UNIVERSITÀ DEGLI STUDI DI SALERNO

UNIVERSITÀ DEGLI STUDI DI SALERNO
Dipartimento di Farmacia

PhD Program

in Drug Discovery and Development

XXXV Cycle — Academic Year 2022/2023

PhD Thesis in

Development of novel anticancer compounds directed towards promising therapeutic targets

Candidate   Tutor

Martina Pierri   Prof. *Stefania Terracciano*

PhD Program Coordinator: Prof. *Gianluca Sbardella*

Firmato digitalmente da: GIANLUCA
SBARDELLA
Luogo: Fisciano
Data: 09/02/2023 15:10:32

Preface

My three-year Ph.D. course in Drug Discovery and Development at the Department of Pharmacy of the University of Salerno started in November 2019 under the supervision of Prof. Stefania Terracciano. My research activity was focused on the design and syntheses of new compounds with potential anti-cancer activity, as part of a major project funded by AIRC (Associazione Italiana per la Ricerca sul Cancro). More specifically, I have been interested in the identification of new binders of Bromodomain-containing protein 9 (BRD9), an epigenetic reader that has recently been receiving growing interest from the scientific community due to its involvement in gene regulation and its overexpression in many human tumors, highlighting it as an attractive target for cancer therapy.

Thus, taking advantage of a multidisciplinary approach, innovative *in silico* techniques and the latest methodologies in the drug discovery field were applied to identify BRD9 binders, exploring thoroughly the biology of this interesting target in cancer.

Finally, during the third year of my Ph.D., I moved to the Centre of Targeted Protein Degradation (CeTPD) at the University of Dundee (UK) for a six-month research period. Here, under the supervision of Prof. Alessio Ciulli, I could pursue my research and knowledge in the protein degradation field and work on promising Leucine-rich repeat kinase 2 (LRRK2) degraders for the potential treatment of Parkinson's disease.

Publications:

- ➢ **Pierri, M.**[†]; Gazzillo, E.[†]; Chini, M. G.; Ferraro, M. G.; Piccolo, M.; Maione, F.; Irace, C.; Bifulco, G.; Bruno, I.; Terracciano, S.*; Lauro, G.* Introducing structure-based three-dimensional pharmacophore models for accelerating the discovery of selective BRD9 binders. *Bioorg. Chem.* **2022***, 118,* 105480*.*

- ➢ Di Micco, S.; Terracciano, S.; **Pierri, M.**; Cantone, V.; Liening, S.; König, S.; Garscha, U.; Hofstetter, R. K.; Koeberle, A.; Werz, O.; Bruno, I.; Bifulco, G. Identification of 2,4-Dinitro-Biphenyl-Based Compounds as MAPEG Inhibitors. *ChemMedChem* **2022**, *17*, e202200327.

- ➢ Gazzillo, E.[†]; **Pierri, M.**[†]; Colarusso, E., Chini, M. G.; Ferraro, M. G.; Piccolo, M.; Irace, C.; Bifulco, G.; Bruno, I.; Terracciano, S.*; Lauro, G.* Exploring the chemical space of [1,2,4]triazolo[4,3-*a*]quinoxaline-based compounds targeting the bromodomain of BRD9. [Manuscript in preparation]

[†]Authors contributed equally to the work.

Conference proceedings:

➢ **Pierri, M.**; Gazzillo, E.; Chini, M. G.; Bifulco, G.; Bruno, I.; Lauro, G.; Terracciano, S. "Design and synthesis of new promising bromodomains binders" poster communication presented at XLV "A. Corbella" International Summer School on Organic Synthesis – ISOS 2021, Virtual, June 14-17, 2021.

➢ **Pierri, M.**; Gazzillo, E.; Chini, M. G.; Bifulco, G.; Bruno, I.; Lauro, G.; Terracciano, S. "Exploring the epigenetic reader BRD9: computational studies and synthesis of new potential binders" poster communication presented at XXVII Congresso Nazionale della Società Chimica Italiana, Virtual, September 14-23, 2021.

➢ **Pierri, M.**; Gazzillo, E.; Chini, M. G.; Bifulco, G.; Bruno, I.; Lauro, G.; Terracciano, S. poster communication presented at the 13th Spanish-Italian Symposium on Organic Chemistry (SISOC-XIII), Tarragona, Spain, September 4-6, 2022.

➢ Terracciano, S.; **Pierri, M.**; Gazzillo, E.; Chini, M.G.; Bifulco, G.; Bruno, I.; Lauro, G. oral communication presented at XL Convegno Nazionale della Società Chimica Italiana, Palermo, Italy, September 11-15, 2022.

➢ Gazzillo, E.; Chini, M. G.; **Pierri, M.**; Terracciano, S.; Colarusso, E.; Giordano, A.; Bruno, I.; Bifulco, G.; Lauro, G. poster communication presented at XL Convegno Nazionale della Società Chimica Italiana, Palermo, Italy, September 11-15, 2022.

Table of Contents

Abstract

Lysine acetylation of histone tails is an epigenetic hallmark that plays a crucial role in the regulation of chromatin structure. Alteration in acetylation levels and/or aberrant activity in proteins involved in this crucial regulation have been linked to the development of several human diseases. Bromodomains are protein modules that, through the recognition of the acetyl-lysine modifications, drive transcriptional programmes that result in phenotypic changes. In this *scenario*, BRD9 has been receiving growing interest in diverse therapeutic areas, particularly oncology. Indeed, acting as a subunit of the mammalian SWI/SNF (mSWI/SNF) chromatin remodeling complex, BRD9 regulates the expression of oncogenes and anti-apoptotic proteins leading to abnormal cell proliferation and survival in different tumor types. These findings stimulated an intensive research activity on BRD9 that emerged as an appealing target in cancer therapy. In addition, recently it has been assessed that targeting BRD9 could hold a potential for the treatment of inflammation.

On these bases, the present research work had been focused on the discovery and development of new agents able to disrupt the activity of BRD9 within the SWI/SNF complex by applying a multi-disciplinary strategy. Intense efforts and coordinated research work between the computational and the synthetic units led to the development of the first 3D structure-based pharmacophore models for BRD9 that represent valid and effective implements for the entire scientific community interested in the identification of new potent and selective ligands. Aided by these pioneering *in silico* tools, three new classes of compounds were effectively explored, supported by the application of modern synthetic methodologies that allowed rapid access to large collections of derivatives.

Abstract

At the beginning of this BRD9 project, an early and simplified version of the three-dimensional pharmacophores, namely the 4-point "pharm-fragment" model, was developed and employed for the design of a class of aryl sulfonamide-based compounds (**49-74**). Nevertheless, the poor activity obtained with these small molecules prompted a careful reevaluation of the computational tool. Therefore, the combination of iterative rounds of *in silico* design with effective syntheses of specific compounds and the final biophysical evaluations of the binding activity on BRD9, have been the cornerstone to optimize the efficiency of the compounds' selection process. Thus, two more precise models consisting of 7 pharmacophoric points were built. Specifically, the development of the "pharm-druglike2" model was crucial for the chemical exploration of a class of compounds featuring the 1-ethyl-[1,2,4]triazolo[4,3-*a*]quinoxaline scaffold. Deepened SAR studies, led to the identification of new interesting BRD9 ligands, specifically four compounds (**1**, **5**, **11**, and **42**) stood out for their potent binding on BRD9 in the low micromolar range and high selectivity across a panel of bromodomains. In collaboration with Prof. Irace (Università degli Studi di Napoli Federico II), compounds **1**, **11**, and **42** showed interesting bioactivity in interfering with tumor growth and proliferation, proving promising outcomes in leukemia cells.

Finally, the employment of the "pharm-druglike2" model, led to the discovery of the latest scaffold, *i.e.*, the 1-ethyl-1*H*-pyrazolo[3,4-*b*]pyridine core. The promising potential, owned by this new class of small molecules as new BRD9 ligands, was assessed by preliminary biophysical data of the hit compound **43**, which disrupted the recognition BRD9 – Histone H4 at 10 μM, presenting 55.0 $\pm$ 1.5 % residual BRD9 activity.

In parallel to the 3D pharmacophore-based discovery, two alternative approaches were explored to circumvent the crosstalk and complexes formation occurring between epigenetic modifiers. These mechanisms often represent a bottleneck for the achievement of a powerful and long-lasting anticancer activity of inhibitors that target specific subunits. Therefore, in addition to the conventional protein inhibition approach, we decided to explore the protein targeted degradation strategy. Herein it is reported a new class of Proteolysis Targeting Chimeras (PROTACs) taking advantage of our identified potent and selective ligand **1** for BRD9 engagement. Initial biological results carried out in collaboration with Prof. Altucci (Università degli Studi della Campania Luigi Vanvitelli), highlighted the promising degradation activity of the PROTAC compound **75**, which showed an evident depletion of BRD9 at 5 μM in U937 treated cells after 24 h, that was also reflected into a strong cytotoxicity in the same cell line.

Moreover, herein is reported the accurate design and the efficient synthesis of the first multi-target probe **81** that could be useful to start a yet unexplored investigation of the ncBAF SWI/SNF complex. The hybrid compound **81** was conceived with the aim to perturb, through a single agent, two crucial subunits belonging to the above-mentioned complex, and both involved in the onset of acute myeloid leukemia: BRD9 and SMARCA4.

As a conclusion of the intense investigations of the biological role exerted in cell environment by BRD9, thanks to a collaboration with Prof. Maione (Università degli Studi di Napoli Federico II), during this project it was assessed the striking anti-inflammatory activity featured by both BRD9 ligands (*e.g.*, compound **1**) and the degrader **75**. All the tested compounds proved a remarkable decrease of IL-6 and TNF-

α in J774 macrophage cells, paving a new interesting therapeutic applicability of BRD9 targeting agents.

Finally, in this Ph.D. project, deepened studies in the emerging protein degradation field were carried out at the University of Dundee (UK) under the supervision of Prof. Ciulli. The results obtained, through the syntheses of specific VHL ligand derivatives followed by both biophysical evaluation and the crystal structure solution of **MP-1-39** bound to VHL protein, could provide important steps forwards to understand the mechanisms of molecular recognition of different stereoisomers and open the rational design of new VHL-based PROTACs. In parallel, the optimization of the degradation profile and pharmacokinetic properties of Leucine-rich repeat kinase 2 (LRRK2) PROTACs for the therapeutic treatment of Parkinson's disease was carried out. Among a small set of newly synthesized degraders, compound **MP01088** qualified as an attractive starting point for future drug development, presenting a strong LRRK2 degradation in mouse embryonic fibroblasts already after 4 h of treatment.

Introduction

My three years Ph.D. project has been focused on the identification of novel anti-cancer agents, which could interfere with specific cancer pathways. Thus, the main goal of the present research study has been the development of new selective small molecule ligands of the target protein Bromodomain-containing protein 9 (BRD9), an epigenetic reader whose gene regulation and overexpression showed a corroborated involvement in many human tumors development.[1] In this context, while bromodomain and extra-terminal (BET) proteins have been extensively studied thanks to the availability of many potent BET ligands, less is known about the biological role of BRD9 beyond the acetyl-lysine recognition. Hence, the identification of selective BRD9 inhibitors could disclose new epigenetic chemical probes useful to elucidate its biological function, as well as for corroborating its importance as a therapeutic target for novel promising anti-cancer drugs.[2] The limited number of highly selective BRD9 inhibitors identified so far highlights the need for the discovery of novel small molecules endowed with high affinity and selectivity. This goal represents a significant challenge since bromodomains' hallmark is both the highly conserved overall fold and the asparagine-mediated protein interaction modules that recognize the ε-*N*-lysine acetylation motifs.

Supported by AIRC (Associazione Italiana per la Ricerca sul Cancro), the application of a multitask protocol was employed, leading to the identification of new selective BRD9 binders (**CHAPTER 2**). In more detail, structure-based 3D BRD9 pharmacophore models recently developed by our research group, have been used as effective computational filters to identify new potential and unexplored chemotypes. The proposed pharmacophore models aid the identification of the key structural features of a BRD9 binder directly into the BRD9 binding site owning a combination

of three-dimensionality, coordinates, and orientation and providing an effective computational implement for rapid identification of new drug-like binders.

The general workflow applied can be summarized as follow:

1. *In silico* studies employing our 3D pharmacophore models that guided the identification of three different and novel molecular chemotypes for the protein target;

2. Choice of modern and efficient synthetic strategies to obtain the most promising *in silico* selected molecules;

3. Syntheses and optimization of the synthetic protocols, purification and full structure characterization by High-Resolution Mass Spectrometry (HRMS) and NMR spectroscopy;

4. Evaluation of the synthesized compounds through biophysical binding assays to verify their affinities for the protein counterpart;

5. Biological screenings of the most efficient disclosed binders on different cancer cell lines aimed to estimate the potential anticancer activity;

6. Focused structural modifications that allowed to build robust SAR studies, which aided the refinement of our 3D pharmacophore models and the improvement of compounds' activity.

7. Whereas a poor or null binding activity was detected, the synthesized compounds were subjected to a biological repositioning by Inverse Virtual Screening (IVS), a useful computational technique previously developed by our research group to identify potential protein targets for a set of compounds.[3]

Particularly, as regard the synthetic approach, in order to obtain large collections of compounds in a relatively short time, we applied fast and versatile synthetic methods. Moreover, microwave-assisted syntheses were also applied in order to improve yields and drastically reduce reaction times.

In parallel, to enhance the biological effect of BRD9 inhibitors, we undertook an alternative approach designing a SWI/SNF multi-target compound combining a well-known BRD9 inhibitor and a high-affinity ligand of the ATPase subunit of the chromatin remodeling complex SMARCA2/4 (**CHAPTER 3**). Notably, the mammalian SWI/SNF complex plays a critical role in human cancers, since its components are mutated in 20% of human tumors.[4] Thus, the development of a bifunctional binder targeting two subunits of the remodeling complex might be a novel promising strategy for the epigenetic therapy of cancer. Moreover, in addition to the conventional protein inhibition approach, in the present thesis is reported our Proteolysis Targeting Chimeras (PROTACs) campaign based on the design and synthesis of potential degraders targeting BRD9 (**CHAPTER 3**).

Concerning our interest in developing small molecule degraders and exploring the PROTAC-mediated protein degradation field, during the third year of my Ph.D. course, I spent six months at the Centre for Targeted Protein Degradation (CeTPD) - University of Dundee (UK), under the supervision of Prof. Alessio Ciulli. Thus, in **CHAPTER 4**, studies on the development of promising PROTACs targeting the Leucine-rich repeat kinase 2 (LRKK2) protein for the potential treatment of Parkinson's disease are reported.

Finally, due to the evidence that this epigenetic reader plays a role in regulating pro-inflammatory cytokines secretion, herein is also reported our preliminary

investigation of a mostly unexplored BRD9 activity in the regulation of inflammatory responses (**CHAPTER 3**).[5]

CHAPTER 1

The role of the target protein Bromodomain-containing protein 9 in epigenetically-defined diseases

1.1 Epigenetic modifications in cancer development

The structural assembly of chromatin, which represents how the genetic information is organized within a cell, plays a crucial role in the ability of genes to be activated or silenced. Therefore, the state of chromatin organization is fundamental for a correct expression of the genome and disruptions of its regulation could lead to aberrant transformations. The "epigenetics" is the genomic branch related to the structural adaptation of chromatin to exogenous signals, and all the epigenetic-related mechanisms are essential for the maintenance of gene expression patterns in mammals.[6] The term "epigenetics" was first defined in 1942 by Conrad Waddington as "the causal interactions between genes and their products, which bring the phenotype into being".[7] However, many further definitions have been given over time due to the implication in a wide variety of biological processes. Indeed, the current definition considers the presence of heritable changes in gene expression established during cell differentiation that are stably maintained through multiple cycles of cell division. The heritability of gene expression patterns is maintained by the so-called "epigenetic modifications" (*i.e.* chemical modifications of DNA and histones), which provide a mechanism for cellular diversity by regulating the accessibility of the cellular machinery to the genetic information contained in the DNA. Dysfunction of the epigenetic regulation can lead to inappropriate activation or inhibition of different signal pathways prompting disease initiation, such as cancer.[8] The chemical modifications implicated in this process are dynamically added and removed by chromatin-modifying enzymes in a highly regulated manner. To date, a number of both DNA and histone modifications have been elucidated, which can alter the chromatin structure and thus, the accessibility to transcription factors. [9-11] In addition, these modifications can be specifically recognized by specialized proteins with unique

domains, called "chromatin readers" able to recruit additional chromatin modifiers and remodelling enzymes that act as the effectors of the modification.

Thus, the information conveyed by epigenetic modifications plays a critical role in regulating DNA processes, such as transcription, DNA repair, and replication. Aberrant expression patterns or genomic alterations in chromatin regulators can lead to the initiation and maintenance of various cancers. However, the reversible nature of the epigenetic changes can be effectively modulated through pharmacological intervention paving the way for the "epigenetic therapy" option. Hence, in the last few years, a great interest from the scientific community has been focused on the discovery of new epigenetic drugs, which have been proven to modulate cell survival and to be less toxic than conventional chemotherapy.[12] Despite significant advances have been made in this field, several mechanisms still remain unsolved, underlining the need for potent and specific chemical probes for deeper understanding of the global patterns of the epigenome.

1.1.1 Regulation of gene expression through histone modifications

All the epigenetic mechanisms, which modify the local dynamics of chromatin structure, work together to regulate its accessibility and compactness. Specifically, four main regulatory mechanisms can be identified: DNA methylation, covalent histone modifications, non-covalent mechanisms (such as the incorporation of histone variants), and non-coding RNAs including microRNAs (miRNAs). For the purpose of this thesis, a specific focus will be on the histone modifications able to regulate key cellular processes such as transcription, replication and repair.[10] Indeed, histone residues are subjected to a wide variety of post-translational processes such as

methylation, acetylation, ubiquitination, sumoylation, and phosphorylation. Although many examples of modifications have been identified, the majority of these occur on the lysine of the *N*-terminal tails of histone proteins, due to their protruding position from the nucleosome core (**Figure *1***).

These epigenetic marks, individually or in combination, are able to change the accessibility of chromatin through the alteration of the interactions with nucleosomes or the recruitment of non-histone effector proteins, which recognize particular histone modifications through specific modules and decode the message included in the modification patterns.[13] Unlike DNA methylation, which always leads to gene silencing, histone modifications are responsible for either activation or repression depending upon which residues are modified and in which combination, defining the so-called "histone code".[14]

1.1.2 Histone acetylation regulates chromatin accessibility and gene expression

Histone acetylation, as part of the covalent histone marks, occurs at lysine residues on the *N*-terminal tails. This modification leads to the neutralization of the positive charge of the histone and, therefore, destabilizes the electrostatic interaction with the DNA. As a consequence, histone acetylation alters nucleosomal conformation increasing the accessibility of transcriptional factors to the genetic code and therefore, it can significantly increase gene expression (**Figure *1***).[15, 16] However, a low level of acetylation has been found also in high transcriptionally active genes; hence, the strictness of this correlation is still under debate.
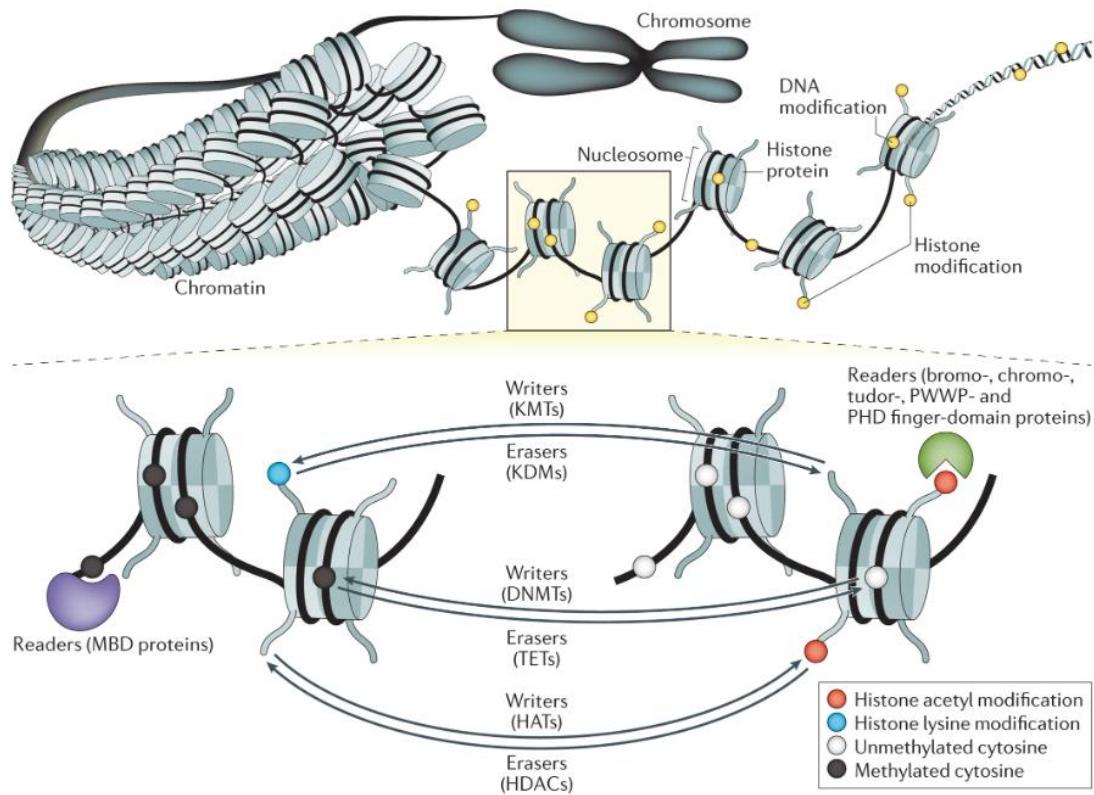
Figure 1. *Schematic representation of covalent histone modifications and their modulation through the action of specific proteins: writers, erasers, and readers.*

Two enzymes are responsible for the addition or removal of the acetylation tag on the histone tails: the histone acetyltransferases (HATs) and histone deacetylases (HDACs). In particular, the histone acetyltransferases (also referred to as "writers") are responsible for transferring acetyl groups from acetyl-CoA cofactors to the ε-amino groups of side chains of lysine residues. This type of process is mainly carried out in the promoting regions, with the preferential targets the histones H3 and H4.[17] In contrast, histone deacetylases (also referred to as "erasers") remove the histone marks added by HATs restoring the positively charged lysine residues, which stabilize the structure of chromatin leading to a suppression of the transcription process.[18]

Finally, the acetylation marks on lysine residues are read by specific protein modules also called "readers", *e.g.* bromodomains (**Figure** *1*). Interestingly,

bromodomains are found in many different chromatin regulators as well as protein complexes that play important roles in human biology and diseases. In this thesis, the attention will be focused on these reader modules due to their attractive implication in cancer development and progression, particularly in leukemias and solid tumors pathogenesis.[19] Moreover, strong evidence assessed an important role of the acetylation mark in the regulation of the inflammatory response and, particularly, a pivotal role is played by the bromodomain-containing proteins.[20, 21]

1.1.3 The key role of bromodomains in chromatin biology regulation

Bromodomains (BRDs) are evolutionarily conserved protein modules able to read the modifications introduced by the writers HATs. Indeed, they selectively recognize and bind the ε-*N*-acetyl-lysine residues on histone tails acting as genetic code readers, and therefore, they play a key role in the regulation of gene expression.

The name "bromodomains" comes from the *Brahma* gene of Drosophila, in which the bromodomain sequence was identified for the first time.[22] The human genome encodes 61 BRDs present in 46 different proteins such as transcriptional co-regulators, chromatin-modifying enzymes, and ATP-dependent chromatin-remodeling complexes.[23] The biological functions of these effector modules, as well as their involvement in several pathological processes, attracted the scientific community for their potential as therapeutic targets.[24]

All bromodomains share a distinctive architecture with a highly conserved ternary structure (***Figure 2***) consisting of a left-handed bundle of four α-helices (αZ, αA, αB, and αC) that are connected by means of two flexible loop regions (ZA and BC), which are variable in sequence and charge and that form the acetyl-lysine binding site (KAc region). Despite the sequence variations among bromodomains in the loop regions, the

amino acid residues responsible for the recognition of the acetyl-lysine in the KAc binding site are highly conserved. Structural data have established that the various bromodomains share the presence of both asparagine (Asn) and tyrosine (Tyr) residues in the binding site, where specific hydrogen bonds and water-mediated interactions occur with the acetyl group (***Figure 2***).[25]
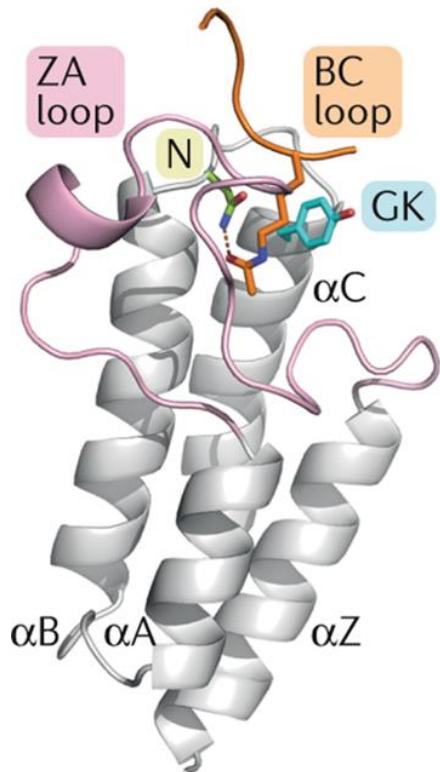
Figure 2. *The left-handed bundle of four α-helices (αZ, αA, αB, and αC) linked by the loop regions (ZA and BC) that define the KAc binding site. The acetyl lysine (represented in orange) interacts with a conserved asparagine residue (represented in green) and a hydrophobic gatekeeper ("GK", represented in cyan).*

Following the most recent structure-based classification, the human BRDs are grouped into eight families that span all 61 domains (***Figure 3***).[25] Among these, the most studied are the bromo and extra terminal (BET) proteins that include BRD2, BRD3, BRD4 and BRDT which display high levels of sequence conservation.

The hydrophobic nature of the acetyl-lysine binding site of bromodomains makes these proteins particularly targetable by small molecules that could interfere with the recognition mediated through protein-protein interactions.[25] In recent years, several bromodomain binders able to disrupt the recognition of the acetyl-lysine have been reported showing great potential as new drugs in cancer therapy. BET bromodomain blockage using small molecules gives rise to selective repression of the transcriptional network driven by c-MYC showing an interesting therapeutic potential for a wide range of malignancies. However, the disruption of the MYC-dependent transcriptional pathway and the Wnt signaling caused by BET ligands, cause critical damage to normal cell proliferation.[26]
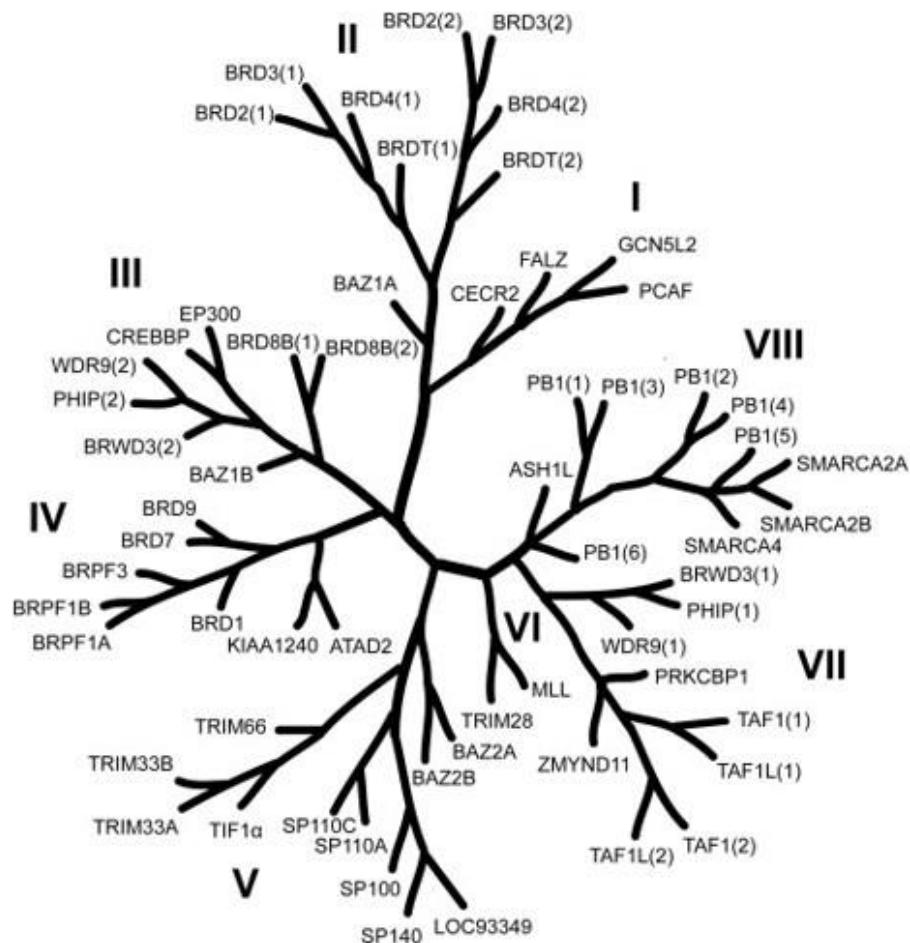
Figure 3. *Phylogenetic tree of human BRDs. The different families are named by roman numerals (I to VIII).*

Most recently, the scientific attention has been focused on the Bromodomain-containing protein 9 (BRD9) that belongs to the IV subfamily together with its close homologue BRD7 with which shares the 72% of similarity. BRD9 is a component of the non-canonical BAF (ncBAF) SWI/SNF chromatin remodeling complex[27] and binds acetylated or butyrate lysine residues, inducing post-translational modifications involved in several diseases including cancer.[28] On the other hand, the Bromodomain-containing protein 7 (BRD7) is a subunit of Polybromo-associated (PBAF) SWI/SNF complex and it is a recognized tumor suppressor whose expression is partially or completely repressed in several types of cancers.[29] Therefore, the achievement of a selective binding toward BRD9, is a compelling goal for the drug discovery field.

1.2 Bromodomain-containing protein 9 (BRD9): an epigenetic target involved in cancer development.

For the purpose of this Ph.D. thesis, particular attention will be focused on Bromodomain-containing protein 9 (BRD9). As previously described, BRD9 is an epigenetic reader, subunit of the non-canonical BAF (ncBAF) switch/sucrose non-fermentable SWI/SNF complex (*Figure 4*) and a member of the bromodomain family IV.[27] Numerous studies confirmed that BRD9 plays a pivotal oncogenic role in multiple cancer types by regulating tumor proliferation and differentiation.[28] Moreover, BRD9 is at the center of multiple signal transduction pathways, chromosomal activities, and nuclear organization.[30] Specifically, the gene coding for BRD9, located on chromosome 5p, is overexpressed in cervical cancer and non-small cell lung cancer.[31, 32] In addition, BRD9 was found often mutated in squamous cell lung cancer, prostatic adenocarcinoma, endometrial cancer, and hepatocellular carcinoma.[33-36] Importantly, several evidences assessed that BRD9 knockdown

suppresses the proliferation of human acute myeloid leukemia (AML) and malignant rhabdoid tumor (MRT).[37, 38] However, although the therapeutic potential of BRD9, the exact biological mechanisms in which it is involved remain elusive. Hence, the discovery of new and highly selective binders targeting BRD9 is an attractive tool to unravel the role of this epigenetic reader in acetyl lysine-dependent reading processes, as well as in the development of human diseases, particularly for cancer.
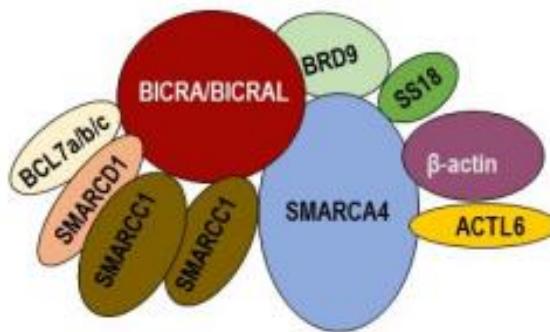
Figure 4. *Schematic representation of the ncBAF SWI/SNF complex.*

1.2.1 Focus on the differences in BRD9 binding sites compared to the other BRDs

The high similarity among bromodomains, specifically in the KAc binding site, represents a significant challenge for the discovery of novel small molecules endowed with high affinity and selectivity. However, as already hinted, there is an urgent necessity for the disclosure of highly selective BRD9 ligands to effectively explore its biology. Although the preserved tridimensional structure, some differences in the amino acid sequence among bromodomains reflect important dissimilarities in the binding site architecture that could be exploited in order to identify new potent and highly selective inhibitors.

BRD9 shares with the other bromodomains the conserved left-handed bundle of four α-helices linked by the ZA and BC loops. An important structural hallmark is a

stretch of three hydrophobic amino acids close to the ZA loop, also called "shelf", which represents a highly conserved motif among the BET family but differs in the other bromodomains. Therefore, this structural feature represents an important hallmark to gain selectivity. The BET family members display the so-called "WPF shelf" due to the presence of Trp81 (W), Pro82 (P) e Phe83 (F); on the other hand, BRD9 presents the peculiar "GFF shelf" consisting of Gly43 (G), Phe44 (F) and Phe45 (F) (**Figure 5**).[39]
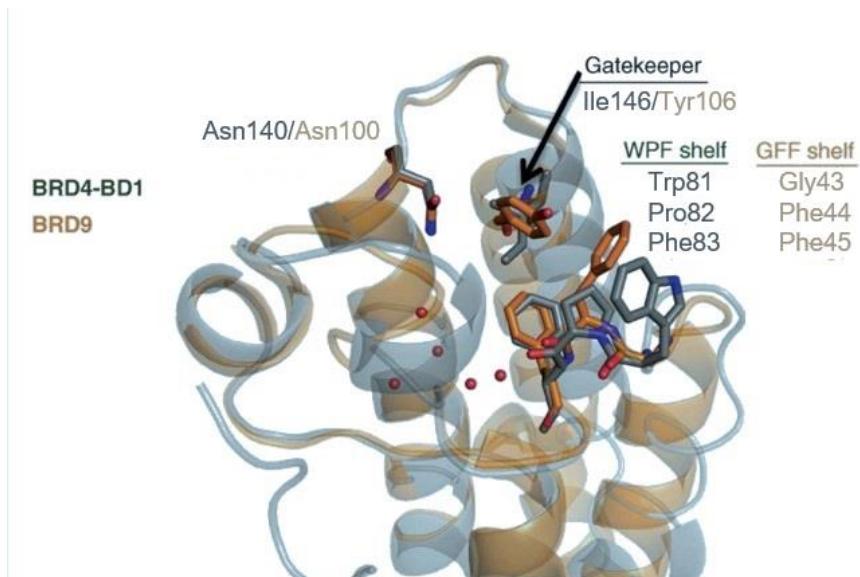
Figure 5. *Superposition of the X-ray structures of BRD4-BD1 (in gray, PDB 3UVW) and BRD9 (in orange, PDB 4Z6I). The amino acids forming the WPF and GFF shelves are represented in gray and orange, respectively. The two different gatekeepers in BRD4 and BRD9 are also shown in gray and orange.*

Structural analyses among bromodomains also revealed a key difference in the first residue of the alpha helix αC, which is called the "gatekeeper" of the binding site. In both BRD9 and BRD7 proteins, the gatekeeper is a tyrosine residue that limits the size of the deeper region of the pocket; on the other hand in the BET family, the gatekeeper is represented by an isoleucine or a valine residue that makes the binding site wider and more accessible (**Figure 5** and *Figure 6*).[40] Moreover, while the deeper region of

BRD9 is less large than that of BRD4 due to the presence of the gatekeeper Tyr106, the ZA channel is characterized by a wider architecture due to the presence of Ala46, Phe47, Pro48, Thr50, and Ile53 residues that form a wide hydrophobic cavity, as observable in *Figure 6*.[39]

Another important difference between BRD9 and the bromodomain BET family arises from the Ala54 residue of BRD9 represented by the Leu94 in BRD4: it has been proven that small molecules featuring chemical groups with basic nature sit more favorably in the less hydrophobic environment alongside Ala54 of BRD9 than beside Leu94 of BRD4. Thus, this small dissimilarity could be exploited to obtain high selectivity on BRD9.[40]
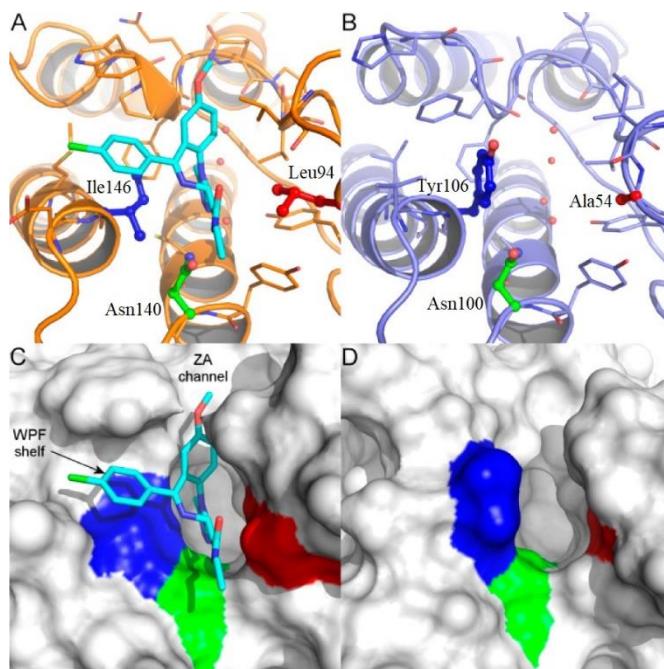
Figure 6. *X-ray crystal structures of (A) BRD4 binding site (orange) in complex with the ligand I-BET762 (cyan); (B) BRD9 binding site (blue); (C) BRD4 binding surface; (D) BRD9 binding surface. In each, the conserved asparagine residue is colored green, while the gatekeeper is colored blue. BRD4 Leu94 and BRD9 Ala54 are colored red.*

However, structural differences between BRD9 and the highly homologous BRD7 are much less evident as shown in **Figure 7**, given its proximity to BRD9 on the phylogenetic tree and sequence similarity within the KAc binding pocket. Despite the similarity, the achievement of high selectivity is possible as demonstrated by the discovery of the first selective BRD9 ligand (compound **I-BRD9**), which showed 200-fold stronger binding affinity to BRD9 than BRD7.[40] Presumably, this activity arises from the differences in the constituent amino acids in the GFF shelf and the ZA channel: the Gly43 of BRD9, in the corresponding position of BRD7 is substituted with a more bulky amino acid represented by Ala154. Moreover, the Ala46 of the BRD9 ZA channel is replaced by Ser157 in BRD7, leading to key structural differences in the architecture of the two bromodomains that could be exploited to design selective binders.

BRD4 BD1	BRD9	BRD7	
TRP81	GLY43	ALA154	WPF motif
PRO82	PHE44	PHE155	WPF motif
PHE83	PHE45	PHE156	WPF motif
GLN84	ALA46	SER157	ZA channel
GLN85	PHE47	PHE158	ZA channel
PRO86	PRO48	PRO159	ZA channel
VAL87	VAL49	VAL160	ZA channel
ASP88	THR50	THR161	ZA loop
ALA89	ASP51	ASP162	ZA loop
LYS91	INS	INS	ZA loop
LEU92	INS	INS	ZA loop
ASN93	ILE53	ILE164	ZA loop
LEU94	ALA54	ALA165	ZA loop
TYR97	TYR57	TYR168	Water-binding Tyr
CYS136	ALA96	ALA207	Conserved amino acid
TYR139	TYR99	TYR210	Conserved Tyr
ASN140	ASN100	ASN211	Conserved Asn
ILE146	TYR106	TYR217	Gatekeeper

Figure 7. *Sequence similarity between the residues of the KAc binding sites of BRD4 BD1, BRD9, and BRD7. The colours represent residue properties: green = aromatic, cyan = hydrophobic, red = acidic, yellow = basic, orange = polar, purple = proline, white = not bulky group. INS = indel.*

1.2.2 BRD9 ligands

In this section are described the most potent and useful ligands identified so far for the epigenetic reader BRD9. For the purpose of this project thesis, it is deemed of interest an insight into their structural and chemical features underling their specific binding mode in the KAc pocket.

1.2.2.1 LP99: a 1,4-dimethylquinolone-based ligand

Considering the structural similarity between the various bromodomains, non-selective binders were the first to be developed. Specifically, LP99 is the first-discovered BRD9/BRD7 ligand (***Figure 8***), which showed a K_D value of 99 nM on BRD9, through ITC (Isothermal Titration Calorimetry) measurement.[41] The development of this compound started from a fragment-hit featuring, as scaffold, the 1-methylquinolone, which presents the *N*-methyl amide portion as mimetic of acetyl-lysine group forming hydrogen bonds with the conserved asparagine and with a structural water molecule present in the binding site. Following a structure-based design approach, different substituents on the core were evaluated. Among these, the heterocycle δ-lactam was inserted in position C-7 in order to exploit the hydrophobic cavity of the ZA channel for a selective binding. Subsequently, a methyl was introduced in position C-4 in order to gain potency through hydrophobic interactions with Ala54 and Tyr106. The valerolactam was further derivatized to increase the selectivity: specifically, a proper phenyl moiety was inserted with the idea to fulfill the adjacent hydrophobic cavity, while a sulfonamide group was introduced in order to form a hydrogen bond with the NH of Gly43. Finally, the stereoisomer mixture was solved in its enantiomers and only the 2*R*,2*S* showed a detectable binding to the protein counterpart. The co-crystal structure of compound LP99 with BRD9 was fundamental to confirm the key interactions with the pocket (***Figure 8B***). Moreover, through DSF (Differential Scanning Fluorimetry), LP99 showed selective binding on BRD9 and BRD7 over a panel of 48 BRDs.

A

LP99

B
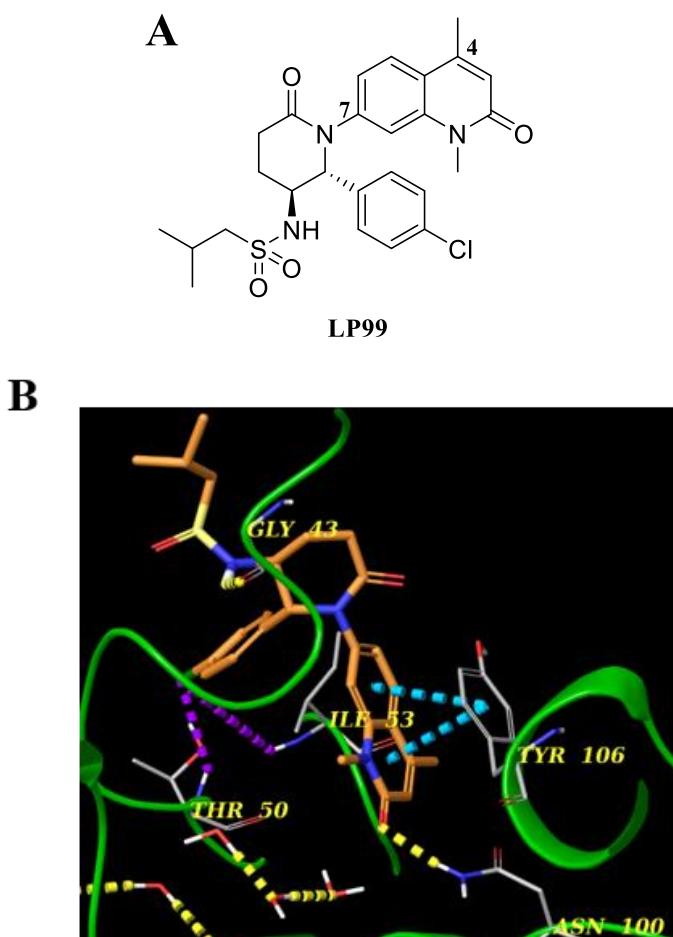
Figure 8. *A) Chemical structure of the first BRD9/BRD7 ligand LP99. B) Co-crystal structure (PDB: 5IGN) of LP99 (orange) in complex with BRD9 (green). Hydrogen bonds are represented in yellow dotted lines, while π-π interactions and halogen bonds are represented in cyan and violet dotted lines, respectively.*

1.2.2.2 I-BRD9: a thienopyridinone-based ligand

A structure-based approach similar to that applied for the ligand LP99, lead to the discovery of the first highly selective and potent chemical probe: compound I-BRD9 (pIC$_{50}$ on BRD9 = 7.3 detected through TR-FRET), characterized by a thienopyridinone scaffold (***Figure 9A***), which showed a more than 700-fold selectivity over the BET family and 200-fold over the highly homologous BRD7.[40] The initial hit was identified through a massive screening on a huge library of compounds, showing

21

a promising selectivity on BRD9 against BRD4. A thorough analysis of the co-crystal structure with BRD9 revealed the goodness of the scaffold in mimicking the *N*-acetyl-lysine, with the carboxyl group establishing the fundamental hydrogen bond with the conserved Asn100, while the aromatic bicyclic scaffold forms π-π stacking with the side chain of Tyr106. After a series of structural modifications and the analysis of the co-crystal structures of the most promising derivatives, it emerged that the amidine moiety is the key group for the achievement of high potency and selectivity on BRD9, mainly thanks to the formation of a H-bond with Ile53 (**Figure *9B***). Furthermore, it was postulated that the increased selectivity over proteins belonging to the BET family is mainly due to the basic nature of this group that, when charged, fits more favorably in the less hydrophobic environment of BRD9. Finally, it was noticed that the *N*-ethyl group on the nitrogen of the pyridinone core enhanced the selectivity on BRD9 over BRD4, while the increase of the length of this alkylic substituent is tolerated by BRD9 but decreases the binding potency.

A

I-BRD9

B
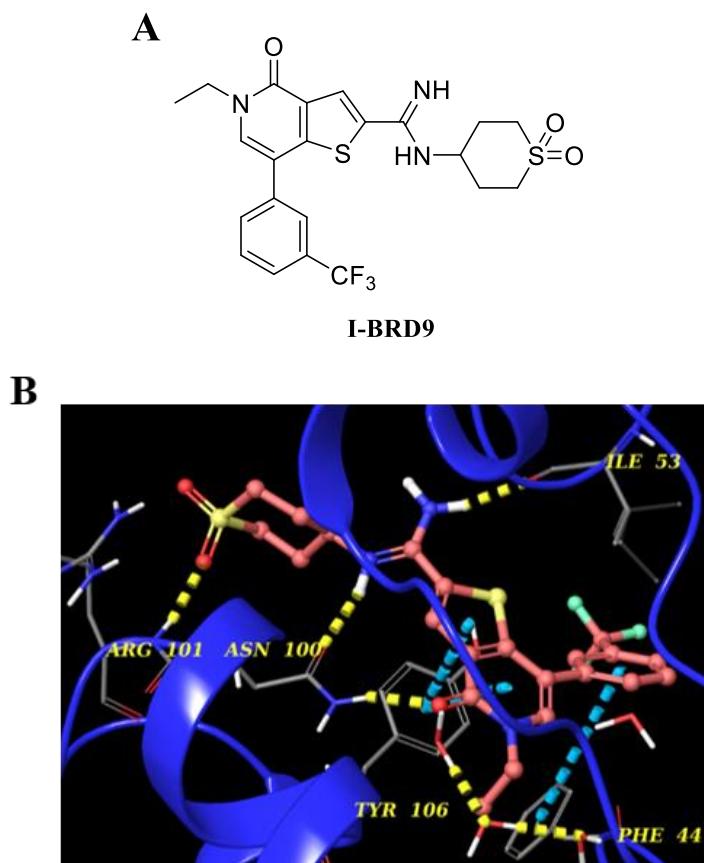
Figure 9. *A) Chemical structure of the first highly selective BRD9 ligand I-BRD9. B) Co-crystal structure (PDB: 4UIW) of I-BRD9 (pink) in complex with BRD9 (blue). Hydrogen bonds and π-π interactions are represented in yellow and cyan dotted lines, respectively.*

1.2.2.3 BI-7273 and BI-9564: naphthyridinone-based ligands

Two chemical probes BI-7273 and BI-9564 (**Figure *10A***) were identified as potent and selective BRD9 ligands (K_D = 15 nM and 14 nM respectively, measured through ITC assay).[42] The two compounds were conceived after an intense structure-based design campaign, starting from a chemical fragment featuring the dimethylpyridinone core co-crystallized with BRD9 that showed an interesting binding to the bromodomain. The enlargement and the structural enrichment of the initial chemical fragment led to the two ring-fused compounds BI-7273 and BI-9564, which showed

an increased selectivity on BRD9 compared to BRD7. After the analysis of the less preserved ZA area of BRD9, the residue Phe44 was highlighted to give key π-π T-stacking interactions with the phenyl on the C-4 position of the naphthyridinone scaffold (*Figure 10B*). The introduction of electron donor groups on the phenyl, *i.e.* the two methoxy moiety, improved the potency and selectivity increasing the strength of the T-stacking interaction and allowing the adoption of the optimal conformation.

In the present thesis, particular attention will be given to compound BI-7273. As described in **CHAPTER 3**, we employed the afore-mentioned ligand in the design of the first SWI/SNF multi-target probe that we conceived as an alternative approach to potentially improve the pharmacological efficacy of BRD9 ligands.

A

BI-7273   BI-9564

B
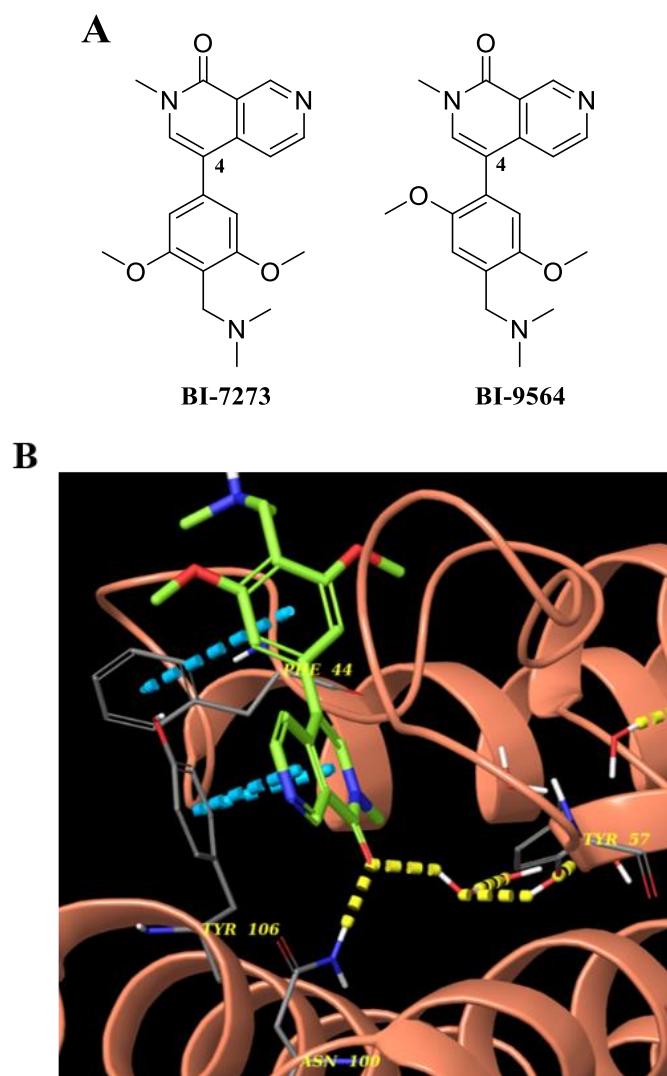
Figure 10. *A) Chemical structures of the two high-affinity BRD9 ligands BI-7273 and BI-9564. B) Co-crystal structure (PDB: 5EU1) of BI-7273 (green) in complex with BRD9 (orange). Hydrogen bonds and π-π interactions are represented in yellow and cyan dotted lines, respectively.*

1.2.2.4 9H-purine-based ligands

In light of the successful fragment-based programs and the reliability for discovering BRDs binders, the purine scaffold was investigated and reported in 2015 by our research group as a putative KAc mimetic that differs from the conventionally employed chemical groups.[43] Starting from the 9*H*-purin-2-amine core, the C-6

position was deeply investigated varying the chemical nature of the substituent in order to explore the space of the ZA channel. A thorough Structure-Activity Relationship (SAR) campaign and co-crystals studies led to a step-by-step structural optimization, which led to the discovery of PUR-5a and PUR-29 (namely, compound 7d and compound 11 in the referenced manuscript,[43] shown in *Figure 11*) as potent BRD9 ligands in the nanomolar scale (K_D measured by ITC = 397 nM and 278 nM, respectively) and only weaker micromolar binders of BRD4. Structural modifications on the 9*H*-purine scaffold, such as the methylation on the N-9, led to a complete loss of the binding affinity, pointing out the importance of a non-substituted nitrogen in this position, which is fundamental in establishing productive H-bonds with Asn100. More importantly, the developed inhibitors induced an appreciable change in the three-dimensional shape of the protein-binding site, resulting in an unprecedented and peculiar induced-fit mechanism that was not observed with the previously reported binders.

Nowadays, it is noteworthy that the inflammatory response predisposes to the development of cancer and promotes tumorigenesis.[44] Considering the close correlation between cancer and inflammation and the recent evidence that BRD9 is a genomic antagonist of the glucocorticoid receptor (GR) in inflammatory-related genes,[5] in the present thesis we investigated the potential anti-inflammatory effect of PUR-29 and other BRD9 ligands. Specifically, the results of our study have been described and reported in **CHAPTER 3**. Moreover, considering the promising biological effect obtained with these ligands, in this thesis is also reported the design of the first PROTAC compound based on the 9*H*-purine scaffold, whose design and synthesis have been reported in **CHAPTER 3**.
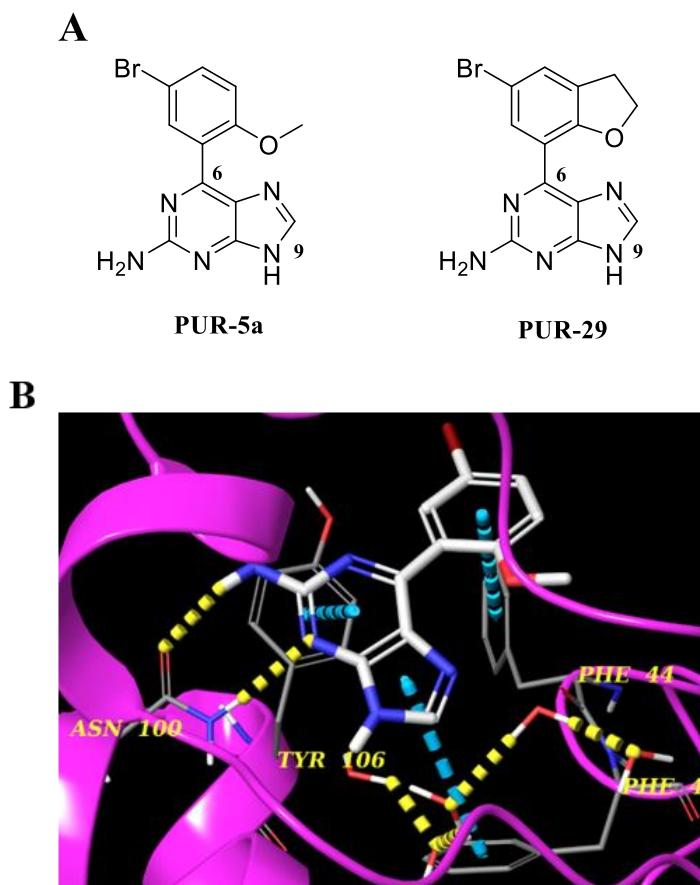
Figure 11. *A) Chemical structures of the two high-affinity ligands compounds PUR-5a and PUR-29. B) Co-crystal structure (PDB: 4XY8) of PUR-5a (white) in complex with BRD9 (purple). Hydrogen bonds and π-π interactions are represented in yellow and cyan dotted lines, respectively.*

1.2.2.5 Other BRD ligands: GNE-375 and compound 28

The inhibitors that have been described so far are the most known and studied ligands for BRD9, but also further compounds have been developed over the years. A similar structure-based approach, as described previously, was the successful option that led to the discovery of the potent and selective *in vitro* tool GNE-375 (IC$_{50}$ = 5 nM on BRD9 measured through TR-FRET, ***Figure 12A***), endowed with >4000-fold selectivity against BRD4.[45] However, while it was highlighted that this compound presented minimal effects in cell viability assays, it showed remarkable potency in

preventing the emergence of a drug-tolerant population in EGFR mutant cells treated with EGFR inhibitors. It is important to note that the modest bioactivity in interfering with tumor growth and proliferation is a common issue for the most selective BRD9 ligands. Presumably, this phenotypic effect is due to the fact that BRD9 works together with other proteins in the large mSWI/SNF complex, thus the bromodomain inhibition is reflected in a reduced but not blocked oncogenic transcription.[46, 47] This topic will be further discussed in the present thesis, as two alternative approaches for circumventing this unwanted effect have been proposed by us in **CHAPTER 3**.

An indolizine BRD9 ligand was also developed starting from a small chemical probe that was initially designed for two different bromodomains, BAZ2A and BAZ2B. A deep SAR study and structural optimization were conducted, which finally led to the discovery of compound 28 (*Figure 12A*) as a BRD9/BRD7 ligand ($K_D = 68$ nM and $K_D = 368$ nM on BRD9 and BRD7 respectively, detected through ITC), whose X-ray structure complexed to BRD9 was determined in order to enlighten the key interactions (*Figure 12B*).[48]

A

GNE-375   **Compound 28**

B
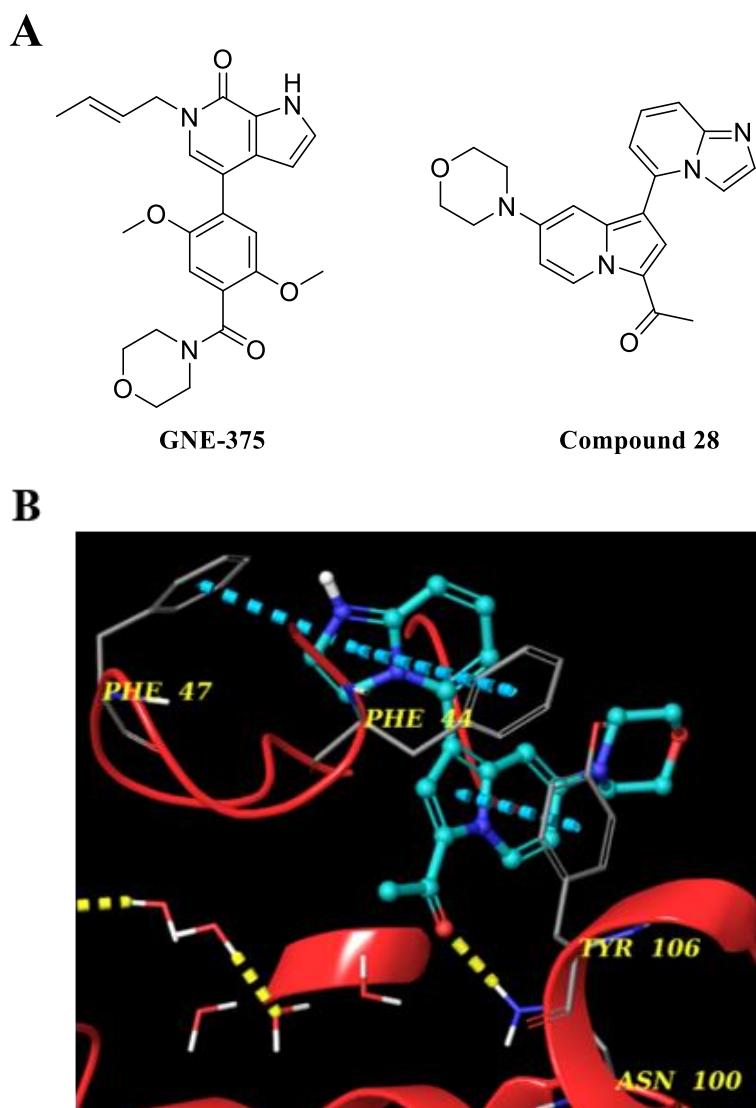
Figure 12. *A) Chemical structures of the two BRD9 ligands: GNE-375 and compound 28. B) Co-crystal structure (PDB: 5E9V) of compound 28 (cyan) in complex with BRD9 (red). Hydrogen bonds and π-π interactions are represented in yellow and cyan dotted lines, respectively.*

Results and Discussion

CHAPTER 2

Identification of new BRD9 binders

2.1 Introduction

As described in **CHAPTER 1**, up to date various BRD9 binders featuring different chemical scaffolds have been identified by combining different experimental structural tools (*e.g.*, X-ray crystallography), screening procedures, and specific biological investigations. Taking advantage of the data collected so far about ligands' interactions with the protein counterpart, and thanks to the availability of a plethora of compounds co-crystallized with BRD9, we developed the first 3D structure-based pharmacophore models defining the common key structural features of known BRD9 binders into the protein binding site.

The fine-tuning of this *in silico* approach promoted effectively the identification of new compounds and oriented the design of new binders in a structure-based fashion.[49] In this chapter is described the detailed project workflow, starting from the *in silico* structure-based design, leading to the identification of novel molecular entities with promising activity and selectivity on BRD9, which have been synthesized through efficient and modern synthetic procedures.

2.2 Development of new 3D structure-based pharmacophore models for the target protein BRD9

The development of 3D structure-based pharmacophore models related to BRD9, combined with virtual screening experiments, provided a useful *in silico* tool for a quick selection of the most promising compounds and paved the way for a new approach for the discovery of BRD9 ligands.[49]
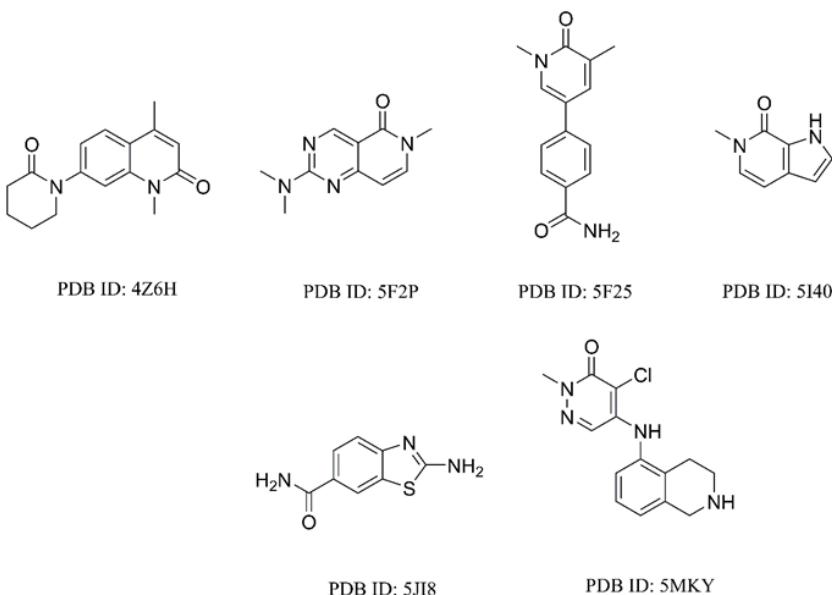
Figure 13. *Chemical structures of six fragment-like ligands co-crystallized with BRD9.*

Specifically, the pharmacophore models were developed by analyzing the binding modes and extrapolating the chemical features of 23 known BRD9 inhibitors determined from the X-ray co-crystal structures available in Protein Data Bank (PDB). Firstly, this set of compounds was split into two groups: a "fragment-like" group (containing 6 out of 23 initial compounds), featuring MW ≤ 300 g/mol and a low number of H-bond acceptor/donor groups (***Figure 13***); and a "drug-like" group, with the remaining 17 ligands endowed with drug-like properties such as MW between ≃350 and ≃500 g/mol and with a maximum of 7 hydrogen bond acceptor and 2 hydrogen bond donor groups (**Figure *14***).
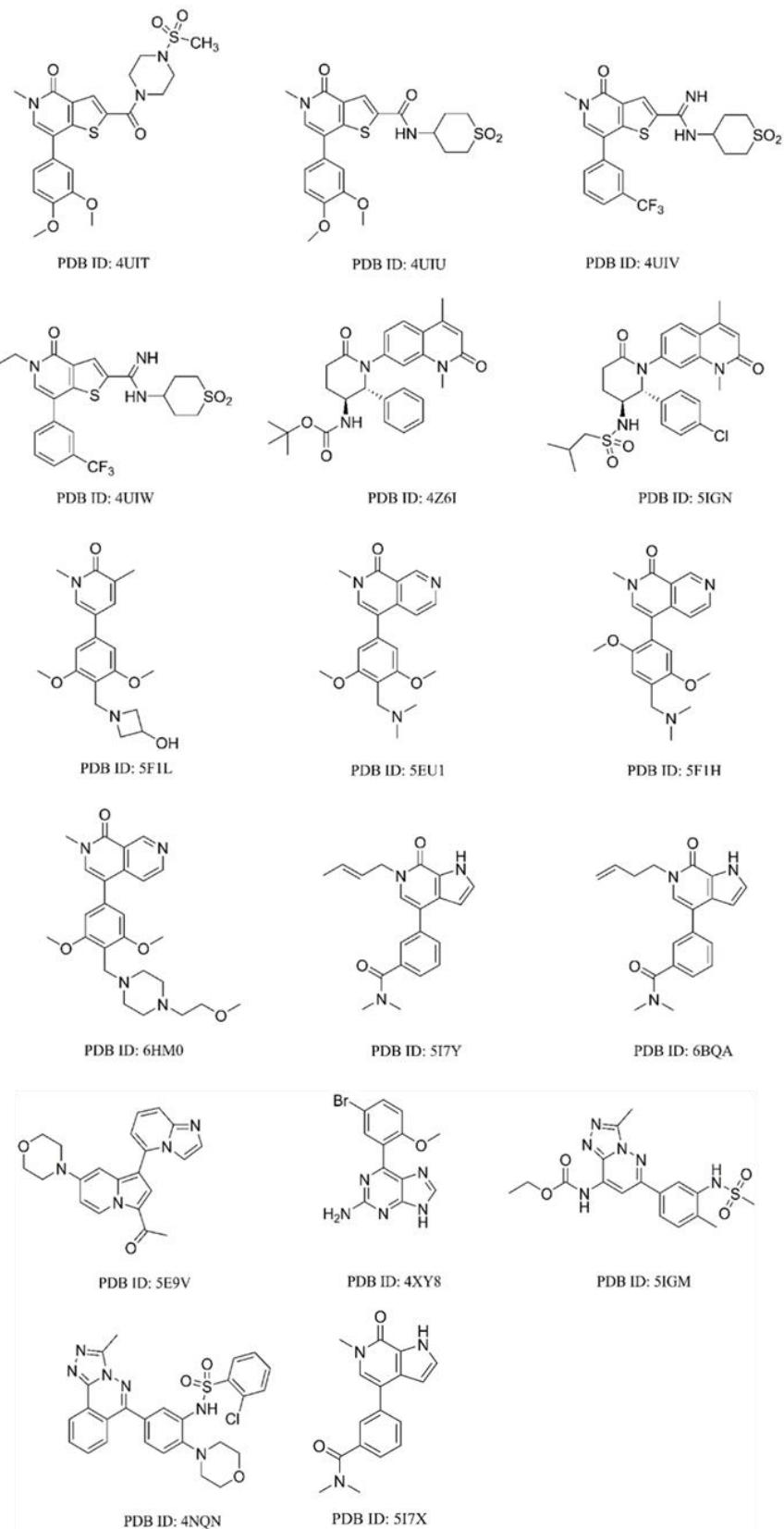
Figure 14. *Chemical structures of seventeen drug-like ligands co-crystallized with BRD9.*

Thus, employing *Phase* software,[50-52] three different pharmacophore models were generated, as shown in ***Figure 15***. Specifically, following the definitions of the specific features as implemented in the software panel, "**A**" indicates an acceptor group, "**H**" is a hydrophobic feature, and "**R**" is an aromatic ring. "**X**" is a customizable group that, in this specific case, includes chemical groups featuring planar geometries.
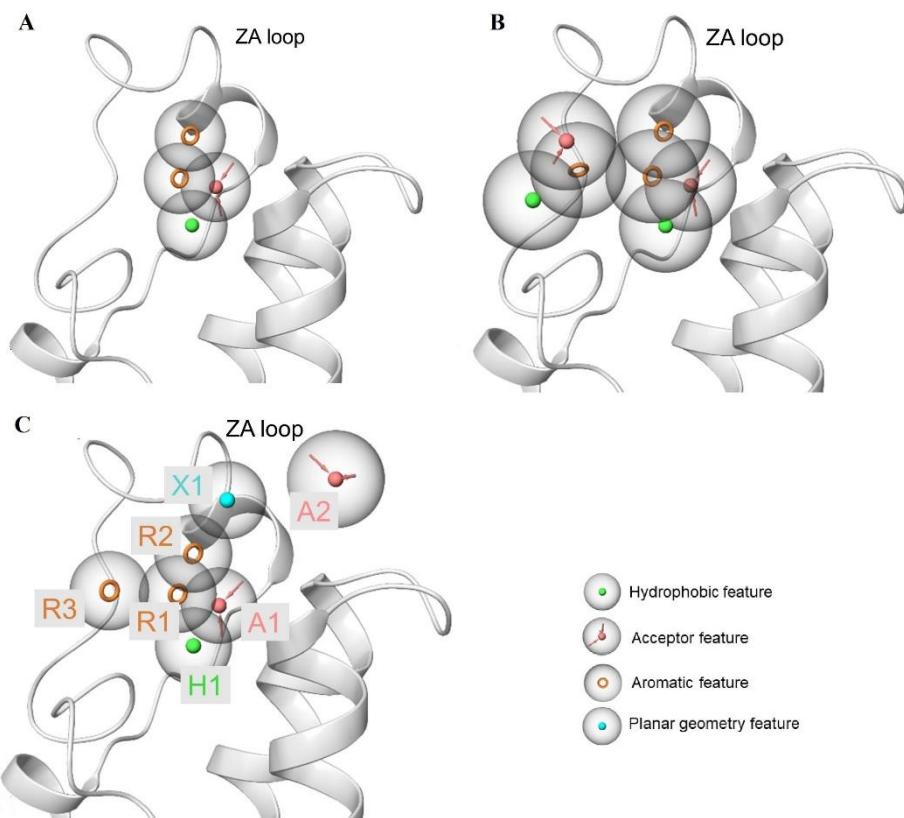
Figure 15. *A)* *AHRR* *4-point "pharm-fragment" model; B)* *AAHHRRR 7-point "pharm-druglike1" model; C)* *AAHRRRX 7-point "pharm-druglike2".*

More in detail, we developed the described pharmacophore models:

- **AHRR** 4-point model (named "pharm-fragment", ***Figure 15A***), using the 6 ligands belonging to the fragment-like group. This model contains the minimal number of chemical and structural features necessary for the binding to BRD9 (*e.g.* the H-bond acceptor group – named "**A**" – is the essential requirement for

the binding to Asn100 in the anchor region, as well as the hydrophobic function – named "**H**" – mimicking the acetyl-lysine group);

- **AAHHRRR** 7-point model (named "pharm-druglike1", ***Figure 15B***), using the 17 ligands belonging to the drug-like group. This model includes the pharmacophore points reported in the previously described "pharm-fragment" and the addition of three more features located in the ZA channel: specifically two aromatic functions – named "**R**" – of which one is substituted in a precise position with an H-bond acceptor feature. This pharmacophore model closely reproduced the most common binding mode among the known BRD9 binders reported in the literature;

- **AAHRRRX** 7-point model (named "pharm-druglike2", ***Figure 15C***), using 4 ligands contained in the co-crystal structures 4UIT, 4UIU, 4UIV, 4UIW. Remarkably, such compounds correspond to the most selective BRD9 binders identified so far (*e.g.*, I-BRD9), presenting a binding mode slightly different from the common ones.[40] Indeed, a new acceptor function "**A**" and a new planar function – named "**X**" – were detected. The latter function is able to recognize planar groups of molecules that point the substituents in such a way to ensure the interaction with some amino acids in the ZA channel important for the achievement of selectivity (*i.e.*, Arg101 and Ile53).

In order to generate such models, all the experimental binding modes of the ligands must be into the same protein coordinate system (crystal structure 5F1H[42] was chosen as the reference protein system for BRD9 for its high resolution). Thus, through docking calculations, the 23 ligands binding modes were reproduced, as the original co-crystal structure, in BRD9 5F1H binding site.

Afterwards, the sampled poses were used as input for generating the 3D pharmacophore models through the *Develop Pharmacophore Hypothesis* panel in *Phase* software.[50] In order to preserve the coordinates and the exact crystallographic conformer of each ligand, the function "use prealigned ligands" was used. Finally, the hypotheses matching at least 60% of the input ligands were used, adjusting the tolerance to 2.0 Å. Thus, the three structure-based 3D pharmacophore models shown in *Figure 15* were generated.

2.2.1 General in silico workflow applied for pharmacophore screenings and molecular docking calculations

The building of three-dimensional pharmacophore models provided an effective computational implement for rapid and accurate identification of new potential chemotypes presenting the pharmacophoric features, as well as improving the *in silico* selection of docked compounds whose structural and conformational properties overlap to the molecular frame of the known inhibitors.

Following this rationale, we took advantage of the pharmacophore models as filters for screening large libraries of small molecules. In particular, the initial collections were first prepared using *Ligprep* software[53] in order to generate, for each compound, all the possible stereoisomers, tautomers and protonation states at a pH = 7.4 ± 1.0.

After structure minimization using OPLS 2005 force field, the libraries were filtered employing the previously described pharmacophore models by means of the *Ligand and database screening* tool in *Phase*.[50] The "generate multiple conformers" option was set in order to perform a conformational search aimed to select the compounds that match at least 6/7 pharmacophoric features *a priori*. Thus, the top-ranked molecules were choose based on the *Phasescreen* score,[50] for the subsequent

molecular docking experiments. Specifically, docking calculations were performed using the *Virtual Screening Workflow* (VSW) tool available in *Glide* software[54-56] and employing the X-ray crystal structure of BRD9 (PDB ID: 5F1H, featuring 1.82 Å resolution). During VSW, molecules have been submitted to three accuracy levels endowed with increasing predictive precision:

- High-Throughput Virtual Screening scoring and sampling (HTVS), saved the best-ranked compounds by docking score and used as input for the next phase;

- Standard Precision scoring and sampling phase (SP), saved the best-ranked compounds by docking score and used them as input for the next phase;

- Extra Precision scoring and sampling phase (XP), generating 20 poses for each ligand and saving the best compounds ranked by docking score as final output.

Subsequently, the docking outputs were again subjected to another filter round, employing the chosen pharmacophore model. It is important to note, that in this step, the specific conformers of each molecule arising from the molecular docking experiments (thus accommodated in the chosen protein structure) were used, skipping any further conformational search.

After this latter step, only the compounds respecting the pharmacophore criteria were selected, considering also:

- The docking score value (*i.e.*, compounds with docking score below < -5.0 kcal/mol);

- PhaseScreen score value, suggestive of the structural congruence of each compound with respect to the pharmacophore features (*i.e.*, compounds with PhaseScreen score > 1.25);

- Ligand interactions with the protein counterpart (*i.e.*, H-bond with Asn100 and π-π interactions with Tyr106 were considered essential);

- No lead-likeness violations [57] (with the aim to identify a lead compound to be optimized).
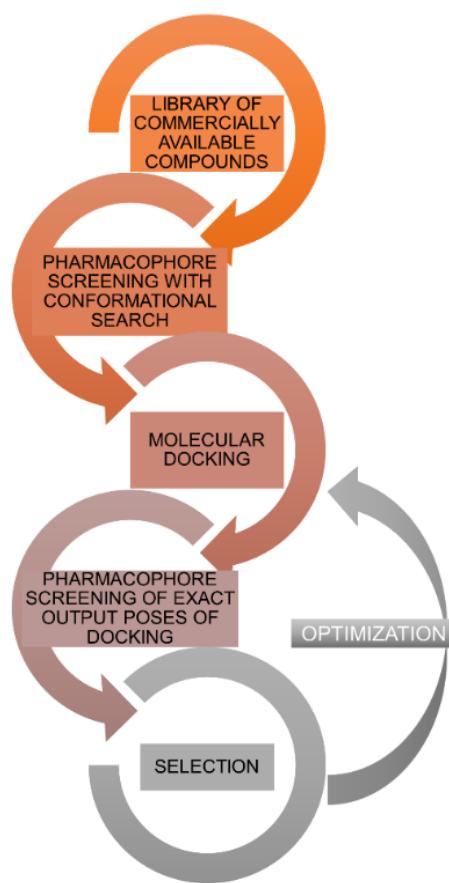
Figure 16. *General in silico workflow applied for the identification of new putative binders for the target protein BRD9 employing our 3D pharmacophore models.*

2.2.2 Identification of new chemical entities employing the 3D pharmacophore models

Employing the described computational workflow (summarized in **Figure *16***), massive screenings were applied on online databases of molecules, leading to the selection of different novel molecular motifs. During the course of this Ph.D. program, 3 molecules (**Figure *17***) featuring novel chemotypes for BRD9, emerged for their correspondence to the pharmacophore models and were thoroughly evaluated. Briefly, compound **1,** featuring the 1-ethyl-[1,2,4]triazolo[4,3-*a*]quinoxaline core, was highlighted as a promising scaffold whose accurate decoration led to the design of new compounds with high binding affinity on BRD9 and strong selectivity against other bromodomains. Compound **2,** which presents the 1-ethyl-1*H*-pyrazolo[3,4-*b*]pyridine core, emerged as a new and unprecedented investigated KAc mimetic, that is currently under active investigation. Lastly, compound **3** emerged as a new small chemical hit, featuring the aryl sulfonamide core, an easily optimizable structure due to its synthetical accessibility.
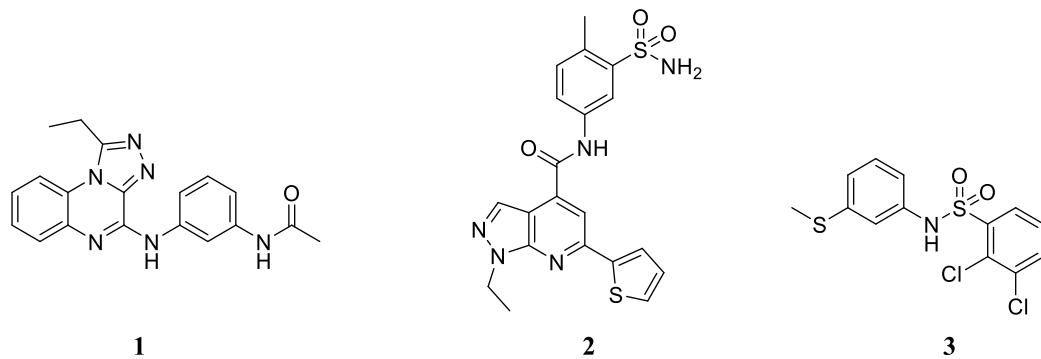
Figure 17. *Chemical structures of the compounds selected after pharmacophore screenings of large online libraries of commercially available compounds.*

After retrosynthetic analyses and detailed computational studies, new pharmacophore-driven libraries of structural derivatives were designed starting from the identified hit compounds (**1-3**). Thus, new sets of drug-like compounds were

synthesized and finally investigated by applying specific biophysical and biological assays.

2.3 Investigation of triazoloquinoxaline-based compounds as BRD9 binders

According to our 3D pharmacophore models, as introduced in the previous paragraph, we investigated the 1-ethyl-[1,2,4]triazolo[4,3-*a*]quinoxaline scaffold to identify new potential anticancer agents that could interfere with the acetyl-lysine reading activity carried out by BRD9 protein. In the following section, are reported in detail the steps of the applied project workflow, describing the *in silico* structure-based approach that led to the design and synthesis of novel drug-like ligands endowed with high affinity and selectivity on the chosen biological target. Moreover, their antiproliferative activity was assessed on a panel of cancer cell lines.[49] Finally, a robust SAR study was developed in order to better clarify the key structural features of a selective BRD9 binder, which aid the optimization of our 3D pharmacophore model, and the development of a second generation of triazoloquinoxaline derivatives.

2.3.1 Identification of the 1-ethyl-[1,2,4]triazolo[4,3-a]quinoxaline scaffold

The application of the *in silico* workflow described in **paragraph 2.2.1**, led to the successful identification of compound **1** (**Figure *18A***), which satisfied all the seven pharmacophoric points of the "pharm-druglike2" model, as shown in **Figure *18B***.

In more detail, compound **1** emerged from *in silico* screenings applied on the online ChemDiv database (www.chemdiv.com) containing a total of 126,416 items. Specifically, considering the involvement of BRD9 in tumor and inflammatory processes,[58, 59] we employed the "Anticancer" and "Anti-Inflammatory" ChemDiv library. After ligands preparation through *Ligprep* software[53] (see **paragraph 2.2.1**), the entire library was filtered employing the pharmacophore "pharm-druglike2"

(AAHRRRX, see *Figure 15C*), which is the model built on the most selective chemical probes identified up to now for BRD9 (*e.g.*, I-BRD9).[40] From the output items, the 1500 top-ranked molecules were selected based on the Phasescreen score for the subsequent molecular docking experiments. The output poses obtained by molecular docking, were re-submitted to a second filter round employing the "pharm-druglike2" model. From this latter step, 1989 compounds showed a good matching with the pharmacophore and only a few were selected considering the interaction patterns, the docking score values, and PhaseScreen scores (as described in **paragraph 2.2.1**). Among these, only compound **1** satisfied all the seven pharmacophoric points, thus indicating the high-performance filtering of our disclosed pharmacophore model.
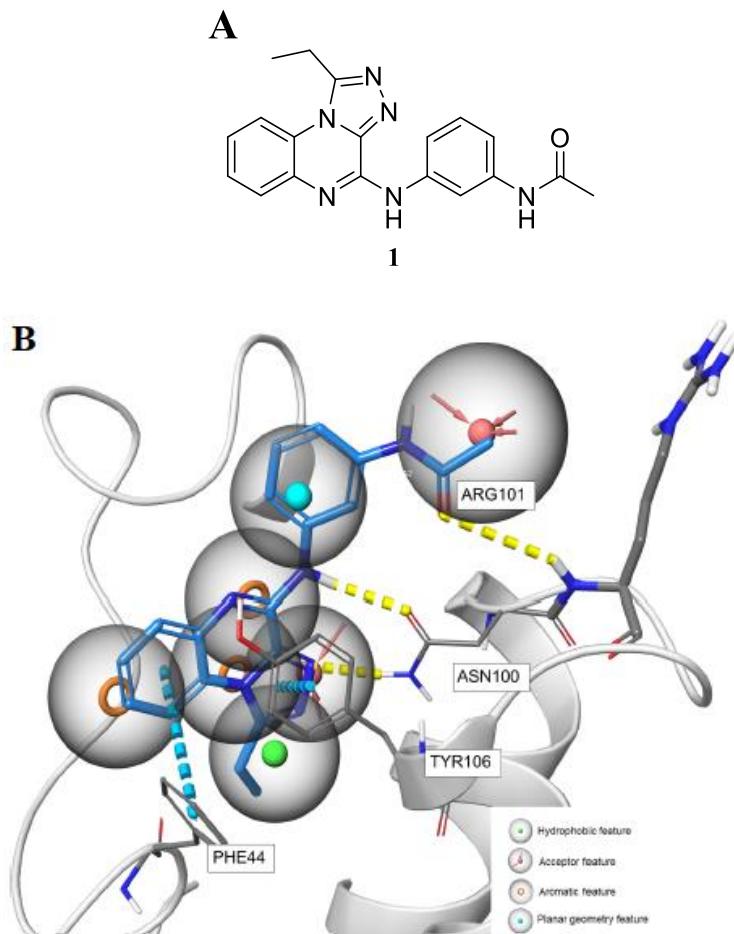
Figure 18. *A) 2D chemical structure of compound **1**. B) Compound **1** in the reference BRD9 protein structure (PDB: 5F1H) superimposed to the 7-point pharmacophore model AAHRRRX. The key amino acids and interactions are reported: H-bonds with Asn100 and Arg101 are represented in yellow dotted lines, π-π interactions with Phe44 and Tyr106 are represented in cyan dotted lines.*

The predicted binding pose of compound **1** (**Figure *18B***), which resulted from molecular docking outcomes, showed that the 1-ethyl-[1,2,4]triazolo[4,3-*a*]quinoxaline moiety fits satisfactorily in the BRD9 anchor region. Good interactions with the two key amino acid residues Asn100 and Tyr106 crucial for binding are made, while the ethyl group at the C-1 position is greatly accommodated in the hydrophobic cavity fundamental for the KAc recognition. Remarkably, this protein region could be appropriately exploited for a selective binding on BRD9 against other bromodomains,

especially those members of the BET family.[49] Interestingly, the triazoloquinoxaline chemical core presented in compound **1**, was already reported in BRD4 binders, even if they present a methyl group on the C-1.[60] On the contrary, as it will be described in the following paragraph, compound **1** and its derivatives featuring an ethyl functionality in this position, did not show binding on BRD4 nor other members of the BET family as assessed in biophysical binding assays. These findings are in accordance with structural evidence reported in literature highlighting that methyl groups are typically suitable for the binding against BRD4, a representative member of the BET family, mainly due to its smaller hydrophobic cavity as compared to that of BRD9.[40] Thus, we thought that the introduction of substituents longer than methyl groups on C-1 position, such as the ethyl, could be crucial for gaining selectivity on BRD9 across the bromodomain families.

Moreover, the accurate analysis of the predicted binding pose of **1**, revealed that the *N*-(3-aminophenyl)acetamide moiety is located in the ZA channel, the least conserved binding area among BRDs that could be largely exploitable to increase binding affinity and selectivity against BET family members.[42] After these considerations, compound **1** emerged as a promising and optimizable compound for targeting BRD9.

To corroborate the *in silico* studies, AlphaScreen biophysical assays[61, 62] were then performed (by Reaction Biology Corporation) to verify the binding of compound **1**. Notably, a very interesting result was obtained since **1** showed binding to BRD9 in the low micromolar scale (IC$_{50}$ = 4.20 ± 1.92 μM) and also great selectivity against a panel of nine additional human bromodomains, as reported in more detail later.

The collected initial outcomes supported the good agreement between experimental data and computational predictions, thus presenting the triazoloquinoxaline scaffold

as a valuable and unprecedented chemical motif for disclosing new potent and selective BRD9 ligands.

2.3.2 Design of a first-generation library of triazoloquinoxaline-based compounds

Starting from the experimental data obtained for compound **1**, the 1-ethyl-[1,2,4]triazolo[4,3-*a*]quinoxaline moiety (**Figure** *19*) had been used for the *in silico* generation of an in-house built combinatorial library of compounds.[49] In particular, the pharmacophore model suggested that effective modifications could be made at the C-4 position. Moreover, a thorough retrosynthetic analysis revealed the synthetical accessibility of this site that could be effectively exploited for the heterocyclic scaffold decoration. Thus, with the aim to explore the substitution pattern at the C-4, a virtual library of [1,2,4]triazolo[4,3-*a*]quinoxaline-based compounds was built using *Combiglide* software[63] and employing primary aromatic amines (downloaded from Sigma-Aldrich on-line database). Following this rationale, a new library of 4349 triazoloquinoxaline-derivatives was generated.

1-ethyl-[1,2,4]triazolo[4,3-*a*]quinoxaline scaffold
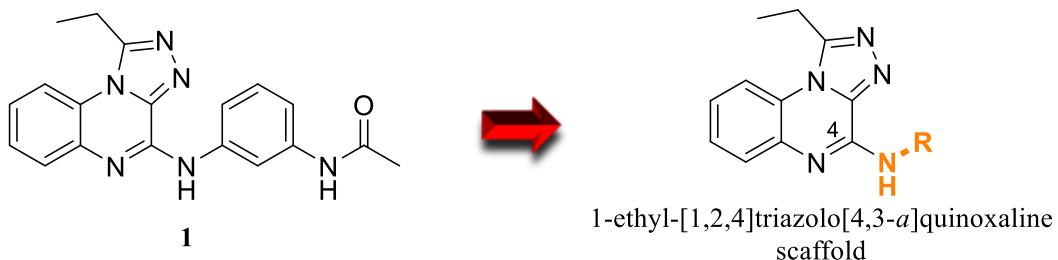
Figure 19. *Chemical structures of the hit compound **1** and the 1-ethyl-[1,2,4]triazolo[4,3-a]quinoxaline moiety employed for the in silico combinatorial library generation.*

In order to consider those molecules with favourable bioavailability, we submitted the initial combinatorial library to pharmacokinetic parameters calculation through *QikProp* software[64, 65] in the Schrödinger Suite. Successively, we applied a

computational filter based on Lipinski's rule of five[66] in order to select those ligands with favourable drug-like properties *i.e.*, optimal molecular weight, adequate number of H-bond donors/acceptors. Successively, the items were subjected to the pharmacophoric filter using the "pharm-druglike2" model and docking calculations. Finally, the accurate analysis of the results, allowed the selection of seven compounds (**4-10**, *Figure 20*), for the following chemical synthesis and biological evaluation steps.
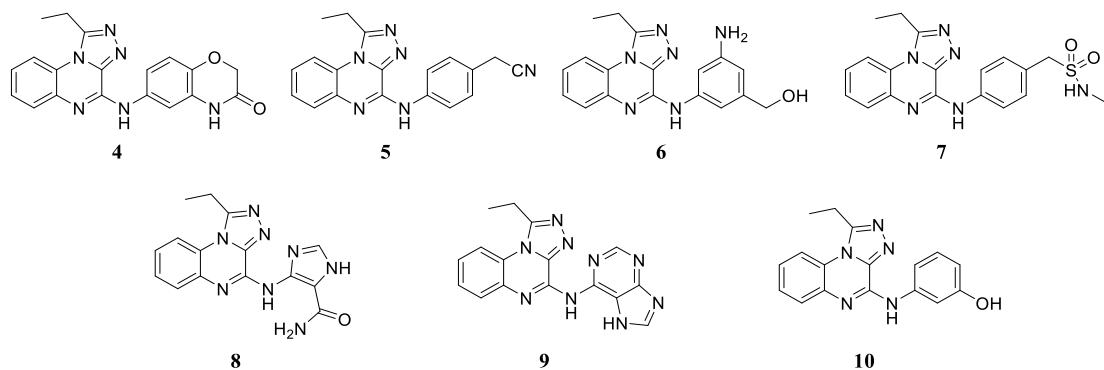
Figure 20. *Chemical structures of the first-generation of triazoloquinoxaline-based compounds (4-10).*

More specifically, among the compounds, four items (**4-7**) were selected considering the best matching to the pharmacophore model and docking scores, thus representing promising BRD9 binders, as shown in **Figure *21***. On the other hand, compound **8**, although able to match the "pharm-druglike2" model, features a low docking score (-2.0 kcal/mol), thus represents a lesser promising compound. Moreover, to further corroborate the reliability and robustness of the chosen pharmacophore model, compounds **9** and **10** were selected as negative controls since they did not match all the criteria of selection (*e.g.*, **9** matched 5/7 pharmacophoric points).

The syntheses of compounds **4-10** were performed *via* an effective synthetic strategy that allowed rapid access to the desired compounds in good to high yields.[49]
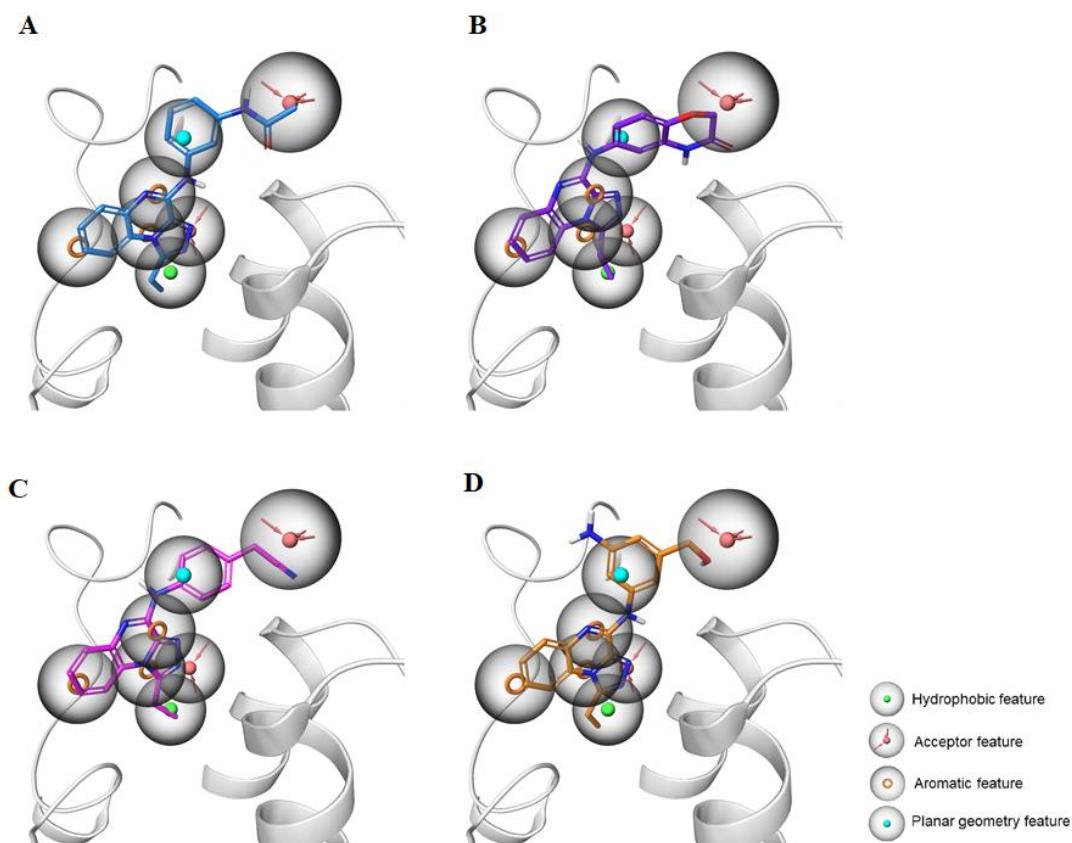
Figure 21. *3D superposition of compound **1** (A) and the most promising selected compounds **4** (B), **5** (C), **6** (D), with the pharm-druglike2 model.*

2.3.3 Chemical synthesis of compounds 4-10

According to the procedure reported by Lee *et al.*, [67] the identified molecules **4-7** and **10** (***Figure 20***) were synthesized using an efficient three-step synthetic procedure, as described in ***Scheme 1***.

More specifically, in the first step, the addition of hydrazine monohydrate to the commercially available 2,3-dichloroquinoxaline at room temperature overnight gave hydrazinyl-quinoxaline **1b** in a quantitative yield. The following cyclization of **1b** with

triethyl orthopropionate overnight, afforded 4-chloro-1-ethyl triazoloquinoxaline **1c** in high yields. Finally, the reaction of **1c** and the selected aryl/heteroaryl amines gave the desired products **4-10**.
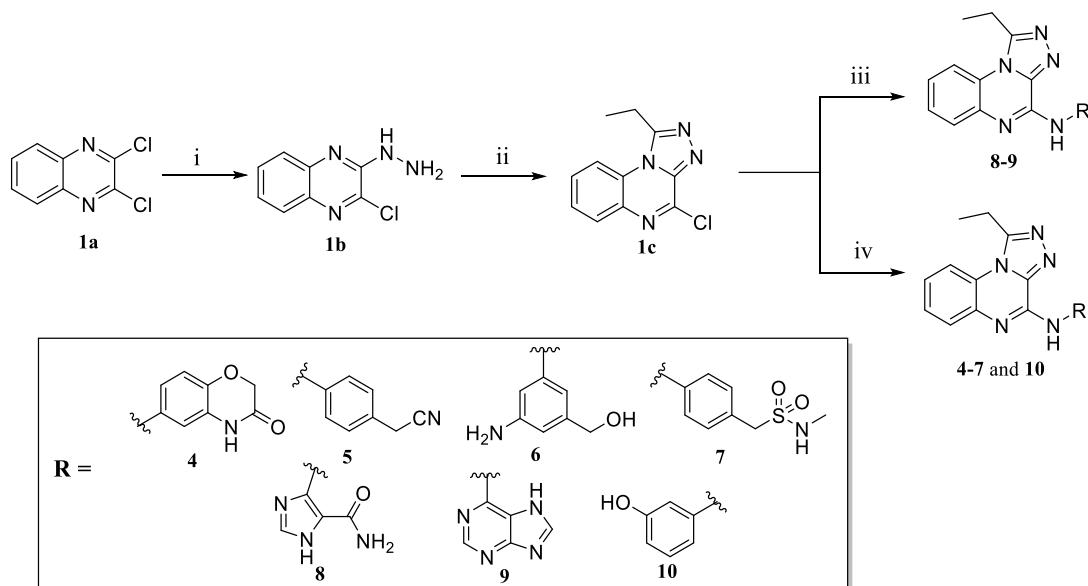
Scheme 1. *Chemical synthesis of compounds **4-10**. Reagents and conditions: i) NH₂NH₂, EtOH, 25 °C, 20h; ii) CH₃CH₂C(OC₂H₅)₃, rt, 16h; iii) RNH₂, K₂CO₃, 80 °C, 1.5-2.5 h, DMSO; iv) RNH₂, 80 or 110 °C MW, 6-8 min, DMSO.*

It is to note that the nucleophilic aromatic substitution in the last step, was initially performed on chlorinated triazoloquinoxaline under conventional heating in the presence of a base (*i.e.*, K₂CO₃). However, the long reaction times and low yields pushed for an optimization of the reaction conditions. Thus, the use of microwave irradiation was explored in the last step of the synthetic route.

To the best of our knowledge, up to now the nucleophilic reaction on 4-chloro-triazoloquinoxaline was carried out only under conventional heating and in presence of bases.[60, 67] Noteworthy, in the microwave-assisted synthetic process, the absorption and transmission of energy differ from conventional heating. The latter is a more superficial heating process and the energy is transferred from the surface to the entire environment by convection and conduction. Therefore, it creates an effect of

inhomogeneous heating with the surface at a higher temperature than the bulk. On the other hand, microwave irradiation produces efficient internal heating by directly coupling microwave energy with the bulk reaction mixture.[68] This efficient mode of heating could result in improved yields and reduce by-products formation and reaction times.

In our synthetic route, reported in *Scheme 1*, microwave irradiations at 80 or 110 °C for 6-8 min using DMSO as solvent and the appropriate aromatic amines, were found as the best experimental conditions for the syntheses of compounds **4-7** and **10**. This approach allowed to synthesize the desired derivatives in high yields and purity and, most of all, to reduce dramatically reaction times (from several hours to maximum of 8 minutes). However, compounds **7** and **9** were synthesized in high yields under conventional heating, using K_2CO_3 and the corresponding heteroaryl amine in DMSO for 1.5–2.5 h to obtain the final compounds.

All synthesized compounds **4-10** were structurally elucidated by spectral data analysis of proton (^1H) and carbon (^{13}C) NMR and by high-resolution mass spectrometry experiments. The purity of all final compounds was $\geq 95\%$ as determined by HPLC analysis and NMR spectra. The detailed experimental section is reported in **CHAPTER 5** (**paragraph 5.2**).

2.3.4 Biophysical binding assays of compounds 4-10 through AlphaScreen technology

All the synthesized compounds were then screened with AlphaScreen assay (by Reaction Biology Corporation) in order to evaluate their potential binding toward the target protein.

This biophysical assay is routinely utilized in bromodomains high throughput screenings, hence we employed this technology to detect the residual BRD9 binding to histone H4. Specifically, the interaction between BRD9 and the histone H4 indicates that the tested compound is not disrupting the protein-protein recognition, therefore it is not able to bind the protein target BRD9. Thus, in the event of no activity of the tested compound, the binding of BRD9 to the H4 enables an energy transfer from the excited donor beads to the acceptor beads and the maximum emission signal is detected. Conversely, if the tested compound is able to displace histone H4, the amplitude of the signal decreases. Noteworthy, AlphaScreen is a quantitative binding assay, since the decrease of the signal's amplitude is related to the affinity of the ligand in binding the protein of interest.[62]

Table 1. *Binding data (AlphaScreen assays) of compounds **4-10** and **1c** on the panel of 10 bromodomain-containing proteins.*

	% RESIDUAL BINDING OF HISTONE/Ac RELATIVE TO DMSO CONTROL										BRD9 IC$_{50}$ (μM)
	BRD9	BRD2-1	BRD2-2	BRD3-1	BRD3-2	BRD4-1	BRD4-2	BRDT-1	BAZ2B	CREBBP	
1	18.9	≥100.0	76.1	56.4	90.6	77.3	64.7	97.0	≥100.0	95.9	4.20±1.92
1c	90.6	n.t.	n.t.	n.t.	n.t.	n.t.	n.t.	n.t.	n.t.	n.t.	n.t.
4	28.7	77.0	83.7	57.1	88.5	65.6	55.0	44.0	92.4	83.2	10.06±2.60
5	2.3	≥100.0	≥100.0	92.9	94.1	97.3	≥100.0	92.8	99.8	≥100.0	4.79±0.49
6	7.0	87.3	86.2	79.8	91.2	81.5	76.3	54.5	96.8	88.5	7.48±2.20
7	57.5	n.t.	n.t.	n.t.	n.t.	n.t.	n.t.	n.t.	n.t.	n.t.	n.t.
8	≥100.0	n.t.	n.t.	n.t.	n.t.	n.t.	n.t.	n.t.	n.t.	n.t.	n.t.
9	97.5	n.t.	n.t.	n.t.	n.t.	n.t.	n.t.	n.t.	n.t.	n.t.	n.t.
10	80.3	n.t.	n.t.	n.t.	n.t.	n.t.	n.t.	n.t.	n.t.	n.t.	n.t.

n.t.: Not tested.

Regarding our study, all the compounds have been evaluated against BRD9 at 10 μM employing Bromosporine as control. The obtained binding data, reported in **Table 1**, were in line with the computational outcomes. In fact, a remarkable binding on BRD9 was detected for the previously described hit compound **1**, and also compounds **4-6** that were respecting all the seven pharmacophore features, while a moderate

binding was found for compound **7**.[49] IC$_{50}$ measurement of the most promising ligands **1** and **4-6** were calculated, presenting binding values in the low micromolar range (**Table** *1* and **Figure** *22*). As we expected, compounds **8-10**, which were selected and synthesized as negative controls (featuring a quite low docking score and/or did not respect all the criteria of the pharmacophore selection), were not able to bind the target protein. Finally, compound **1c** which presents the triazoloquinoxaline scaffold lacking the substituent in C-4 did not bind BRD9, highlighting the importance of the correct substitution in this position.

Once validated the binding to BRD9, in order to assess the selectivity over other bromodomain subfamilies, the most promising ligands (**1** and **4-6**) were tested on a panel of nine additional BRDs in order to cover most of the related human phylogenetic tree. Also in this case, all the compounds have been tested at 10 μM employing specific controls for each bromodomain. Noteworthy, all the tested molecules showed a comparable profile exhibiting strong selectivity against BRD9 over other human BRDs, thus emerging as new strong and selective BRD9 ligands (**Table** *1*).
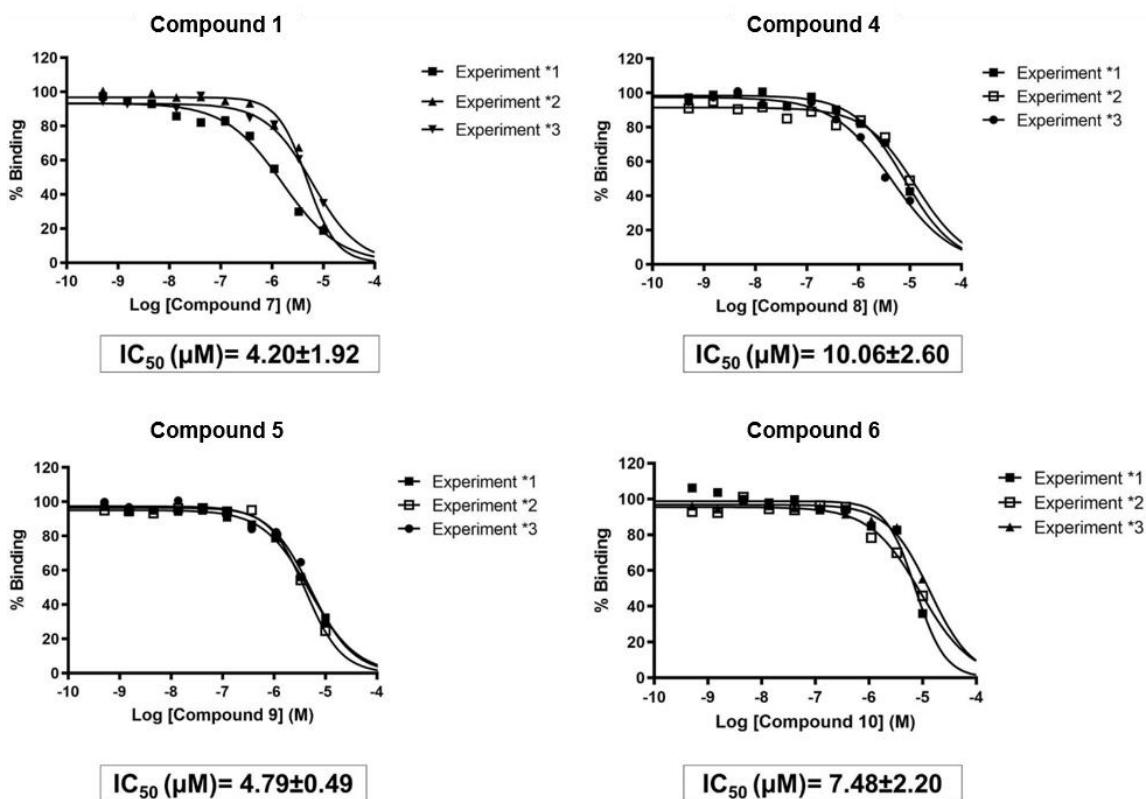
Figure 22. *Dose-response curves for compounds **1** and **4-6** against BRD9. Compounds were tested in 10-dose IC$_{50}$ mode with 3-fold serial dilution starting at 10 μM. Data are expressed as mean ± SD, n = 3.*

Overall, the application of the described approach, which involved a great synthetic effort that assisted the achievement of the desired compounds in relatively short times, led to the identification of potent binders confirming the computational predictions of our in-house 3D pharmacophore model "**AAHRRRX**" and the applicability of our straightforward tools.[49]

2.3.5 Biological evaluation of the potential anticancer activity of the most promising compounds

Following the identification of potent and highly selective binders among our first generation of compounds, preclinical biological assays were carried out in collaboration with Prof. Irace's group (from Università degli Studi di Napoli Federico

II), with the aim to assess their potential anticancer activity. Specifically, the antiproliferative effect of the most promising compounds (**1** and **4-6**) was investigated through the estimation of the "cell survival index" arising from the combination of cell viability evaluation (MTT assay) and automatic cell count, on selected human cancer models representing leukemia, melanoma, breast and colon cancers. These specific systems were chosen both because of the high levels of endogenous BRD9,[69-72] and also to assess the putative effect of the tested compounds on different cancer cell lines. Among these, compound **1** emerged as the most bioactive of the series, proving promising outcomes in leukemia cells (see ***Table 2*** and ***Figure 23***).[49]

Table 2. *Anticancer activity was reported as IC$_{50}$ values (µM) in Jurkat, MDA-MB-231, A375, and HCT-116 human cancer cell lines for compounds **1** and **4-6** after 48 h of incubation in vitro. The calculation of the IC$_{50}$ is based on plots of data and repeated three times. IC$_{50}$ values are expressed as mean ± SEM of three independent experiments.*

	IC$_{50}$ (µM)			
Compounds	**Jurkat**	**MDA-MB-231**	**A375**	**HCT-116**
1	77 ± 7	125 ± 8	133 ± 5	145 ± 3
4	184 ± 5	>250	150 ± 2	250 ± 8
5	150 ± 4	241 ± 1	172 ± 7	>250
6	100 ± 5	246 ± 3	169 ± 6	>250
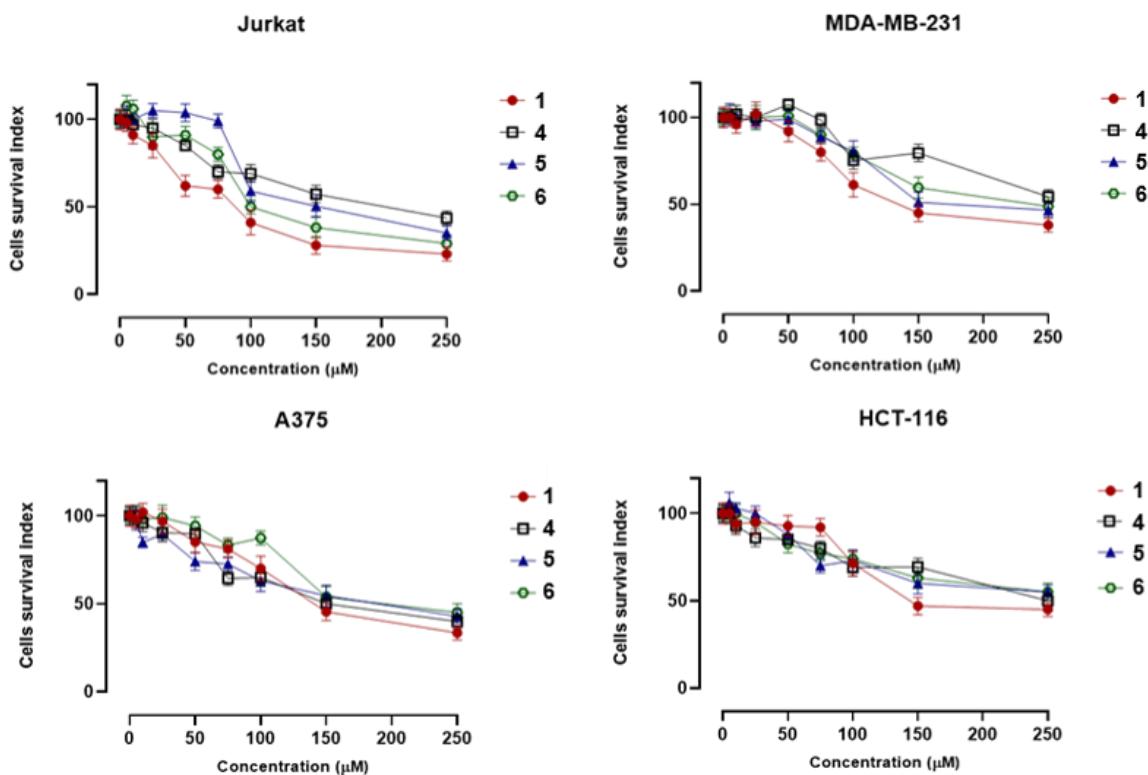
Figure 23. *Cell survival index by concentration-response curves, evaluated by the MTT assay and live/dead cell ratio analysis. Cells were incubated for 48h with a range of concentrations (5 - 250 μM). Results are expressed in lines graph as the percentage of cell survival index to untreated control cultures and are reported as mean ± SEM of three independent experiments.*

The moderate antiproliferative activity detected is in perfect agreement with recent outcomes regarding potent and selective BRD9 binders.[46, 47, 73] Indeed, it is to note that high-affinity BRD9 binders already identified in previous studies and also able to inhibit the binding of BRD9 to the chromatin (*e.g.*; LP99 and I-BRD9), have not shown a significant alteration of cell proliferation, probably due to a compensation effect carried out by other subunits of the SWI/SNF complex.

In conclusion, following a multidisciplinary approach, the triazoloquinoxaline scaffold emerged as a new interesting chemical core and a promising starting point for

a thorough structure-activity relationship (SAR) study, in order to enhance the biological profile.

2.3.6 SAR studies: design and syntheses of a second-generation library of triazoloquinoxaline-based compounds

To accomplish a deep SAR study, we investigated further the newly disclosed triazoloquinoxaline core through the design and synthesis of new derivatives, with the aim to optimize the biological outcomes of the disclosed binders and also to optimize the precision of our pharmacophore model.

Following the initial assumption that the ethyl group at the C-1 position is crucial for a selective binding on BRD9 against other bromodomains, we primarily started our structural investigation maintaining unchanged the central core while investigating the chemical space around the C-4 position (***Figure 24***), which is accommodated in the ZA loop of BRD9 binding site.
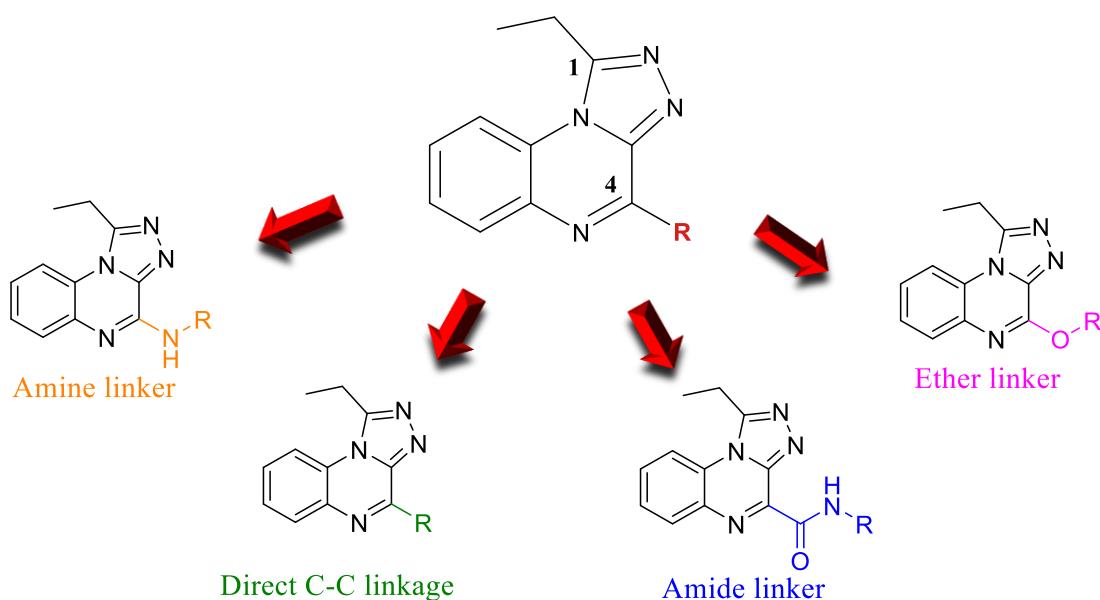
Figure 24. *Structural modifications applied to the C-4 position of the triazoloquinoxaline scaffold.*

A retrosynthetic analysis revealed that this position is accessible with different synthetic routes that would allow a wide exploration of the ZA channel, *i.e.* the least conserved binding area among BRDs largely exploitable to increase binding affinity and selectivity.[42] Hence, guided by *in silico* studies, four new collections were designed, synthesized, and biophysically evaluated to discern the influence on the binding affinity linked to different chemical substitutions at the C-4 (*Figure 24*).

Moreover, structural insights of the anchor region of BRD9, in which the triazoloquinoxaline scaffold is greatly accommodated making crucial interactions with the key residues Asn100 and Tyr106, pushed for the exploration of the deepest surrounding of this hydrophobic cavity that is fundamental for the acetyl-lysine recognition. As we previously demonstrated,[49] this protein region can be appropriately exploited for a selective binding on BRD9 over other bromodomain subfamilies, especially those members of the BET family. Indeed, structural evidences highlighted that small hydrophobic groups, such as methyl, are typically suitable for binding against BRD4, a representative member of the BET family, mainly due to its smaller hydrophobic cavity as compared to that of BRD9.[74] The highly selective 1-ethyl-[1,2,4]triazolo[4,3-*a*]quinoxaline compounds that we identified, confirmed the ethyl group at the C-1 position as crucial for a selective binding on the target protein, since BRD9 is able to tolerate bulky alkyl group on the contrary of other bromodomains. Thus, we decided to explore how the length and the volume of this alkylic substituent affects the binding to the protein target, designing and synthesizing two derivatives presenting a longer hydrophobic chain at the C-1 position of the scaffold (**Figure 25**).

Figure 25. *Structural modifications applied to the C-1 position of the triazoloquinoxaline scaffold.*

Hereafter, it is described the design of new collections belonging to the second generation of triazoloquinoxaline-based compounds according to our pharmacophore model, that were synthesized and biologically evaluated to assess the potential activity against BRD9. The obtained structure-activity relationship profile lead to an optimization and updating of our previously identified "pharm-druglike2" model featuring an improved accuracy.

2.3.6.1 Modification on the C-4 position: collection of derivatives (11-21) featuring the amine functionality

Firstly, in light of the activity data of the bioactive compounds **1** and **4-6**, we extended our initial selection of triazoloquinoxaline derivatives substituted on the C-4 position with the amine functionality by making an *in silico* revaluation of the output compounds obtained from molecular docking and pharmacophore screenings. Thus, we selected a new set of 11 drug-like compounds **11-21** (**Figure** *26*) featuring promising selection parameters and a variety of aromatic and heteroaromatic amines on the C-4.
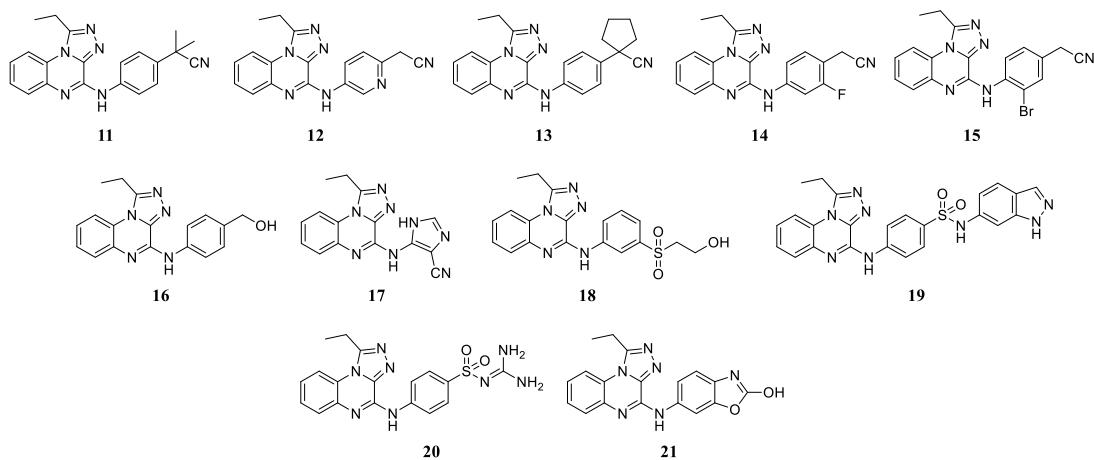
Figure 26. *Compounds **11-21** belong to the collection of triazoloquinoxaline derivatives featuring the amine functionality.*

The new compounds **11-21** match all the features of the "pharm-druglike2" model (as clearly shown in ***Figure 27***), thus representing novel promising BRD9 compounds. Specifically, **11-15** (***Figure 27A, B*** and ***C***) were selected as close derivatives of compound **5** (***Figure 20***), which exhibited a promising activity on BRD9 ($IC_{50} = 4.79 \pm 0.49 \, \mu$M) and the best selectivity profile (as reported in **Table *1***).
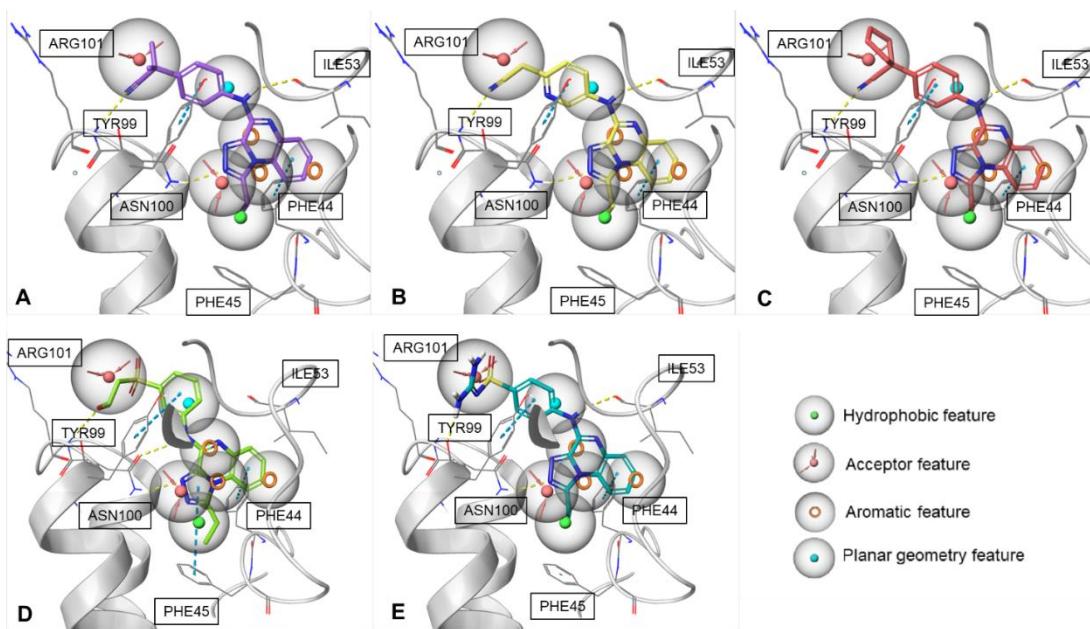
Figure 27. *Binding poses of **11** (A), **12** (B), **13** (C), **18** (D), and **20** (E), in BRD9 binding site superimposed to the "pharm-druglike2" model. H-bonds and π-π interactions are reported in yellow and cyan dotted lines, respectively.*

Compounds **11-21** were then synthesized in high yields following the three steps synthetic routes, already described in **paragraph 2.3.3**, exploiting the nucleophilic reaction of primary aromatic or heteroaromatic amines for the chemical core decoration (*Scheme 2*).[49]
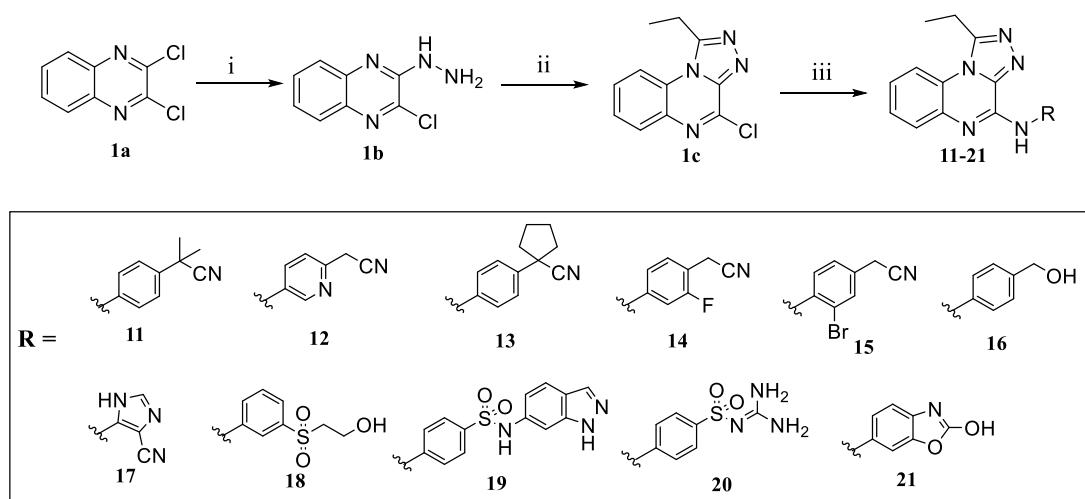
Scheme 2. *Chemical synthesis of compounds **11-21**. Reagents and conditions: i) NH₂NH₂, EtOH, 25 °C, 20h; ii) CH₃CH₂C(OC₂H₅)₃, r.t., 16h; iii) RNH₂, 110 °C MW, 6 min, DMSO.*

For the synthesis of compound **14**, it was required a further synthetic step for the nitro group reduction employing Fe and NH_4Cl (**Scheme 3**).
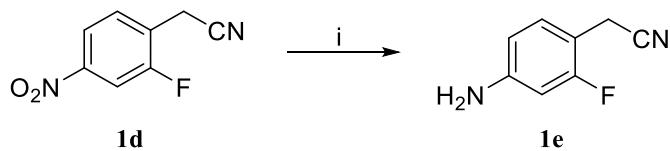
Scheme 3. *Reagents and conditions for the synthesis of the required amine **1e**: i) Fe, NH₄Cl, EtOH/H₂O, reflux, 2.5h.*

The synthesized compounds **11-21** were structurally elucidated by NMR analysis of proton (^{1}H) and carbon (^{13}C) and by high-resolution mass spectrometry. The purity of the final compounds was ≥ 95% as required by biophysical experiments. The detailed experimental section is reported in **CHAPTER 5** (**paragraph 5.2**).

2.3.6.2 Modification on the C-4 position: collection of derivatives (22-37) featuring direct C-C linkage

With the aim of exploring the chemical space of the BRD9 binding site, the removal of the linker between the central core and the substituent at C-4 was also considered in order to evaluate the effect of both reduced distance between the central core and the C-4 substituent and also the loss of the NH functionality. The retrosynthetic analysis of the 1-ethyl-[1,2,4]triazolo[4,3-*a*]quinoxaline moiety revealed that the C-4 position is easily accessible for the heterocyclic scaffold decoration employing the Suzuki-Miyaura cross-coupling reaction,[75] allowing the formation of a carbon-carbon bond between the scaffold and the aromatic moiety.

Thus, through *Combiglide* software,[63] a new *in silico* combinatorial library consisting of 589 compounds was generated employing commercially available boronic acids. The calculation of the pharmacokinetic parameters through *QikProp* software[64] and the application of the computational filter based on Lipinski's rule of five[66] allowed the selection of compounds with favourable drug-like properties. Then, the obtained combinatorial library was filtered employing the 7-point "pharm-druglike2" model "**AAHRRRX**" through *Phase* software[50] (as described in **paragraph 2.2.1**). Finally, the accurate analysis of the results based on the protein-ligand predicted binding affinities, as well as the respect of key interactions within the protein-binding site and a favorable Phasescreen score (see **paragraph 2.2.1**), allowed the final selection of a new collection of 16 derivatives **22-37** (**Figure *28***). It is important to note that compounds **22** and **23** were designed as close derivatives of our identified BRD9 ligands **1** and **5**, respectively, (see **Figure *19*** and ***Figure 20***) lacking the NH functionality.
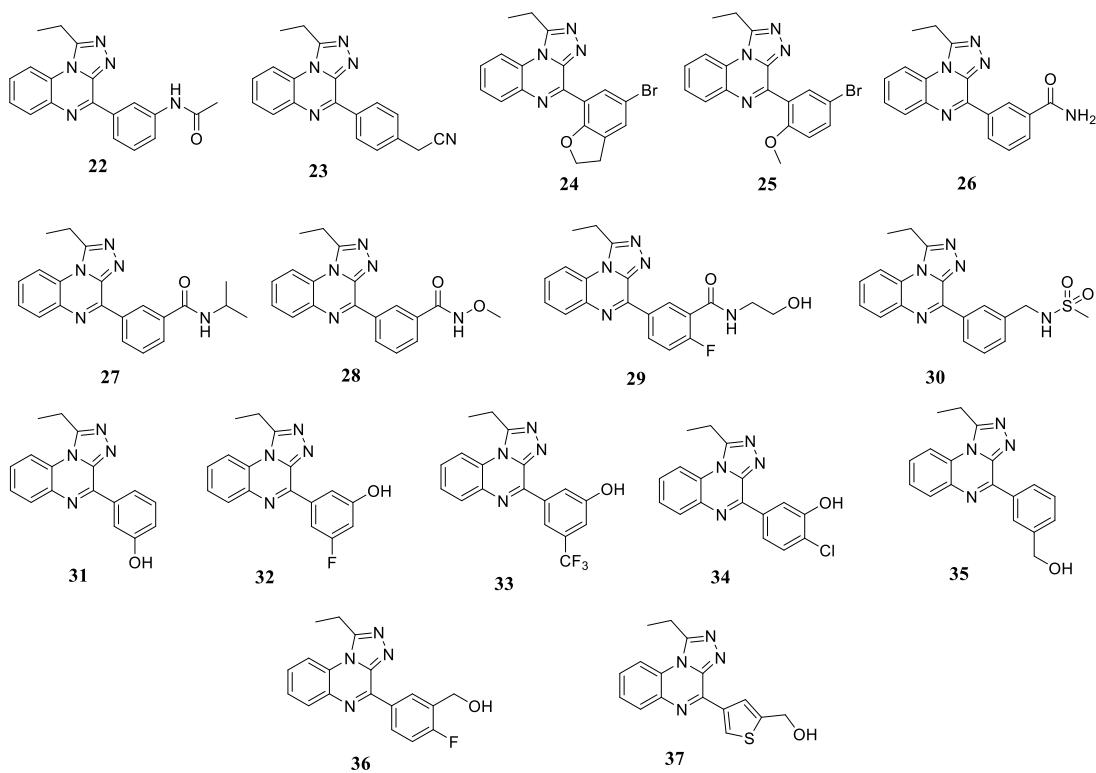
Figure 28. *Compounds 22-37 belong to the collection of triazoloquinoxaline derivatives featuring direct C-C linkage.*

The *in silico* results showed the loss of an important interaction with Ile53 (see **Figure *29A* and *B*) or partial matching to the "pharm-druglike2" model (6/7 points matched for most of the selected compounds, see **Figure *29B***).

65
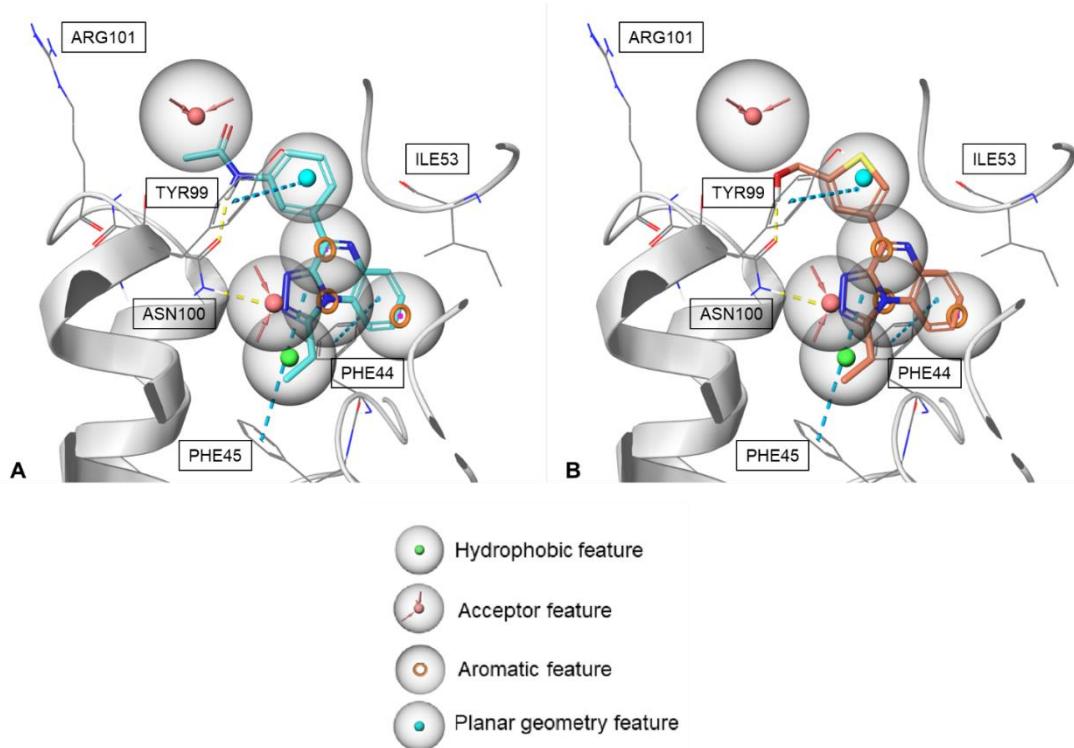
Figure 29. *Binding poses of **22** (A) and **37** (B) in the BRD9 binding site superimposed on the "pharm-druglike2" model. H-bonds and π-π interactions are reported in yellow and cyan dotted lines, respectively.*

The identified molecules **22-37** were synthesized *via* an effective three steps synthetic route that allowed rapid access to the desired compounds in good yields. In particular, the applied synthetic protocol (described in **Scheme *4***) shares the first two steps with the synthetic strategy previously described in *Scheme 2* leading to the common intermediate **1c**. Differently, in this last step, it was employed the Suzuki-Miyaura cross-coupling reaction in order to form a C-C bond between the triazoloquinoxaline scaffold with the selected organoboron species. Noteworthy, we choose the application of these specific reaction conditions considering its efficiency and versatility, and the stability and low toxicity of the organometallic partner in comparison to other reagents. Specifically, as reported in *Scheme 4*, the reaction was carried out in a solution of 1,4-dioxane/H_2O at 80 °C overnight employing the Suzuki

reaction condition using bis(triphenylphosphine)palladium (II) dichloride as the catalyst, tricyclohexylphosphine as ligand, and cesium carbonate as the base.[76] The synthesized compounds **22-37** were structurally elucidated by spectral data analysis of proton (^{1}H) and carbon (^{13}C) NMR and by high-resolution mass spectrometry experiments. The purity of the final compounds was ≥ 95% as determined by HPLC analysis and NMR spectra. The detailed experimental section is reported in **CHAPTER 5** (**paragraph 5.2**).
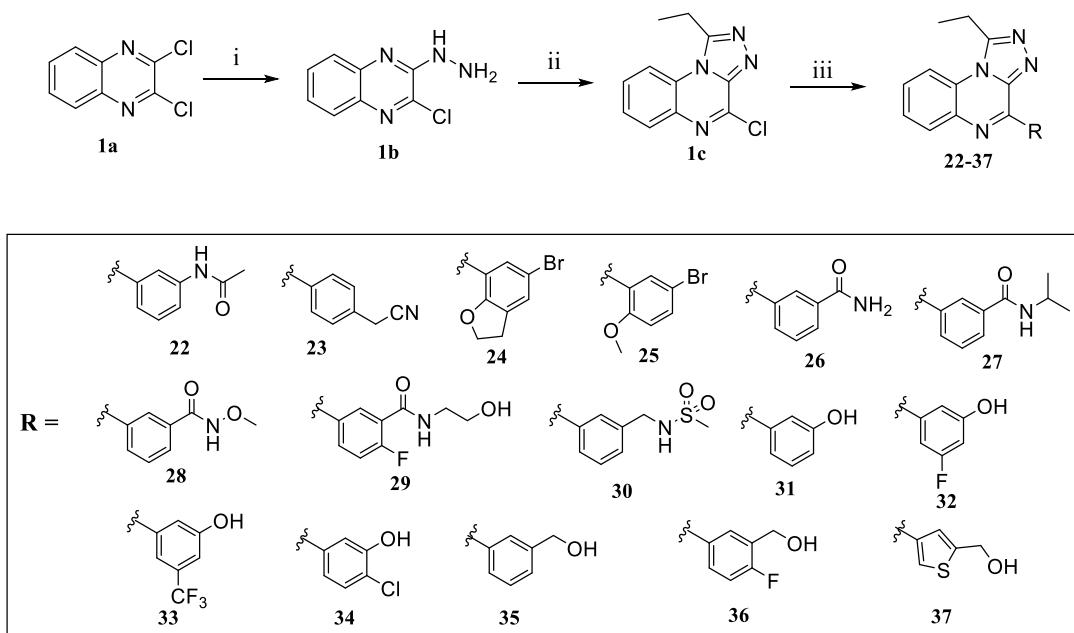
Scheme 4. *Chemical synthesis of compounds **22-37**. Reagents and conditions: i) NH₂NH₂, EtOH, 25 °C, 20h; ii) CH₃CH₂C(OC₂H₅)₃, r.t., 16h; iii) RB(OH)₂, (PPh₃)₂PdCl₂, Cs₂CO₃, PCy₃, 1,4-dioxane/H₂O (8:2), 80 °C, overnight.*

2.3.6.3 Modification on the C-4 position: derivatives featuring the amide (38-39) and ether linker (40)

For the development of a robust SAR study, we decided to explore the influence of the chemical nature of the linker between the triazoloquinoxaline scaffold and the aromatic moiety. Thereby, we designed two close derivatives of the most bioactive

compounds identified in this study (compounds **1** and **5**, see **Figure** *30*) inserting an amide linker at the C-4 position, exploiting the planar geometry with restricted rotations of this functional group. The rationale for the insertion of an amide linker is related to the evaluation of both the effect of a longer spacer and the respect of the planar feature "**X**" reported in the "pharm-druglike2" model. For preferable synthetic accessibility, the two derivatives **38** and **39** (**Figure** *30*) were designed with the carboxyl group directly conjugated with the triazoloquinoxaline scaffold.
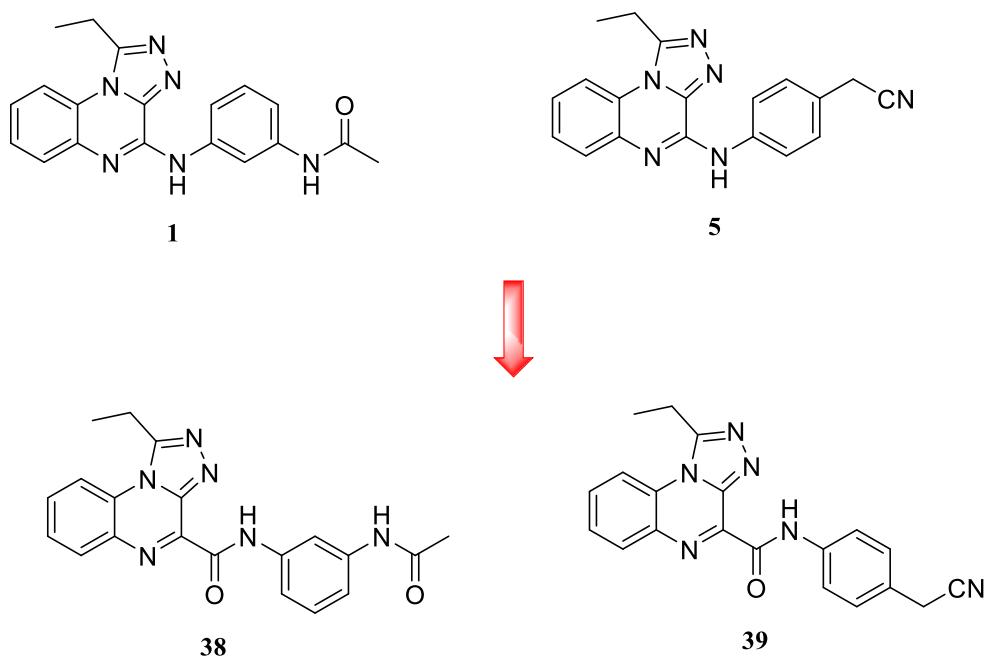
Figure 30. *Compounds 38 and 39 were designed as close derivatives of the most bioactive compounds 1 and 5.*

Through a feasible synthetic procedure,[77] as shown in *Scheme 5*, the commercially available compound **1f** was coupled to the desired primary aromatic amine using peptide coupling conditions (EDC/HOBt) to obtain the intermediate **1g**. The latter was used for the following addition of hydrazine monohydrate at room temperature for 20 h to give the intermediate **1h** in good yields. The final cyclization with triethyl orthopropionate overnight afforded the desired compounds **38** and **39** in moderate

yields, which were purified and used for the following biological assays. The detailed experimental protocol is reported in **CHAPTER 5** (**paragraph 5.2**).
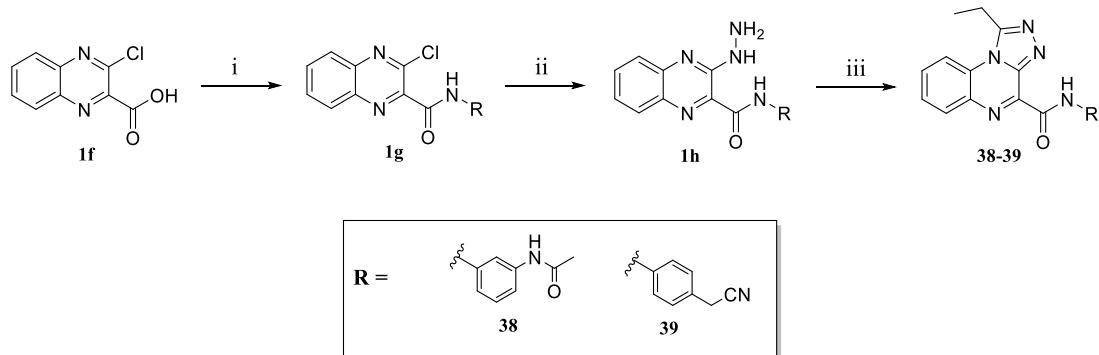
Scheme 5. *Chemical synthesis of compounds **38** and **39**. Reagents and conditions: i) RNH₂, EDC·HCl, HOBt, DMF, rt, overnight; ii) NH₂NH₂, EtOH, 25 °C, 20h; iii) CH₃CH₂C(OC₂H₅)₃, r.t., 16h.*

In parallel, in order to evaluate the influence of the oxygen as chemical functionality between the central core and the aromatic substituent, we designed compound **40** (**Figure *31***), conceived as a close derivative of the bioactive compound **1**.
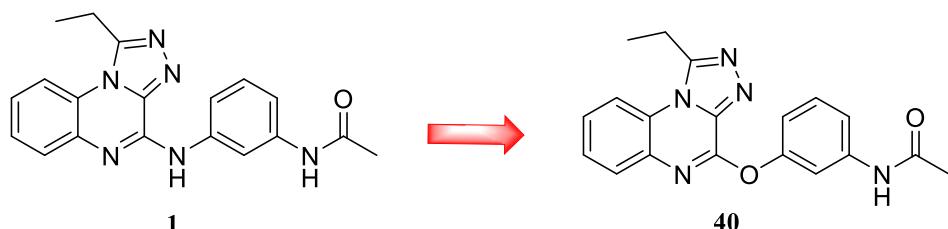
Figure 31. *Compound **40** was designed as a close derivative of the bioactive compound **1**.*

Precisely, compound **40** was synthesized in high yields through nucleophilic aromatic substitution on the intermediate **1c** in DMSO in the presence of cesium carbonate, as reported in *Scheme 6*, which ensured the deprotonation of the phenol

enhancing the nucleophilicity of the oxygen. The detailed experimental protocol is reported in **CHAPTER 5** (**paragraph 5.2**).
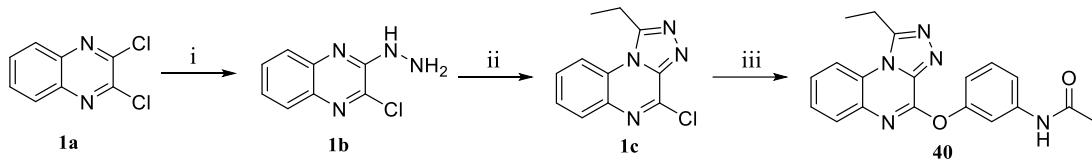
Scheme 6. *Chemical synthesis of compound **40**. Reagents and conditions: i) NH₂NH₂, EtOH, 25 °C, 20h; ii) CH₃CH₂C(OC₂H₅)₃, r.t., 16h; iii) 3-acetamidophenol, Cs₂CO₃, 80 °C, DMSO, 3 h.*

The molecular docking experiments and pharmacophore screening of compounds **38** and **39** showed that they respected all the pharmacophoric points (**Figure *32A*** and **Figure *32B***), while compound **40** matched only 6/7 features (**Figure *32C***), lacking the interaction with Arg101.
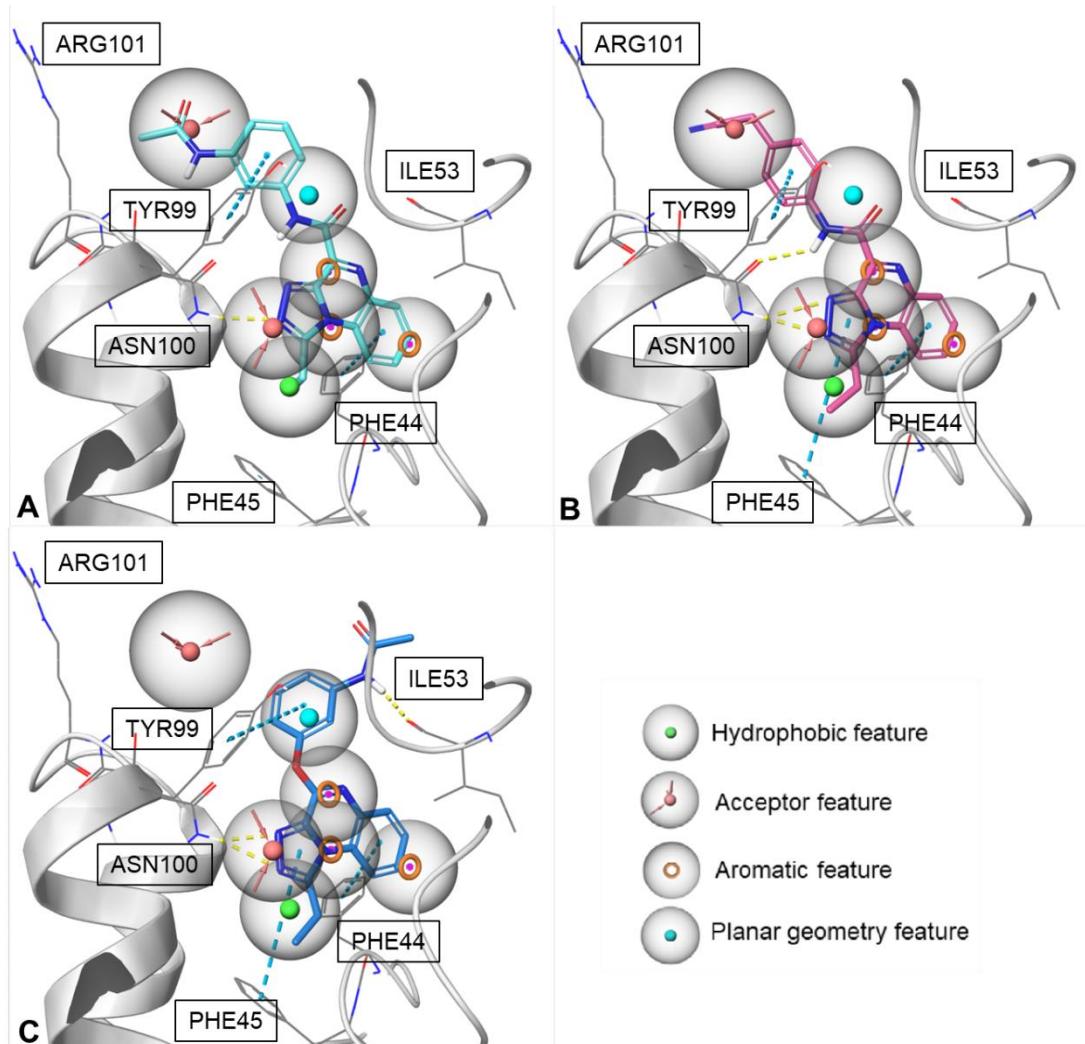
Figure 32. *Binding poses of **38** (A), **39** (B), and **40** (C) in the BRD9 binding site superimposed on the "pharm-druglike2" model. H-bonds and π-π interactions are reported in yellow and cyan dotted lines, respectively.*

2.3.6.4 Biophysical binding assays of compounds 11-40 modified on the C-4 position

The four collections belonging to the second generation of triazoloquinoxaline-based compounds (**11-40**) were then biophysically evaluated to detect the potential binding on the target protein BRD9 and to discern the influence of the length and chemical properties of the linker between the central scaffold and the aromatic substituent.

Thus, all the synthesized compounds were tested, through AlphaScreen technology carried out by Reaction Biology Corporation, against BRD9 at 10 μM employing Bromosporine as control. As reported in **Table 3**, the biophysical binding assay showed a remarkable binding for compounds **11-13**, which were designed as close derivatives of our previously identified bioactive compound **5**. Conversely, in the case of the close derivatives **14** and **15**, the additional presence of a halogen atom, therefore an electron-attractor group (*i.e.*, F and Br, respectively) on the aromatic ring, caused a decrease in activity compared to the reference compound **5**.

Together with compounds **11-13**, also **18** and **20** emerged as new promising binders with an IC_{50} in the low micromolar scale.

Overall, the compounds presenting the amine functionality showed the ability to bind BRD9, thus confirming the goodness of the scaffold and of the NH group, which is able to establish effective hydrogen bonds with the BRD9 binding site. On the other hand, the removal of the linker or its substitution with another functional group (amide or ether) resulted in the lack of the necessary length and adequate spatial arrangement of chemical groups in the binding site of BRD9 (see *Figure 29* and *Figure 32*), leading to a none binding (as reported in *Table 3*). Moreover, the absence of the NH group on the C-4 position of the triazoloquinoxaline scaffold does not encourage the binding to BRD9 confirming that an H-bond donor directly linked to the scaffold is fundamental for the interaction with Ile53 in the ZA region.

Table 3. *Residual binding of Histone H4Ac to BRD9 after treatment with synthesized compounds 11-40 and related IC$_{50}$ values for the most promising compounds. Values are shown as the average of separate experiments.*

Compound	R$_1$	R$_2$	BRD9 IC$_{50}$ ± SD (μM)	% residual binding of histone /Ac ± SD [Compound] = 10μM
DERIVATIVES FEATURING THE NH FUNCTIONALITY				
11	CH$_2$CH$_3$		3.93 ± 0.54	
12	CH$_2$CH$_3$		8.24 ± 1.44	
13	CH$_2$CH$_3$		4.41 ± 1.16	
14	CH$_2$CH$_3$			96.2 ± 2.4
15	CH$_2$CH$_3$			85.7 ± 9.2
16	CH$_2$CH$_3$			48.7 ± 7.2
17	CH$_2$CH$_3$			84.6 ± 4.5
18	CH$_2$CH$_3$		8.31 ± 0.85	
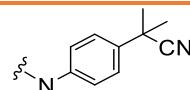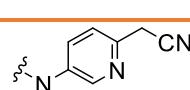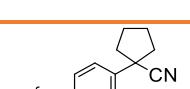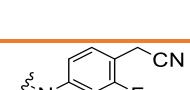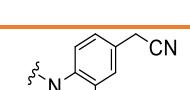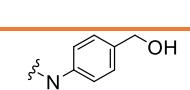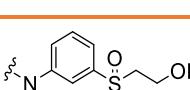
19	CH₂CH₃			60.2 ± 0.1
20	CH₂CH₃		5.26 ± 1.15	
21	CH₂CH₃			69.7 ± 1.8
DERIVATIVES FEATURING DIRECT C-C LINKAGE				
22	CH₂CH₃			98.4 ± 6.0
23	CH₂CH₃			92.2 ± 5.7
24	CH₂CH₃			90.9 ± 1.0
25	CH₂CH₃			88.4 ± 2.2
26	CH₂CH₃			91.7 ± 0.8
27	CH₂CH₃			>100
28	CH₂CH₃			>100
29	CH₂CH₃			93.0 ± 0.7
30	CH₂CH₃			>100

31	CH$_2$CH$_3$			>100
32	CH$_2$CH$_3$			>100
33	CH$_2$CH$_3$			93.7 ± 1.7
34	CH$_2$CH$_3$			>100
35	CH$_2$CH$_3$			95.6 ± 2.4
36	CH$_2$CH$_3$			>100
37	CH$_2$CH$_3$			99.1 ± 0.4
DERIVATIVES FEATURING THE AMIDE LINKER				
38	CH$_2$CH$_3$			>100
39	CH$_2$CH$_3$			94.7 ± 3.8
DERIVATIVE FEATURING THE ETHER LINKER				
40	CH$_2$CH$_3$			85.1 ± 2.9

2.3.6.5 Exploration of the linker at the C-1 position of the triazoloquinoxaline scaffold and biophysical results

The exploration of chemical modifications at the C-4 position led to the identification of compound **11**, which emerged as the most promising binder of the series. With the aim to trace a complete SAR study, the afore-mentioned compound was selected for further investigation on the C-1 position. Indeed, structural evidence assessed that BRD9 is able to accommodate bulkier alkyl groups due to a wider hydrophobic cavity as compared to that of other bromodomains, including BRD7.[74] On these bases, two novel derivatives (compounds **41** and **42**, **Figure** *33*), conceived as derivatives of compound **11,** were designed accounting for a propyl and a butyl groups at the C-1.
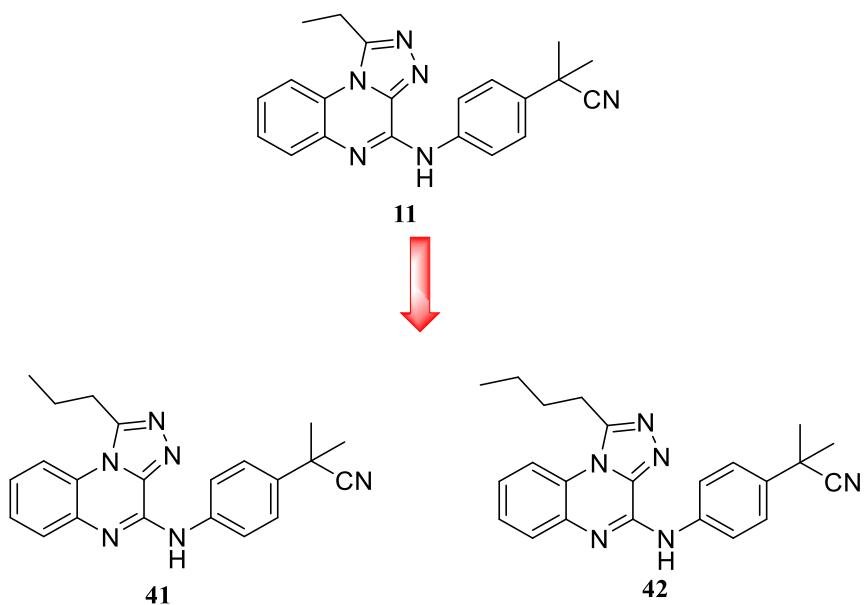
Figure 33. *Compounds 41 and 42 were designed as close derivatives of the potent compound 11 featuring bulkier alkyl groups on the C-1*

Molecular docking calculations and pharmacophore screening assessed that the two compounds **41** and **42** are greatly accommodated in the binding site making effective

interactions with the key residues (**Figure** *34*). In addition, both compounds match all the seven pharmacophoric features of the "pharm-druglike2" model (**Figure** *34*).
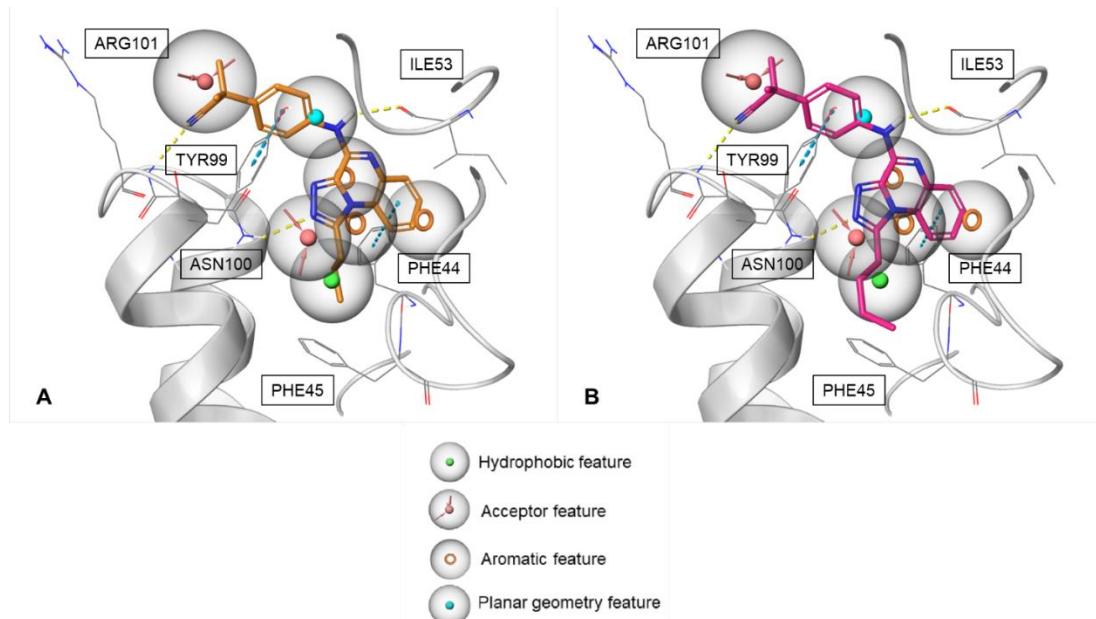
Figure 34. *Binding poses of **41** (A) and **42** (B) in the BRD9 binding site superimposed on the "pharm-druglike2" model. H-bonds and π-π interactions are reported in yellow and cyan dotted lines, respectively.*

Compounds **41** and **42** were synthesized, as described in **Scheme 7**, applying a similar synthetic strategy reported for the library featuring the amine linker (see *Scheme 1*, **paragraph 2.3.3**). Specifically, in the second step, it was employed 1,1,1-triethoxybutane or 1,1,1-triethoxypentane depending on the length of the alkylic substituent in C-1. The detailed experimental protocol is reported in **CHAPTER 5** (**paragraph 5.2**).
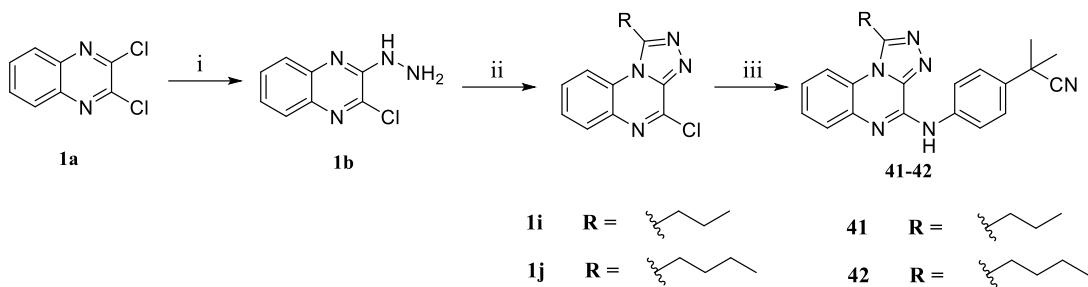
Scheme 7. *Chemical synthesis of compounds* **41** *and* **42**. *Reagents and conditions: i) NH₂NH₂, EtOH, 25 °C, 20h; ii) 1,1,1-triethoxybutane (for* **41***) or 1,1,1-triethoxypentane (for* **42***), r.t., 16h; iii) 2-(4-aminophenyl)-2-methylpropanenitrile, 110 °C MW, 6 min, DMSO.*

Despite the increased volume of the alkylic substituents, the two homologous compounds **41** and **42** preserved a considerable binding to BRD9. Indeed, compound **42** displayed an $IC_{50} = 6.73 \pm 1.55\ \mu M$ comparable with the parental compound **11**, which showed $IC_{50} = 3.93 \pm 0.54\ \mu M$. These findings clearly suggest that more bulky groups are well tolerated in the large hydrophobic anchor region of BRD9 and that this structural element could be effectively employed for the design of new ligands.

2.3.6.6 SAR studies: final considerations on triazoloquinoxaline-based compounds and optimization of the 3D pharmacophore model "pharm-druglike2"

In conclusion, after molecular docking experiments combined with pharmacophore screenings and the biophysical evaluation of 32 new derivatives, the structure-activity relationship profile on the newly disclosed triazoloquinoxaline compounds could be summarized as follows:

- The substitution of the NH linker with amide or ether groups or its removal is not tolerated;

- Halogen atoms on the substituents at C-4 are not tolerated;

- The linker between the central scaffold and the substituent oriented towards the ZA loop should present H-bond donor properties;

- The substituents at the C-4 position require aromatic and heteroaromatic rings with a number of atoms > 6;

- The substituents at the C-4 position need *para*-substitutions with H-bond acceptor groups;

- The increase of the length of the alkylic substituent at C-1 is tolerated up to 4 carbon atoms.

Importantly, the obtained results highlighted the crucial role performed by a hydrogen bond donor group on the ligand for anchoring the ZA region. Based on this consideration, we implemented an optimization of the "pharm-druglike2" model, inserting a new donor feature "**D**" in correspondence with the planar group (**Figure *35A***), in order to guarantee an additional hydrogen bond with Asn100 or Ile53. Moreover, the presence in this specific position of a hydrogen bond donor group in the most potent BRD9 binders (*e.g.*, I-BRD9, see **Figure *35B***) strengthen our adjustment.

We believe that the optimized and updated 3D pharmacophore model will aid the identification of compounds with improved activity and selectivity.
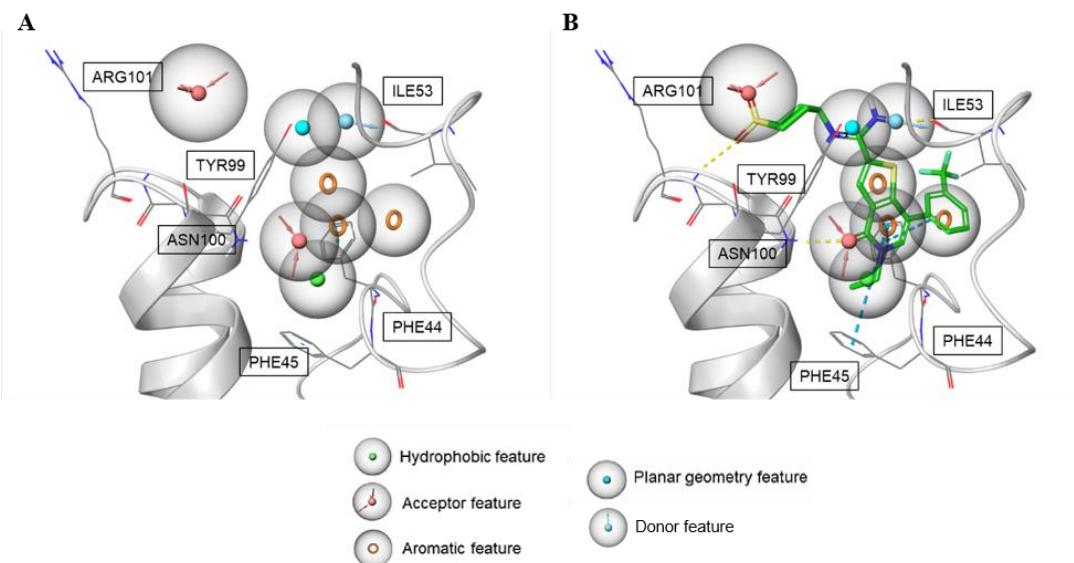
Figure 35. *A) Optimized "pharm-druglike2" model in BRD9 binding site. B) I-BRD9 superimposed to the optimized "pharm-druglike2" model.*

2.3.6.7 Evaluation of the selectivity profile of compound 11

The obtained binding data for compound **11** showed its remarkable potency on BRD9 (IC_{50} = 3.93 ± 0.54 μM), hence it was selected as representative compound among the second generation of ligands for further studies. Thereby, BromoMELT™ Assay was carried out by Reaction Biology Corporation, for profiling the binding of compound **11** to a large collection of 76 human bromodomain proteins.

Briefly, BromoMELT™ is a thermal stability assay, where the protein denaturation is detected by the exposure of the hydrophobic surfaces that, interacting with a dye, increase its fluorescence. A plot of fluorescence versus the increase of the temperature is analyzed to obtain a melting temperature value (Tm), represented by an inflection of the curve. The interaction between the protein and the ligand increases protein stability, leading to an increment in Tm. Thus, the interaction of a ligand to a protein is detected as ΔTm value (*i.e.*, $Tm_{compound} - Tm_{dmso}$).[78] It is important to note that the

BromoMELT™ assay is predominantly a semi-quantitative technique, useful to identify if a compound is able to bind the protein of interest.

As reported in our extensive selectivity profile (**Figure *36***), **11** emerged as a highly selective compound among bromodomains, binding BRD9 and its close homolog BRD7, which shares with BRD9 the 72% of similarity. Moreover, **11** appears to bind the bromodomains of BRPF1 (Bromodomain and PHD finger containing 1) whose activity will be further evaluated. Indeed, recently, it has emerged that depletion of BRPF1 interferes with the upregulation of HOX gene expression which is frequently associated with the development of leukemia. Therefore, the therapeutic targeting of BRPF1 may be valuable in acute myeloid leukemia (AML).[79] Moreover, BRPF1 emerged recently as the most significantly upregulated gene in human hepatocellular carcinoma (HCC) often associated with poor patient survival. Gene ablation or pharmacological inactivation of BRPF1 significantly attenuated cell growth *in vitro* and *in vivo* of hepatocellular carcinoma, proving the potentiality of this protein target for the treatment of HCC.[80]

Hence, we evaluated the IC_{50} values of binding to BRD7 and BRPF1 of compound **11** and its close derivative **42** through the application of the AlphaScreen technique. According to our computational analysis, the longer alkyl chain on the C-1 featured by **42** strongly enhances the selectivity on BRD9 over the highly homologous BRD7. Indeed, compound **42** presented a considerable decreased affinity on BRD7 with IC_{50} = 95.76 ± 2.74 μM compared to **11** that presented IC_{50} = 18.38 ± 2.06 μM.

Notably, a strong binding affinity on BRPF1 was detected for both compounds **11** and **42** (IC_{50} = 4.50 ± 0.31 μM and 1.48 ± 0.24 μM, respectively), highlighting an interesting dual activity on two proteins involved in carcinogenesis, paving the way to a new class of BRD9/BRPF1 epidrugs.
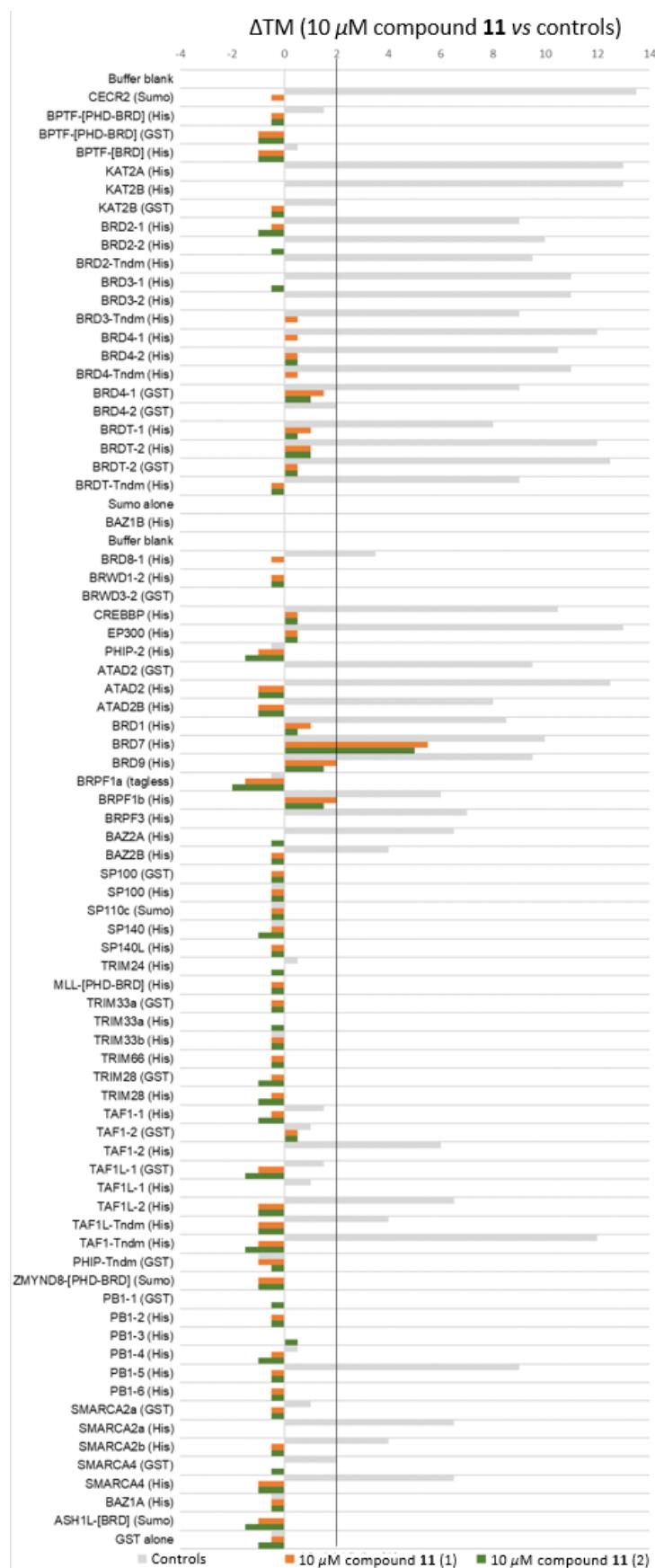
Figure 36. *BromoMELT™ profile for compound 11*.

2.3.6.8 Biological evaluation of the potential anticancer activity of the most promising compounds belonging to the second generation of triazoloquinoxaline derivatives.

In order to complete the biological activity investigation of the newly identified potent binders belonging to the second generation of compounds, preclinical biological assays were carried out in collaboration with Prof. Irace's group (from Università degli Studi di Napoli Federico II). Specifically, the antiproliferative effects of the most interesting compounds **11** and **42** were investigated on selected human leukemia cell lines (*i.e.*, THP-1, Kasumi-1, HL-60, K-562, and CCRF-CEM) and healthy cells (*i.e.*, HaCaT and HDFa) through the evaluation of the cell survival index obtained by the MTT assay and monitoring of live/dead cell ratio. As reported in **Table *4***, highly attractive results were achieved confirming improved bioactivity for the second generation of triazoloquinoxaline compounds. The obtained data highlighted an interesting cytotoxicity for compound **42** in all treated leukemia cells that was not observed in healthy cells (HaCaT and HDFa). In particular, among the selected tumor cell lines, the best activity was detected on CCRF-CEM, where compound **11** showed $IC_{50} = 50 \pm 5 \mu M$ and compound **42** presented $IC_{50} = 35 \pm 4 \mu M$.

The enhanced antiproliferative activity of **42** is probably related to its higher selectivity on BRD9 over BRD7 with respect to compound **11**, as assessed by the previously described AlphaScreen assays. Indeed, BRD7 plays a tumor suppressive role in carcinogenesis,[29] whose activity is therefore in contrast with that of the highly homologous BRD9.

Table 4. IC_{50} *values (μM) relative to* **11** *and* **42** *in human leukemia cell lines (THP-1, Kasumi-1, HL-60, K-562, and CCRF-CEM) and healthy cells (HaCaT and HDFa) following 48 h of incubation (concentration range 1 - 100 μM). The calculation of the IC_{50} is based on plots of data and repeated five times. IC_{50} are expressed as mean ± SEM of five independent experiments.*
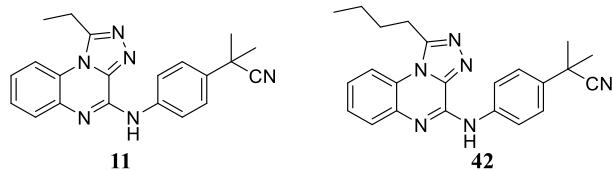
Compound	THP-1	Kasumi-1	HL-60	K-562	CCRF-CEM	HaCaT	HDFa
			IC_{50} **(μM)**				
11	95 ± 6	97 ± 4	>100	90 ± 5	50 ± 5	>100	>100
42	60 ± 5	72 ± 5	81 ± 5	65 ± 4	35 ± 4	>100	>100

2.4 Exploration of new BRD9 ligands through the syntheses of pyrazolopyridine-based compounds

The combined pharmacophore/virtual screening *in silico* workflow (described in **paragraph 2.2.1**) was successfully applied as a valid computational tool for the identification of another chemotype that, at the moment, is under investigation for the development of a new class of potential BRD9 inhibitors. In this paragraph, it is described the selection of an initial hit featuring the pyrazolopyridine motif, which represents an unexplored chemical entity for the development of BRD9 binders. The promising data prompted us to pursue focused structural modifications on the newly identified core through the application of an effective synthetic protocol.

2.4.1 Identification of the 1-ethyl-1H-pyrazolo[3,4-b]pyridine scaffold

The latest application of the 7-point "pharm-druglike2" model **AAHRRRX**, explored during this Ph.D. project, led to the discovery of the hit compound **2** (***Figure 37A***), which successfully matched all the chemical and structural features of the 3D pharmacophore. In more detail, employing our effective tool as selection filter, compound **2** emerged from a massive screening of a huge library of compounds available on Sigma-Aldrich database (www.aldrichmarketselect.com). Indeed, as predicted by docking calculations, compound **2** is anchored in BRD9 binding pocket by making powerful interactions (illustrated in ***Figure 37B***): the key amino acids Asn100 and Arg101 are engaged by a multiple H-bond network, while important π-π stackings are made with Tyr106, Phe44, and Tyr99. Similarly to the previously described triazoloquinoxaline ligands (**paragraph 2.3**), compound **2** presents an ethyl group at the N-1 position correctly accommodated in the deepest hydrophobic cavity of BRD9, in agreement with the feature **H** of the model. Moreover, the two

substitutions at the C-4 and C-6 sites appear located at the appropriate distance and orientation from the scaffold, and engage perfectly the pharmacophoric requirements, enabling an efficient occupation of the binding site.
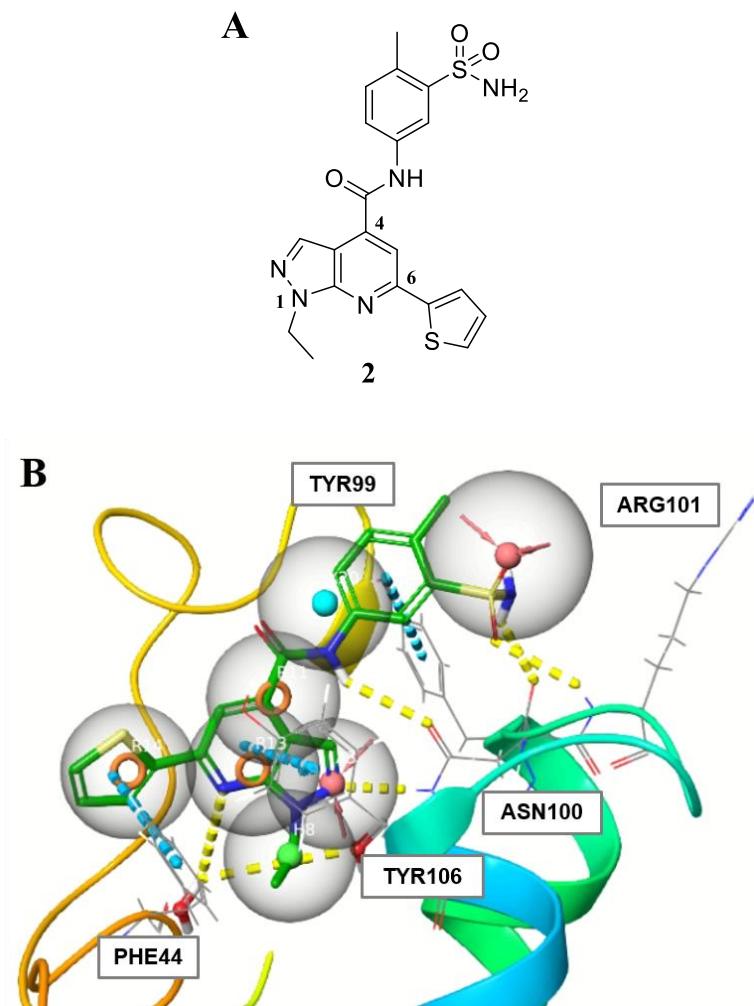
Figure 37. *A) 2D Chemical structure of hit compound **2**. B) Compound **2** in the reference BRD9 protein structure (PDB: 5F1H) superimposed to the 7-point "pharm-druglike2" model. H-bonds and π-π interactions are reported in yellow and cyan dotted lines, respectively.*

With the aim to corroborate the reliability of the *in silico* predictions, we employed AlphaScreen technique to verify the ability of compound **2** to bind the target protein. The results showed that the treatment with the selected compound at 10 μM, disrupted

the recognition BRD9 – Histone H4, presenting 55.0 ± 1.5 % residual BRD9 activity. For this reason, **2** was highlighted as a promising starting point for the development of more potent BRD9 ligands.

2.4.2 Design and synthesis of pyrazolopyridine-based compounds

The discovery of compound **2**, featuring the pyrazolopyridine scaffold, paved the way for a wide exploration of this new interesting chemical motif. A retrosynthetic analysis revealed the possibility to carry out a thorough investigation around the central core ensuring the respect of the pharmacophore features. As shown in *Figure 38*, three different portions of the molecules are currently under exploration with the aim to fulfill a comprehensive and robust SAR study.
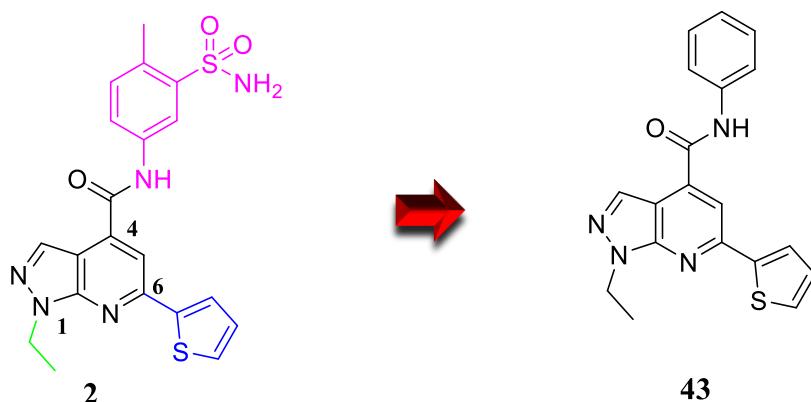
Figure 38. *Chemical structure of the hit compound **2** and the first synthesized derivative **43**. In green, violet and blue are highlighted the three synthetically accessible moieties that will be explored for the heterocyclic scaffold decoration.*

In particular, modifications of the blue moiety (corresponding to the C-6 position) could be exploited to probe the chemical space of the shelf of BRD9, close to the anchor region, where reside important amino acids for the binding, *i.e.,* Gly43, Phe44, and Phe45. Moreover, the diversification of the length and bulkiness of the green aliphatic group (corresponding to the N-1 position) will be useful to investigate the

impact on the selectivity against other bromodomain proteins. Finally, variations of

the violet group (corresponding to the C-4 position) are highly instrumental to probe

the ZA channel with the aim to enhance both the potency and the selectivity of the

designed compounds. For the development of detailed SAR investigations, we first

explored the effect on the binding affinities of different chemical substitutions on the

C-4, retaining constant the thiophene group at C-6 as well as the ethyl group at the N-

1 position. Thus, we designed one initial derivative bearing a simplified

phenylacetamide moiety (compound **43**, *Figure 38*) to validate the minimal chemical

requirements necessary for the binding. Moreover, the synthesis of such compound

was useful to probe the efficiency of the chosen synthetic protocol and its applicability

for the syntheses of a large set of derivatives.
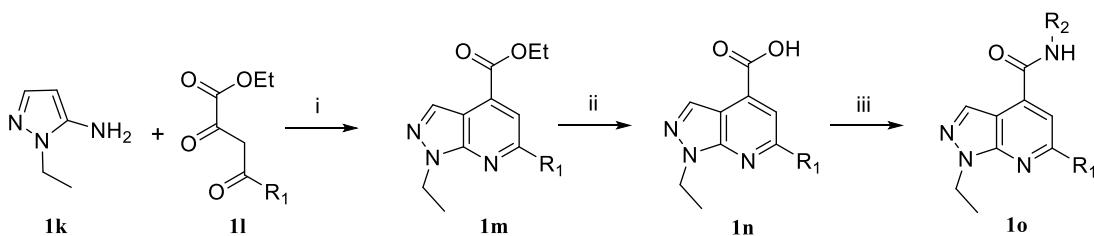
Scheme 8. *General synthetic protocol applied for the synthesis of compound 43. Reagents and conditions: i) AcOH, reflux, 2 h; ii) KOH, iPrOH, reflux, 2.5 h; iii) a. oxalyl chloride, dry DCM, 0 °C to r.t. for 2 h; b. R$_2$NH$_2$, dry toluene, reflux, 12 h.*

In *Scheme 8* is shown the efficient three-step synthetic procedure selected for the

synthesis of pyrazolopyridine-based compounds. More specifically, to ensure a high

diversity of the library, a Combes-type reaction of 4-substituted-2,4-diketoesters with

different amino heterocycles will be employed. Hence, the initial step consists in the

reaction between the commercially available 1-ethyl-1*H*-pyrazol-5-amine with the 4-

substituted-2,4-diketoester in acetic acid, which yields the intermediate **1m**.

Subsequently, the hydrolysis of **1m** with KOH gives the formation of the

corresponding acid, which is activated to the acid chloride with oxalyl chloride and finally coupled with the selected aniline to afford the desired compound.[81] The described synthetic protocol was successfully employed for the obtainment of compound **43** in high yields, and it was considered useful for the syntheses of new collections of the designed pyrazolopyridine compounds. The detailed experimental section for the synthesis of compound **43** is described in **CHAPTER 5** (**paragraph 5.3**).

2.4.3 Binding assay and future SAR studies

In order to test the influence on the binding affinity of the simplified derivative **43** (*Figure 38*) and to assess the importance of an appropriate substitution pattern on the C-4 position, the compound was then evaluated for its binding on BRD9, through AlphaScreen performed by Reaction Biology. As we were expecting, the binding assay detected a decreased affinity on BRD9 compared to the initial hit: in fact, the biophysical measurement reported a 74.1 ± 1.6 % BRD9 residual activity after treatment at 10 μM with compound **43** *vs* 55.0 ± 1.5 % residual activity with **2** in the same experimental conditions. Such differences in the binding affinities between the two derivatives underlined that the C-4 modifications of the scaffold are fundamental to gain more potent binders. Therefore, we are deeply investigating the substitution pattern of this aromatic moiety, in order to establish more favourable interactions within the BRD9 binding site. Thus, considering the possibility to diversify this position with different decorated aromatic substituents through the high-quality synthetic protocol described in *Scheme 8*, the 1-ethyl-1*H*-pyrazolo[3,4-*b*]pyridine scaffold was used for the *in silico* generation of a combinatorial library with various primary aromatic amines (*Figure 39*).
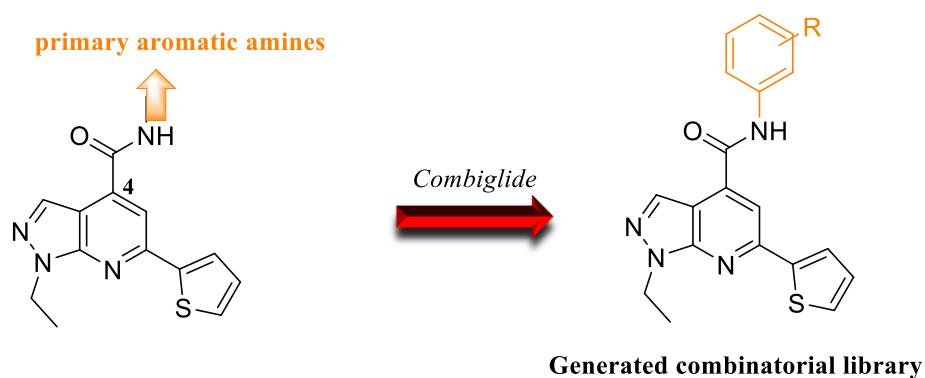
Figure 39. *In silico combinatorial library generation on the pyrazolopyridine core.*

Thus, an in-house library of 5256 pyrazolopyridine-derivatives was generated. After pharmacokinetic parameters calculation employing *QikProp*,[64] and the selection of those ligands with favourable drug-like properties, the library was screened employing the "pharm-druglike2" model. The top-ranked molecules presenting the best *Phasescreen* values of correspondence with the pharmacophore model were submitted to molecular docking calculations. Hence, the predicted binding modes were carefully analyzed to select an initial and focused set of five compounds **44-48** (**Figure 40**). Despite the high chemical variability, all the compounds satisfied with high performances our **AAHRRRX** model. Indeed, we deemed of great interest the selection of compounds presenting different substitution patterns on the C-4 with the aim to effectively probe the chemical space around this position.
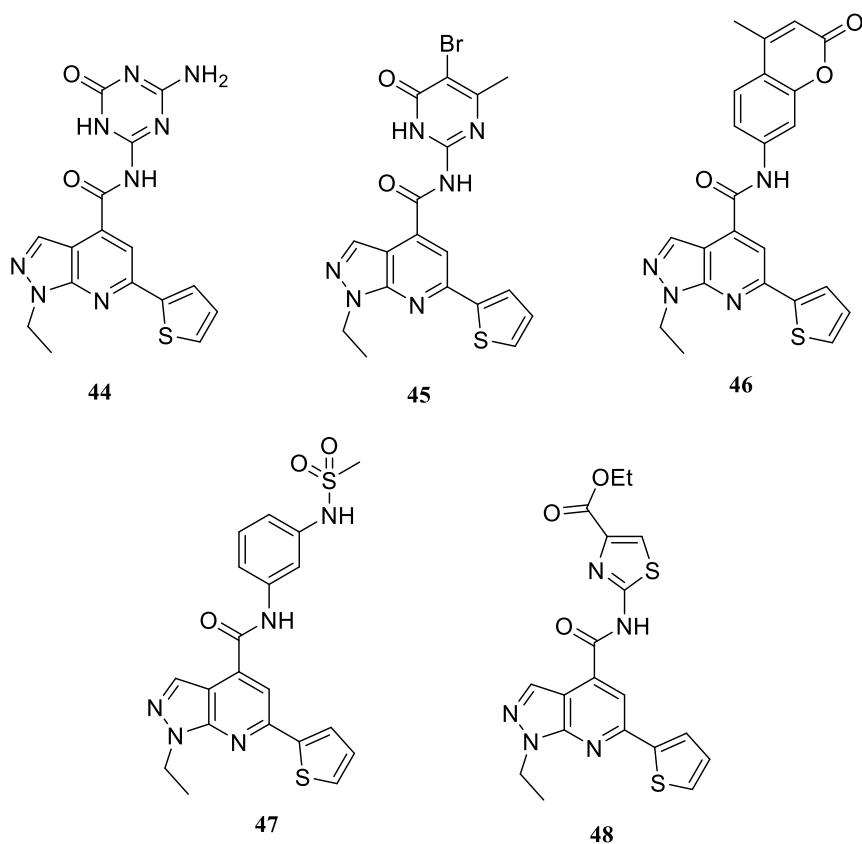
Figure 40. *Chemical structures of the pyrazolopyridine derivatives **44-48** selected employing the "pharm-druglike2" model.*

At present, the syntheses of the most promising derivatives **44-48** are ongoing employing the procedure previously described in *Scheme 8*. Eventual modifications and/or optimizations of the proposed synthetic protocol will be evaluated whereas the efficiency of the reaction is considered not completely satisfying.

Finally, both the evaluation of the binding affinities of compounds **44-48** on BRD9 and their selectivity on a panel of bromodomain proteins, will be critical to drive future SAR studies. Hence, in order to optimize the disclosed BRD9 ligands, systematic modifications of the two synthetically accessible groups will be performed, as indicated in **Figure *41***.
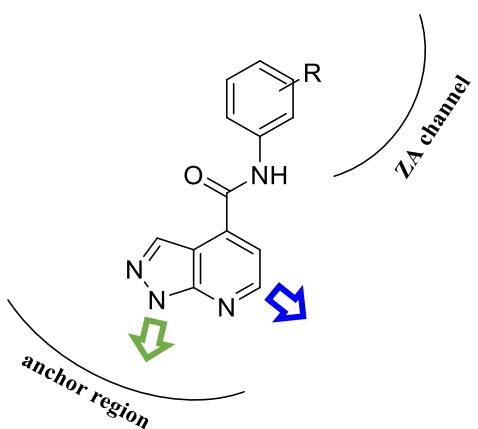
Figure 41. *General chemical structure of the pyrazolopyridine under evaluation. The arrows indicate the two positions that will be explored for future SAR studies.*

2.5 Investigation of aryl sulfonamide-based compounds as potential BRD9 ligands

The successful identification of new BRD9 binders, reported in the previous paragraphs, is the final result of rounds of fine-tuning and optimization processes of *in silico* studies coupled to targeted syntheses of collections of small molecules, which have allowed to explore the chemical space of KAc binding site. The achievement of such effective computational tools implied great efforts and concerted work between the computational and the synthetic units, due to the necessity to probe and adjust, step-by-step, the pharmacophore features of the three-dimensional model.

In this paragraph will be described the early stages of our research project on BRD9, whose outcomes had been beneficial for the improvement and refinement of the final model.

2.5.1 Exploration of a new chemical motif identified through the "pharm-fragment" AHRR model

At the very beginning of our BRD9 project, a simplified version of the pharmacophore model was developed. In particular, a 4-point "pharm-fragment" AHRR model, was initially applied as a computational tool to identify new potential chemotypes presenting the minimal number of chemical and structural features necessary for the binding to BRD9, and that could be easily modified in a structure-based fashion to develop a new class of potential inhibitors. The employment of the "pharm-fragment" as pharmacophore filter for screenings of large libraries of compounds, lead to the identification of the hit compound **3** (**Figure** *42A*), which emerged from the online Sigma-Aldrich Market database (www.aldrichmarketselect.com). As shown in **Figure** *42B*, compound **3** successfully

matched the minimal requirements of the 4-point model. The predicted binding pose resulted from molecular docking, displayed that the aryl sulfonamide moiety is located in the BRD9 anchor region, and despite the low structural complexity, establishes promising interactions with the key amino acids Asn100 and Tyr99. The methyl substituent on the sulfur functionality is correctly accommodated in the hydrophobic cavity fundamental for the KAc recognition; however, a thorough structural analysis revealed that a longer substituent could be exploited for a better occupancy of the pocket.

A retrosynthetic analysis immediately highlighted compound **3** for its synthesis feasibility and flexibility towards chemical diversification, both instrumental for a wide chemical exploration of this new chemical entity. At this stage, we deemed necessary the synthesis of a large collection of derivatives featuring chemical diversity in order to probe the quality of selection provided by this minimal pharmacophore model and to explore widely the potentiality of this new chemical fragment.

A

3

B
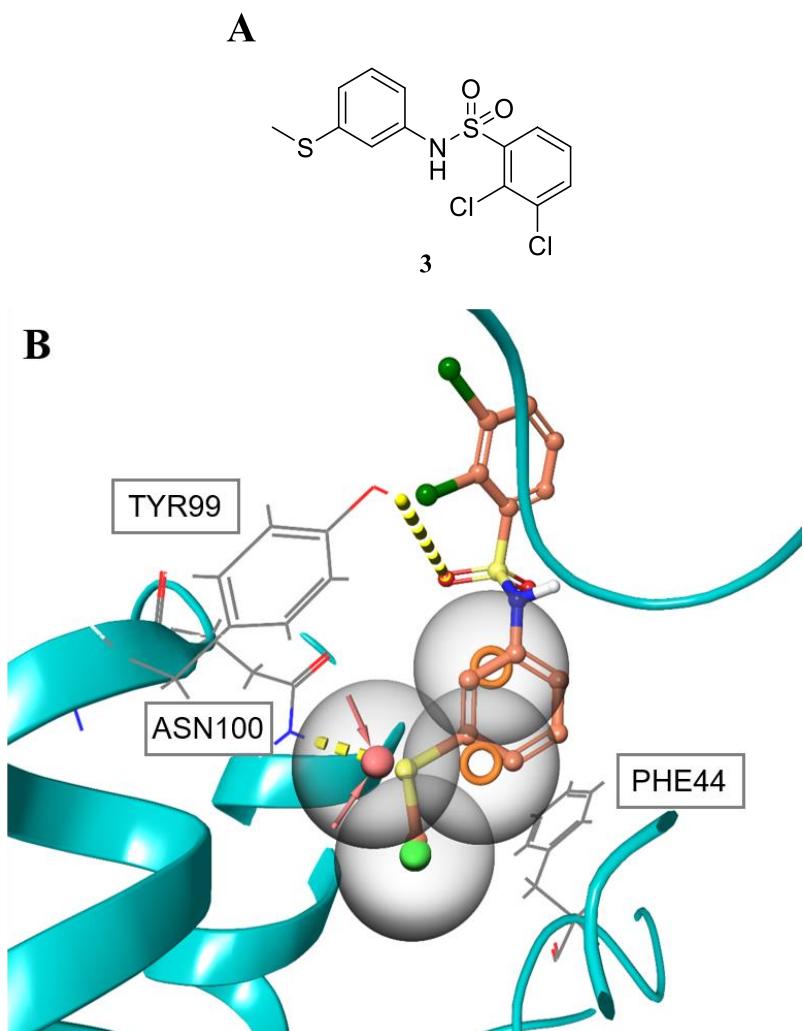
Figure 42. *A) 2D Chemical structure of compound **3**. B) Compound **3** in the reference BRD9 protein structure (PDB: 5F1H) superimposed to the 4-point "pharm-fragment" model. H-bonds are reported in yellow dotted lines.*

Starting from the predicted binding pose of compound **3**, on the basis of the chemical and structural features of the "pharm-fragment" **AHRR**, we designed a structurally related library of derivatives (**49-69**) through various functionalization of the aryl sulfonamide core (**Figure *43***).

A

3
Hit compound
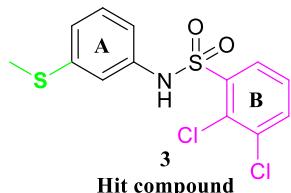
B
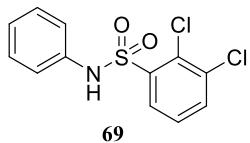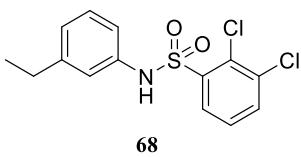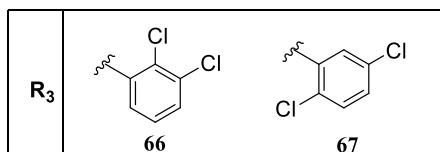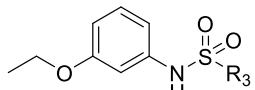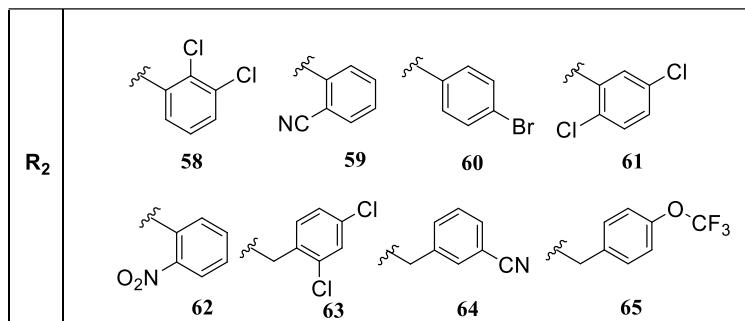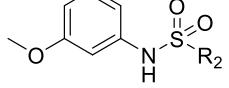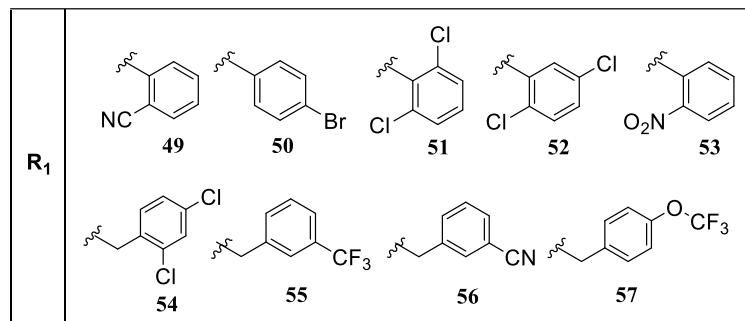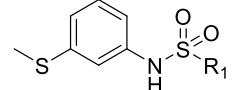
Figure 43. *A) Chemical structure of hit compound **3**. The two portions of the molecule that have been modified for the design of structural derivatives are highlighted in green and purple. B) Chemical structures of the designed and synthesized compounds **49-69**.*

In order to extend the chemical variability of the compounds, we started the exploration of the aryl sulfonamide core through systematical modification of two

portions of the initial hit **3**, highlighted in different colours in **Figure *43A***. More in detail, according to the strict requirement of the pharmacophore model of a H-bond acceptor group (**A**) directly conjugated to the ring A, we replaced the sulfur, a poor H-bond acceptor, with a more effective group. Hence, we designed a total of 10 derivatives (**58-67**) presenting the oxygen functionality aiming to improve the binding with the key amino acid Asn100 in the BRD9 binding site. Additionally, for this initial set of compounds, we also explored in correspondence of the hydrophobic feature (**H**) on the "pharm-fragment" model, ethyl groups (**66-67**). Moreover, as a proof-of-concept of the essentiality of both the H-bond acceptor and hydrophobic features mimicking the acetyl-lysine function, we designed compounds **68** and **69** considering the removal of such chemical groups.

In combination with the modification applied on ring A, we also modified the substitution pattern on ring B. Moreover, a careful *in silico* analysis of the binding mode of the designed compounds, suggested the introduction of a spacer between the sulfonamide group and the aromatic ring B with the aim to point the aromatic substituents in such a way to facilitate the interaction with key amino acids in the ZA channel (*i.e.*, Arg101 and Ile53). Thus, compounds **54-57** and **63-65** were designed considering the insertion of a methylene spacer.

2.5.2 Chemical synthesis of aryl sulfonamide-based compounds 49-69

The applied synthetic protocol, promptly supported the necessity to obtain a wide variety of derivatives featuring different substitution patterns and chemical properties, in order to carry out an extended investigation of this new potential chemical core. Indeed, 21 derivatives **49-69** (shown in ***Figure 43***), designed according to the "pharm-fragment" model, were synthesized in high yields through a fast and facile one-step

synthetic route. As reported in *Scheme 9*, all compounds have been obtained following a similar synthetic procedure starting from commercially available 3-substituted anilines that have been coupled with the appropriate aryl sulfonyl chloride by using anhydrous pyridine.[82]
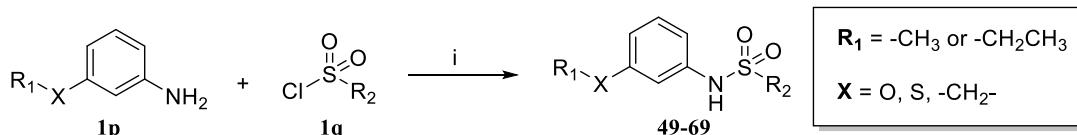
Scheme 9. *Chemical synthesis of compounds **49-69**. Reagents and conditions: i) pyridine, r.t., 2h.*

2.5.3 Biophysical binding assays of compounds 49-69 through AlphaScreen technology

All the synthesized compounds **49-69** and the initial hit **3** were then evaluated through AlphaScreen binding assay (by Reaction Biology Corporation) in order to evaluate their potential binding toward the target protein.

However, none of the tested compounds showed an appreciable binding to the protein counterpart at 10 μM ligand concentration. The initial poor data obtained are probably due to the low chemical complexity of the designed compounds which is not adequate for the recognition of BRD9. To date, a review of these preliminary results does not surprise us, since the *in silico* selection that drove the choice of these compounds was based on an initial proposal of the pharmacophore model in course of construction. Nevertheless, the obtained results prompted us to pursue a new design and, on the other hand, to reevaluate an optimization of our *in silico* pharmacophore that requires to be more specific and stringent.

Thus, the computational unit subsequently built more effective models incorporating additional pharmacophore features that lead to the final 7-point models

AAHHRRR and **AAHRRRX** (described in **paragraph 2.2**). Confident that these optimized models could assist the improvement of the binding affinity toward BRD9, we carried out a reevaluation of the aryl sulfonamide-based compounds.

2.5.4 Design and syntheses of a new collection of optimized aryl sulfonamide-based compounds

A careful structural insight of the binding modes of compounds **49-69**, predicted by molecular docking experiments, was then performed. In this initial phase of optimization, we decided to focus our attention on those molecules presenting the oxygen functionality at the C-3 position of ring A due to the more effective H-bond interaction that this atom can perform when compared to the sulfur. Moreover, the binding mode inspections, combined with the structural information provided by the model **AAHRRRX**, suggested that effective derivatization could be made at the C-5 position of ring A in order to fulfill the additional pharmacophore point **R** and establish potential interactions with key amino acids in the ZA channel of BRD9 (*Figure 44*).
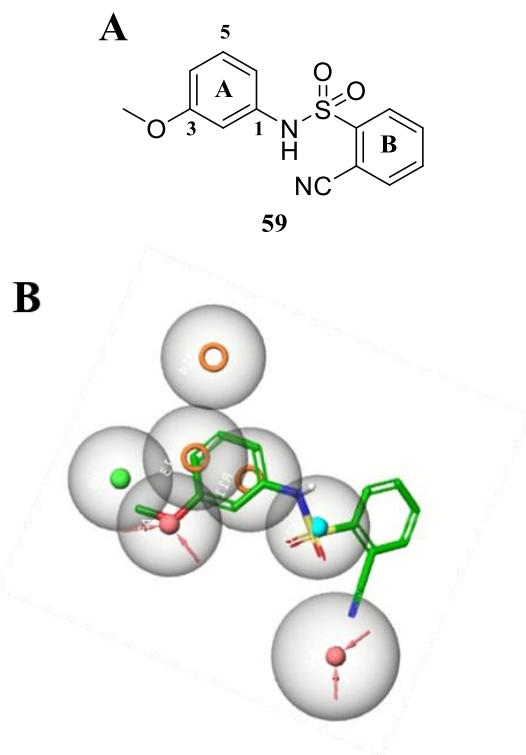
Figure 44. *A) 2D Chemical structure of compound **59**. B) Compound **59** superimposed to the 7-point model "pharm-druglike2" model AAHRRRX.*

A thorough retrosynthetic analysis revealed the synthetical accessibility of this site that could be effectively exploited for the heterocyclic scaffold decoration through different approaches. To start our structural optimization, we first investigated a direct C-C conjugation at the C-5 position with aromatic substituents to effectively satisfy the additional **R** feature. The commercial availability of the 3-bromo-5-methoxyaniline, pushed us to employ the Suzuki-Miyaura cross-coupling reaction[75] for an efficient compounds decoration. Therefore, an *in silico* collection was built employing *Combiglide* software,[63] considering two sites for combinatorial library generation: the amine functionality on the C-1 position that was substituted with aryl sulfonyl chlorides, and the C-5 position that was derivatized with boronic acid derivatives (**Figure *45***).
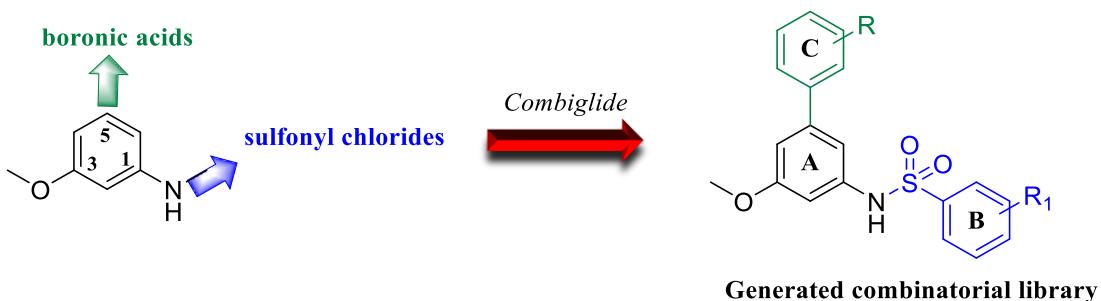
Figure 45. *Generation of an in silico combinatorial library of aryl sulfonamide derivatives.*

Following this rationale, a new library of 116,688 aryl sulfonamide-derivatives was generated. In order to consider those molecules with favourable bioavailability, the combinatorial library was then submitted to pharmacokinetic parameters calculation through *QikProp* software.[64, 65] Successively, the application of the computational filter based on Lipinski's rule of five[66] led to the selection of those ligands with favourable drug-like properties. Successively, the items were subjected to the pharmacophoric filter using the "pharm-druglike2" model and docking calculations. Finally, a careful analysis of the results based on the docking score values and the correspondence with the pharmacophore model, allowed the selection of five compounds (**70-74**, **Figure** *46*), for the following chemical synthesis and biophysical evaluation steps.
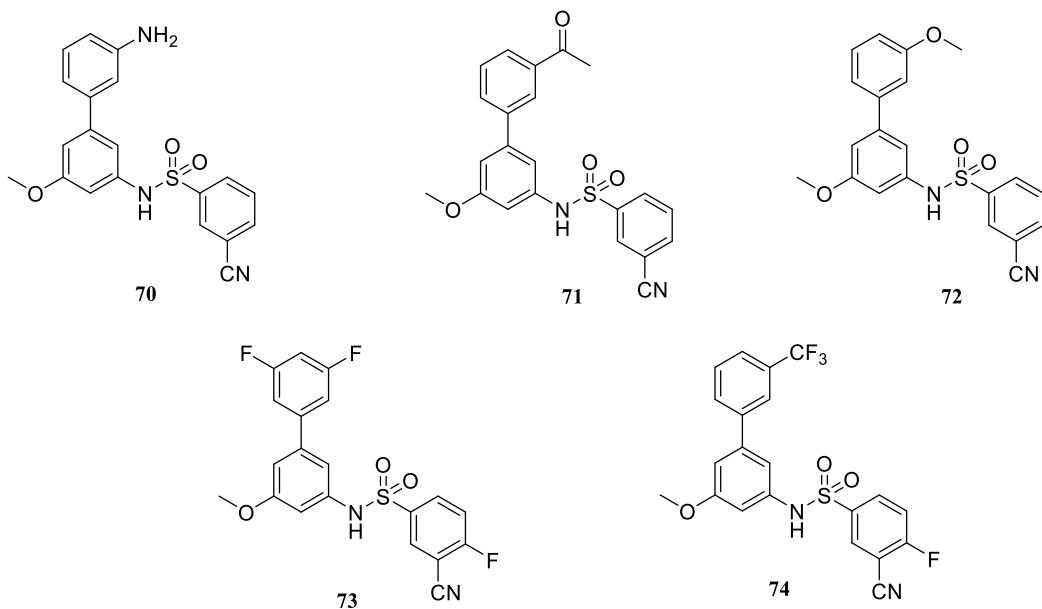
Figure 46. *Chemical structures of the aryl sulfonamide derivatives **70-74** selected employing the "pharm-druglike2" model.*

The identified molecules **70-74** (***Figure 46***) were synthesized using an efficient two-step synthetic procedure, as described in ***Scheme 10***, which led to the desired items from good to high yields. More specifically, in the first step, the reaction between the commercially available 3-bromo-5-methoxyaniline (**1r**) and the proper aryl sulfonyl chloride led to the formation of an intermediate featuring a sulfonamide linkage.[82] The obtained compound was then cross-coupled with the selected boronic acids under standard Myaura-Suzuki condition,[75] yielding the desired five compounds (**70-74**), selected as the most promising through *in silico* inspection.

All synthesized compounds were structurally elucidated by spectral data analysis of proton (^{1}H) and carbon (^{13}C) NMR and by high-resolution mass spectrometry experiments. The corresponding experimental section is reported in **CHAPTER 5** (**paragraph 5.4**).
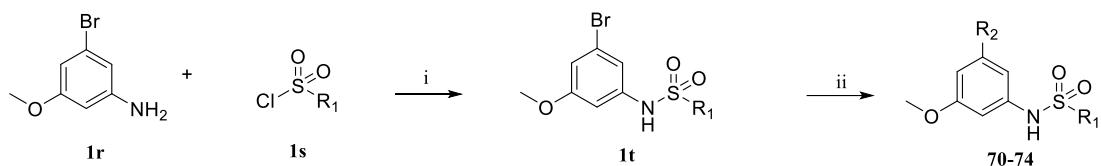
Scheme 10. *Chemical synthesis of compounds 70-74. Reagents and conditions: i) pyridine, r.t., 2h; ii) $R_2B(OH)_2$, $(PPh_3)_2PdCl_2$, Cs_2CO_3, PCy_3, 1,4-dioxane/H_2O (8:2), 80 °C, overnight.*

2.5.5 Biophysical binding assays of compounds 70-74

Compounds **70-74** were evaluated employing AlphaScreen binding assay (by Reaction Biology Corporation) to analyse their interactions with the target protein. As the previous compounds, the molecules were tested against BRD9 at 10 μM employing Bromosporine as control.

Despite the *in silico* analysis of this set of optimized compounds was more encouraging than the previous one, the preliminary biophysical assays did not detect any binding to the protein counterpart (**Table 5**).

Table 5. *Residual binding of Histone H4Ac to BRD9 after treatment with synthesized compounds **70-74**. Data are expressed as means ± SD, n = 2.*

Compound	R₁	R₂	% residual binding of histone /Ac ± SD [Compound] = 10 μM
70	CN	NH₂	97.5 ± 0.3
71	CN	O (acetyl)	>100
72	CN	O-methyl	>100
73	CN, F	F, F	95.9 ± 7.8
74	CN, F	CF₃	94.3 ± 0.7

In our experience, as reported in the SAR study for triazoloquinoxaline-derivatives in **paragraph 2.3.6**, even small modifications on the molecule could reverse significantly the binding to BRD9. For this reason, we believe that *in silico* tools, such as our pharmacophore model, are indeed necessary to assist in the discovery and

optimization of new chemical probes for this target protein. At present, pharmacophore-driven modifications of this chemical motif are ongoing. In particular, the insertion of a fused aromatic ring between rings A and C has been considered, as well as the possibility to replace the sulfonamide group with a H-bond donor moiety, such as an amidine, that could increase the activity through direct interaction with Ile53 or Asn100 (**Figure *47***). The latter modification is strongly motivated both by the latest update of our pharmacophore suggesting a H-bond donor group in correspondence with the **X** feature of the pharmacophore model (see **paragraph 2.3.6.6**), but also by the presence of the amidine moiety in a potent BRD9 inhibitor (I-BRD9).[40]
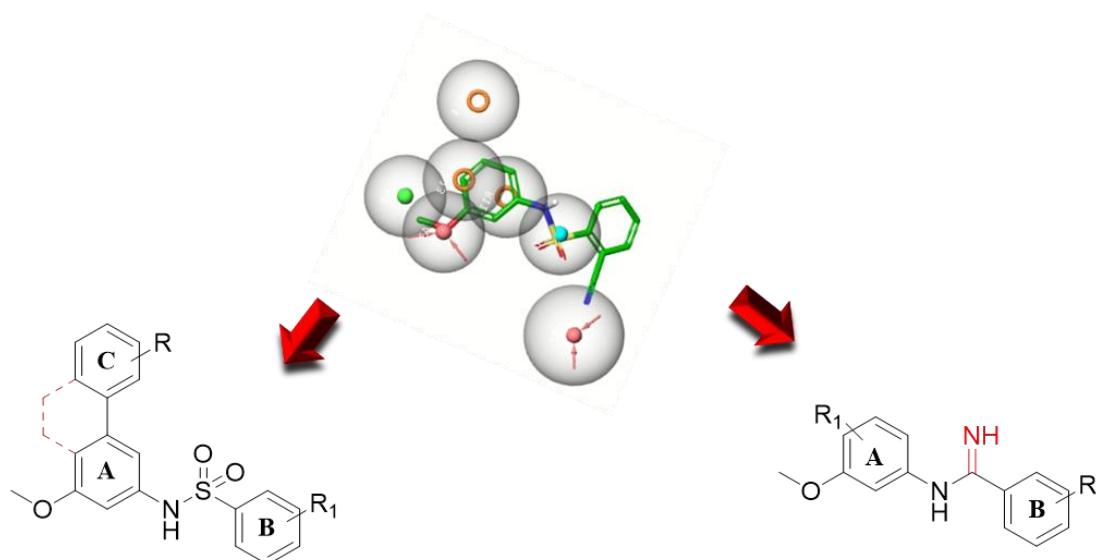
Figure 47. *Ongoing structural optimization.*

2.5.6 Repositioning of aryl sulfonamide-based compounds through Inverse Virtual Screening

The unsatisfying results of the synthesized compounds **49-74** and the hit **3** on BRD9, pushed us to reposition these molecules through Inverse Virtual Screening (IVS) method.[3] More specifically, this *in silico* methodology had been developed and

successfully used in these years by our research group, for the rapid search of potential targets for a small set of molecules.[83, 84]

Thus, through the application of this computational technique, the entire library of aryl sulfonamide-based compounds was docked *versus* a panel of proteins involved in the development of cancer and inflammation. From the obtained data, six promising target proteins emerged: the estrogen receptor β (Erβ), thymidine phosphorylase (TP), tankyrase 2 (TANK2), retinoid X receptor (RXR), soluble epoxide hydrolases (sEH), microsomal prostaglandin E synthase-1 (mPGES-1). Following these results, the most appropriate assay for detecting the activity *versus* the protein of interest will be applied in order to corroborate the computational predictions and to further investigate their potential applicability.

At present, in collaboration with Prof. Oliver Werz (University of Jena), cell-free assays to evaluate the inhibitory activity of the selected compounds on mPGES-1 are ongoing. Specifically, mPGES-1 is the terminal enzyme responsible for the production of inducible prostaglandin E_2, and it represents an interesting protein target largely investigated by our research group for its attractive biological involvement in inflammation and cancer pathologies. [85, 86]

CHAPTER 3

Exploration of alternative therapeutic approaches and

further investigation of the BRD9 biological profile

The investigation described in the previous chapter, highlighted the intense efforts, during this Ph.D. program, in the identification of new BRD9 binders guided by innovative structure-based 3D pharmacophore models, which paved the way to a new and effective approach in BRD9 drug design. In parallel, the focus of this Ph.D. project was also fueled by a thorough exploration of BRD9's role in the mSWI/SNF chromatin remodeling complex, with the final goal to enhance the bioactivity in interfering with tumor growth and proliferation featured by classical BRD9 ligands.[46, 87] Indeed, we investigated two different approaches to target the protein, with the aim to perturb the stability and/or the activity of the remodeling complex, and subsequently study the consequences on the downstream effects. Hence, in this chapter, it is presented the application of two innovative techniques, aiming to fulfill a comprehensive study of the possible targeting strategies for this epigenetic reader.

Firstly, it will be presented our Proteolysis Targeting Chimeras (PROTACs) campaign based on the design and synthesis of potential degraders targeting BRD9, and the obtained encouraging results. Next, it will be described the design and synthesis of the first SWI/SNF multi-target probe aiming to disrupt the activity of the ncBAF complex targeting two key subunits involved in cancer development: BRD9 and SMARCA4. Finally, in this chapter, it will be reported our investigation of a mostly unexplored BRD9 activity in regulating the inflammatory response.

3.1 Design and synthesis of new BRD9 PROTACs

3.1.1 Induced target protein degradation: a paradigm-shifting drug discovery approach

For years, the classical drug discovery approach has been based on the use of small molecules that, through the binding of well-defined binding sites, are able to modulate

the activity of target proteins.[88] However, several proteins lack binding pockets and/or catalytic activity, making their modulation difficult to achieve. At the same time, some proteins work in large complexes that could compensate for the reduced activity due to inhibition.[89]

Over the past decades, different alternative approaches have been explored in order to overcome these limits, such as antisense oligonucleotides (ASOs),[90] monoclonal antibodies (mAbs),[91] or small-interfering RNAs (siRNAs).[92] Nevertheless, small molecules continue to be the cornerstone of pharmaceutical research, playing a critical role in newly approved drugs.[93] Unequivocally, the revolutionary modality based on PROteolysis TArgeting Chimeras (PROTACs), represents one of the most emerging and innovative approaches, especially for cancer treatment,[94] belonging to the small molecules class of therapeutics.

In recent years, PROTAC technology was highlighted as a novel drug discovery strategy with the potential to offer therapeutic interventions not achievable *via* conventional medicinal chemistry approaches, demonstrating to be advantageous when compared to inhibition, especially for proteins previously described as undruggable.[95, 96] The first study about PROTACs was published in 2001 by the groups of Craig M. Crews and Raymond J. Deshaies,[97] but the field remained for years largely unexplored, until 2015 when PROTACs started to gain the attention from the entire scientific community.[98]

This innovative approach relies on the use of small molecules to decrease protein levels in cells rather than modulate their function.[99] More specifically, PROTACs are bifunctional degraders that hijack the intracellular ubiquitin-proteasome system (UPS) to induce the degradation and elimination of a target protein. A protein-of-interest ligand (also called "warhead") is connected *via* a linker of different lengths and

chemical nature to an E3 ubiquitin ligase ligand (***Figure 48A*** and ***Figure 48B***).[99] In this way, the target protein is brought close to the E3 ligase that promotes its polyubiquitination and degradation through proteasome activity (***Figure 48C***).[100] Hence, PROTACs rely their activity on the formation of a stable and cooperative ternary complex (protein-of-interest:PROTAC:E3 ligase), which is usually predictive of the ability of the PROTAC to degrade the target protein. Specifically, the ability of a degrader to form a ternary complex is quantitatively expressed by the cooperativity (α) value, which is defined as the ratio of binary *vs* ternary dissociation constants. Stable ternary complex features positive cooperativity ($\alpha > 1$), and generally, the higher is the cooperativity, the more favorable is the formation of the ternary complex over binary complex formation that results in higher degradation of the protein-of-interest.[101, 102]
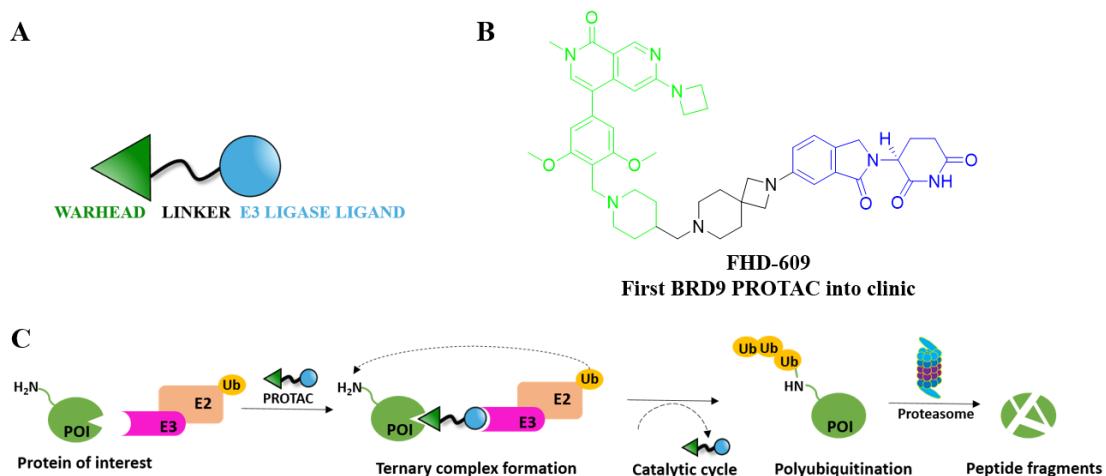
Figure 48. *A) Schematic representation of a PROTAC molecule. B) The first BRD9 PROTAC in Phase 1 clinical trial[103] reported as a representative example of the chemical functionalities of a PROTAC: the warhead is highlighted in green, the linker in black, and E3 ligase ligand in blue. C) Schematic representation of the mechanism of action of PROTACs.*

The emerging strategy of PROTAC-mediated protein degradation offers a range of potential advantages relative to traditional small molecule inhibitors that are hereinafter described.

- Increased cellular potency due to the catalytic effect. Generally, the activity of a typical inhibitor is driven by the maintenance of high target occupancy, which in turn requires high-affinity ligands and, from a clinical perspective, a high drug dose that is often associated with off-target effects. Conversely, PROTACs are not limited to this paradigm. The ability of a single degrader molecule to remove many molecules of a target protein underlies the potent activity at low concentrations of PROTACs. Hence, a low level of target occupancy may be sufficient to maintain a rate of protein degradation that quickly depletes the protein-of-interest from the cell. [104] This catalytic mode of action allows a potent activity of PROTACs at sub-stoichiometric concentrations. Thus, this effect can compensate for ligands presenting low affinity for the protein-of-interest or problems related to low cell permeability.

- Improved selectivity. One of the main achievements of traditional medicinal chemistry is the development of highly selective molecules in order to minimize off-target effects. PROTACs strategy offers the possibility to improve selectivity, even with the employment of non-selective ligands as a warhead.[105] Although the phenomenon has yet to be completely explained, recent works assessed that PROTAC linkers, as well as the recruitment of the E3 ligase, yield productive secondary interactions during the formation of the ternary complex that leads to increased selectivity.[106]

- Possibility to target the undruggable. Many proteins, although are appealing pharmacological targets, do not have a well-defined binding/catalytic site whose function can be blocked. On the other hand, other proteins present multiple catalytic domains or work together with other proteins in large complexes, and the blockage of only one may have partial or no efficacy. In these cases, the PROTACs strategy could offer a possible solution since they can recruit proteins *via* any binding site, which does not need to be the functional one. Moreover, the depletion of a single protein subunit could lead to the disruption of the function of the entire complex.[89]

- Potential to extend the pharmacodynamics duration of action. The targeted protein degradation is time-dependent and, generally, protein depletion mediated by PROTACs is faster than protein synthesis carried out by the cell.[104] This effect, combined with the catalytic activity of PROTACs, allows excellent knockdown of the protein levels driven by low dose and long administration intervals.[107]

However, despite the potential and the numerous advantages of this ground-breaking approach, nowadays PROTAC drug design is predominantly an iterative process, with structure optimization guided mostly by chemical intuition, due to the limited availability of ternary complex crystal structures. Hence, the necessity to identify a more systematic approach to drive PROTAC design is of critical importance.

3.1.2 The employment of BRD9 PROTACs in cancer therapy

In the last decades, there has been much devotion from the scientific community for the development of innovative therapeutic approaches in order to circumvent limitations of small molecules for cancer treatment (*e.g.*, the necessity of high target

occupancy, high selectivity). Moreover, a high number of proteins involved in cancer pathologies consist of multiple domains and the use of small molecules targeting specific subunits is often reflected in a phenotypic inefficiency.[94]

Among the newly explored technique in cancer therapy, the PROTACs strategy is certainly one of the most exciting. To confirm the targeted protein degradation success and the striking potential of this approach in tumor pathologies, in 2019, Arvinas Therapeutics started the first-ever clinical study of a PROTAC (ARV-110), which is an orally bioavailable degrader of the androgen receptor (AR) for the treatment of metastatic castration-resistant prostate cancer.[108]

In addition to nuclear hormone receptors, a great interest from the scientific community was also focused on the development of PROTAC degraders targeting epigenetic proteins, especially bromodomain. To date a large number of PROTACs have been developed for the degradation of these protein modules, with particular attention to BET proteins, BRD9, and SMARCA 2/4, [109-113] reporting promising outcomes in cancer therapies. The degradation of these epigenetic readers is very attractive since bromodomain inhibition, in contrast to genetic knockdown, has not always been associated with a phenotypic response. The critical limitation of bromodomain inhibitors arises from the fact that these epigenetic proteins typically contain multi-domain arrangements and are often part of multi-subunit complexes. Thus, as described previously, the blockage of a single catalytic activity or the disruption of a single interaction with a classical inhibitor may not lead to an effective outcome, since the many other activities and interactions will remain unaffected *via* such intervention.[114] As a matter of fact, potent and selective BRD9 inhibitors reported in literature yielded contradictory results, presenting modest bioactivity in interfering with tumor growth and proliferation. Recently, it has been demonstrated that albeit

chromatin occupancy of BRD9 is reduced in cells treated with inhibitors, some BRD9 proteins remain associated with chromatin. These findings confirmed that BRD9 associates with chromatin also independently of its bromodomain function, therefore traditional BRD9 inhibitors do not fully ablate oncogenic transcription (***Figure 49***).[87] On the other hand, BRD9 degradation induces downregulation of oncogenic transcriptional programs leading to a potent inhibition of cancer progression in mouse models (***Figure 49***).[87]
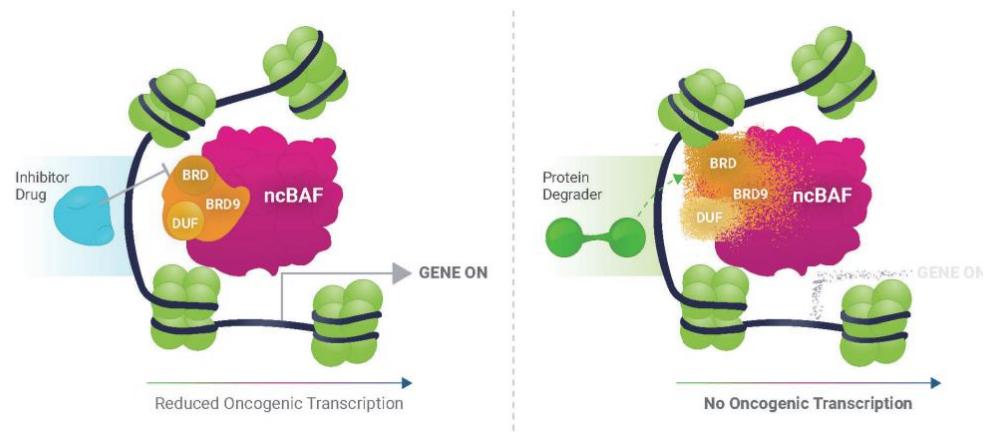
Figure 49. *Schematic representation of BRD9 inhibition vs degradation. BRD9 does not rely only on the bromodomain function to associate with chromatin.*

At present, FHD-609 (***Figure 48B***), developed by Foghorn Therapeutics, recently entered in Phase 1 to be tested in patients with advanced synovial sarcoma, representing the first BRD9 PROTACs to reach clinical trials.[103] Furthermore, in March 2022, another BRD9 degrader, CFT8634 developed by C4 Therapeutics, started phase I trials for the same form of rare sarcoma.[115]

In this scenario, considering the encouraging results coming from the scientific literature, we pursued this innovative technology designing and synthesizing potential PROTAC degraders targeting BRD9 based on our recently discovered triazoloquinoxaline binders (described in **CHAPTER 2**, **paragraph 2.3**).

3.1.3 Design, syntheses and biological evaluation of new BRD9 PROTACs based on triazoloquinoxaline compounds

3.1.3.1 Design of BRD9 PROTACs

To date, the design of efficient PROTACs is a laborious and often unguided process. Structure-activity relationship (SAR) studies are largely empirical and the design of new PROTACs still represents a bottleneck. Emerging evidences suggest that to maximize the opportunity for achieving potent degraders, it could be beneficial to develop parallel chemical series varying both linker length and chemical composition, and hijacking different E3 ligases.[110, 116] A critical role, it is mostly played by the linker, generally featuring alkyl or polyethylene glycol (PEG) units. Indeed, its length and chemical composition have been shown to have a great impact on PROTAC's rigidity, solubility and ternary complex cooperativity.[116] Hence, one of the major goals of PROTAC design is to make a wide linkers' diversification. Similarly, the choice of the E3 ligase ligand is critical for PROTAC activity. Around 600 different E3 ligases are encoded by the human genome,[117] with different cellular localization and expression, but only a few of them have been successfully employed for PROTACs design. Thus, a systematic and iterative approach is needed for the design and optimization of potent degraders. Given these premises, we initiated a PROTAC campaign designing a small set of degraders (**75-80**), shown in *Figure 50*.
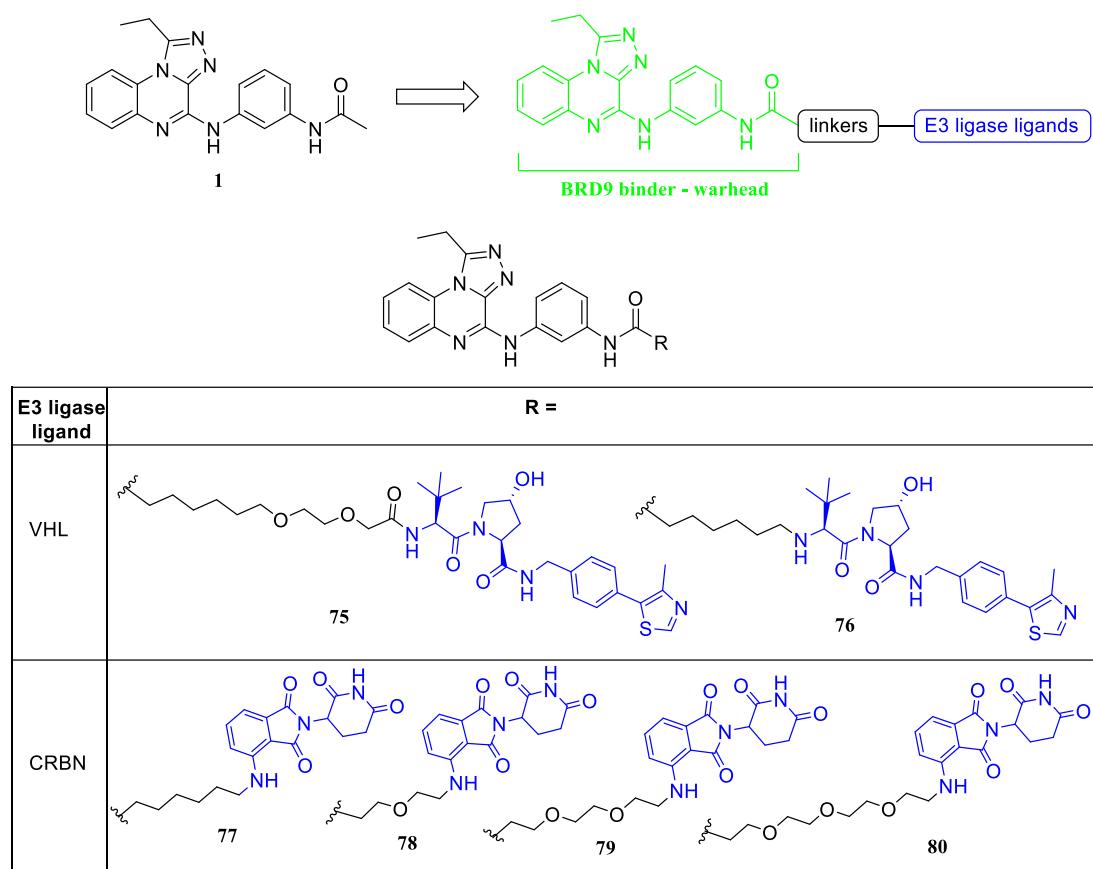
Figure 50. *Design of novel VHL- and CRBN-based PROTACs (**75-80**) presenting the potent and selective BRD9 binder compound **1** as warhead.*

Compound **1** (see **CHAPTER 2**, **paragraph 2.3.1**) was chosen as warhead on the basis of its remarkable affinity on BRD9 and selectivity over other bromodomain proteins. Structure insight of **1** binding mode into BRD9 pocket obtained through molecular docking (***Figure 51***), showed that the *N*-phenylacetamide moiety is solvent exposed and thus it has been exploited as exit vector to readily conjugate a linker *via* amide bond formation, without impairing the binding to the target protein. Linkers with different lengths and PEG units were chosen to sample enough chemical space and chemical properties; moreover, two well-known E3 ubiquitin ligases ligands were employed to generate this initial set of PROTACs: the von Hippel−Lindau (VHL) and cereblon (CRBN).
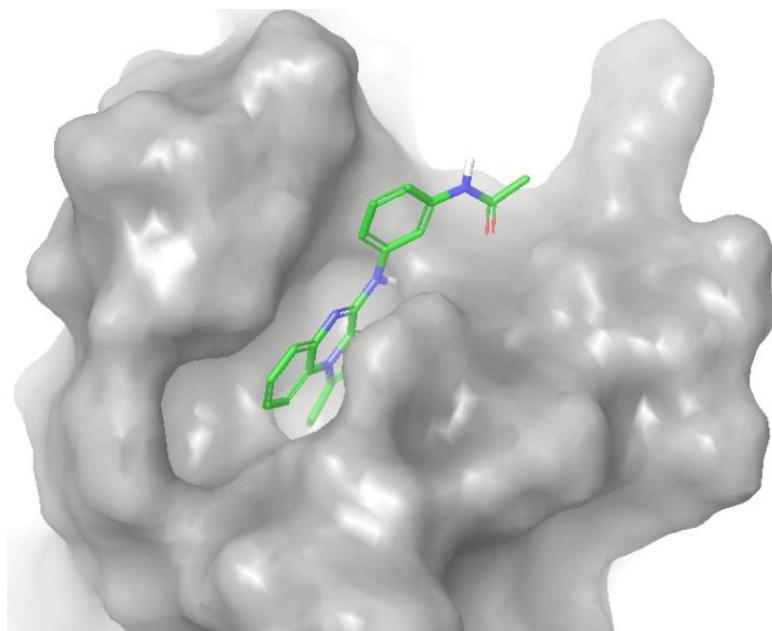
Figure 51. *Binding mode of compound **1** in the BRD9 binding pocket predicted through molecular docking experiments. The solvent-exposed N-phenylacetamide moiety has been used as exit vector for linker conjugation.*

3.1.3.2 Syntheses of the designed PROTAC compounds

Compounds **75-80** were then synthesized *via* an efficient synthetic protocol, shown in *Scheme 11*. The key intermediate triazoloquinoxaline core **1u** was obtained in high yields following the synthetic procedure described in **CHAPTER 2**, **paragraph 2.3.3**.[49] Compound **1u** was then conjugated on the primary amine functionality with commercially available building blocks, constituted by a linker and E3 ligase ligands, *via* amide bond formation using HATU as coupling reagent, yielding final compounds **75-80**. The detailed experimental section is described in **CHAPTER 6** (**paragraph 6.2**).
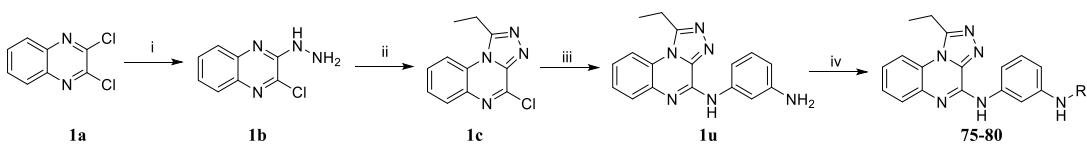
Scheme 11. *Syntheses of compounds 75-80. Reagents and conditions: i) NH₂NH₂,*
EtOH, 25 °C, 20h; ii) CH₃CH₂C(OC₂H₅)₃, r.t., 16h; iii) m-phenylendiamine, 110 °C
MW, 6 min, DMSO; iv) RCOOH, HATU, TEA, DMF, r.t, 1h.

3.1.3.3 Biophysical and biological evaluation of the synthesized PROTACs

At this point, it is essential to verify that the binding to the protein-of-interest is not affected by the linker conjugation to the warhead, thus binary binding affinity assay on BRD9 was performed. AlphaScreen confirmed the ligand-protein recognition of **75**, the first-synthesized compound of the series, which showed 10.1 ± 0.2 % residual binding of Histone H4 at 10 μM ligand concentration validating the goodness of the chosen vector point for linker conjugation.

Subsequently, in collaboration with Prof. Altucci's group from Università degli Studi della Campania Luigi Vanvitelli, **75** was biologically evaluated by Western blotting for the degradation activity in pro-monocytic human myeloid leukemia cell line (U937), that represents a powerful *in vitro* model for hematological studies. U937 cells were treated with compound **75** at 1 and 5 μM for 24 h, and the intracellular levels

of BRD9 were determined. Interestingly, **75** showed an evident degradation activity, demonstrating > 50% depletion of BRD9 at 5 μM (***Figure 52A***). We next assessed the impact of **75** degradation on the viability of U937 cells through Cell Counting Kit 8 assay (CCK8) which showed encouraging cytotoxicity (~30% residual viability) already at 5 μM after 24 h of treatment. Noteworthy, this initial *in vitro* evaluation confirmed an enhanced cytotoxicity in pro-monocytic human myeloid leukemia cell line, which is the result of the degradation activity carried out by the PROTAC. Together, these data qualify compound **75** as a novel and promising degrader probe of BRD9 suitable for further biological investigations, such as the evaluation of BRD7 degradation.

At present, ongoing studies are evaluating the degradation profile for compounds **76-80**, and future dose-dependent degradation assay for the most promising degraders will be carried out.
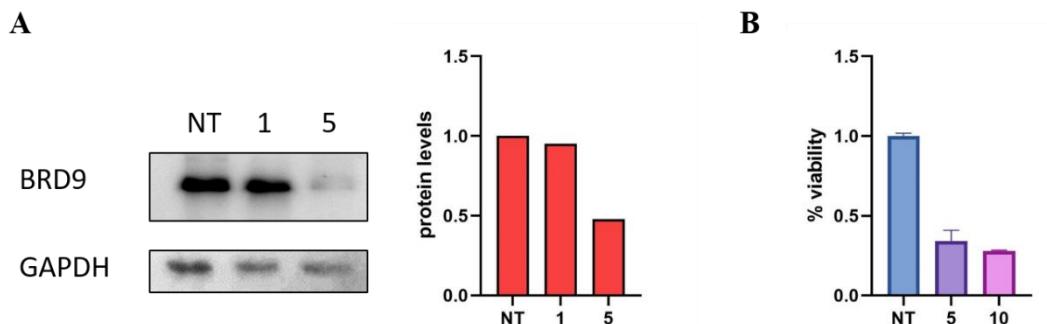
Figure 52. *A) Western blot and quantitative analysis monitoring BRD9 levels in U937 cells following treatment with compound **75** at 1 and 5 μM or DMSO (NT) for 24 h. B) Viability of U937 cells detected in CCK-8 assay after treatment with compound **75** at 5 and 10 μM or DMSO (NT) for 24 h.*

3.2 Design and synthesis of a SWI/SNF multi-target probe

3.2.1 Principles of polypharmacology: from combination therapy to a multi-target approach

For years, the modern drug discovery research has been focused on the design of highly selective compounds for a particular target. On the other hand, the combined use of multiple drugs acting on different protein targets simultaneously is commonly employed to treat several diseases, especially cancer and neurological disorders. Indeed, homeostasis and compensative effects are often exploited by cells resulting in an inadequate biological outcome of the single-target strategy.[118] For this reason, it is intuitive that the simultaneous modulation of more than one protein target is often necessary to achieve the desired therapeutic effect. This observation led, in 2006, to the origin of the so-called "polypharmacology" concept.[119] The exact definition of "polypharmacology" was established by the National Library of Medicine (NLM) in 2014 as "the design or use of pharmaceutical agents that act on multiple targets or disease pathways". Hence, this new concept encompasses two different possibilities: multiple drugs binding to different targets, or a single drug binding to multiple targets within a specific biological pathway. However, it is important to underline that the polypharmacology category is a purposeful approach to target more than one protein in a given biological pathway, and it differs from the so-called "promiscuous compounds" that unintentionally modulate a wide spectrum of diverse proteins and, therefore, are responsible for several adverse reactions.[120] Multi-target compounds are often also termed "hybrid molecules"[121] since they contain a combination of two, or more than two, domains with different biological functions, that ideally work synergistically as distinct units on different biological targets. Generally, the two

domains are joined together through a linker that could be cleavable in a cell environment or also non-cleavable.[122]

Over the last ten years, the so-called multi-target drug (MTD) approach has received increasing interest from the scientific community due to the significant benefits that this technology could offer and the opportunity to design more potent and efficacious compounds. In this regard, epigenetics-based polypharmacology could represent one of the most innovative approaches to future anticancer drug discovery campaigns, highlighting the advantages of this new generation of compounds.[123]

3.2.2 Epigenetic multi-target compounds

At present, in the field of the epigenetic-based polypharmacology, there are several compounds under investigations featuring fused or linked ligands that benefit from the synergistic effect of the multi-target approach. Hence, the combination of multiple compounds, especially in cancer therapy, should in principle have a lower risk of drug-drug interactions and drug resistance compared to the classical drug cocktails employed in chemotherapy.[124] Moreover, in epigenetic therapies, the crosstalk and complexes formation that occur between epigenetic modifiers, could be circumvented with the application of the polypharmacology approach.

Nowadays, a number of epigenetic multi-target compounds showed promising biological outcomes, and most of them are hybrid molecules containing a histone deacetylase (HDAC) inhibitor fused or linked to another anticancer compound acting on a different target. The reason underlining the popularity of HDAC inhibitors combined in dual agents it is mostly due to the extensive studies in the last 15 years that led to the availability of a multitude of high-affinity HDAC inhibitors. Moreover, a plethora of co-crystal structures of compounds in complex with HDAC facilitated

the identification of the portion of the molecule protruding from the active channel that could be exploited for the linkage to form the dual compound. Noteworthy, Curis developed two dual compounds that reached clinical trials, presenting HDAC inhibitors in combination with compounds targeting different proteins.[125, 126] Another interesting example, it is the design by GlaxoSmithKline of a dual HDAC/BET inhibitor that showed potent cellular activity in both immune and cancer cells, although no synergistic effect was observed after cellular treatment.[127]

On these bases, we considered of interest to deepen the above-described multi-target epigenetic approach studying the yet unexplored effect of a dual action of a BRD9 ligand in combination with another compound that exerts its biological activity within the SWI/SNF chromatin remodeling complex: SMARCA4.

3.2.3 Design, synthesis and preliminary biophysical evaluation of the first multi-target probe targeting BRD9 and SMARCA2/4

3.2.3.1 Design of the BRD9 and SMARCA2/4 multi-target probe

In the last few years, a number of high affinity and selective BRD9 binders (such as LP99[41] and I-BRD9[40]) have been disclosed. However, although they are able to inhibit the binding of BRD9 to chromatin, have not shown a significant alteration of cell proliferation in leukemic cells. The lack of a strong pharmacological efficacy is probably due to different protein interaction domains or to a combination of interaction domains that are able to anchor the SWI/SNF complex to specific sets of chromatin sites, independently from BRD9. This hypothesis has been recently supported also by a similar behavior shown by selective SMARCA2/4 inhibitors, such as PFI-3.[73] In order to circumvent the described issues and to investigate the interplay between complex subunits, in addition to the development of PROTACs (described in

paragraph 3.1), we conceived a previously unreported multi-target probe with the aim to disrupt, through a single chemical entity, the activity of the SWI/SNF ncBAF complex acting on two different subunits: BRD9 and SMARCA4 (**Figure *53***).[27] Remarkably, the mammalian SWI/SNF complex plays a pivotal role in human malignancies, since its components are mutated in 19.6% of all human tumors.[4] For this reason, the development of a bifunctional binder, designed for targeting two subunits of the same remodeling complex, could represent a new promising strategy.
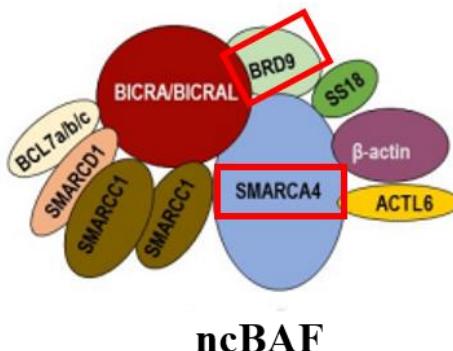
Figure 53. *Schematic representation of the ncBAF SWI/SNF chromatin remodeling complex. BRD9 and SMARCA4 subunits are highlighted in a red box.*

With this aim, we designed compound **81** (**Figure *54***), in which two known ligands for two different target subunits of the ncBAF complex have been linked together to form a hybrid molecule. Specifically, careful consideration of structural biology and chemical tractability led us to focus our efforts on the design of a chimeric molecule consisting of BI-7273,[42] a well-known BRD9 ligand markedly superior as BRD9 chemical probe over other ligands, in combination with SMARCA^BD, a high-affinity ligand for the ATPase SMARCA2/4 subunits.[128] It is important to note, that SMARCA2/4, as well as BRD9, are proteins whose activity in acute myeloid leukemia (AML) is essential to maintain the oncogenic transcription program and drive proliferation.[129]
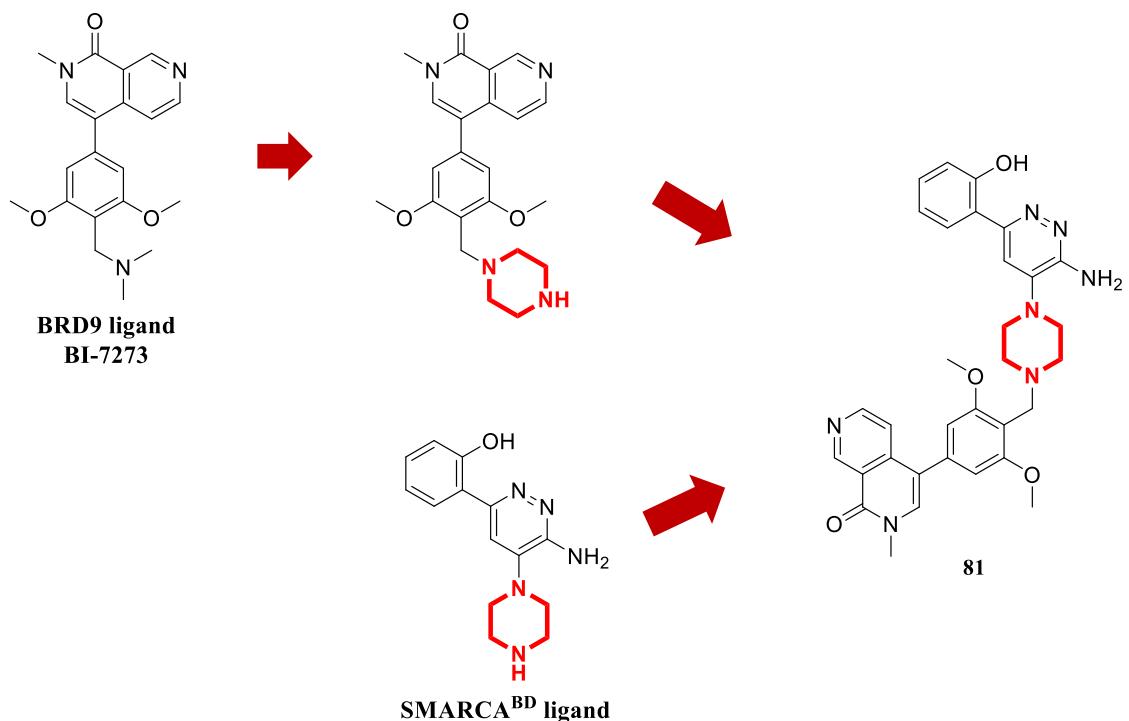
Figure 54. *The rational strategy applied for the design of compound **81**, the first SWI/SNF multi-target probe targeting BRD9 and SMARCA2/4.*

Great efforts had been applied by the scientific community to discover SMARCA inhibitors, so we focused our attention on the compound SMARCA[BD] which has been reported to possess robust SMARCA2/4 binding.[111, 128] Moreover, this choice was also strongly supported by its low molecular weight and the availability of the co-crystal structure of SMARCA[BD] in complex with SMARCA2. This structural information aided the rational design of the dual compound, identifying the piperazine group as the portion of the molecule protruding from the binding site suitable for the conjugation with the other ligand. At the same time, the co-crystal structure of compound BI-7273 with BRD9 showed the dimethylamine group as a solvent-exposed moiety, suggestive of a suitable vector for the linkage with the SMARCA ligand. For this reason, the dimethylamine group of BI-7273 was replaced by a piperazine group in order to

provide a convenient isosteric handle for the conjugation with the SMARCA[BD] ligand, which also displays a piperazine ring protruding out into the solvent (***Figure 54***).

3.2.3.2 Synthesis of the multi-target compound 81

After a careful retrosynthetic analysis, the designed hybrid compound **81** was synthesized as reported in (**Scheme** *12*). Reductive amination between the commercially available **1v** and Boc-piperazine led to the formation, in high yields, of the intermediate **1w**, which was then cross-coupled with **1y** obtained by a previous methylation of the commercially available compound **1x**. The Boc-removal under acidic conditions gave the key intermediate **1z**.[110] At this point, **1z** was linked to 4-bromo-6-chloropyridazin-3-amine through nucleophilic substitution to obtain compound **2a**, which was finally coupled through Myaura−Suzuki cross-coupling to the commercially available (2-hydroxyphenyl)boronic acid yielding the desired hybrid compound **81**. The detailed experimental section is described in **CHAPTER 6** (**paragraph 6.3**).
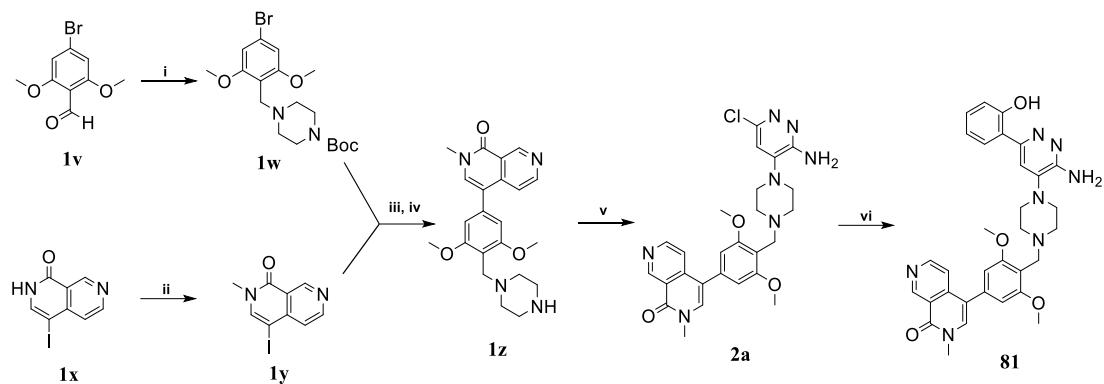
Scheme 12. *Synthesis of the multi-target compound* **81**. *Reagents and conditions: i) 1-Boc-piperazine, NaBH(OAc)$_3$, THF, TEA, r.t., overnight; ii) NaH, CH$_3$I, DMF, 0 °C, 5 h; iii) a.* **1w**, *B$_2$pin$_2$, KOAc, Pd(dppf)Cl$_2$, 1,4-dioxane, 140 °C MW, 40 min; b.* **1y** *and K$_2$CO$_3$ (aq) are added to step a., 120°C MW, 30 min; iv) DCM/TFA 1:1, r.t., 1h; v) 4-bromo-6-chloropyridazin-3-amine, DIPEA, DMSO, 100°C, overnight; vi) (2-hydroxyphenyl)boronic acid, Xphos-Pd-G3, K$_2$CO$_3$, dioxane/H$_2$O, 90°C, overnight.*

3.2.3.3 Preliminary biophysical assay and future investigations

Compound **81** was initially tested in AlphaScreen binding assay on BRD9 to assess that the structural variation applied to obtain the chimeric molecule did not compromise the binding to the protein. Not surprisingly, biophysical data performed by Reaction Biology Corporation revealed a good binding affinity for BRD9 (IC$_{50}$ = 3.34 ± 0.15 μM). At present, the evaluation of the binding to SMARCA4 is in progress, although we are quite confident that the structural modification did not affect the protein recognition since the same conjugation site has been used as exit vector for linkers attachment in a PROTACs campaign reported in the literature.[111]

The evaluation of the cellular response to BRD9 and SMARCA2/4 inhibition is currently in progress in a broad cancer cell line panel, in collaboration with Prof. Altucci's group (Università degli Studi della Campania Luigi Vanvitelli). Thus, the

investigation of the interdependencies between these two epigenetic subunits in the ncBAF complex and the possible synergistic effect of the dual inhibition will follow.

We are confident that this innovative and, up-to-date, unreported approach for a BRD9 ligand, could provide a useful chemical probe for elucidating the interplay between protein subunits belonging to the same SWI/SNF complex and, conceivably, open a new strategy for enhancing the pharmacological activity of these epigenetic proteins.

3.3 Investigation of BRD9 activity in regulating inflammatory responses

3.3.1 Inflammation and oncogenesis: a close connection

The connection between inflammation and cancer is a notion discovered in 1863 by Virchow, who was the first to assess that the sites of chronic inflammation are potential sources for cancer development. It is estimated that around 20% of cancers derive from a persistent inflammatory state, [130] hence the correlation between the two pathologies had been widely studied among academics and industries. A multitude of factors are responsible for neoplastic development and, one of the most important is an environment rich in inflammatory agents that potentiate and support tumor growth. The purpose of the inflammatory response is to repair and regenerate tissues that are exposed to injuries through increased cell proliferation. When the damage is repaired, proliferation is blocked and inflammation stops. In cancers, it has been observed that the proliferation of damaged cells persists in microenvironments of inflammation.[131] However, although the relationship between inflammation and cancer is broadly known, many of the molecular and cellular mechanisms underlying the development of cancer-related inflammation are yet not fully disclosed.[132]

During the inflammatory state, the recruited cells and factors play a crucial role in the defense of the damaged tissue. Notably, the control of the duration of the response is fundamental to avoid a long-lasting exposure to the inflammatory environment.[133] In the transition from tissue-damage to tissue-repair, both pro-inflammatory and anti-inflammatory mechanisms are involved since, for the maintenance of cellular homeostasis, it is crucial the correct balance between the promotion of the inflammatory state and its suppression. Hence, the removal of inflammatory cells from damaged tissues and the following resolution of the response is carried out by specific cells, especially macrophages, the main cellular component in chronic inflammation.[134] A dysregulation in the arrest of the inflammatory response causes the persistence of macrophages and other inflammatory-related cells in the cellular environment. This effect consequently leads to the production of growth factors, cytokines, and reactive oxygen species that may cause DNA damage. Moreover, the release of both the tumor necrosis factor-α (TNF-α) and the macrophage migration inhibitory factor (MIF), contribute to the accumulation of oncogenic mutations.[135] Altogether, these conditions clearly predispose to cancer development and its progression.[136]

On these bases, we decided to investigate a mostly unexplored BRD9 activity in regulating inflammatory responses, which is deemed of interest due to the evidence that this epigenetic reader plays an important role in regulating pro-inflammatory cytokine secretion.[5]

### 3.3.2 The potential involvement of BRD9 in inflammatory disease

For years, the scientific community mainly focused the attention on the important role that BRD9 exerts in cancer proliferation and development.[137, 138] However, recent

studies revealed broader biological functions of this interesting protein target also in pluripotency[139] and inflammatory responses,[140] making it a favorable target for therapeutic intervention.

In regard to inflammatory diseases, BRD9 emerged as essential for macrophages activation and the modulation of glucocorticoid responses. As a matter of fact, the inhibition, degradation, or genetic depletion of BRD9 in macrophages significantly attenuated their responses to both liposaccharides and interferon inflammatory *stimuli*.[5] These late findings revealed a potential for BRD9 ligands to increase the therapeutic efficacies of dexamethasone due to an overlap of the genes regulated by this epigenetic reader and the genes regulated by the synthetic glucocorticoid.

However, the putative activity that BRD9 inhibitors could have as anti-inflammatory agents is mostly unexplored. Compound LP99 is one of the few BRD9 ligands that has been investigated for its activity in regulating pro-inflammatory cytokine secretion.[41] Specifically, the influence of LP99 on the secretion of interleukin 6 (IL-6) was measured on human THP-1 monocytic cells stimulated with lipopolysaccharide (LPS) by an enzyme-linked immunosorbent assay (ELISA) (***Figure 55***). LP99 inhibited IL-6 secretion in a dose-dependent manner, demonstrating for the first time that BRD9 could act as a potential target for anti-inflammatory treatment.

The striking evidence that BRD9 is a genomic antagonist of the glucocorticoid receptor (GR) in inflammatory-related genes in macrophages and that BRD9 ligands could act as potential anti-inflammatory agents, pushed us to investigate this evidence further and explore the influence of some of our identified compounds, as described below.
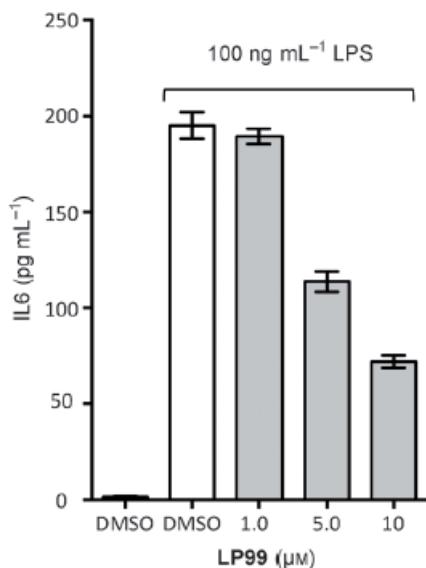
Figure 55. *LP99 inhibits the secretion of IL-6 in LPS-stimulated THP-1 cells in a dose-dependent manner.*

3.3.3 In vitro investigation of the anti-inflammatory activity of BRD9 inhibitors

With the aim to broadly explore the effect of BRD9 inhibition in cells, we decided to investigate the expression of pro-inflammatory cytokines after treatment with selected compounds. More specifically, we choose compound **1** (identified during this Ph.D. project and thoroughly described in **paragraph 2.3.1**),[49] **PUR-29** (a BRD9 inhibitor featuring the 9*H*-purine scaffold, previously reported by our research group),[43] and **I-BRD9** a well-known selective BRD9 inhibitor; [40] the chemical structures of the tested compounds are shown in *Figure 56A*.

For this purpose, in collaboration with Prof. Maione's group (from Università degli Studi di Napoli Federico II), J774 murine macrophages cells were stimulated with 10 μg/ml lipopolysaccharide (LPS), and the effect of the above-mentioned compounds at the concentration of 1 μM on the secretion of IL-6 and TNF-α was measured by an enzyme-linked immunosorbent assay (ELISA), using dexamethasone as control at 0.3

μM. Notably, TNF-α and IL-6 are key cytokines released during inflammatory responses, and it has been demonstrated that both are involved in most of the processes for cancer development acting as tumor promoters that modulate cellular proliferation, transformation, invasion, angiogenesis, and metastasis.[141, 142]
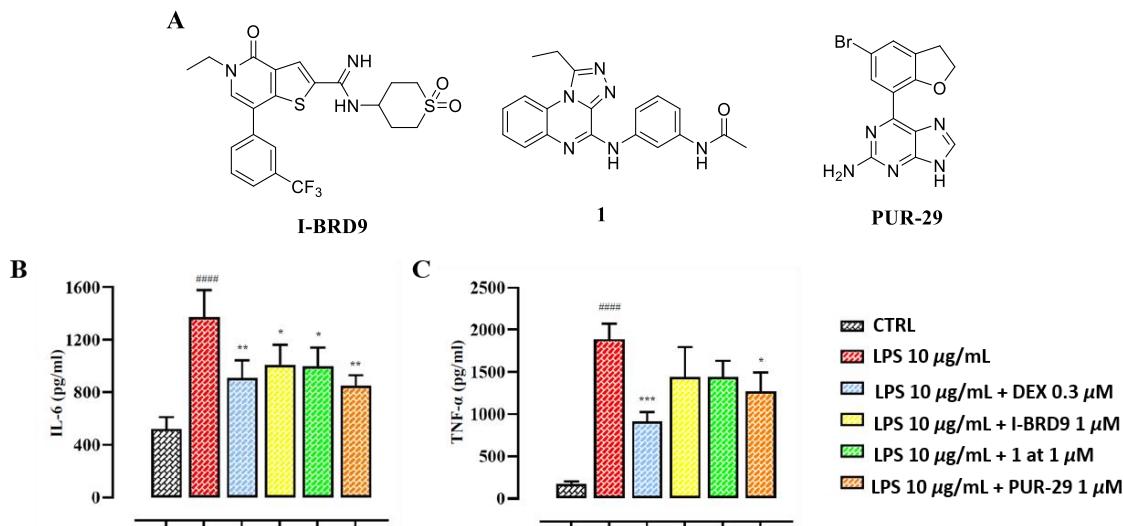
Figure 56. *Effect of dexamethasone (DEX), I-BRD9, 1 and PUR-29 on (B) IL-6, (C) TNF-α release under inflammatory conditions. Data were expressed as pg/ml and presented as means $\pm$ S.D. of 3 independent experiments. [####]P $\le$ 0.0001 vs Ctrl group, *P $\le$ 0.05, **P $\le$ 0.01 vs LPS. Statistical analysis performed by one-way ANOVA followed by Bonferroni's for multiple comparisons.*

Interestingly, as shown in **Figure 56**, all the tested BRD9 ligands inhibited IL-6 and TNF-α secretion from J774 cells already after 4 h, with a remarkable activity reported by **PUR-29** that emerged as the most potent among the tested compounds.

Encouraged by the results, we turned our attention to the evaluation of the release of TNF-α and IL-6 exerted by our identified PROTAC compound **75** (**Figure 57A**) that features as warhead compound **1** (described in **paragraph 3.1.3**). Treatment of J774 murine macrophages cells for 4 h with **75** at the concentration of 1 μM (**Figure 57**) revealed an enhanced anti-inflammatory effect when compared to the classical

inhibitor **1**, conceivably associated with BRD9 depletion in cells as demonstrated in previous Western blot assays (reported in **paragraph 3.1.3**).
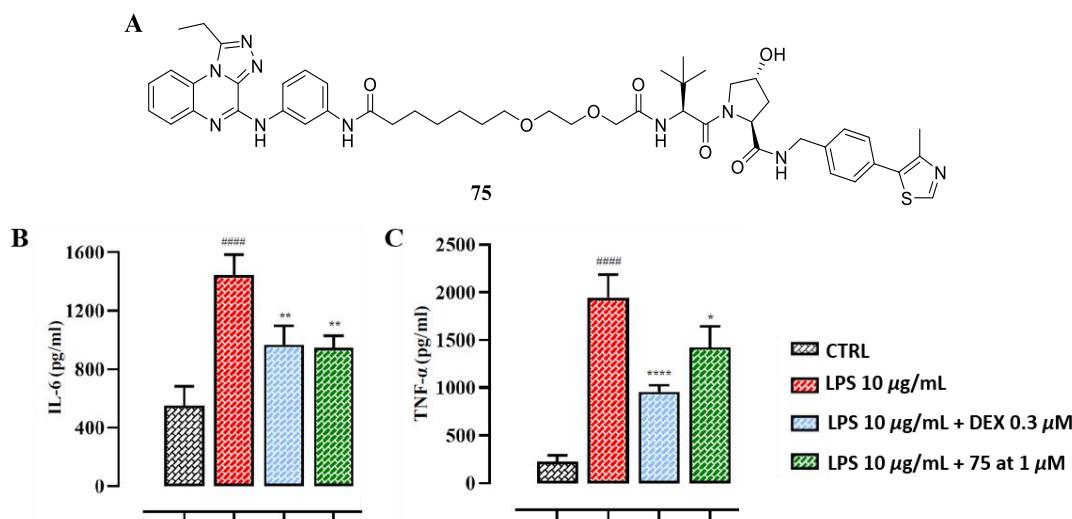
Figure 57. *Effect of dexamethasone (**DEX**) and **75** on (B) IL-6 and (C) TNF-α release under inflammatory conditions. Data were expressed as pg/ml and presented as means ± S.D. of 3 independent experiments. ####P ≤ 0.0001 vs Ctrl group, *P ≤ 0.05, **P ≤ 0.01 vs LPS. Statistical analysis performed by one-way ANOVA followed by Bonferroni's for multiple comparisons.*

The impressive outcomes highlighted **PUR-29** and **75** as the most potent compounds able to limit the inflammatory response by reducing the secretion of IL-6 and TNF-α from macrophages through the inhibition or the degradation of BRD9. Notably, these data disclose an additional therapeutic effect for our compounds able to disrupt the activity of this epigenetic reader, which will arouse great interest from the scientific community due to the close correlation between cancer and inflammation.

At present, our investigation is ongoing to further characterize the effect of the most promising compounds **PUR-29** and **75** on the secretion of a large number of cytochemokines.

Moreover, prompted by the obtained results and with the aim to maximize the promising biological effect obtained by the inhibitor **PUR-29**, we started the design of a new PROTAC degrader based on the 9*H*-purine scaffold.

3.3.4 Design and synthesis of a new BRD9 PROTAC based on the 9H-purine scaffold

Notably, the anti-inflammatory effect of the degrader **75** is enhanced when compared to the activity of the corresponding BRD9 ligand compound **1**. Thus, we considered of great interest the design of new PROTACs based on the 9*H*-purine scaffold of the ligand **PUR-29**, whose remarkable activity in reducing pro-inflammatory cytokines secretion has stood out together with the degrader **75**.

The lack of a co-crystal structure of **PUR-29** in complex with BRD9, led us to consider the high-affinity derivative **PUR-5a** as warhead for PROTAC design (*Figure 58*).[43] Indeed, comparable to **PUR-29**, **PUR-5a** showed a nanomolar affinity on the target of interest, and the available co-crystal structure allowed a careful ligand-protein inspection. The bromine function at the *meta* position was recognized as a solvent-exposed group not involved in interaction with BRD9 binding site, hence linker conjugation on this site should not affect ligand-protein recognition (*Figure 58*).
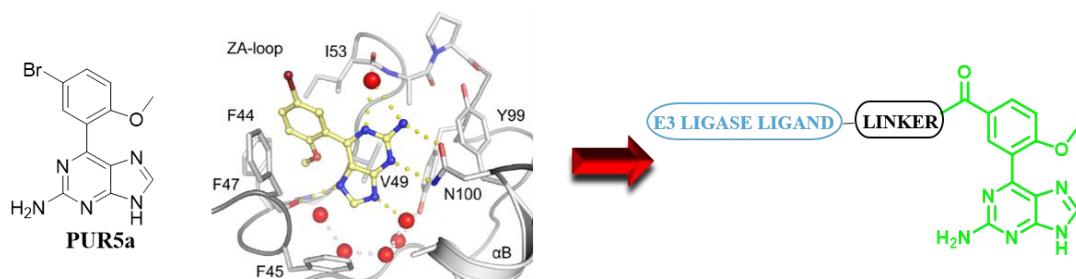
Figure 58. *Design of novel degraders based on 9H-purine scaffold ligands. The co-crystal structure (PDB: 4XY8) of* ***PUR-5a*** *in complex with BRD9 guided the choice of the exit vector for linker conjugation.*

For synthetic reasons, the bromine function of compound **PUR-5a** was replaced by a carboxylic moiety (***Figure 58***), providing a convenient isosteric handle for linker attachment. On this basis, we designed and synthesized the first PROTAC based on the 9*H*-purine scaffold as described in ***Scheme 13***. More specifically, the both commercially available 2-amino-6-bromopurine and 2-methoxy-5-carboxyphenylboronic acid were cross-coupled through an aqueous-phase Suzuki-Miyaura reaction to obtain the key intermediate **2c** in excellent yield. Compound **2c** was then conjugated on the carboxylic acid functionality with the commercially available building block **2d**, constituted by a linker with two PEG units and the VHL E3 ligase ligand, *via* amide bond formation using HATU and HOAt as coupling reagents yielding the final compound **82** in moderate yield. The detailed experimental section is described in **CHAPTER 6** (**paragraph 6.4**).
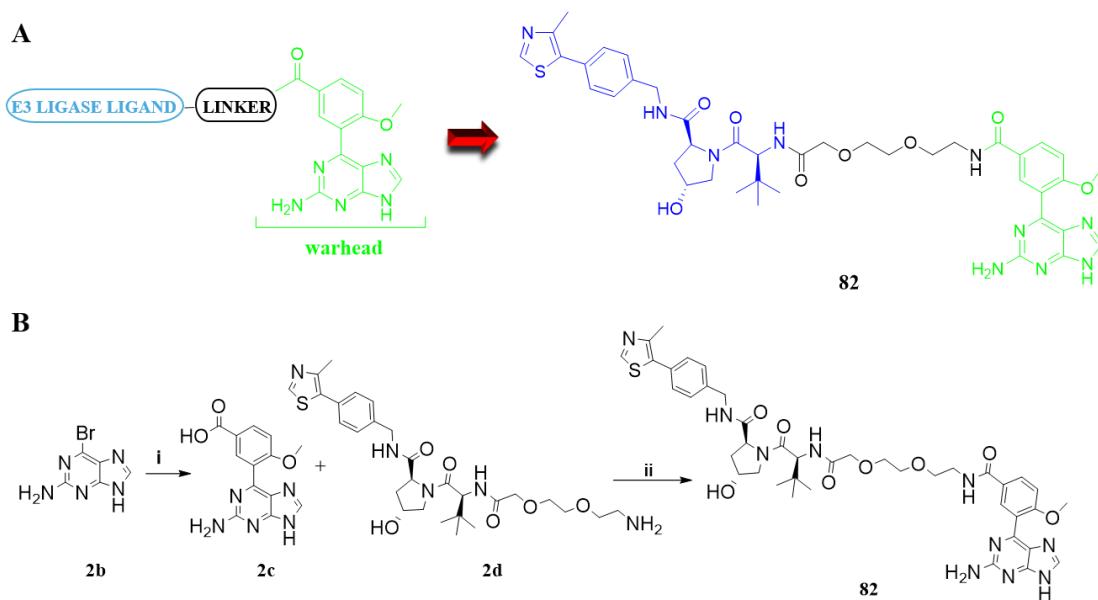
Scheme 13. *A) Design of the first purine-based PROTAC* **82** *for BRD9 degradation. B) Synthesis of compound* **82**. *Reagents and conditions: i) 2-Methoxy-5-carboxyphenylboronic acid, Pd(OAc)$_2$/P(C$_6$H$_4$SO$_3$Na)$_3$, Cs$_2$CO$_3$, CH$_3$CN/H$_2$O (1:2), MW, 150 °C, 15 min; ii) HATU, HOAt, DIPEA, DMF, 2h, r.t.*

At present, the syntheses of new purine-based PROTACs varying linker compositions as well as the E3 ligase ligands are ongoing, in order to enrich the collection with compounds presenting different chemical properties. In parallel, we are testing the ability of the first synthesized purine-based PROTAC **82** to bind BRD9 through AlphaScreen assay with the aim to assess the goodness of the chosen attachment point for linker conjugation. Finally, Western Blot to measure the potential degradation activity of the synthesized compounds will follow.

In the case of the discovery of new potent degraders, it will be interesting to evaluate both the anticancer and the anti-inflammatory activity of the new purine-based PROTACs and, above all, whether BRD9 degradation induces a more enhanced therapeutic effect when compared to the classical inhibition.

CHAPTER 4

# Effects of linkers and decreased VHL binding affinity on

LRRK2 PROTACs

4.1 Introduction

In the course of the third year of this Ph.D. project, I spent 6 months at the Centre for Targeted Protein Degradation (CeTPD) - University of Dundee (UK), under the supervision of Prof. Alessio Ciulli and Dr. Xingui Liu. During this period, I worked on promising small molecule degraders of Leucine-rich repeat kinase 2 (LRRK2) protein for the potential treatment of Parkinson's disease, focusing the study on two potent LRRK2 PROTACs recently discovered by CeTPD.[143] Herein, it is reported the project workflow, which was focused on two different but related topics: 1) molecular mechanism studies of the effect of linkers in the two LRRK2 PROTACs identified by CeTPD; 2) optimization of the degradation profile and pharmacokinetic properties of LRRK2 degraders. More specifically, thanks to the daily guide of Dr. Xingui Liu, and other members of the Ciulli's group (*i.e.*, Dr. Alena Kroupova for the crystallography, and Dr. Zoe Rutter for the Isothermal Titration Calorimetry), I took part to every scientific investigation herein described.

4.1.1 Leucine-rich repeat kinase 2 (LRRK2) in Parkinson's disease

Parkinson's disease (PD) is a progressive neurodegenerative disorder responsible for both motor (*e.g.*, bradykinesia, rigidity, postural instability, tremor) and non-motor (*e.g.*, memory loss, hyposmia) disabilities, but also for shortening life expectancy.[144] It is the second most frequent neurodegenerative disorder after Alzheimer's disease, and, according to the Global Burden of Disease study,[145] PD is the fastest-growing neurological disorder that has exponentially increased over the last 15 years. To date, around 10 million people worldwide are living with this pathological condition, and some specific factors (*e.g.*, aging, increasing longevity) fuel the incidence in the population, which will lead the possible burden of Parkinson's to 17 million by 2040

(*Figure 59*).[146] These data clearly suggest that, nowadays, PD is a major health problem. Hence, the scientific community is highly motivated in the research of novel therapeutic approaches for Parkinson's disease, since the most up-to-date therapies are limited to motor symptom management with dopamine replacement or by enhancing the activity of the remaining dopaminergic neurons.
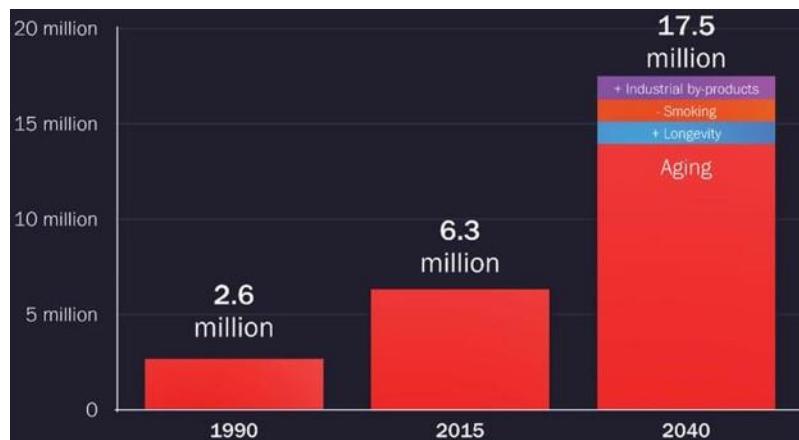
Figure 59. *Projected global burden of Parkinson's disease.[146]*

Although the cause of Parkinson's remains unknown, in the last few years significant steps have been made in understanding the pathological mechanisms underlying the disorder, contributing to the discovery of new potential therapeutic targets.

More than 20 genes have been identified to be associated with the onset and progression of PD, highlighting leucine-rich repeat kinase 2 (LRRK2) mutations as the most implicated in the pathogenesis of both familial and sporadic PD.[147, 148] LRRK2 is a large protein that includes several domains and motifs involved in protein-protein interactions (*Figure 60*). Very recently, much progresses had been made in deciphering the structure of the full-length LRRK2 (*Figure 60*) using single-particle cryo-EM, which aided the elucidation of the architecture and interdomain interactions.[149]
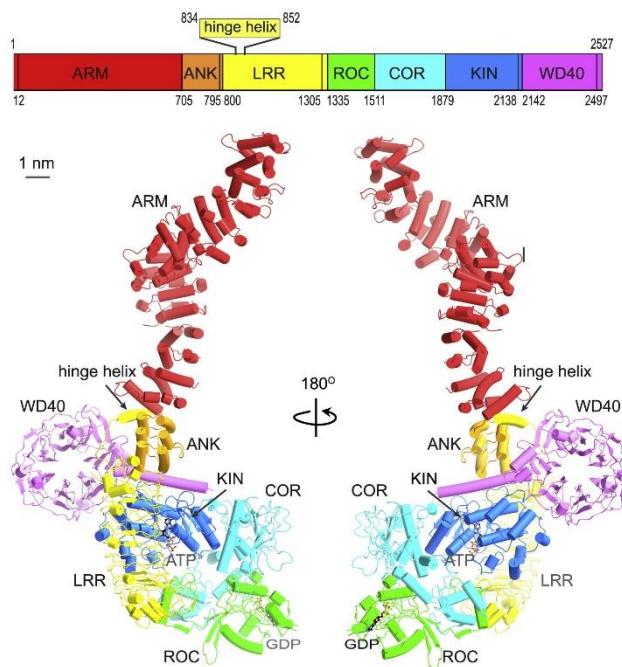
Figure 60. *Domain scheme of LRRK2 (top) and architecture of the full-length human LRRK2 monomer (bottom) elucidated through cryo-EM.[149]*

Studies have identified numerous pathogenic mutations in LRRK2: among these G2019S, a missense mutation Gly2019Ser, is the most common in LRRK2-related PD patients,[150] responsible for the hyperactive kinase activity of the protein that eventually leads to pathogenic hallmarks associated with the pathological condition. However, independently from LRRK2 mutations, an increased LRRK2 kinase activity has also been found in idiopathic PD patients.[151] These observations clearly suggest that LRRK2-targeting is one of the most promising therapeutic interventions for PD.

4.1.2 Proposed therapeutic strategies for targeting LRRK2

Over the past years, different LRRK2-targeting strategies have been proposed and are currently under active investigation.

The attention had been initially focused on the design of ATP-competitive type 1 LRRK2 kinase inhibitors and the development of selective LRRK2 inhibitors started in 2011 thanks to the work of Deng *et al.* that led to the discovery of the first selective

ligand (LRRK2-IN-1).[152] Subsequently, several new selective LRRK2 inhibitors were reported including HG-10-102-01, which represents the first blood-brain barrier (BBB) penetrant LRRK2 inhibitor, fundamental for the eventual clinical development.[153] The intense research activity lead to a big step forward with the discovery of two compounds DNL201 and DNL151, manufactured by Denali Therapeutics, which represent the first two LRRK2 kinase inhibitors in clinical trials.[154] Interestingly, in both Phase 1 and Phase 1b, DNL201 achieved robust target engagement and it was well tolerated in healthy volunteers and patients with PD. Moreover high levels of cerebrospinal fluid (CSF) exposure were observed in both groups of patients.

Altogether, these data corroborate the therapeutic potential achieved with LRRK2 inhibitors and push for further development of LRRK2 inhibitors as a therapeutic modality for PD. However, there have been some concerns about the safety of ATP-competitive type 1 kinase inhibitors that, stabilizing the closed conformation of LRRK2, lead to dephosphorylation of Ser935 and other biomarker sites, LRRK2 aggregation, and mislocalization to microtubules.[155, 156] As a result, ATP-competitive type 1 kinase inhibitors may be responsible for side effects on lungs and kidneys observed *in vivo* studies in mice.[157, 158]

Nevertheless, there are plenty of proposed therapeutic strategies, under active exploration, for reducing the activity of LRRK2 that do not involve the use of classical ATP-competitive inhibitors. Hence, these most recent alternative LRRK2-targeting strategies include: antisense oligonucleotide (currently in a Phase 1 clinical trial),[159] G2019S mutation selective inhibitors,[160, 161] type 2 LRRK2 kinase inhibitors,[162] GTPase inhibitors,[163, 164] dimerization inhibitors,[165] and finally, LRRK2 proteolysis targeting chimeras (PROTACs).[143, 166-168]

Despite, three compounds targeting LRRK2 are already in clinical trials, there is still the necessity to fully understand the LRRK2 biology mechanism and to shed light on pathways upstream and downstream of LRRK2 signaling.

4.1.3 Identification of a potent and selective PROTAC degrader of LRRK2 by the University of Dundee

Thanks to a well-conducted and comprehensive medicinal chemistry exploration, the Centre for Targeted Protein Degradation (CeTPD) in collaboration with the Medical Research Council Protein Phosphorylation and Ubiquitylation Unit (MRC-PPU) and the support of Ono Pharmaceutical, has recently discovered a potent and selective LRRK2 PROTAC degrader, which qualified as a valuable chemical probe to study LRRK2 biology.[143]

More specifically, through the application of fine-tuned design, syntheses, and biological screenings, compounds **XL01126** and **XL01134** (*Figure 61*) emerged as potent and fast von Hippel-Lindau (VHL)-based degraders, featuring as LRRK2 ligand the type 1 kinase inhibitor HG-10-102-01. Intriguingly, despite the two PROTACs being epimers of each other (**XL01126** is the *trans* epimer while **XL01134** is the *cis*), this small difference in the stereochemistry of the linker gives rise to very different degradation profiles and different binary binding affinities to VHL.
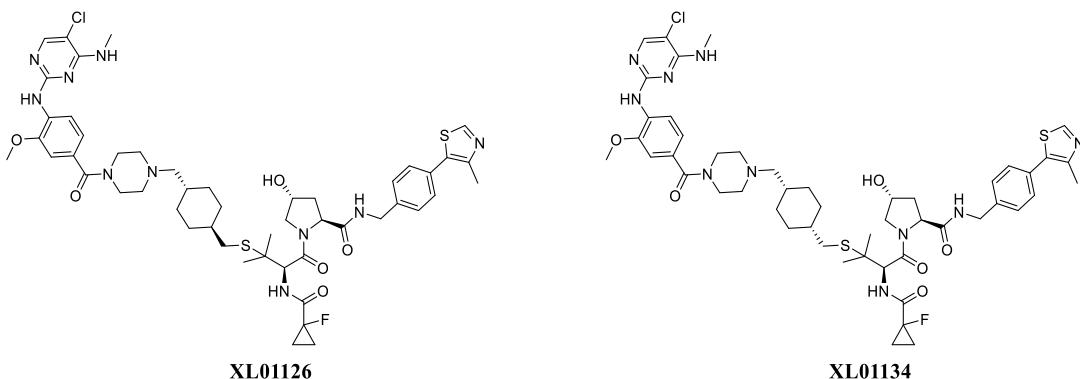
Figure 61. *Chemical structures of the degraders XL01126 and XL01134 identified by CeTPD and MRC.*

Hence, despite **XL01126** has >10-fold weaker binding affinity to VHL ligase than **XL01134**, as measured by Fluorescence Polarization binding assay (FP) (see ***Figure 62A***), dose-dependent and time-dependent degradation assays assessed that **XL01126** induces a more efficient and faster degradation of LRRK2, while **XL01134** showed a strong "hook effect" as demonstrated by the typical bell-shaped curve (***Figure 62B***). In line with the degradation potency, **XL01126** induces a more cooperative ternary complex as indicated by its positive cooperativity (α = 5.7), compared to the epimer

XL01134 which presents a significantly lower value ($\alpha = 1.4$), thus confirming that

the ternary binding affinity plays a critical role in the PROTAC-induced degradation.
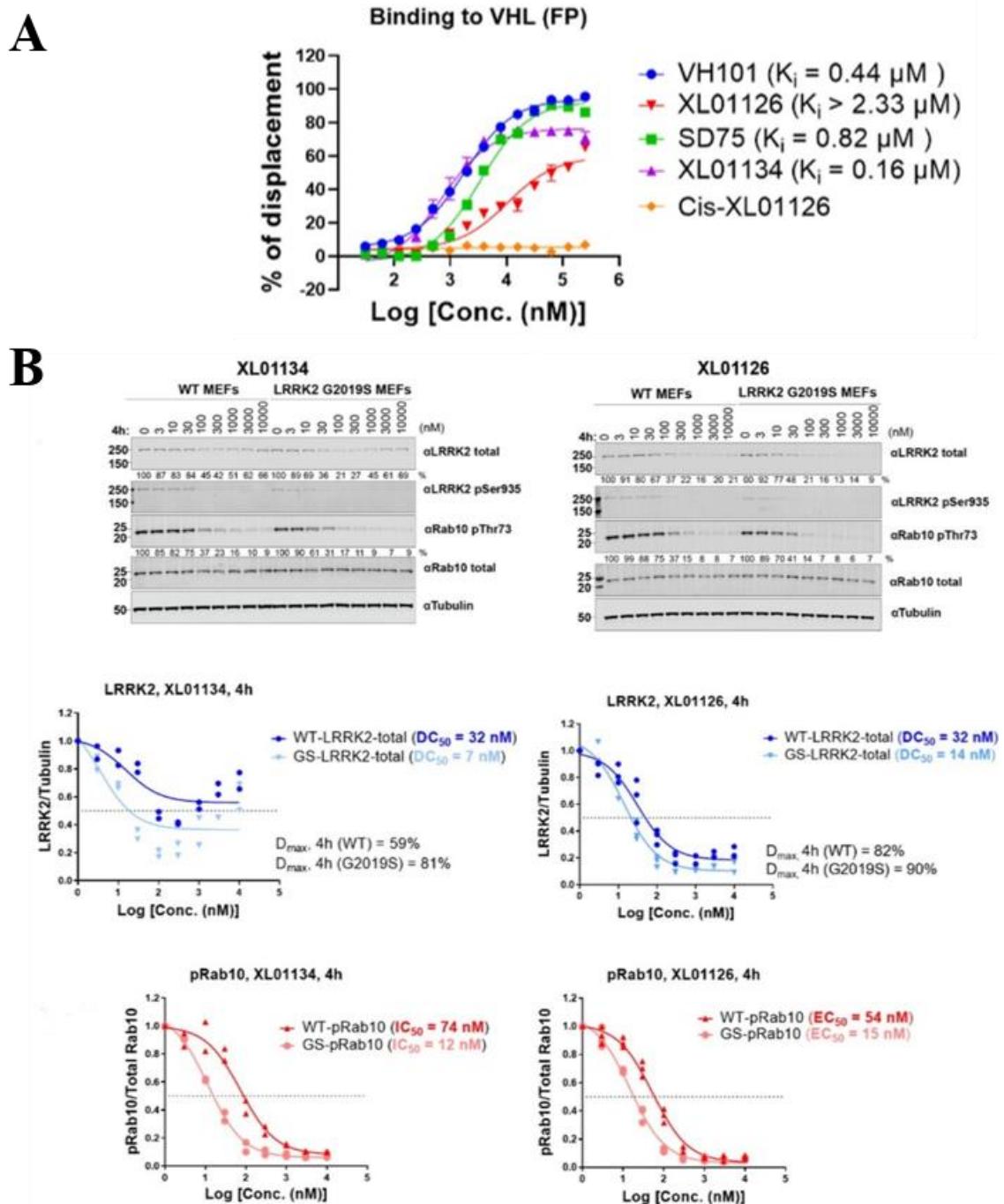
Figure 62. *A) Binary binding affinity (detected through FP assay) of the tested compounds to VHL reported in the manuscript (among these **XL01126** and **XL01134**). B) Dose-dependent LRRK2 degradation, LRRK2 dephosphorylation, and Rab10 dephosphorylation by XL01134 and XL01126 in Wild Type and G2019S LRRK2 Mouse Embryonic Fibroblasts (MEFs).*[143]

Further biological investigations assessed that **XL01126** is a potent degrader in multiple cell lines with a high cell permeability, orally bioavailable, and importantly, can penetrate the blood-brain barrier (BBB) after either oral or parental dosing in mice. Moreover, proteomic data corroborated that **XL01126** is a selective degrader, which does not degrade LRRK1 and other related proteins, nevertheless showed a low level of depletion (~30%) of phosphodiesterase 6δ (PDE6D).[143]

Altogether, these data qualified **XL01126** as a degrader probe for studying LRRK2 activity *in vitro* and *in vivo*.

4.1.4 Aims of the investigation carried out during the research visiting period

In the presented *scenario*, it is deemed of interest to investigate how the stereochemistry of the linker of **XL01126** and **XL01134** (*Figure 61*) affects greatly the binary binding to VHL and, at the same time, the ternary complex formation. Hence, a focused collection of compounds was designed and synthesized in order to thoroughly explore the molecular mechanism underlying the differences, between the two epimers, in both biophysical and biological outcomes. Thus, Fluorescence Polarization (FP) and Isothermal Titration Calorimetry (ITC) techniques were applied in this study in order to perform binary binding assays to the VHL protein and to investigate the effects caused by the stereocenter. Moreover, the structure determination of one of the designed epimers by X-ray crystallography, revealed a peculiar binding to VHL, suggesting the hypothesis that the binding mechanism is greatly affected by different conformer stabilities in the two stereoisomers.

In parallel, the promising biological outcomes observed with the *trans* epimer **XL01126** pushed for a medicinal chemistry optimization with the aim to achieve enhanced therapeutic performances improving the drug-like properties and, possibly,

the degradation activity and the ternary complex cooperativity. Thus, a small set of PROTACs, structurally related to **XL01126** and **XL01134**, was designed, synthesized, and biologically tested through Western blotting for the evaluation of the degradation activity.

**4.2 Molecular mechanism studies of the effect of linkers in compounds XL01126 and XL01134**

4.2.1. Design and syntheses of a small set of truncated derivatives

With the aim to explore how the stereochemistry of the cyclohexyl linker affects the binary binding to the VHL ligase, we started our investigation by designing and synthesizing three derivatives (*i.e.*, compounds **MP-1-21**, **MP-1-23** and **MP-1-39**, *Figure 63*) of the two identified PROTACs **XL01126** and **XL01134**. Specifically, compounds **MP-1-21**, and **MP-1-39**, similarly to the full-PROTACs, features the thioether VHL-ligand conjugated with the cyclohexyl linker (*trans* and *cis*, respectively), though lacking most part of the warhead in order to eliminate possible interferences in the binding due to the bulkiness of this moiety. Hence, the piperazine group, which is the terminal portion of the warhead, was replaced by a morpholine as a capping group. Whereas, compound **MP-1-23,** was designed considering solely the VHL-ligand substituted with a methyl on the thiol group.
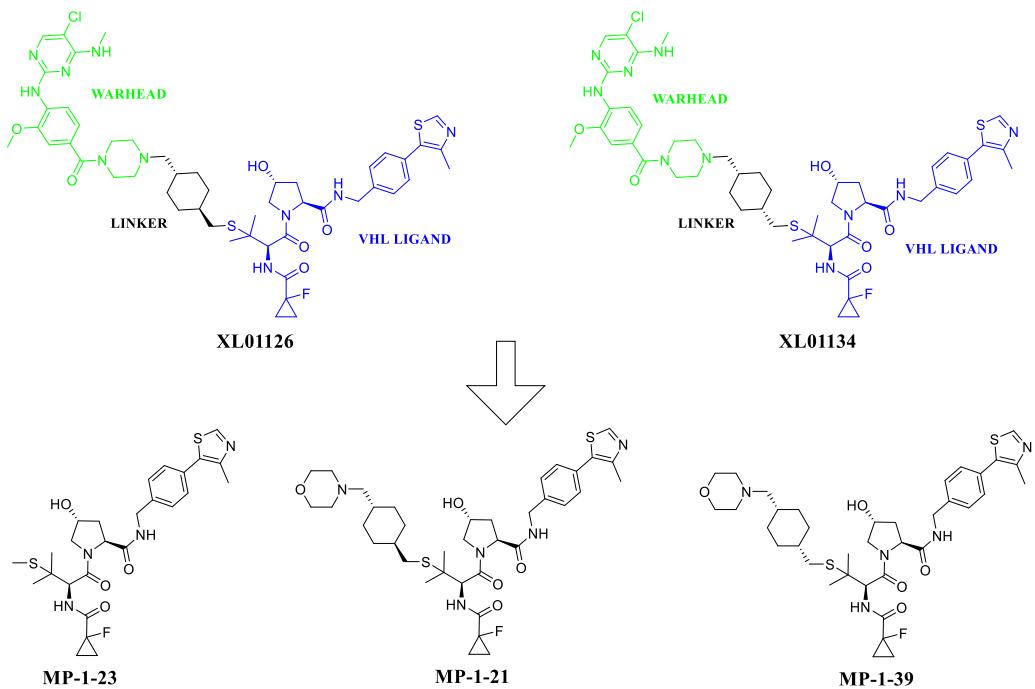
Figure 63. *Chemical structures of the designed MP-1-21, MP-1-23 and MP-1-39 deriving from warhead removal of the two degraders XL01126 and XL01134. In compounds XL01126 and XL01134, the three functional moieties of a PROTAC (warhead, linker and ligase ligand) are highlighted in different colours.*

The designed compounds were then synthesized *via* an efficient synthetic protocol. More specifically, the synthesis of the VHL ligand intermediate (**2k**), outlined in *Scheme 14*, was carried out with excellent yields by applying the synthetic procedure reported in the literature for compounds **XL01126** and **XL01134**.[143]
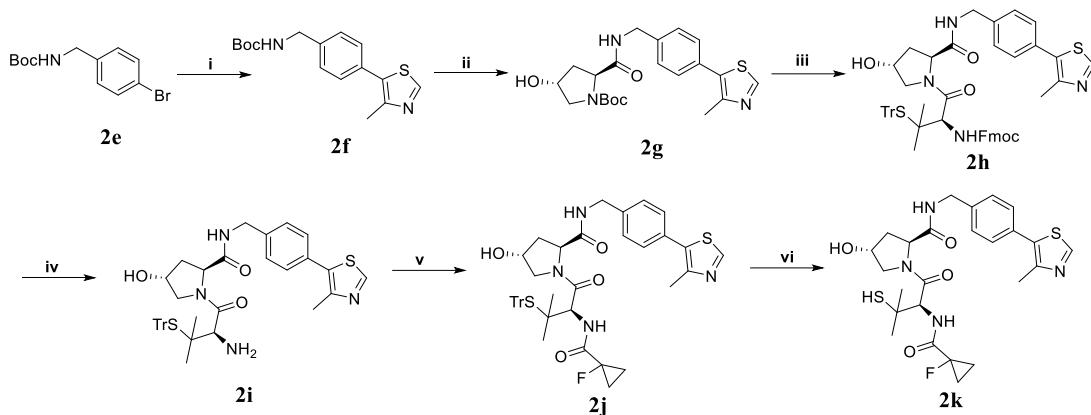
Scheme 14. *Synthesis of the VHL ligand moiety* **2k**. *Reagents and conditions: i) 4-methyl thiazole, Pd(OAc)₂, KOAc, DMA, 100 °C, overnight; ii) a. 2N HCl in dioxane and DCM, r.t., 1.5h, b. (2S,4R)-1-(tert-butoxycarbonyl)-4-hydroxypyrrolidine-2-carboxylic acid, HATU, TEA, DCM, r.t., 1.5h; iii) a. 2N HCl in dioxane and DCM, r.t., 1h, b. Fmoc-S-trityl-L-penicillamine, HATU, TEA, DMF, 0 °C, 1h; iv) Piperidine, DCM, r.t., 1h; v) 1-fluorocyclopropane-1-carboxylic acid, HATU, TEA, DCM, r.t., 1h; vi) TFA, triisopropylsilane, DCM, 0 °C, 10 min.*

Briefly, the commercially available compound **2e** was coupled with the 4-methyl thiazole through the Heck reaction to give compound **2f**. Subsequently, the cleavage of the *tert*-butyloxycarbonyl protecting group in acidic conditions and then the amide coupling with (2*S*,4*R*)-1-(tert-butoxycarbonyl)-4-hydroxypyrrolidine-2-carboxylic acid produced the intermediate **2g** with excellent yields. Then, deprotection of the Boc group and amidation with Fmoc-*S*-trityl-L-penicillamine at 0 °C afforded compound **2h**, of which the following Fmoc deprotection was carried out in basic conditions giving **2i**. Finally, compound **2i** was conjugated with 1-fluorocyclopropane-1-carboxylic acid using HATU as coupling reagent, yielding the key intermediate compound **2j**, which was converted into the final VHL ligand **2k** by deprotection of the trityl group after trifluoroacetic acid (TFA) treatment.

In parallel, the syntheses of both *trans* and *cis* linkers were carried out, as shown in *Scheme 15*.[143] Specifically, the commercially available *trans*-cyclohexane-dimethanol

2l was converted in high yields into the corresponding toluenesulfonate ester **2m**, which was then di-brominated using LiBr yielding compound **2n**. Finally, the mono-nucleophilic substitution with morpholine gave the key intermediate **2o** in moderate yield. The epimer **2t** was obtained through a similar synthetic procedure, starting from the commercially available *cis*-cyclohexane-dicarboxylic acid **2p**, which was converted into the corresponding dimethanol-derivative **2q** through reduction using borane dimethylsulfide. In the last step, the use of cesium carbonate as inorganic base did not improve the final yield that resulted very low, giving compound **2t** with 12% yield. It is not unlikely that either the replacement of the inorganic carbonate with other stronger bases or longer reaction times could considerably improve reaction yields. However, due to the short period of time that I spent at CeTPD, further optimization conditions were not investigated.
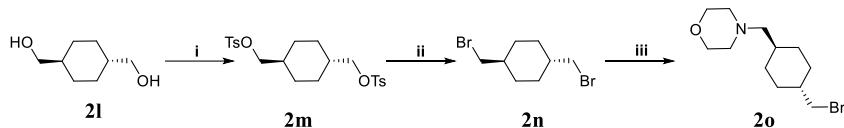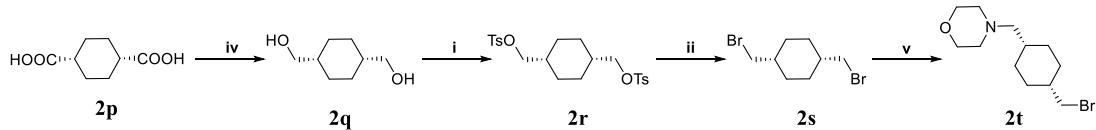
Scheme 15. *Syntheses of trans and cis linkers **2o** and **2t**. Reagents and conditions: i) TsCl, DMAP, TEA, DCM, r.t., overnight; ii) LiBr, acetone, reflux, overnight; iii) Morpholine, K₂CO₃, acetone, reflux, overnight; iv. BMS, THF, 0 °C, overnight; v) Morpholine, Cs₂CO₃, acetone, reflux, overnight.*

Finally, the desired compounds **MP-1-21**, **MP-1-23** and **MP-1-39**, were obtained through nucleophilic substitution of **2o** and **2t** with the thiol group of **2k** by use of DBU, yielding the corresponding thioether compounds, as described in *Scheme 16*.
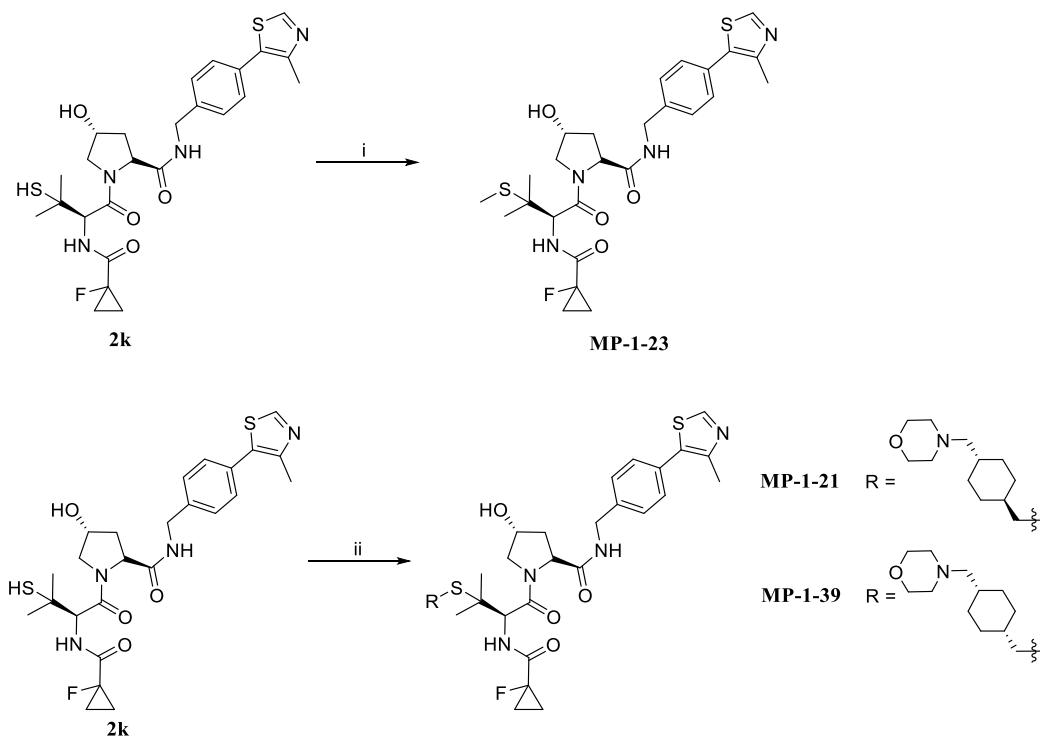
Scheme 16. *Syntheses of the final compounds **MP-1-21**, **MP-1-23** and **MP-1-39**. Reagents and conditions: i) CH₃I, DBU, DCM, r.t., 1h; ii) 2o or 2t, DBU, THF, r.t., overnight.*

In the final step of the synthesis of **MP-1-23**, the use of DCM appeared deleterious to the final yield (23%) probably due to an interference of the solvent in the nucleophilic reaction that, therefore, was replaced with THF for the syntheses of compounds **MP-1-21** and **MP-1-39**. Indeed, Liquid Chromatography - Mass Spectrometry (LC-MS) employed for monitoring the reaction, showed in the condition **i** (*Scheme 16*), the formation of a peculiar 15% byproduct not observed in the reaction carried out in THF, featuring ESI$^+$ m/z = 541.4 probably related to the $[M + 2H]^{2+}$ ion of the hypothesized byproduct structure showed in *Figure 64*. However, purification

and NMR structural characterization of such compound will be done to confirm the suggested structure.
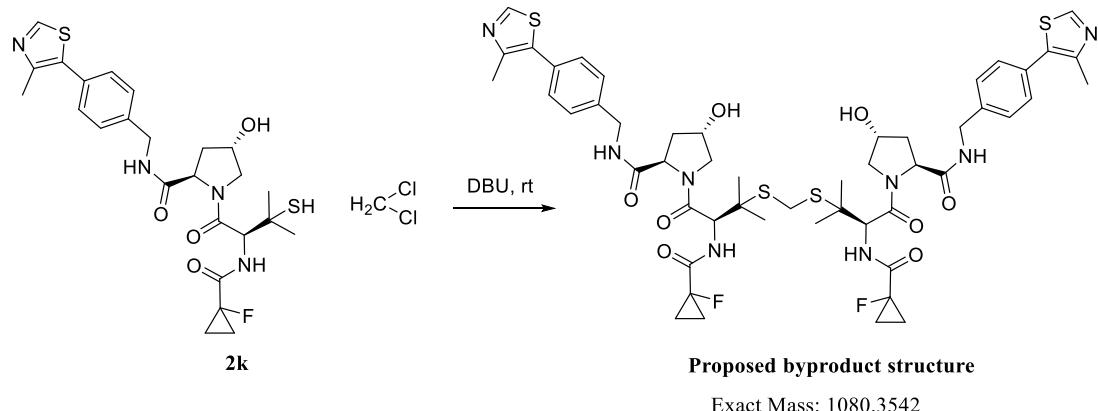
Figure 64. *Hypothesized formation of the obtained byproduct.*

The detailed experimental section for the syntheses of compounds **MP-1-21, MP-1-23**, and **MP-1-39** is described in **CHAPTER 7 (paragraph 7.1.2)**.

4.2.2 Evaluation of the binary binding affinity to VHL through biophysical binding assays

4.2.2.1 Fluorescence Polarization (FP) binding assay

The designed compounds **MP-1-21**, **MP-1-23** and **MP-1-39** were then tested for the evaluation of their affinities to the specific E3 ubiquitin ligase. Thus, the binary binding to the recombinant VCB protein (VHL complexed with elongin B and elongin C) was detected through Fluorescence Polarization (FP) competitive binding assay using VH101 as a positive control, and the full-PROTACs (**XL01126** and **XL01134**) for binding comparisons.

The fluorescence polarization assay is a biophysical technique that is commonly used in high-throughput screening (HTS) programs to quantitatively analyze the binding of a fluorescent molecule (or a molecule that competes with it) to a protein.

The assay relies on the principle that the degree of fluorescence polarization of a fluorescent compound is proportional to its rotational relaxation time. The interaction of the fluorescent ligand with the protein can alter its rotational relaxation time and, therefore, its polarization that is detected through plane-polarized light. Thus, the binding affinity of the fluorescent ligand for the protein can be quantitatively measured through the emission light, which could be: polarized (when the ligand is bound to the protein) or depolarized (in case the ligand is not binding) (see *Figure 65*).[169] In the PROTAC field, the FP technique represents a powerful tool to determine binary or ternary binding affinities and cooperativities, as shown in numerous published studies.[111, 170, 171] More specifically, in this study, the competitive FP assay was employed to detect the binary binding of the synthesized ligands (*e.g.*, **MP-1-21**, **MP-1-23** and **MP-1-39**) to VHL provided by the displacement from the protein of the FAM-labeled HIF-1α peptide (namely, JC9), used as the fluorescent probe.
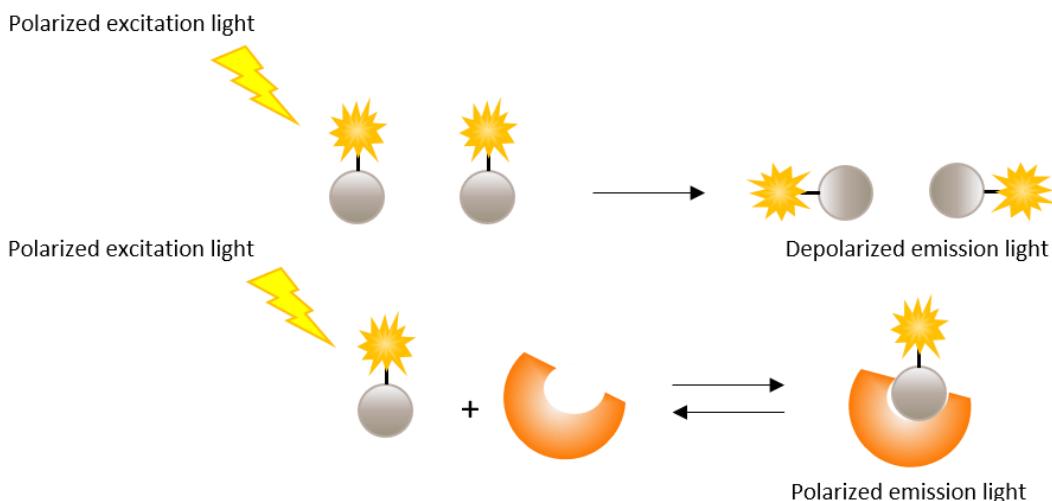

Figure 65. *Schematic representation of the mechanism of the fluorescence polarization (FP) assay.*

More in detail, 14 concentrations of the tested compounds were titrated to a solution of VCB protein and JC9 (a FAM-labeled probe that binds to VCB) to displace JC9.

The percentage of displacement was then calculated based on the ratio between the measured RFU (relative fluorescence units) value of the condition and the reference RFU value in the absence of displaced molecules, and plotted against the compounds' concentration and fitted into the "nonlinear regression, one site-log IC_{50}" to obtain the IC_{50} values, which were used to back-calculate the Ki values. The detailed experimental section related to FP experiments is described in **CHAPTER 7** (**paragraph 7.2**).

As shown in *Figure 66*, the *trans* compound **MP-1-21** has ~1.5-fold weaker binding affinity to VHL ligase than the *cis* epimer **MP-1-39**, confirming that the stereochemistry of the linker, although protruding out into the solvent and not apparently involved in the binding to VHL, greatly affects the binding to the protein independently from the presence or absence of the warhead.
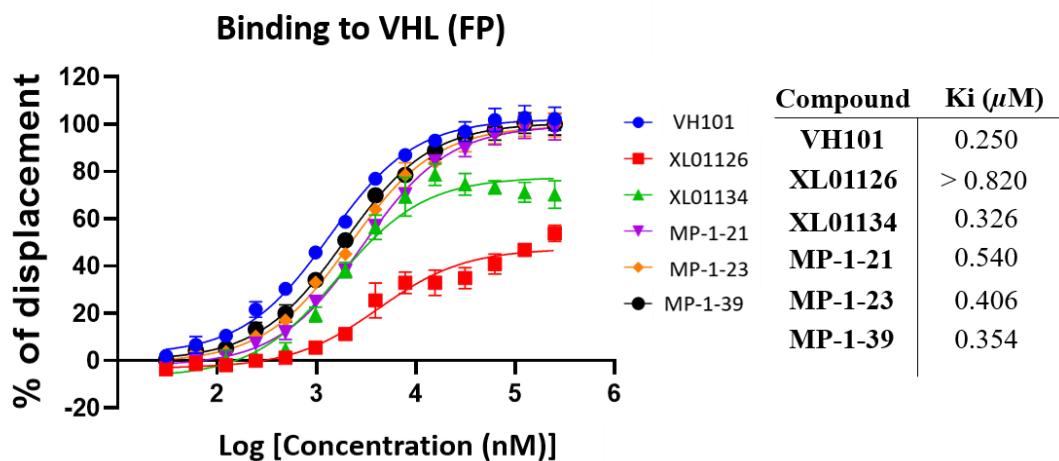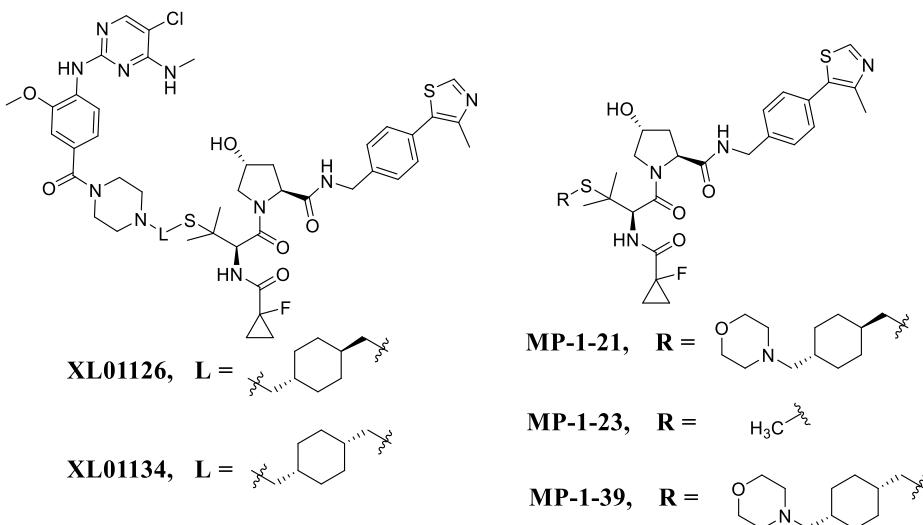
Figure 66. *Binding affinities of the tested compounds to VHL through FP assay. Data points are presented as mean $\pm$ SEM from three independent experiments.*

4.2.2.2 Isothermal Titration Calorimetry (ITC) assay

To further validate the data obtained by the FP assay for the two epimers **MP-1-21** and **MP-1-39**, Isothermal Titration Calorimetry (ITC) assay, that is a "gold-standard" technique for detecting direct binding equilibria, was also applied as orthogonal biophysical analysis.

ITC is a technique commonly used for the direct binding measurement of small molecules to larger macromolecules (*e.g.*, proteins). More specifically, through its

employment, important binding parameters can be determined in a single experiment, including the dissociation constant (K_d), binding stoichiometry (N), changes in enthalpy (ΔH), and changes in entropy (ΔS). This biophysical technique relies on the monitoring of the generation or consumption of heat (exothermic or endothermic processes, respectively) following the stepwise titration of a ligand solution into a calorimetric cell containing the protein solution (or the reverse). The analysis of the heat of the reaction mixture, as a function of the analyte concentration, provides a complete thermodynamic characterization of the binding event.[169]

Nowadays, in the PROTAC field, ITC represents an important tool to determine, both for binary and ternary complexes, the thermodynamic parameters and cooperativities of the degraders.

Thus, for our ITC experiment, 19 injections of VCB protein solution into the cell containing the ligand were performed. The analysis of each compound was done in a single experiment as, in our opinion, it represented sufficient data as an orthogonal assessment. The detailed experimental section related to ITC is described in **CHAPTER 7** (**paragraph 7.3**).

The obtained results (see ***Figure 67***) assessed a comparable trend of binding to those obtained by FP, reporting the *trans* compound as a 2.4-fold weaker binder of VHL than the *cis* epimer **MP-1-39**, confirming our previous assumptions.
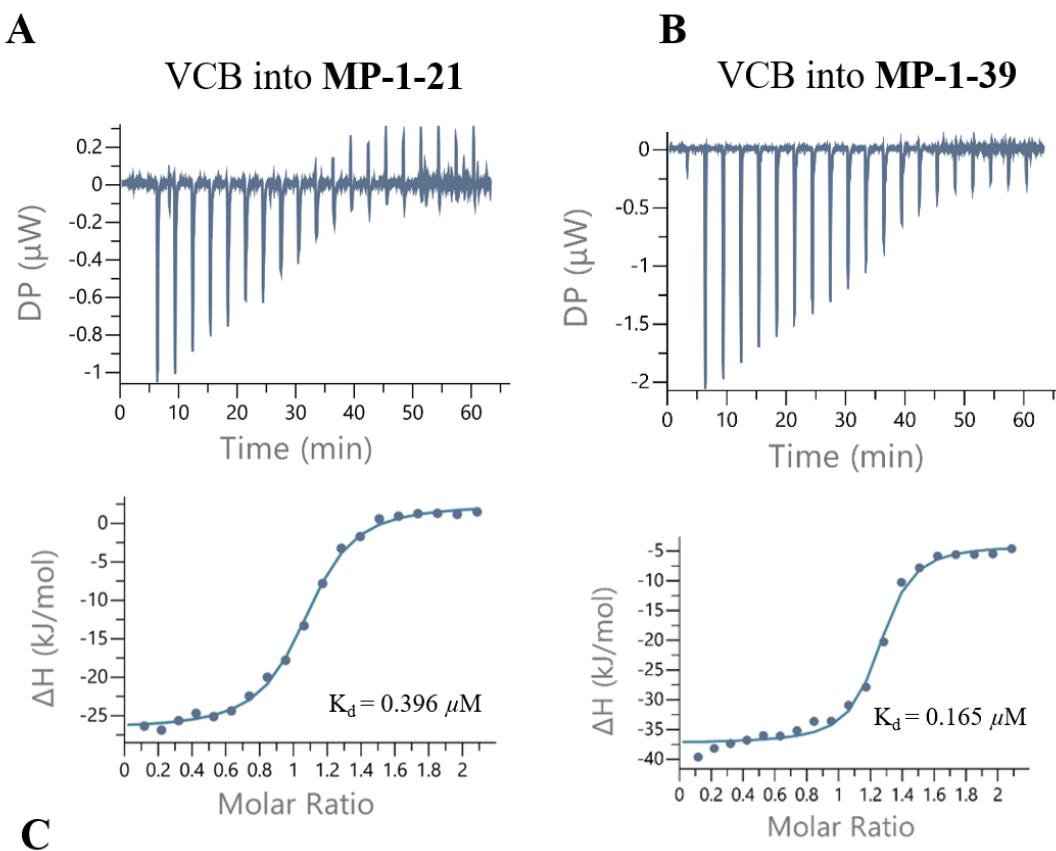

Figure 67. *Binary binding data measured by ITC A) Raw heat and Wiseman plots obtained by VCB titration into **MP-1-21**. B) Raw heat and Wiseman plots obtained by VCB titration into **MP-1-39**. C) Thermodynamic parameters related to each binary complex formation. All ITC titrations were performed at 25 °C.*

4.2.3 Structure determination of the binding mode of the two epimers: X-ray crystallography and future studies

The evidence that the two epimers are able to bind VHL ligase with different binding affinities and that this is mainly ascribable to the stereocenter in the cyclohexyl linker, motivated us to conduct a thorough structural characterization aimed to dissect the molecular basis underpinning these different binding modalities. Such understanding will be undoubtedly crucial for providing a guidance for future optimization campaigns. Hence, we attempted to crystallize compounds **MP-1-21** and **MP-1-39** with VHL pursuing both the soaking process and the co-crystallization method, in order to expand the crystallization space explored and, therefore, increase the chances to obtain high-quality diffraction data. Moreover, we considered of great importance the employment of both techniques to obtain a biologically relevant conformation of the ligand bound to the protein, thereby minimizing interference or artifacts from crystal packing.

The soaking approach is often the method of choice for the crystallization of protein-ligand complexes due to the high-throughput nature of the method leveraging existing crystal forms. In this technique, the compound is soaked into pre-formed crystals of the target protein crystallized in the absence of the ligand (*i.e.*, apocrystals) (***Figure 68A***).[172] Once the crystallization conditions for a specific protein have been established, many ligands could be quickly screened employing apocrystals of the same type, provided that the binding site of interest is accessible from solvent channels within the crystal. On the other hand, in the co-crystallization technique, the ligand is incubated with the protein prior to the formation of protein crystals (***Figure 68B***), thus the conditions often need to be optimized for each protein-ligand complex. For this reason, compared with soaking, the co-crystallization method requires more resources

and time. However, it is the best option when conformational changes occur as a result of ligand binding or crystal packing prevents ligand from accessing the binding site.[173] Moreover, differently from soaking, automated processes could be implemented.
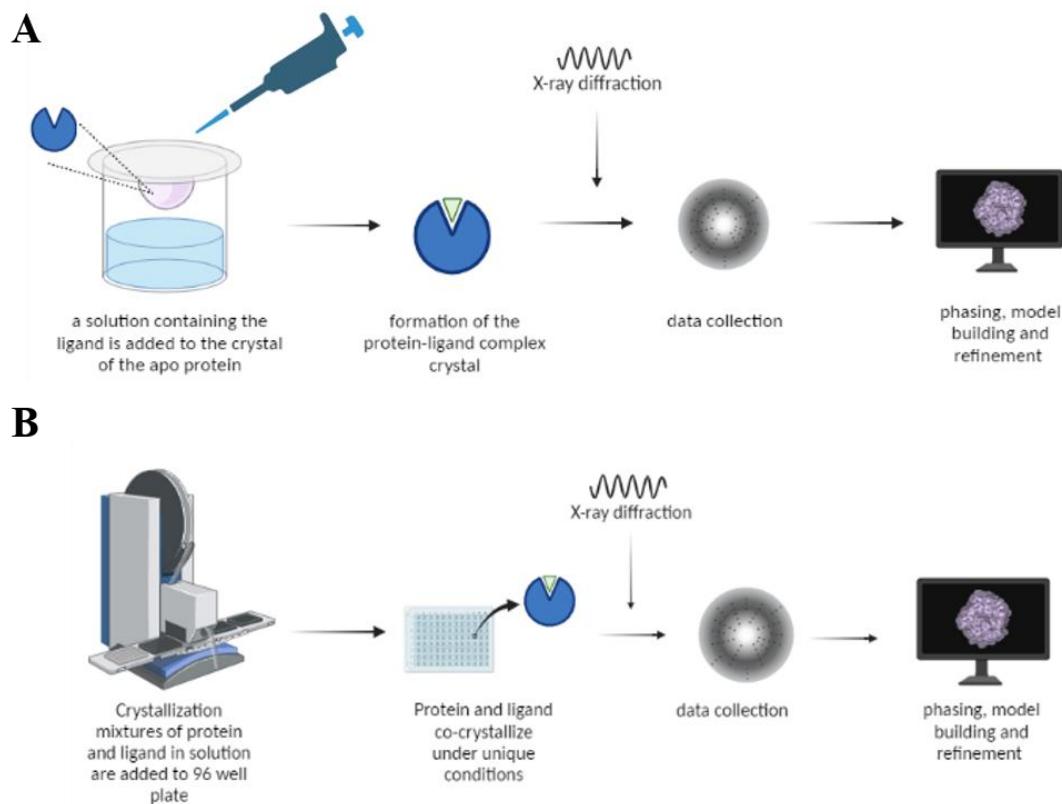
Figure 68. *Schematic representation of the two crystallization techniques employed in this study: A) Soaking approach; B) Co-crystallization.*

In our investigation, apo-VCB crystals for the soaking experiment were produced applying the crystallization conditions described in a previous work,[174] considering two protein concentrations (3 mg/mL and 5 mg/mL) while varying the pH of the buffer, the precipitant and salt concentrations. For the co-crystallization, we took advantage of an automated drop setting process (implemented by the Mosquito® SPT LabTech robot) for screening a large number of different crystallization conditions covering a wide range of pH, precipitants and salt additives. More specifically, four different and commercially available 96-well crystallization plates were used.

A total of 48 crystals were then harvested (selecting the ones with more appropriate shapes and dimensions), and diffraction data were collected at Diamond Light Source beamline. Finally, the structures were solved by molecular replacement, subjecting the initial model to iterative rounds of model building and refinement. The detailed experimental section related to X-ray crystallography is described in **CHAPTER 7** (**paragraph 7.4**).

The best diffracting crystal resulted from co-crystallization in a 2.0 Å structure of **MP-1-39** bound to VHL (see *Figure 69*), which showed a peculiar folding back of the cyclohexyl linker onto the VHL ligand anchored in the binding site, suggesting a favored conformer stability for the *cis* compound. The H-bonding interactions of the VHL warhead are conserved with respect to the usual binding network of VHL ligands, and no new direct interactions are formed that would be thought as instrumental in stabilizing the back-folded conformation of the linker.

Conversely, no good-quality diffraction data suitable for structure determination were collected for the *trans* compound **MP-1-21**, suggestive of a strikingly different binding mode. At the moment, at the University of Dundee, different co-crystallization methods and conditions for compound **MP-1-21** are under exploration with the aim to improve the diffraction resolution of these crystals.
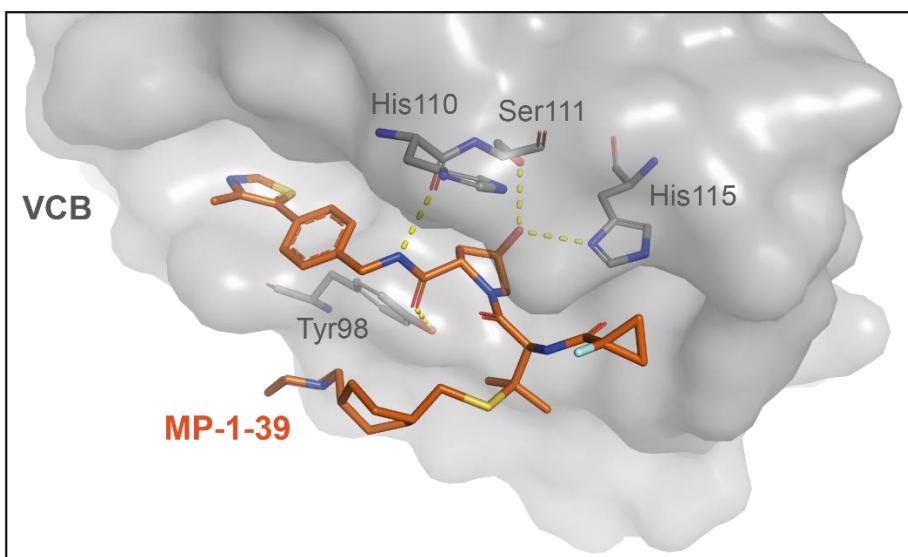
Figure 69. *Binding mode of compound **MP-1-39** co-crystallized with VHL. H-bonds are represented in yellow dotted lines.*

The solution of a high-quality electron density for compound **MP-1-21** and the determination of its conformation when bound to VHL will be the keystone to rationalize how a single stereocenter can induce such differences in the binding affinities to the ligase. Moreover, this structural information could be a big step forward to understand how this is reflected in the ternary complex formation, which conversely displays the opposite trend whereby the weaker ligand forms more stable and efficient ternary complexes. On the other hand, the solution of a ternary complex crystal structure VHL:PROTAC:LRRK2 appears yet to be a major challenge to overcome for the entire scientific community.

Moreover, NMR studies of the two epimers aimed to determine the conformational ensembles in different solvents, mimicking different cellular environments, are ongoing at the University of Dundee. Notably, the two PROTACs **XL01126** and **XL01134** also displayed different cell permeability, where compound **XL01126** was found to be more permeable than its epimer. This data could be suggestive that the two stereoisomers are represented by different conformers' populations in solution and in

the membrane interior. Hence, it could be deemed of interest to investigate if the stereocenter in the linker could also promote the so-called "chameleonicity", namely the ability of a compound to adopt different conformations depending on the environment. For example, compounds able to adopt a more extended conformation in extra- and intracellular compartments, while a more folded and compact conformation in a cell membrane interior, have been observed as promoting cell permeability as a result of minimization of polar surface area and shielding of solvating group during the permeation process.[175]

Altogether, these data could guide the rational design and optimization of new degraders displaying similar linkers and thus have a great impact in the protein degradation field.

4.2.4 Ongoing investigation of the influence in the binding affinity of cyclohexyl linker substitutions

In order to investigate how much the bulkiness of the substituent on the cyclohexyl linker affects the binding to VHL, four new compounds featuring different substitutions were designed and synthesized varying the size of the R group (***Figure 70***). Specifically, **MP-1-85** and **MP-1-95**, similar to the full-PROTACs **XL01126** and **XL01134**, present the VHL-ligand conjugated with the cyclohexyl linker (*trans* and *cis*, respectively), but the piperazine group was replaced by a smaller dimethylamine moiety. Conversely, compounds **MP-1-105** and **MP-1-106** were designed considering the 3-methoxybenzoyl group conjugated with the piperazine of the warhead, reproducing partially the full structure of **XL01126** and **XL01134**.
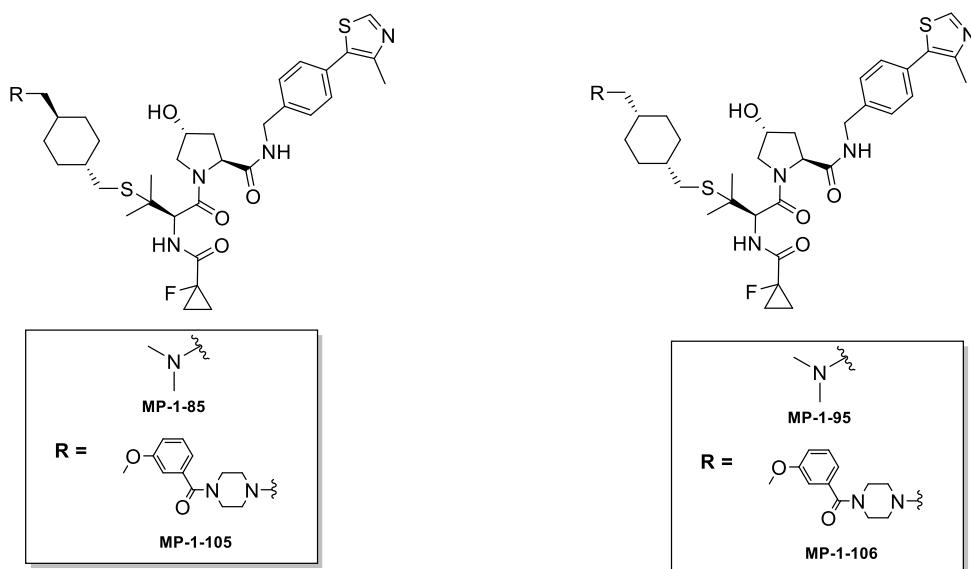
Figure 70. *Chemical structures of the designed compounds featuring groups with different sizes on the cyclohexyl linker.*

The designed derivatives were then synthesized through an efficient synthetic procedure. Specifically, for both **MP-1-85** and **MP-1-95**, the synthetic conditions are outlined in *Scheme 17*. The mono-nucleophilic substitution with dimethylamine hydrochloride on the previously synthesized 1,4-bis(bromomethyl)cyclohexane (**2n** *trans*, **2s** *cis*) gave the intermediates **2u** and **2v** in moderate yields. Finally, by use of DBU, the nucleophilic substitution of the intermediates **2u** and **2v** respectively, with the thiol group of the already synthesized VHL-linker **2k**, yielded the desired compounds **MP-1-85** and **MP-1-95** in good yields.

Synthesis of the trans VHL ligand
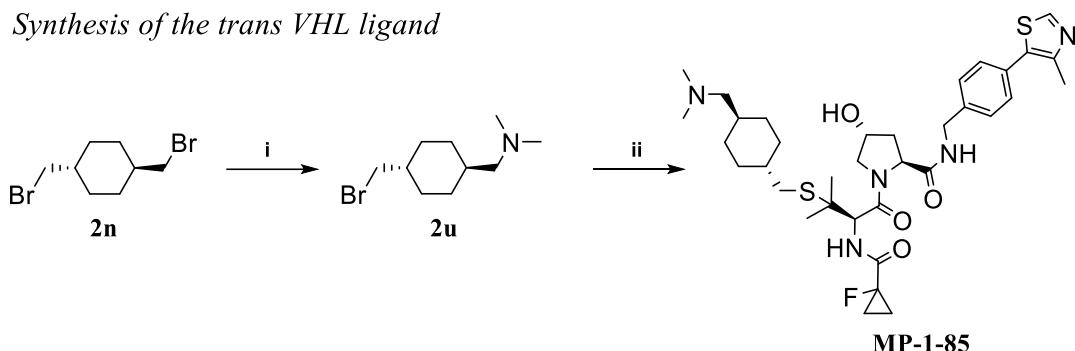
Synthesis of the cis VHL ligand
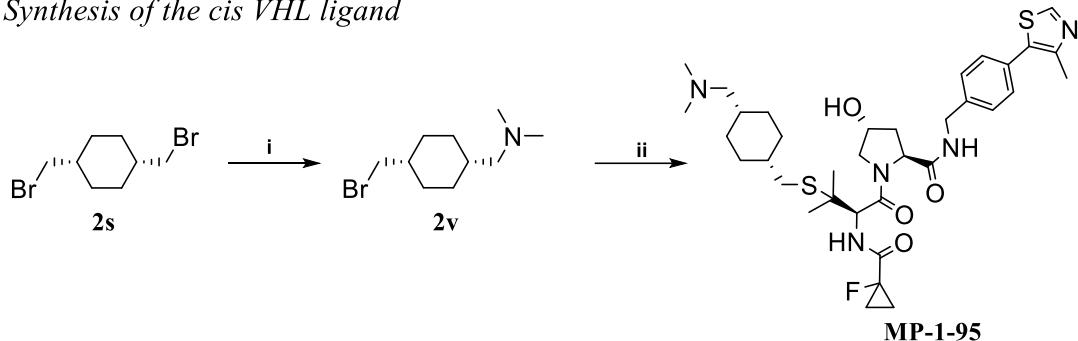
Scheme 17. *Syntheses of compounds **MP-1-85** and **MP-1-95**. Reagents and conditions: i) (CH₃)₂NH HCl, DBU, EtOH, 50 °C, overnight; ii) **2k**, DBU, THF, r.t., overnight.*

In parallel, the syntheses of compounds **MP-1-105** and **MP-1-106** were carried out as described in **Scheme 18**. Starting from the commercially available 3-methoxybenzoic acid **2w**, the amide coupling reaction with Boc-piperazine and subsequently cleavage of the protecting group in acidic conditions yielded the common intermediate **2x**. Consequently, the mono-nucleophilic substitution on the already synthesized 1,4-bis(bromomethyl)cyclohexane (**2n** *trans*, **2s** *cis*) yielded the intermediates **2y** and **2z**, respectively. Ultimately, the obtained intermediates were coupled through nucleophilic substitution with the VHL-linker **2k**, to give the desired compounds **MP-1-105** and **MP-1-106** in high yields. The detailed experimental

section for the syntheses of compounds **MP-1-85**, **MP-1-95**, **MP-1-105** and **MP-1-106** is described in **CHAPTER 7** (**paragraph 7.1.2**).
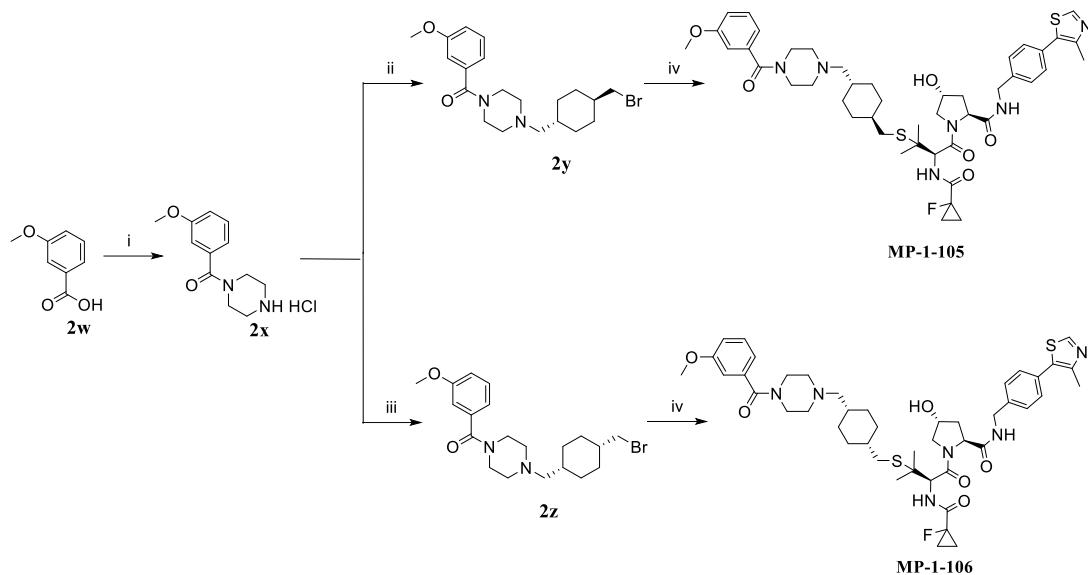
Scheme 18. *Syntheses of compounds **MP-1-105** and **MP-1-106**. i) a. Boc-piperazine, DIPEA, DCM, PyOxim, 0 °C, 2h; b. 2N HCl in dioxane and DCM, r.t., 2.5h; ii) **2n**, K₂CO₃, acetone, reflux, overnight; iii) **2s**, K₂CO₃, acetone, reflux, overnight; iv) **2k**, DBU, THF, r.t., overnight.*

At the moment, FP assays aimed to detect the binding affinity to VHL for compounds **MP-1-85**, **MP-1-95**, **MP-1-105**, and **MP-1-106** are ongoing. A careful analysis of the binding results will be important to evaluate if the substituent on the cyclohexyl linker affects and/or enhances the differences in the affinities of the two stereoisomers. Moreover, in combination with the data obtained by the above-described investigations (*i.e.,* X-ray crystallography, NMR conformational studies), it could represent a valuable information to complete the picture underlying the mechanism of binding of the two different epimers.

4.3 Optimization of the pharmacokinetic properties and/or degradation profile of the two LRRK2 degraders XL01126 and XL01134

4.3.1 Design and syntheses of new LRRK2 PROTACs with decreased VHL binding affinity

The discovery of compounds **XL0116** and **XL01134** offered new precious chemical tools for deciphering the biology of LRRK2. However, the achievement of a favorable pharmacokinetic (PK) profile to pursue future clinical trials is quite challenging, especially for PROTACs featuring multiple violations of the Rule of 5 (Ro5). Although orally bioavailable and BBB permeable, **XL01126** showed low concentration in the brain and CSF, with a low brain-to-plasma ratio.[143] For this reason, further lead-optimization aimed to improve the drug-like properties are important for maximizing compound exposure in the brain. Moreover, considering the strong hook effect showed by **XL01134** in dose-dependent LRRK2 degradation assays and the low cooperativity ($\alpha = 1.4$) in the ternary complex formation,[143] it is deemed of interest to improve the displayed degradation profile. Thus, we started a medicinal chemistry optimization aimed to achieve enhanced therapeutic performances for the two degraders **XL01126** and **XL01134**.

For this purpose, starting from the chemical structures of **XL01126** and **XL01134**, we designed modified PROTACs derivatives endowed with both lower molecular weight to enhance potentially the pharmacokinetic profile and, at the same time, decreased VHL binding affinity in order to potentially improve the low cooperativity displayed by **XL01134** and eliminate the strong hook effect. Hence, we focused on the benzylamine moiety of the VHL ligand because this portion is known to be critical in modulating the binary binding to VHL. Specifically, we designed compounds

MP01077, **MP01083**, **MP01088** and **MP01089** (*Figure 71*) replacing the 4-methylthiazole moiety in the *para*-position of the benzylamine with chlorine or a nitrile group, which are both reported as alternative groups able to decrease the binary binding affinity to the VHL ligase.[176-178] Moreover, this modification aims to decrease the molecular weight of the degraders and potentially improve the PK parameters.

MP01077: R = Cl
MP01088: R = CN

MP01083: R = Cl
MP01089: R = CN
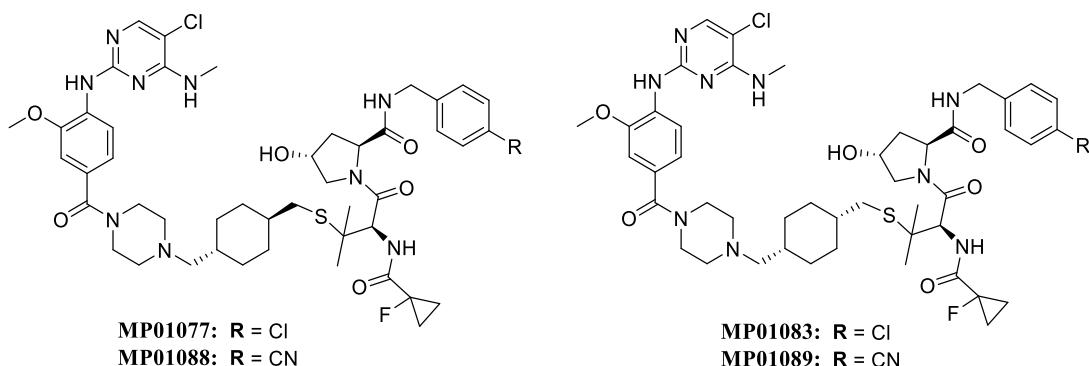
**Figure 71.** *Chemical structures of the newly designed LRRK2 PROTACs.*

Similarly to the above-described protocol, the modified VHL ligands **3k** and **3l** were synthesized in high yields following the synthetic approach reported in *Scheme 19*, starting from the commercially available (4-chlorophenyl)methanamine hydrochloride and 4-(aminomethyl)benzonitrile hydrochloride, respectively.
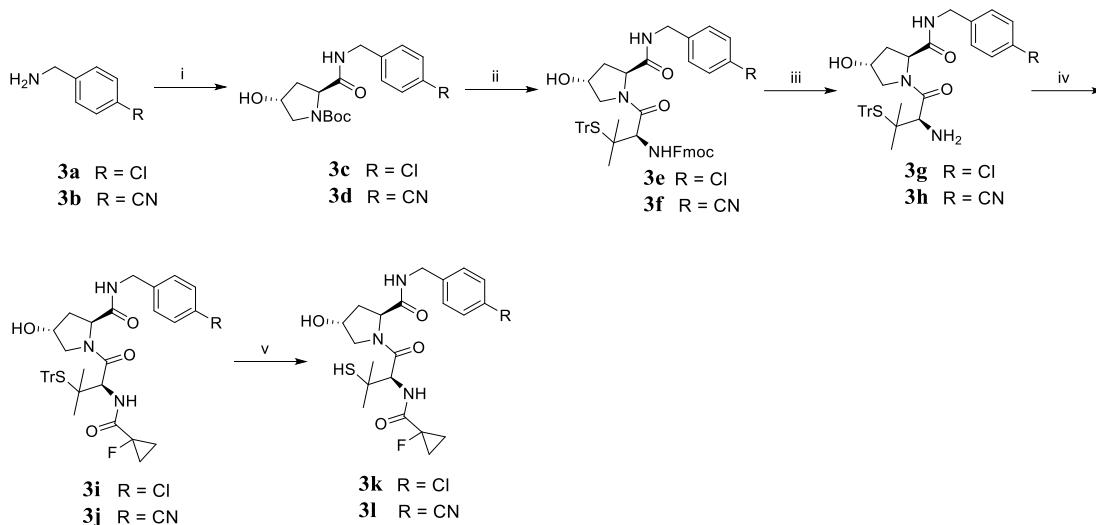
Scheme 19. *Syntheses of the modified VHL ligands **3k** and **3l**. Reagents and conditions: i) (2S,4R)-1-(tert-butoxycarbonyl)-4-hydroxypyrrolidine-2-carboxylic acid, HATU, TEA, DCM, r.t., 1.5h; ii) a. 2N HCl in dioxane and DCM, r.t., 1h; b. Fmoc-S-trityl-L-penicillamine, HATU, TEA, DMF, 0 °C, 1h; iii) piperidine, DCM, r.t., 1h; iv) 1-fluorocyclopropane-1-carboxylic acid, HATU, TEA, DCM, r.t., 1h; v) TFA, triisopropylsilane, DCM, 0 °C, 10 min.*

The final PROTACs were then synthesized as reported *in Scheme 20*. Specifically, the intermediate **3m** (provided by an internal CeTPD library of synthesized compounds) was conjugated with the 1,4-bis(bromomethyl)cyclohexane (**2n** and **2s**, *trans* and *cis* respectively), through nucleophilic substitution using K_2CO_3. The key intermediates **3n** and **3o** were finally linked to the modified VHL ligands **3k** and **3l**, to obtain the desired compounds in high yields. The detailed experimental section for the syntheses of compounds **MP01077**, **MP01083**, **MP01088** and **MP01089** is described in **CHAPTER 7** (**paragraph 7.1.3**).
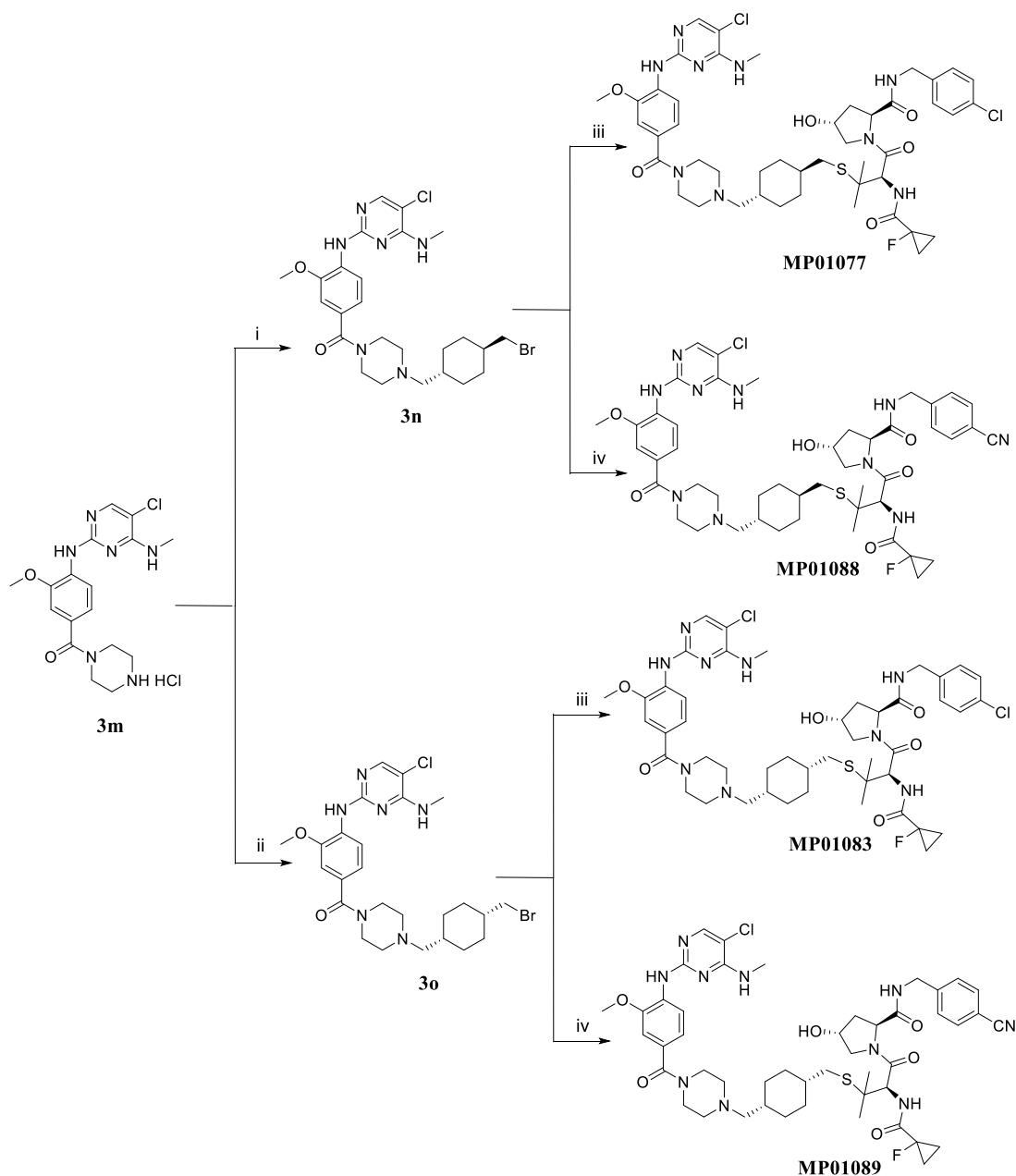
Scheme 20. *Syntheses of the final compounds **MP01077**, **MP01083**, **MP01088** and **MP01089**. Reagents and conditions: i) **2n**, K₂CO₃, acetone, reflux, overnight; ii) **2s**, K₂CO₃, acetone, reflux, overnight; iii) **3k**, DBU, THF, r.t., overnight; iv) **3l**, DBU, THF, r.t., overnight.*

4.3.2 Evaluation of the target protein degradation through Western blot

Hence, the synthesized compounds **MP01077**, **MP01083**, **MP01088** and **MP01089** were biologically evaluated for their degradation activity in both wild-type (WT) and

LRRK2 G2019S (representative of a pathogenic hallmark mutation in PD) mouse embryonic fibroblasts (MEFs) by Western blotting. Briefly, both WT and LRRK2 G2019S MEFs were treated with the compounds at 33 nM and 1 μM for 4 h, and the intracellular levels of LRRK2, phosphorylated LRRK2 at Ser935 (pSer935), and phosphorylated Rab10 at Thr73 (pThr73) were determined. It is important to note that Rab10 is a key physiological substrate of LRRK2, thus its phosphorylation status is directly affected by the kinase activity and protein levels of LRRK2.[179, 180] The phosphorylation at Ser935 is a well-studied biomarker site widely exploited to assess the efficacy of type 1 inhibitors, since LRRK2 inhibition leads to its dephosphorylation at Ser935.[162, 181, 182] The detailed experimental section related to Western Blot experiments is described in **CHAPTER 7** (**paragraph 7.5**).

Interestingly, the obtained results showed a preserved degradation activity of LRRK2 (see *Figure 72*), despite the modification on the VHL ligand potentially decreased the binary binding to the ligase. Among the tested compounds, the *trans* derivatives emerged as the most active: **MP01077** achieved ~60% of G2019S LRRK2 degradation at 1 μM/4h, while **MP01088** degraded ~80% of G2019S LRRK2 at 1 μM/4h, emerging as the most potent PROTACs of the series. Noteworthy, **MP01088** showed almost the same degradation activity as the potent degrader **XL01126**, therefore it will be interesting to deepen the investigation of the newly identified PROTAC **MP01088**, evaluating the pharmacokinetic effects due to the decreased molecular weight of the compounds. Moreover, a dose-dependent degradation assay and the evaluation of the cooperativity in the ternary complex formation will be carried out. Hence, it will be compelling to assess if the *cis* compounds **MP01083** and **MP01089** still feature the strong hook effect observed for the *cis* degrader **XL01134**.
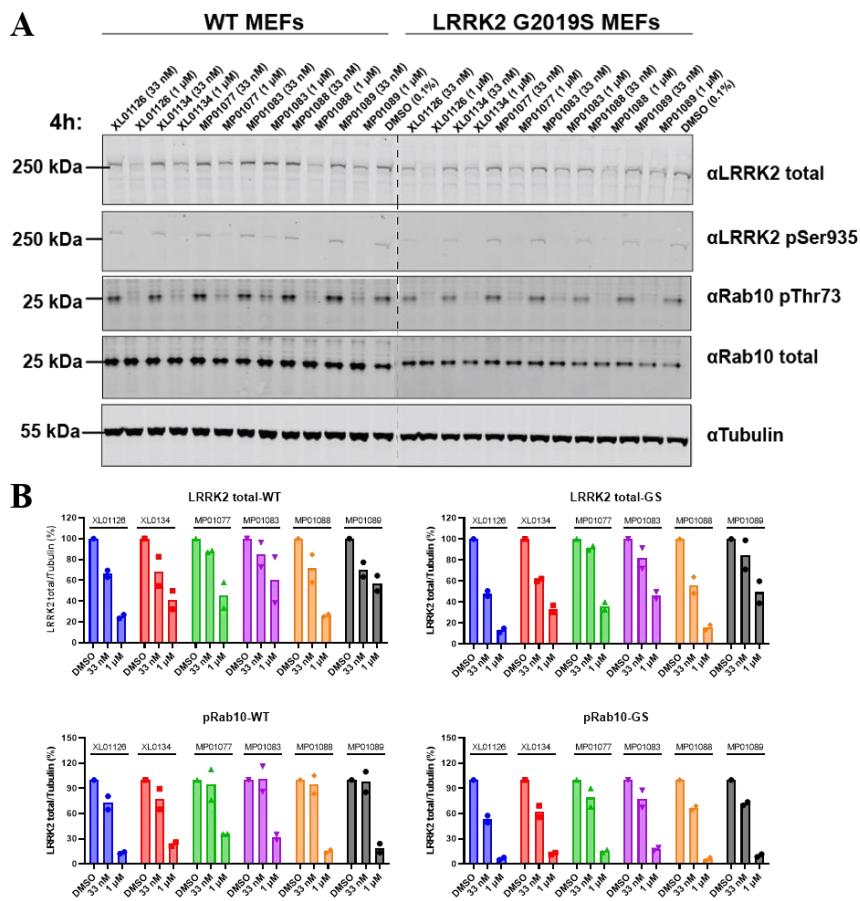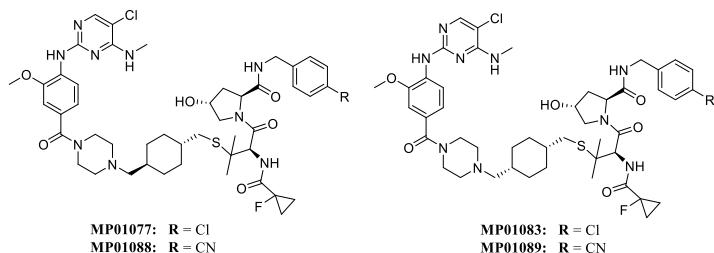
Figure 72. *Evaluation of the degradation activity of designed compounds in WT and G2019S MEFs. A) Representative Western blots monitoring the total LRRK2, LRRK2-pSer935, Rab10-pThr73, total Rab10, and tubulin levels following the treatment with the indicated compounds at 33 nM, 1 μM, or DMSO for 4h. B) Quantitative analysis of the relative LRRK2 and Rab10-pThr73 levels, which are presented as ratios of total LRRK2/tubulin or Rab10-pThr73/total Rab10, normalized to the DMSO-treated sample. Data were obtained from two biological independent experiments.*

Conclusions

The present research work carried out in the frame of my Ph.D. project was based on the unceasing and dynamic application of a multi-disciplinary approach. In the course of this three-year program, I had the possibility to follow, step-by-step, the entire research workflow and to be an active participant in it. More importantly, I acquired, explored, and developed new techniques. Specifically, I followed closely the computational design for the pharmacophore buildings and SAR studies, and I had been fully employed for the syntheses of all the designed compounds, optimization of synthetic protocols, purification steps, and full characterization through NMR and mass spectrometry experiments. Moreover, I could learn important biophysical techniques, such as Surface Plasmon Resonance (SPR), Isothermal Titration Calorimetry (ITC), and Fluorescence Polarization (FP) to detect the binding between small molecules and target proteins. Finally, during my visiting research period at the University of Dundee, I could improve my synthetic expertise in organic chemistry, and also, learn and apply Western blot techniques and X-ray crystallography for PROTACs studies.

As thoroughly described in this thesis, a broad exploration of the epigenetic reader BRD9 had been done. The development of 3D pharmacophore models had been the keystone for the identification and selection of new hit compounds that were derivatized and structurally optimized after rounds of concerted work between the chemical synthesis and the *in silico* design. New items belonging to the triazoloquinoxaline-derivatives collection emerged as new potent and highly selective BRD9 ligands in the low micromolar scale. In addition, **11** and **42** belonging to the second generation of triazoloquinoxaline compounds, presented an enhanced

antiproliferative effect on a broad panel of leukemia models with no cytotoxicity on healthy cells, proving promising outcomes for future investigations. Importantly, a thorough SAR study, carried out thanks to the syntheses of specific derivatives and the following biophysical evaluations, was crucial for the introduction of a new pharmacophoric feature on our "pharm-druglike2" model that could be useful for future studies. The improved accuracy of the three-dimensional selection tool will aid the identification of new compounds with increased activity and selectivity on BRD9. Moreover, a preliminary biophysical evaluation carried out through BromoMELT™ assay on a panel of 78 human bromodomain proteins, highlighted the binding of compound **11** to BRPF1 (Bromodomain and PHD finger containing 1). Further insights are ongoing to evaluate the effect of the disclosed compound on this interesting and less explored protein involved in the development of acute myeloid leukemia and hepatocellular carcinoma.

Thanks to the employment of the "pharm-druglike2" model, a newly disclosed class of pyrazolopyridine-based compounds was also investigated. Promising binding results have been achieved with the identification of the hit **43**, which effectively displaced the histone H4 from BRD9. Hence, we are currently working on thorough SAR studies with the aim to enhance the detected potency.

On the other hand, the class of aryl sulfonamide-based compounds **49-74**, which was identified by means of an initial and simplified version of the pharmacophore, namely the "pharm-fragment" model, did not lead to interesting results on BRD9. For this reason, a careful optimization process is ongoing. In addition, a repositioning of the inactive aryl sulfonamide derivatives through our successful methodology of the Inverse Virtual Screening was made. By this approach, six diverse proteins involved

in the development of cancer and inflammation have emerged as possible biological targets that will be further evaluated through the most appropriate assays.

The first attempt by our research group of the application of the PROTACs technology also led to important results for BRD9. Albeit at present the biological evaluation through Western Blotting of five of the synthesized degraders is ongoing, the potent degradation activity displayed by the first compound of the series **75**, strongly assessed the goodness of our design and project workflow. Indeed, the initial *in vitro* evaluation qualified **75** as a novel effective degrader probe for BRD9, able to induce > 50% cellular degradation of BRD9 in pro-monocytic human myeloid leukemia cell line at 5 μM after 24 h of treatment, also reflected into strong cytotoxicity (~30% residual viability).

Concurrently to our PROTACs campaign, the development of the hybrid multi-target probe **81**, targeting BRD9 and SMARCA2/4 subunits of the highly mutated SWI/SNF complex in tumors, opens a new and unexplored strategy to the field of the epigenetic-based polypharmacology. Preliminary AlphaScreen binding assays assessed that compound **81** strongly binds BRD9 with IC_{50} = 3.34 ± 0.15 μM. At present, the evaluation of the binding to SMARCA4 is in progress, although we are quite confident that the potent recognition of the protein is conserved. In parallel, the analysis of the cellular response due to the combined BRD9 and SMARCA2/4 inhibition is ongoing with the aim to investigate the possible synergistic effect obtained with the dual inhibitory activity.

Finally, the pharmacological potential held by both BRD9 inhibitors (*i.e.*, compound **1**, **I-BRD9**, **PUR-29**) and our disclosed degrader **75** for the treatment of inflammation was assessed through the evaluation of pro-inflammatory cytokines levels: notably, all the compounds strongly decreased IL-6 and TNF-α secretion, and

PUR-29 and **75** stood out for their potent activity. Moreover, following the clear evidence that the anti-inflammatory effect of the PROTAC **75** is stronger of the classical inhibitor **1** (representing the protein-of-interest ligand employed for **75** design), we initiated a new series of PROTACs based on the 9*H*-purine scaffold of **PUR-29** with the aim to enhance the anti-inflammatory activity displayed by this promising inhibitor. All these data strongly enrich the potential therapeutic applications of BRD9 agents.

As a conclusion of my Ph.D. research activity, I spent 6 months at the University of Dundee, where I had the possibility to further expand my scientific knowledge concerning the emerging field of targeted protein degradation. Specifically, investigations aimed to dissect the mechanism of binding related to epimer compounds were carried out through the syntheses of specific VHL ligands and the evaluation of their binary binding affinities to the VHL ligase. Crystallographic studies of the *cis* compound **MP-1-39**, showed a peculiar folding back of the cyclohexyl linker onto the VHL ligand anchored in the binding site, suggesting different conformer stabilities related to the stereochemistry of the linker. However, no solid conclusions could be made at the moment, since more data are needed and further investigations are currently ongoing.

In parallel, structural optimizations aimed to improve both the degradation profile and the pharmacokinetic properties of known LRRK2 PROTACs were investigated. Thus, new LRRK2 PROTACs were designed by modifying the VHL ligand portion of the degraders, in order to combine the effect of decreased VHL binding affinity with the lower molecular weight of the final molecules. A first Western blot screening confirmed that, despite the substantial chemical modification, all the newly designed PROTACs are able to efficiently degrade the target protein. In particular, **MP01088**

emerged as the most promising compound presenting ~80% degradation of G2019S LRRK2 in mouse embryonic fibroblasts after 4 h of treatment at 1 μM. Further exploration and optimization for future drug development are therefore ongoing at the University of Dundee.

Experimental Section

CHAPTER 5

Syntheses of new small molecules targeting BRD9

5.1 Chemistry general information

All commercially available starting materials were used as purchased from Sigma-Aldrich and Fluorochem without further purification. All solvents used for the synthesis were of HPLC grade (Sigma-Aldrich). Chemical reactions were monitored on silica gel 60 F254 plates (Merck) and spots were visualized under UV light (λ = 254 nm). Proton (^{1}H) and carbon (^{13}C) NMR spectra were recorded on Bruker Avance 400, 500 or 600 MHz spectrometer at T = 298 K. All compounds were dissolved in 0.5 mL of CDCl$_3$, CD$_3$OD or DMSO-d_6 (Sigma-Aldrich, 99.8 Atom % D). Chemical shifts (δ) are given in parts per million (ppm) relative to the solvent peak as internal reference: CDCl$_3$ (δH = 7.26 ppm/δC = 77.16 ppm), CD$_3$OD (δH = 3.31 ppm/δC = 49.00 ppm), or DMSO-d_6 (δH = 2.50 ppm/δC = 39.52 ppm). Coupling constants (J) are reported in Hertz (Hz). Signal patterns are reported as: s = singlet, d = doublet, t = triplet, q = quartet, p = quintet, h = sextet, m = multiplet, brs = broad, or a combination of the listed splitting patterns. High resolution mass spectrometry experiments were performed using a LTQ Orbitrap XL mass spectrometer (Thermo Scientific). Semi-preparative reversed-phase HPLC was performed on Agilent Technologies 1200 Series high-performance liquid chromatography using Nucleodur C8 reversed-phase column (250 × 10 mm, 4 μm, 80 Å, flow rate = 4 mL/min, Phenomenex®) or Luna C18 reversed-phase column (250 × 10 mm, 5 μm, 100 Å, flow rate = 4 mL/min, Phenomenex®). The binary solvent system (A/ B) was as follows: 0.1% TFA in water (A) and 0.1% TFA in CH$_3$CN (B). The absorbance was detected at 240 nm. The purity of all biologically tested compounds (>96%) was determined following HPLC and NMR spectra evaluation. Microwave irradiation reactions were carried out in a dedicated CEM-Discover SP focused microwave synthesizer, operating with continuous irradiation power from 0 to 300 W utilizing the standard absorbance level

of 300 W maximum power. Reactions were carried out in 10 mL sealed microwave glass vials. The Discover system also included controllable ramp time, hold time (reaction time), and uniform stirring. After the irradiation period, reaction vessels were cooled rapidly (60–120 s) to ambient temperature by air jet cooling.

## 5.2. Syntheses and characterization of triazoloquinoxaline derivatives 4-42

Synthesis of 2-chloro-3-hydrazinyl-quinoxaline (1b)
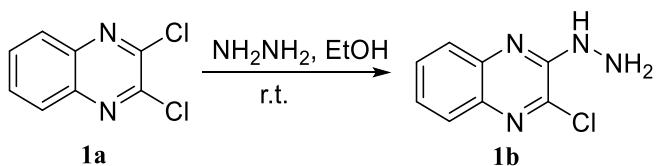
A solution of the commercially available 2,3-dichloroquinoxaline (1.0 equiv., 0.50 mmol) and hydrazine monohydrate (2.2 equiv., 1.10 mmol) in ethanol (1.8 mL) was stirred overnight at 25 °C. The reaction mixture was then allowed to precipitate in an ice bath. The resulting precipitate was filtered, washed with ice-cold ethanol and dried under nitrogen atmosphere to give **1b** (99% yield) which was then used without any further purification. ^{1}H NMR (600 MHz, CDCl$_3$) δ 7.85 (d, *J* = 8.3 Hz, 1H), 7.77 (d, *J* = 8.3 Hz, 1H), 7.63 (t, *J* = 7.7 Hz, 1H), 7.46 (t, *J* = 7.7 Hz, 1H), 6.81 (s, 1H), 4.17 (s, 2H). ^{13}C NMR (150 MHz, CDCl$_3$) δ 149.6, 140.9, 137.3, 136.8, 130.6, 128.3, 126.2, 126.0. HRMS: calcd for C$_8$H$_7$ClN$_4$ 194.0359, found *m/z* 195.0434 [M + H]$^+$.

General synthetic procedure (A) for the synthesis of the intermediates 4-chloro-1-alkyl-[1,2,4]triazolo[4,3-a]quinoxaline (1c, 1i, 1j)
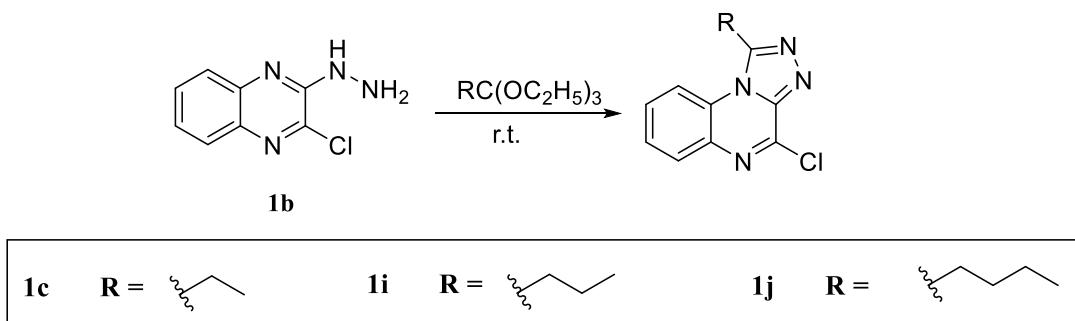

2-chloro-3-hydrazinyl-quinoxaline (**1b**) (1.0 equiv., 0.379 mmol) and the proper 1,1,1-triethoxyalkane derivative (*e.g.*, 1,1,1-triethoxypropane, 1,1,1-triethoxybutane or 1,1,1-triethoxypentane) (10.0 equiv., 3.787 mmol) were stirred 16 h at room temperature. The resulting mixture was then washed with cyclohexane and filtered off. The precipitate was collected with chloroform and dried under nitrogen atmosphere to give the desired intermediate compound, which was used without any further purification.

Synthesis of the intermediate 2-(4-amino-2-fluorophenyl)acetonitrile (1e)
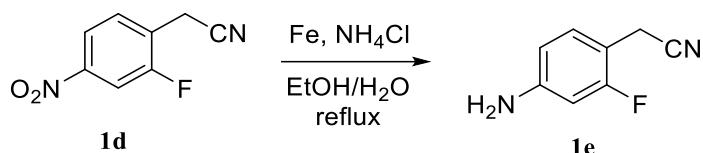
The commercially available 2-(2-fluoro-4-nitrophenyl)acetonitrile **1d** (1 equiv., 0.22 mmol), iron powder (3 equiv., 0.66 mmol), and NH_4Cl (5 equiv., 1.11 mmol) were dissolved in 1 mL of a $EtOH/H_2O$ mixture (1:1.6) and stirred at reflux for 2.5 h. After completion, the reaction mixture was filtered and DCM was added. The organic phase was then washed with water and brine, dried over sodium sulfate, filtered, and finally condensed under reduced pressure to afford a residue which was used for the following step without further purification (55% yield). ^1H NMR (400 MHz, $CDCl_3$) δ 7.08 (t, J = 8.4 Hz, 1H), 6.44 – 6.34 (m, 2H), 3.90 (brs, 2H), 3.59 (s, 2H). HRMS: calcd for $C_8H_7FN_2$ 150.0593, found m/z = 151.0664 $[M + H]^+$.

General synthetic procedure (B) for the syntheses of triazoloquinoxaline-derivative compounds 4-7, 10-21, 41 and 42, obtained under MW irradiation
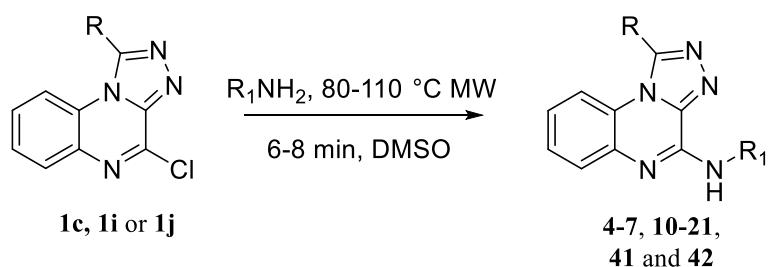
A mixture of 4-chloro-1-alkyl-[1,2,4]triazolo[4,3-*a*]quinoxaline (**1c, 1i** or **1j**) (1 equiv., 0.14 mmol) and the required aromatic amine (3 equiv., 0.41 mmol) in DMSO (0.4 mL) was heated under microwave irradiation at 80–110 °C for 6–8 min. After

irradiation, the vial was cooled to ambient temperature by air jet cooling and the reaction mixture was diluted with CH_2Cl_2 (1.0 mL) and acidified with 1 N HCl. The resulting crude precipitate was filtered using a Büchner funnel under reduced pressure. The solid was then collected and precipitated in methanol to give the desired compounds. For the biology testing purity (>96%), all the compounds were purified by semi-preparative reversed-phase HPLC using the gradient conditions from 5% B to 100% B over 50 min, flow rate of 4 mL/min, $\lambda = 240$ nm. All final products were characterized by mass spectrometry experiments and NMR analysis.

General synthetic procedure (C) for the syntheses of triazoloquinoxaline-derivative compounds 8 and 9 obtained under conventional heating
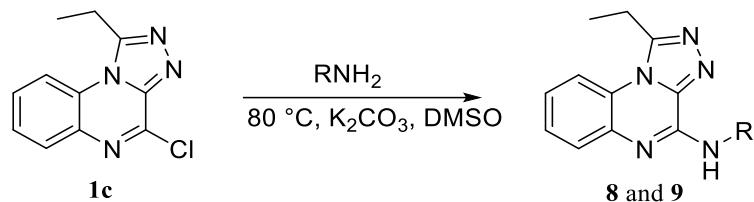
A mixture of 4-chloro-1-ethyl-[1,2,4]triazolo[4,3-*a*]quinoxaline (**1c**) (1.5 equiv., 0.16 mmol), the required heteroaryl amine (1 equiv., 0.11 mmol) and potassium carbonate (1.2 equiv., 0.13 mmol) in DMSO (0.5 mL) was stirred for 1.5–2.5 h at 80 °C. After cooling to room temperature, the reaction mixture was diluted with CH_2Cl_2 (1.25 mL) and acidified with 1 N HCl. The resulting crude precipitate was filtered using a Büchner funnel under reduced pressure then collected and purified through precipitation in methanol giving compounds **8** and **9**. The final products were characterized by mass spectrometry experiments and NMR analysis.

General synthetic procedure (D) for the syntheses of triazoloquinoxaline-derivative compounds 22-37
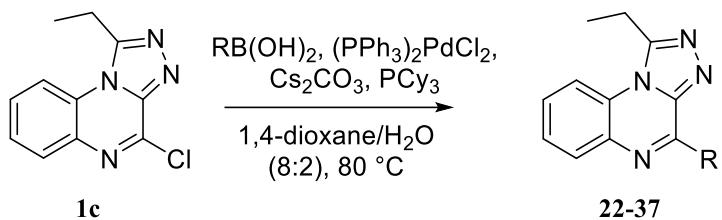
In a two-neck flask were added the intermediate 4-chloro-1-ethyl-[1,2,4]triazolo[4,3-*a*]quinoxaline (**1c**) (1.00 equiv., 0.251 mmol), the selected phenyl boronic acid (1.50 equiv., 0.376 mmol), PCy$_3$ (0.05 equiv. 0.013 mmol), (PPh$_3$)$_2$PdCl$_2$ (0.05 equiv. 0.013 mmol) and Cs$_2$CO$_3$ (3.90 equiv., 0.979 mmol). The flask was evacuated and backfilled with nitrogen three times. Then a degassed solution (2.2 mL) of 1,4-dioxane (80%) and water (20%) was added and the mixture was stirred overnight at 80 °C under nitrogen atmosphere. After completion of the reaction, the mixture was cooled to room temperature, ethyl acetate was added and extracted with distilled water (x2) and brine (x1). The organic phase was dried over anhydrous Na$_2$SO$_4$, filtered and concentrated under vacuum. The crude was purified by semi-preparative reversed-phase HPLC by using the gradient conditions from 5% B to 100% B over 50 min, flow rate of 4 mL/min, λ = 240 nm, to achieve the final compounds **22-37**, whose purity was determined by HPLC (>96%). All final products were characterized by mass spectrometry experiments and NMR analysis.

General synthetic procedure (E) for the syntheses of the intermediate 3-chloro-N-substituted-quinoxaline-2-carboxamide compounds 1g-I and 1g-II
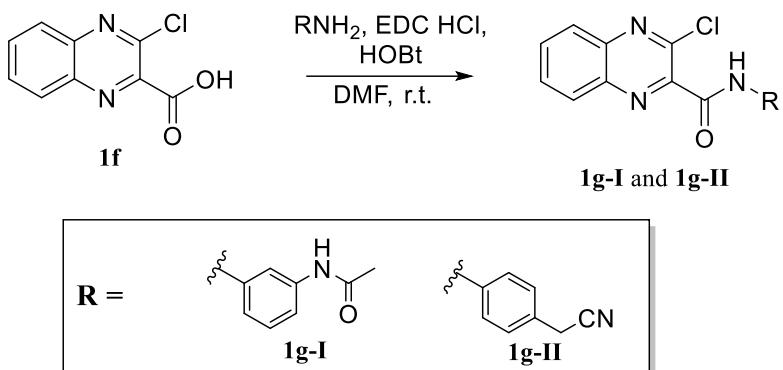
To a solution of the commercially available 3-chloroquinoxaline-2-carboxylic acid **1f** (1.05 equiv., 0.240 mmol) in dry DMF (1.9 mL), the proper amine (1 equiv., 0.228 mmol), EDC HCl (2.80 equiv., 0.639 mmol), HOBt (4 equiv., 0.913 mmol) were added. The reaction mixture was stirred at room temperature overnight under nitrogen atmosphere. After completion of the reaction, ethyl acetate was added and the organic phase was washed with a saturated solution of NH_4Cl (x3) and $NaHCO_3$ (x3). The organic layer was then dried over sodium sulfate, filtered, and condensed to afford a crude that was purified on silica gel column chromatography in hexane/ethyl acetate.

General synthetic procedure (F) for the syntheses of the intermediate 3-hydrazineyl-N-substituted-quinoxaline-2-carboxamide compounds 1h-I and 1h-II
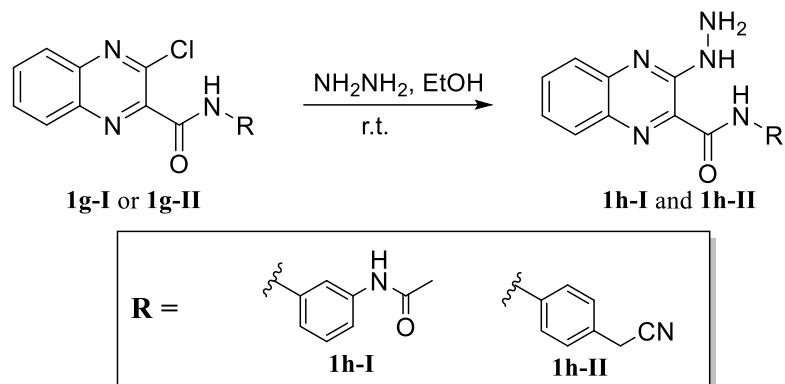
To a solution of the intermediate 3-chloro-*N*-substituted-quinoxaline-2-carboxamide compound (1.0 equiv., 0.050 mmol) in ethanol (0.7 mL), hydrazine monohydrate (2.2 equiv., 0.110 mmol) was added and the reaction mixture was stirred overnight at 25 °C. The crude was then precipitated in an ice bath. The resulting precipitate was filtered, washed with ice-cold ethanol and dried under nitrogen atmosphere to give the desired intermediate compound, which was then used without any further purification.

General synthetic procedure (G) for the syntheses of the final compounds 38 and 39
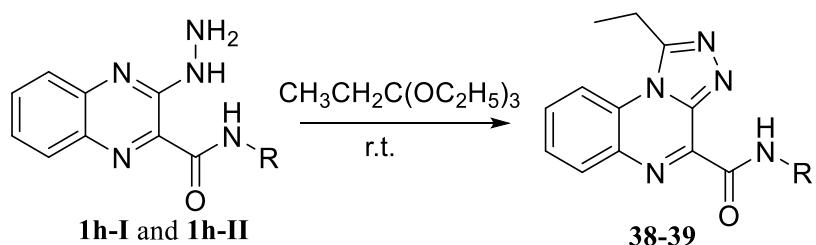
The intermediate compound 3-hydrazineyl-*N*-substituted-quinoxaline-2-carboxamide (1.0 equiv., 0.022 mmol) and triethyl orthopropionate (10.0 equiv., 0.220 mmol) were stirred 16 h at room temperature. The resulting crude was then washed several times

with cyclohexane and filtered off. The precipitate was collected, dried and purified by semi-preparative reversed-phase HPLC by using the gradient conditions from 5% B to 100% B over 50 min, flow rate of 4 mL/min, λ = 240 nm, to achieve the final compounds **38-39**, whose purity was determined by HPLC (>96%). All final products were characterized by mass spectrometry experiments and NMR analysis.

Synthesis of compound N-(3-((1-ethyl-[1,2,4]triazolo[4,3-a]quinoxalin-4-yl)oxy)phenyl)acetamide (40)
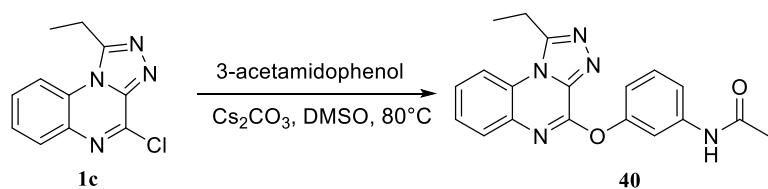
To a solution of 4-chloro-1-ethyl-[1,2,4]triazolo[4,3-*a*]quinoxaline (**1c**) (1 equiv., 0.179 mmol) in DMSO (0.50 mL) were added 3-acetamidophenol (1 equiv., 0.179 mmol) and cesium carbonate (1.2 equiv., 0.214 mmol). The reaction mixture was heated to 80 °C and stirred for 3 h. After cooling to room temperature, the reaction mixture was diluted with dichloromethane (1.25 mL) and acidified with 1 N HCl. The obtained precipitate was filtered under reduced pressure and collected for further purification. In order to achieve the desired biology testing purity (>96%), semi-preparative reversed-phase HPLC was carried out by using the gradient conditions from 5% B to 100% B over 50 min, flow rate of 4 mL/min, λ = 240 nm. The final compound **40** was obtained with 99% overall yield and characterized by mass spectrometry experiments and NMR analysis.

^{1}H NMR (400 MHz, DMSO-*d$_6$*) δ 10.16 (s, 1H), 8.25 (d, *J* = 8.0 Hz, 1H), 7.74 (s, 1H), 7.67 – 7.60 (m, 2H), 7.55 (t, *J* = 7.2 Hz, 1H), 7.48 – 7.40 (m, 2H), 7.08 (dt, *J* = 7.5,

2.0 Hz, 1H), 3.51 (q, J = 7.3 Hz, 2H), 2.06 (s, 3H), 1.52 (t, J = 7.3 Hz, 3H). ^{13}C NMR (150 MHz, DMSO-d_6) δ 168.7, 153.1, 152.0, 151.2, 140.7, 139.6, 134.3, 129.8, 128.1, 127.4, 127.3, 125.7, 116.4, 116.4, 116.2, 112.3, 24.1, 21.6, 11.0. HRMS: calcd for $C_{19}H_{17}N_5O_2$ 347.1382, found m/z = 370.1280 [M + Na]$^+$.

*4-chloro-1-ethyl-[1,2,4]triazolo[4,3-a]quinoxaline (**1c**)*

1c
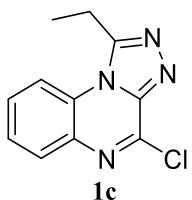
Compound **1c** was obtained following the general synthetic procedure (**A**) (70% yield). ^{1}H NMR (400 MHz, CDCl$_3$) δ 8.13 (dd, J = 8.2, 1.4 Hz, 1H), 8.08 (dd, J = 8.2, 1.4 Hz, 1H), 7.76 – 7.65 (m, 2H), 3.52 (q, J = 7.4 Hz, 2H), 1.66 (t, J = 7.4 Hz, 3H). ^{13}C NMR (100 MHz, CDCl$_3$) δ 153.6, 143.2, 142.7, 135.7, 130.5, 130.0, 128.1, 126.3, 115.6, 22.5, 11.4. HRMS: calcd for $C_{11}H_9ClN_4$ 232.0516, found m/z = 233.0585 [M + H]$^+$.

*4-chloro-1-propyl-[1,2,4]triazolo[4,3-a]quinoxaline (**1i**)*

1i
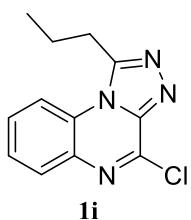
Compound **1i** was obtained following the general synthetic procedure (**A**) (65% yield). ^{1}H NMR (400 MHz, CDCl$_3$) δ 8.14 – 8.04 (m, 2H), 7.73 (t, J = 7.3 Hz, 1H), 7.67 (t, J = 7.3 Hz, 1H), 3.46 (t, J = 7.5 Hz, 2H), 2.10 (h, J = 7.5 Hz, 2H), 1.19 (t, J = 7.5 Hz, 3H). ^{13}C NMR (100 MHz, CDCl$_3$) δ 152.5, 143.3, 142.9, 135.9, 130.6, 130.0, 128.1,

126.4, 115.6, 30.7, 20.3, 14.0. HRMS: calcd for $C_{12}H_{11}ClN_4$ 246.0672, found $m/z =$ 269.0570 $[M + Na]^+$.

*4-chloro-1-butyl-[1,2,4]triazolo[4,3-a]quinoxaline (1j)*

1j
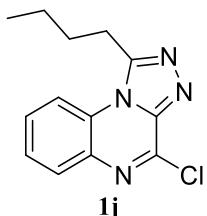
Compound **1j** was obtained following the general synthetic procedure (**A**) (65% yield).

^{1}H NMR (400 MHz, CDCl$_3$) δ 8.14 – 8.04 (m, 2H), 7.77 – 7.63 (m, 2H), 3.51 – 3.45 (m, 2H), 2.03 (p, J = 7.4 Hz, 2H), 1.60 (h, J = 7.4 Hz, 2H), 1.04 (t, J = 7.4 Hz, 3H).

^{13}C NMR (100 MHz, CDCl$_3$) δ 152.8, 143.3, 142.9, 135.9, 130.6, 130.0, 128.1, 126.5, 115.6, 28.8, 28.5, 22.6, 13.9. HRMS: calcd for $C_{13}H_{13}ClN_4$ 260.0829, found $m/z =$ 283.0725 $[M + Na]^+$.

6-((1-ethyl-[1,2,4]triazolo[4,3-a]quinoxalin-4-yl)amino)–2H-benzo[b][1,4]oxazin-

3(4H)-one (4)

4
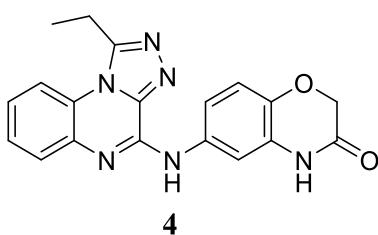
Compound **4** was obtained following the general synthetic procedure (**B**) (79% overall yield). ^{1}H NMR (400 MHz, DMSO-d_6) δ 10.83 (s, 1H), 10.13 (s, 1H), 8.22 (d, J = 2.5 Hz, 1H), 8.13 (dd, J = 8.4, 1.5 Hz, 1H), 7.80 (dd, J = 8.1, 1.5 Hz, 1H), 7.58 – 7.50 (m, 2H), 7.43 (td, J = 8.7, 8.0, 1.6 Hz, 1H), 6.94 (d, J = 8.7 Hz, 1H), 4.56 (s, 2H), 3.48 (q, J = 7.3 Hz, 2H) 1.51 (t, J = 7.3 Hz, 3H). ^{13}C NMR (100 MHz, DMSO-d_6) δ 165.2,

153.0, 143.3, 139.6, 138.8, 136.8, 134.5, 127.0, 124.4, 124.0, 116.0, 115.7, 115.3, 108.9, 66.9, 21.5, 11.0. HRMS: calcd for $C_{19}H_{16}N_6O_2$ 360.1335, found m/z = 383.1220 [M + Na]$^+$.

2-(4-((1-ethyl-[1,2,4]triazolo[4,3-a]quinoxalin-4-yl)amino)phenyl)acetonitrile (5)
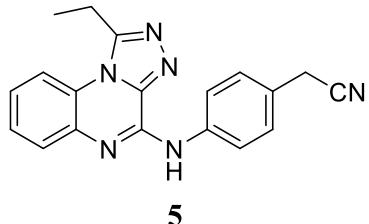
Compound **5** was obtained following the general synthetic procedure (**B**) (39% overall yield). ^{1}H NMR (400 MHz, DMSO-d_6) δ 10.23 (s, 1H), 8.20 (d, J = 8.6 Hz, 2H), 8.14 (d, J = 8.2 Hz, 1H), 7.77 (dd, J = 8.0, 1.5 Hz, 1H), 7.53 (td, J = 7.8, 1.5 Hz, 1H), 7.44 (td, J = 7.8 Hz, 7.3 Hz, 1.5 Hz, 1H), 7.35 (d, J = 8.6 Hz, 2H), 4.01 (s, 2H), 3.48 (q, J = 7.3 Hz, 2H) 1.51 (t, J = 7.3 Hz, 3H). ^{13}C NMR (100 MHz, DMSO-d_6) δ 153.0, 143.4, 139.6, 139.1, 136.6, 128.2, 127.1, 127.1, 125.3, 124.6, 124.1, 121.0, 119.4, 116.0, 21.9, 21.6, 11.0. HRMS: calcd for $C_{19}H_{16}N_6$ 328.1436, found m/z = 351.1329 [M + Na]$^+$.

(3-amino-5-((1-ethyl-[1,2,4]triazolo[4,3-a]quinoxalin-4-yl)amino)phenyl)methanol

(6)

6
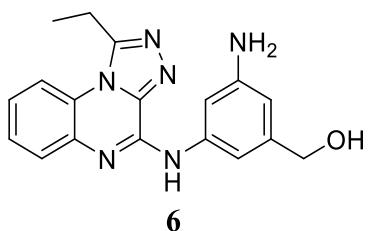
Compound **6** was obtained following the general synthetic procedure (**B**) (61% overall

yield). ^{1}H NMR (400 MHz, MeOD) δ 8.40 (s, 1H), 8.21 (d, J = 8.5 Hz, 1H), 7.92 (d,

J = 8.0 Hz, 1H), 7.85 (s, 1H), 7.59 (t, J = 8.0 Hz, 1H), 7.52 (t, J = 8.5 Hz, 1H), 7.06 (s,

1H), 4.70 (s, 2H), 3.56 (q, J = 7.3 Hz, 2H), 1.63 (t, J = 7.3 Hz, 3H). ^{13}C (100 MHz,

DMSO-d_6) δ 153.1, 144.6, 143.4, 140.5, 139.6, 136.5, 127.2, 127.1, 124.9, 124.1,

116.1, 115.2, 113.2, 111.2, 62.7, 21.6, 11.0. HRMS: calcd for $C_{18}H_{18}N_6O$ 334.1542,

found m/z = 335.1616 [M + H]$^+$.

1-(4-((1-ethyl-[1,2,4]triazolo[4,3-a]quinoxalin-4-yl)amino)phenyl)-N-

methylmethanesulfonamide (7)

7
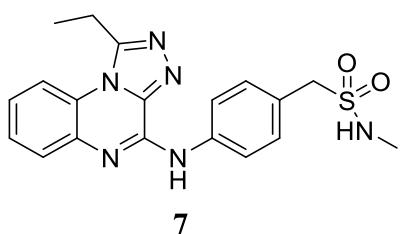
Compound **7** was obtained following the general synthetic procedure (**B**) (78% overall

yield). ^{1}H NMR (400 MHz, DMSO-d_6) δ 10.21 (s, 1H), 8.21 (d, J = 8.6, 2H), 8.15 (dd,

J = 8.4, 1.3 Hz, 1H), 7.79 (dd, J = 8.0, 1.3 Hz, 1H), 7.54 (t, J = 7.3 Hz, 1H), 7.46 (td,

J = 8.4 Hz, 1.3 Hz, 1H), 7.38 (d, J = 8.6 Hz, 2H), 6.91 (q, J = 4.7 Hz, 1H), 4.32 (s,

2H), 3.49 (q, J = 7.3 Hz, 2H), 2.60 (d, J = 4.7 Hz, 3H), 1.52 (t, J = 7.3 Hz, 3H). ^{13}C

NMR (100 MHz, DMSO-d_6) δ 153.1, 143.3, 139.6, 139.5, 136.6, 130.9, 127.2, 127.1,

124.7, 124.5, 124.1, 120.3, 116.0, 55.4, 28.9, 21.6, 11.0. HRMS: calcd for

$C_{19}H_{20}N_6O_2S$ 396.1368, found m/z = 419.1252 [M + Na]$^+$.

4-((1-ethyl-[1,2,4]triazolo[4,3-a]quinoxalin-4-yl)amino)-1H-imidazole-5-

carboxamide (8)
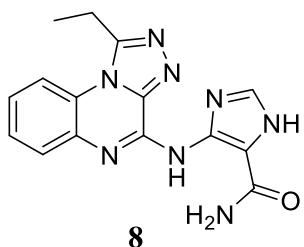
Compound **8** was obtained following the general synthetic procedure (**C**) (59% overall

yield). ^{1}H NMR (400 MHz, DMSO-d_6) δ 8.83 (s, 1H), 8.36 (dd, J = 8.2 Hz, 1.5 Hz,

1H), 8.23 (dd, J = 7.7, 1.9 Hz, 1H), 7.83–7.70 (m, 2H), 7.09 (s, 2H), 3.56 (q, J = 7.3

Hz, 2H) 1.54 (t, J = 7.3 Hz, 3H). ^{13}C NMR (100 MHz, DMSO-d_6) δ 166.4, 153.1,

143.7, 140.1, 140.0, 133.8, 129.3, 129.3, 127.7, 125.5, 116.4, 111.1, 21.7, 10.9.

HRMS: calcd for $C_{15}H_{14}N_8O$ 322.1291, found m/z = 345.1183 [M + Na]$^+$.

*1-ethyl-N-(7H-purin-6-yl)-[1,2,4]triazolo[4,3-a]quinoxalin-4- amine (**9**)*

9
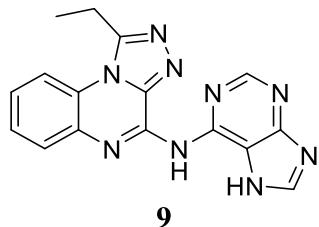
Compound **9** was obtained following the general synthetic procedure (**C**) (79% overall yield. ^{1}H NMR (400 MHz, DMSO-d_6) δ 9.73 (s, 1H), 8.71 (s, 1H), 8.46 (dd, J = 8.5 Hz, 1.2 Hz, 1H), 8.11 (dd, J = 8.0, 1.6 Hz, 1H), 7.90 (td, J = 8.5, 8.0, 1.6 Hz, 1H), 7.82 (td, J = 8.6, 7.8, 1.2 Hz, 1H), 3.63 (q, J = 7.3 Hz, 2H) 1.56 (t, J = 7.3 Hz, 3H). ^{13}C NMR (100 MHz, DMSO-d_6) δ 153.4, 152.5, 150.1, 148.2, 141.1, 138.6, 134.0, 130.3, 129.1, 128.1, 126.0, 116.7, 109.2, 21.5, 11.0. HRMS: calcd for $C_{16}H_{13}N_9$ 331.1294, found m/z = 354.1190 [M + Na]$^+$.

*3-((1-ethyl-[1,2,4]triazolo[4,3-a]quinoxalin-4-yl)amino)phenol (**10**)*

10
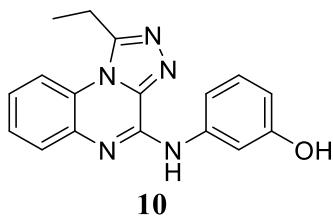
Compound **10** was obtained following the general synthetic procedure (**B**) (76% overall yield). ^{1}H NMR (600 MHz, DMSO-d_6) δ 9.98 (s, 1H), 9.43 (s, 1H), 8.14 (dd, J = 8.4, 1.5 Hz, 1H), 7.85 (t, J = 2.2 Hz, 1H), 7.76 (dd, J = 8.1, 1.5 Hz, 1H), 7.57–7.53 (m, 2H), 7.47–7.43 (m, 1H), 7.15 (t, J = 8.1 Hz, 1H), 6.50 (dd, J = 8.1 Hz, 1.5 Hz, 1H), 3.48 (q, J = 7.3 Hz, 2H), 1.51 (t, J = 7.3 Hz, 3H). ^{13}C NMR (150 MHz, DMSO-d_6) δ 157.5, 153.1, 143.4, 140.7, 139.7, 136.8, 129.1, 127.2, 127.1, 124.6, 124.1, 116.2, 111.5, 110.0, 107.8, 21.6, 11.1. HRMS: calcd for $C_{17}H_{15}N_5O$ 305.1277, found m/z = 328.1164 [M + Na]$^+$.

2-(4-((1-ethyl-[1,2,4]triazolo[4,3-a]quinoxalin-4-yl)amino)phenyl)-2-

methylpropanenitrile (11)

11
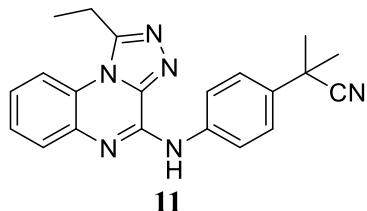
Compound **11** was obtained following the general synthetic procedure (**B**) (73% yield).

^{1}H NMR (400 MHz, DMSO-d_6) δ 10.25 (s, 1H), 8.23 (d, J = 8.8 Hz, 2H), 8.15 (dd, J

= 8.4, 1.4 Hz, 1H), 7.76 (dd, J = 8.0, 1.5 Hz, 1H), 7.56 – 7.50 (m, 3H), 7.45 (td, J =

8.0, 7.5, 1.6 Hz, 1H), 3.49 (q, J = 7.3 Hz, 2H), 1.71 (s, 6H), 1.51 (t, J = 7.3 Hz, 3H).

^{13}C NMR (100 MHz, DMSO-d_6) δ 153.1, 143.4, 139.6, 139.1, 136.6, 135.6, 127.2,

127.1, 125.3, 124.8, 124.7, 124.1, 120.8, 116.1, 36.1, 28.4, 21.6, 11.0. HRMS: calcd

for $C_{21}H_{20}N_6$ 356.1749, found m/z = 379.1646 [M + Na]$^+$.

2-(5-((1-ethyl-[1,2,4]triazolo[4,3-a]quinoxalin-4-yl)amino)pyridin-2-yl)acetonitrile

(12)

12
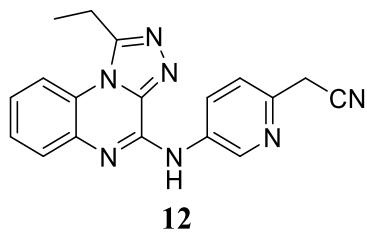
Compound **12** was obtained following the general synthetic procedure (**B**) (46% yield).

^{1}H NMR (400 MHz, DMSO-d_6) δ 10.53 (s, 1H), 9.34 (d, J = 2.6 Hz, 1H), 8.66 (dd, J

= 8.5, 2.6 Hz, 1H), 8.16 (d, J = 8.2 Hz, 1H), 7.80 (dd, J = 8.0, 1.5 Hz, 1H), 7.56 (t, J =

7.6 Hz, 1H), 7.53 – 7.44 (m, 2H), 4.20 (s, 2H), 3.50 (q, J = 7.3 Hz, 2H), 1.52 (t, J =

7.3 Hz, 3H). ^{13}C NMR (100 MHz, DMSO-d_6) δ 153.6, 144.9, 143.8, 141.9, 140.0,

136.7, 136.5, 129.3, 127.8, 127.7, 125.6, 124.7, 123.1, 118.8, 116.6, 25.3, 22.1, 11.5.

HRMS: calcd for $C_{18}H_{15}N_7$ 329.1389, found m/z = 352.1281 $[M + Na]^+$.

1-(4-((1-ethyl-[1,2,4]triazolo[4,3-a]quinoxalin-4-yl)amino)phenyl)cyclopentane-1-

carbonitrile (13)

13
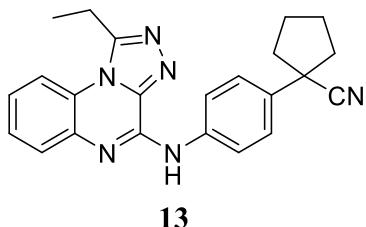
Compound **13** was obtained following the general synthetic procedure (**B**) (80% yield).

^{1}H NMR (400 MHz, DMSO-d_6) δ 10.26 (s, 1H), 8.24 (d, J = 8.8 Hz, 2H), 8.16 (dd, J

= 8.4, 1.3 Hz, 1H), 7.78 (dd, J = 8.1, 1.5 Hz, 1H), 7.58 – 7.44 (m, 4H), 3.50 (q, J = 7.3

Hz, 2H), 2.47 – 2.40 (m, 2H), 2.17 – 2.05 (m, 2H), 1.95 – 1.87 (m, 4H), 1.52 (t, J =

7.3 Hz, 3H). ^{13}C NMR (100 MHz, DMSO-d_6) δ 153.1, 143.4, 139.6, 139.2, 136.6,

133.6, 127.2, 127.1, 126.3, 124.7, 124.4, 124.1, 120.8, 116.1, 46.7, 39.2, 23.4, 21.5,

11.0. HRMS: calcd for $C_{23}H_{22}N_6$ 382.1906, found m/z = 405.1788 $[M + Na]^+$.

2-(4-((1-ethyl-[1,2,4]triazolo[4,3-a]quinoxalin-4-yl)amino)-2-

fluorophenyl)acetonitrile (14)

14
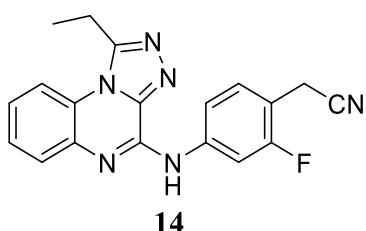
Compound **14** was obtained following the general synthetic procedure (**B**) employing

the in-house synthesized aromatic amine **1e** (70% yield). ^{1}H NMR (400 MHz, DMSO-

d_6) δ 10.47 (s, 1H), 8.30 (dd, J = 13.0, 2.1 Hz, 1H), 8.18 (dd, J = 8.3, 1.4 Hz, 1H), 8.05

(dd, J = 8.3, 2.1 Hz, 1H), 7.84 (dd, J = 8.3, 1.4 Hz, 1H), 7.57 (td, J = 7.6, 1.4 Hz, 1H),

7.52 – 7.42 (m, 2H), 4.03 (s, 2H), 3.50 (q, J = 7.3 Hz, 2H), 1.52 (t, J = 7.3 Hz, 3H).

^{13}C NMR (100 MHz, DMSO-d_6) δ 159.7 (d, J = 242.9 Hz), 153.2, 143.3, 141.3 (d, J

= 11.3 Hz), 139.6, 136.3, 130.2 (d, J = 4.6 Hz), 127.3 (d, J = 14.1 Hz), 125.2, 124.2,

118.3, 116.5 (d, J = 2.4 Hz), 116.1, 111.9 (d, J = 16.1 Hz), 107.4, 107.2, 21.6, 16.4,

11.0. HRMS: calcd for $C_{19}H_{15}FN_6$ 346.1342, found m/z = 369.1214 [M + Na]$^+$.

2-(3-bromo-4-((1-ethyl-[1,2,4]triazolo[4,3-a]quinoxalin-4-

yl)amino)phenyl)acetonitrile (15)

15
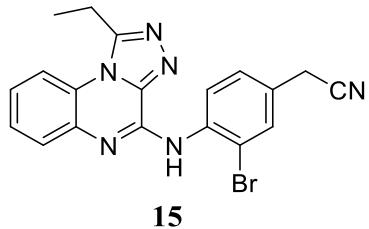
Compound **15** was obtained following the general synthetic procedure (**B**) (35% yield).

^{1}H NMR (400 MHz, DMSO-d_6) δ 9.34 (brs, 1H), 8.40 (d, J = 8.3 Hz, 1H), 8.16 (d, J

= 8.3 Hz, 1H), 7.75 (s, 1H), 7.71 (d, J = 7.8 Hz, 1H), 7.55 – 7.46 (m, 3H), 4.10 (s, 2H),

3.49 (q, J = 7.3 Hz, 2H), 1.51 (t, J = 7.3 Hz, 3H). ^{13}C NMR (100 MHz, DMSO-d_6) δ

153.3, 143.4, 139.6, 136.3, 136.1, 132.2, 129.0, 128.2, 127.3, 127.2, 125.2, 125.0,

124.3, 119.0, 117.0, 116.2, 79.2, 21.5, 11.0. HRMS: calcd for $C_{19}H_{15}BrN_6$ 406.0542,

found m/z = 429.0436 [M + Na]$^+$.

*(4-((1-ethyl-[1,2,4]triazolo[4,3-a]quinoxalin-4-yl)amino)phenyl)methanol (**16**)*
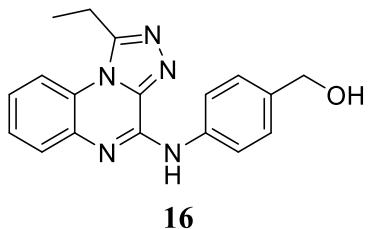
16

Compound **16** was obtained following the general synthetic procedure (**B**) (36% yield).

^{1}H NMR (400 MHz, DMSO-d_6) δ 10.08 (s, 1H), 8.15 (d, J = 8.3 Hz, 1H), 8.11 (d, J = 8.5 Hz, 2H), 7.75 (dd, J = 8.0, 1.5 Hz, 1H), 7.53 (t, J = 7.6 Hz, 1H), 7.44 (t, J = 7.9 Hz, 1H), 7.28 (d, J = 8.3 Hz, 2H), 3.96 (d, J = 9.0 Hz, 2H), 3.49 (q, J = 7.3 Hz, 2H), 1.51 (t, J = 7.3 Hz, 3H). HRMS: calcd for $C_{18}H_{17}N_5O$ 319.1433, found m/z = 320.2542 [M + H]$^+$.

5-((1-ethyl-[1,2,4]triazolo[4,3-a]quinoxalin-4-yl)amino)-1H-imidazole-4-

*carbonitrile (**17**)*
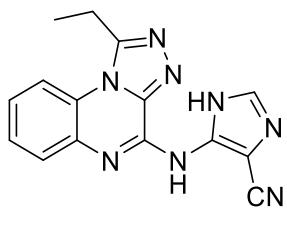
17

Compound **17** was obtained following the general synthetic procedure (**B**) (80% yield).

^{1}H NMR (600 MHz, DMSO-d_6) δ 8.18 (d, J = 8.0 Hz, 1H), 7.87 (d, J = 8.0 Hz, 1H), 7.79 (s, 1H), 7.56 (t, J = 7.8 Hz, 1H), 7.49 (t, J = 7.8 Hz, 1H), 3.51 (d, J = 7.4 Hz, 2H), 1.51 (t, J = 7.4 Hz, 3H). ^{13}C NMR (100 MHz, DMSO-d_6) δ 158.4, 158.1, 149.4, 131.8, 131.7, 127.2, 125.3, 117.4, 116.2, 116.0, 114.5, 21.5, 11.0. HRMS: calcd for $C_{15}H_{12}N_8$ 304.1185, found m/z = 327.1076 [M + Na]$^+$.

2-((3-((1-ethyl-[1,2,4]triazolo[4,3-a]quinoxalin-4-yl)amino)phenyl)sulfonyl)ethan-1-

ol (18)
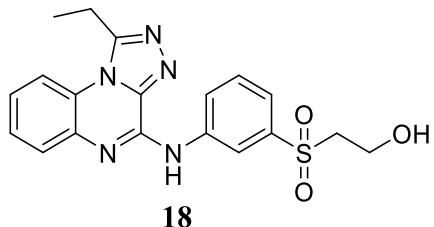
Compound **18** was obtained following the general synthetic procedure (**B**) (48% yield).

^{1}H NMR (400 MHz, DMSO-d_6) δ 10.60 (s, 1H), 8.95 (t, J = 2.0 Hz, 1H), 8.41 (d, J =

8.1 Hz, 1H), 8.18 (d, J = 7.1 Hz, 1H), 7.76 (dd, J = 8.1, 1.6 Hz, 1H), 7.65 (t, J = 7.9

Hz, 1H), 7.61 – 7.55 (m, 2H), 7.54 – 7.47 (m, 1H), 4.93 (t, J = 5.6 Hz, 1H), 3.75 (q, J

= 7.3 Hz, 2H), 3.55 – 3.43 (m, 4H), 1.52 (t, J = 7.3 Hz, 3H).^{13}C NMR (100 MHz,

DMSO-d_6) δ 153.2, 143.4, 140.5, 140.1, 139.6, 136.2, 129.6, 127.3, 125.2, 125.1,

124.3, 121.4, 119.3, 116.2, 57.7, 55.1, 21.6, 11.0. HRMS: calcd for $C_{19}H_{19}N_5O_3S$

397.1209, found m/z = 420.1102 [M + Na]$^+$.

*4-((1-ethyl-[1,2,4]triazolo[4,3-a]quinoxalin-4-yl)amino)-N-(1H-indazol-6-*

yl)benzenesulfonamide (19)
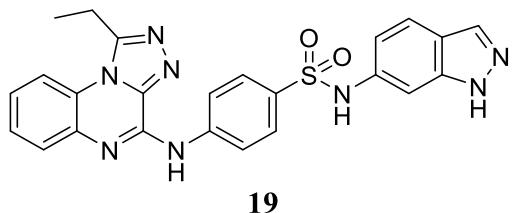
Compound **19** was obtained following the general synthetic procedure (**B**) (40% yield).

^{1}H NMR (400 MHz, DMSO-d_6) δ 10.54 (s, 1H), 10.34 (s, 1H), 8.38 (d, J = 9.0 Hz,

2H), 8.17 (d, J = 8.3 Hz, 1H), 7.93 (s, 1H), 7.84 (dd, J = 7.9, 1.6 Hz, 1H), 7.77 (d, J =

9.0 Hz, 2H), 7.63 – 7.54 (m, 2H), 7.55 – 7.46 (m, 1H), 7.29 (s, 1H), 6.92 (dd, J = 8.3,

1.6 Hz, 1H), 3.49 (q, J = 7.3 Hz, 2H), 1.51 (t, J = 7.3 Hz, 3H). ^{13}C NMR (150 MHz,

DMSO-d_6) δ 153.7, 144.3, 143.6, 140.6, 140.0, 136.7, 136.5, 133.9, 132.8, 128.1, 128.0, 127.7, 126.0, 124.8, 121.7, 120.3, 120.1, 116.7, 115.2, 100.1, 22.1, 11.5. HRMS: calcd for $C_{24}H_{20}N_8O_2S$ 484.1430, found m/z = 507.1312 [M + Na]$^+$.

N-(diaminomethylene)-4-((1-ethyl-[1,2,4]triazolo[4,3-a]quinoxalin-4-yl)amino)benzenesulfonamide (20)
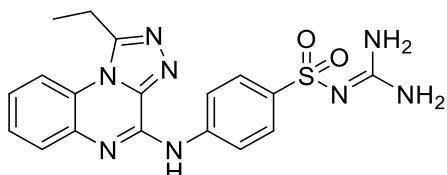
20

Compound **20** was obtained following the general synthetic procedure (**B**) (95% yield).

^{1}H NMR (600 MHz, DMSO-d_6) δ 10.48 (s, 1H), 8.33 (d, J = 8.8 Hz, 2H), 8.18 (dd, J = 8.4, 1.3 Hz, 1H), 7.84 (dd, J = 8.0, 1.5 Hz, 1H), 7.75 (d, J = 8.8 Hz, 2H), 7.57 (td, J = 7.7, 1.3 Hz, 1H), 7.50 (td, J = 7.7, 7.2, 1.5 Hz, 1H), 6.72 (brs, 3H), 3.50 (q, J = 7.3 Hz, 2H), 1.52 (t, J = 7.3 Hz, 3H). ^{13}C NMR (150 MHz, DMSO-d_6) δ 158.1, 153.2, 143.3, 142.2, 139.7, 138.2, 136.3, 127.5, 127.3, 126.3, 125.2, 124.3, 119.8, 116.2, 21.6, 11.1. HRMS: calcd for $C_{18}H_{18}N_8O_2S$ 410.1273, found m/z = 433.1161 [M + Na]$^+$.

6-((1-ethyl-[1,2,4]triazolo[4,3-a]quinoxalin-4-yl)amino)benzo[d]oxazol-2-ol (21)
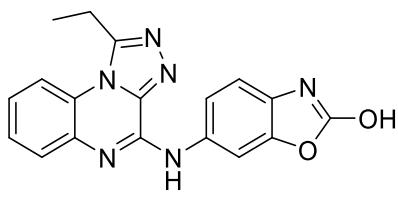
21

Compound **21** was obtained following the general synthetic procedure (**B**) (98% yield).

^{1}H NMR (400 MHz, DMSO-d_6) δ 11.55 (s, 1H), 10.22 (s, 1H), 8.30 (d, J = 1.9 Hz, 1H), 8.14 (dd, J = 8.4, 1.3 Hz, 1H), 7.89 (dd, J = 8.5, 2.0 Hz, 1H), 7.76 (dd, J = 8.1,

1.5 Hz, 1H), 7.53 (td, *J* = 7.9, 7.2, 1.3 Hz, 1H), 7.44 (td, *J* = 7.9, 7.2, 1.3 Hz, 1H), 7.10

(d, *J* = 8.5 Hz, 1H), 3.48 (q, *J* = 7.3 Hz, 2H), 1.51 (t, *J* = 7.3 Hz, 3H). ^{13}C NMR (100

MHz, DMSO-d_6) δ 154.7, 153.1, 143.4, 143.1, 139.6, 136.7, 134.5, 127.2, 127.1,

125.6, 124.6, 124.1, 116.3, 116.1, 109.3, 103.0, 21.6, 11.1. HRMS: calcd for

$C_{18}H_{14}N_6O_2$ 346.1178, found *m/z* = 369.1066 [M + Na]$^+$.

2-(4-((1-propyl-[1,2,4]triazolo[4,3-a]quinoxalin-4-yl)amino)phenyl)-2-

*methylpropanenitrile (**41**)*

41
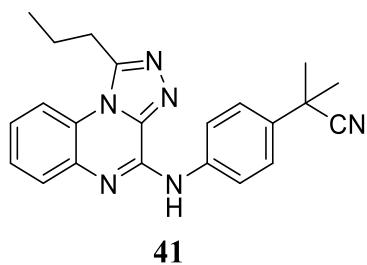
Compound **41** was obtained following the general synthetic procedure (**B**) (85% yield).

^{1}H NMR (400 MHz, DMSO-d_6) δ 10.24 (s, 1H), 8.23 (d, *J* = 8.8 Hz, 2H), 8.13 (dd, *J*

= 8.4, 1.6 Hz, 1H), 7.76 (dd, *J* = 8.0, 1.6 Hz, 1H), 7.56 – 7.50 (m, 3H), 7.46 (td, *J* =

8.0, 7.4, 1.6 Hz, 1H), 3.44 (t, *J* = 7.4 Hz, 2H), 1.97 (h, *J* = 7.4 Hz, 2H), 1.71 (s, 6H),

1.10 (t, *J* = 7.4 Hz, 3H). ^{13}C NMR (100 MHz, DMSO-d_6) δ 151.9, 143.4, 139.6, 139.1,

136.6, 135.6, 127.2, 125.3, 124.8, 124.7, 124.1, 120.8, 116.0, 36.1, 29.5, 28.4, 19.5,

13.6. HRMS: calcd for $C_{22}H_{22}N_6$ 370.1906, found *m/z* = 371.1988 [M + H]$^+$.

2-(4-((1-butyl-[1,2,4]triazolo[4,3-a]quinoxalin-4-yl)amino)phenyl)-2-

methylpropanenitrile (42)
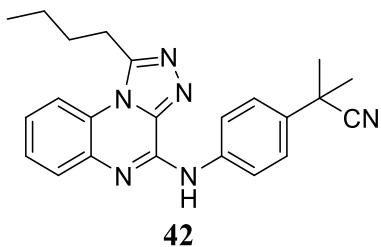
42

Compound **42** was obtained following the general synthetic procedure (**B**) (80% yield).

^{1}H NMR (400 MHz, DMSO-d_6) δ 10.24 (s, 1H), 8.23 (d, J = 8.8 Hz, 2H), 8.13 (dd, J

= 8.0, 1.5 Hz, 1H), 7.77 (dd, J = 8.0, 1.5 Hz, 1H), 7.57 − 7.50 (m, 3H), 7.47 (td, J =

8.0, 7.5, 1.5 Hz, 1H), 3.46 (t, J = 7.5 Hz, 2H), 1.93 (p, J = 7.5 Hz, 2H), 1.71 (s, 6H)

1.53 (h, J = 7.5 Hz, 2H), 0.99 (t, J = 7.4 Hz, 3H). ^{13}C NMR (100 MHz, DMSO-d_6) δ

152.0, 143.4, 139.6, 139.1, 136.6, 135.6, 127.2, 125.3, 124.8, 124.7, 124.1, 120.8,

116.0, 36.1, 28.3, 28.2, 27.4, 21.7, 13.7. HRMS: calcd for $C_{23}H_{24}N_6$ 384.2062, found

m/z = 385.2133 [M + H]$^+$.

N-(3-(1-ethyl-[1,2,4]triazolo[4,3-a]quinoxalin-4-yl)phenyl)acetamide (22)
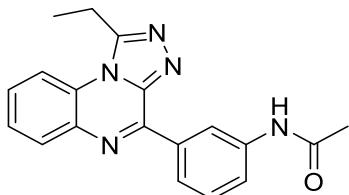
22

Compound **22** was obtained following the general synthetic procedure (**D**) (27%

yield). ^{1}H NMR (400 MHz, DMSO-d_6) δ 10.25 (s, 1H), 8.81 (t, J = 1.9 Hz, 1H), 8.47

(dt, J = 7.9, 1.4 Hz, 1H), 8.36 (dd, J = 8.3, 1.4 Hz, 1H), 8.15 (dd, J = 7.9, 1.4 Hz, 1H),

7.96 (d, J = 9.1 Hz, 1H), 7.82 − 7.69 (m, 2H), 7.54 (t, J = 8.0 Hz, 1H), 3.56 (q, J = 7.3

Hz, 2H), 2.10 (s, 3H), 1.54 (t, J = 7.3 Hz, 3H). ^{13}C NMR (100 MHz, DMSO-d_6) δ

168.5, 152.1, 148.5, 143.9, 139.4, 135.8, 135.3, 130.1, 129.5, 128.7, 127.4, 125.9, 124.5, 121.9, 119.9, 116.4, 24.0, 21.7, 11.0. HRMS: calcd for $C_{19}H_{17}N_5O$ 331.1433, found m/z = 332.1508 $[M + H]^+$.

2-(4-(1-ethyl-[1,2,4]triazolo[4,3-a]quinoxalin-4-yl)phenyl)acetonitrile (23)

23
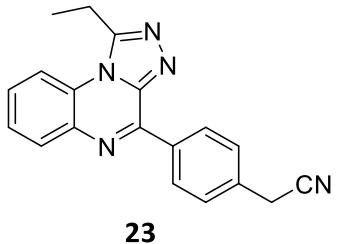
Compound **23** was obtained following the general synthetic procedure (**D**) (25% yield). ^{1}H NMR (400 MHz, DMSO-d_6) δ 8.81 (d, J = 8.4 Hz, 2H), 8.37 (d, J = 8.1 Hz, 1H), 8.18 (dd, J = 7.9, 1.7 Hz, 1H), 7.84 – 7.67 (m, 2H), 7.62 (d, J = 8.1 Hz, 2H), 4.21 (s, 2H), 3.56 (q, J = 7.3 Hz, 2H), 1.54 (t, J = 7.3 Hz, 3H). ^{13}C NMR (100 MHz, DMSO-d_6) δ 152.1, 147.9, 143.9, 135.7, 134.5, 134.1, 130.1, 130.0, 129.6, 128.2, 127.4, 125.9, 119.0, 116.4, 22.4, 21.7, 11.0. HRMS: calcd for $C_{19}H_{15}N_5$ 313.1327, found m/z = 336.1227 $[M + Na]^+$.

4-(5-bromo-2,3-dihydrobenzofuran-7-yl)-1-ethyl-[1,2,4]triazolo[4,3-a]quinoxaline

(24)

24
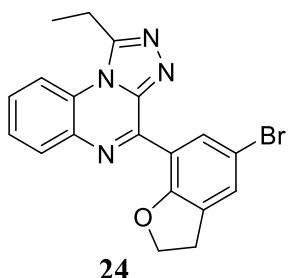
Compound **24** was obtained following the general synthetic procedure (**D**) (35% yield). ^{1}H NMR (400 MHz, DMSO-*d*₆) δ 8.35 (d, *J* = 8.6 Hz, 1H), 8.11 (dd, *J* = 8.0, 1.6 Hz, 1H), 7.91 (d, *J* = 2.2 Hz, 1H), 7.81 (td, *J* = 8.4, 7.8, 1.6 Hz, 1H), 7.73 (td, *J* = 7.7, 1.3 Hz, 1H), 7.63 (d, *J* = 2.2 Hz, 1H), 4.61 (t, *J* = 8.7 Hz, 2H), 3.54 (q, *J* = 7.4 Hz, 2H), 3.34 – 3.27 (m, 2H), 1.52 (t, *J* = 7.3 Hz, 3H). ^{13}C NMR (100 MHz, DMSO-*d*₆) δ 157.8, 152.2, 147.6, 143.7, 135.8, 132.0, 131.2, 130.1, 129.8, 129.6, 127.4, 125.9, 119.2, 116.5, 110.5, 72.1, 28.8, 21.6, 11.0. HRMS: calcd for $C_{19}H_{15}BrN_4O$ 394.0429, found *m/z* = 417.0308 [M + Na]⁺.

*4-(5-bromo-2-methoxyphenyl)-1-ethyl-[1,2,4]triazolo[4,3-a]quinoxaline (25)*

25
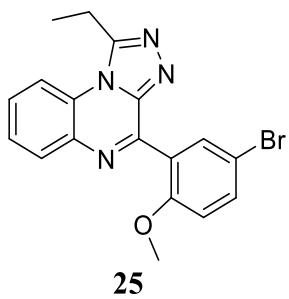
Compound **25** was obtained following the general synthetic procedure (**D**) (63% yield). ^{1}H NMR (400 MHz, DMSO-*d*₆) δ 8.37 (dd, *J* = 8.5, 1.3 Hz, 1H), 8.13 (dd, *J* = 8.0, 1.6 Hz, 1H), 7.83 (td, *J* = 8.5, 7.9, 1.6 Hz, 1H), 7.77 – 7.71 (m, 2H), 7.69 (d, *J* = 2.6 Hz, 1H), 7.23 (d, *J* = 8.9 Hz, 1H), 3.73 (s, 3H), 3.55 (q, *J* = 7.3 Hz, 2H), 1.52 (t, *J*

= 7.3 Hz, 3H). ^{13}C NMR (100 MHz, DMSO-d_6) δ 156.9, 152.0, 149.4, 144.2, 135.8, 133.7, 132.6, 130.1, 129.8, 127.4, 127.0, 126.0, 116.6, 114.4, 111.5, 56.1, 21.6, 11.0.

HRMS: calcd for $C_{18}H_{15}BrN_4O$ 382.0429, found m/z = 383.0508 [M + H]$^+$.

*3-(1-ethyl-[1,2,4]triazolo[4,3-a]quinoxalin-4-yl)benzamide (**26**)*

26
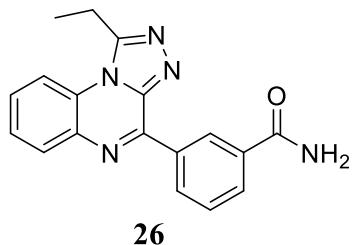
Compound **26** was obtained following the general synthetic procedure (**D**) (77% yield). ^{1}H NMR (600 MHz, DMSO-d_6) δ 9.19 (t, J = 1.6 Hz, 1H), 8.94 (d, J = 8.0 Hz, 1H), 8.39 (d, J = 8.3 Hz, 1H), 8.23 (dd, J = 7.9, 1.6 Hz, 1H), 8.17 (s, 1H), 8.11 (d, J = 7.7 Hz, 1H), 7.82 (td, J = 8.4, 7.9, 1.6 Hz, 1H), 7.77 (td, J = 7.7, 1.2 Hz, 1H), 7.72 (t, J = 7.8 Hz, 1H), 7.54 (s, 1H), 3.58 (q, J = 7.3 Hz, 2H), 1.55 (t, J = 7.3 Hz, 3H). ^{13}C NMR (150 MHz, DMSO-d_6) δ 167.7, 152.2, 148.2, 143.9, 135.8, 134.9, 134.7, 132.3, 130.2, 129.8, 129.7, 128.8, 128.4, 127.5, 126.0, 116.5, 21.7, 11.0. HRMS: calcd for $C_{18}H_{15}N_5O$ 317.1277, found m/z = 340.1170 [M + Na]$^+$.

*3-(1-ethyl-[1,2,4]triazolo[4,3-a]quinoxalin-4-yl)-N-isopropylbenzamide (**27**)*

27
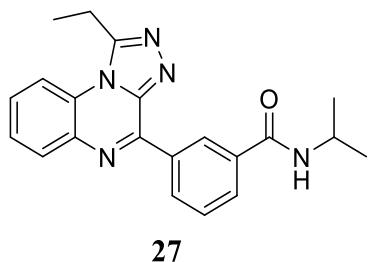
Compound **27** was obtained following the general synthetic procedure (**D**) (80% yield). ^{1}H NMR (400 MHz, DMSO-d_6) δ 9.11 (s, 1H), 8.90 (d, J = 7.2 Hz, 1H), 8.42

(d, *J* = 7.6 Hz, 1H), 8.37 (d, *J* = 8.3 Hz, 1H), 8.20 (d, *J* = 7.9 Hz, 1H), 8.07 (d, *J* = 7.5 Hz, 1H), 7.82 – 7.68 (m, 3H), 4.21 – 4.10 (m, 1H), 3.56 (q, *J* = 7.3 Hz, 2H), 1.55 (t, *J* = 7.2 Hz, 3H), 1.22 (d, *J* = 6.1 Hz, 6H). ^{13}C NMR (100 MHz, DMSO-d_6) δ 165.2, 152.1, 148.2, 143.9, 135.7, 135.3, 134.8, 132.0, 130.2 129.6, 129.5, 128.5, 128.2, 127.4, 125.9, 116.4, 41.1, 22.3, 21.7, 11.0. HRMS: calcd for $C_{21}H_{21}N_5O$ 359.1746, found *m/z* = 382.1649 [M + Na]$^+$.

*3-(1-ethyl-[1,2,4]triazolo[4,3-a]quinoxalin-4-yl)-N-methoxybenzamide (**28**)*

28
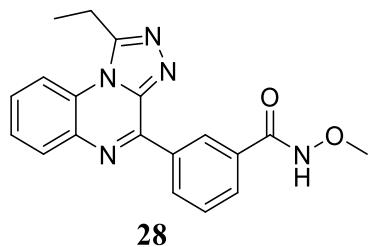
Compound **28** was obtained following the general synthetic procedure (**D**) (38% overall yield). ^{1}H NMR (400 MHz, DMSO-d_6) δ 11.97 (s, 1H), 9.11 (s, 1H), 8.96 (d, *J* = 7.9 Hz, 1H), 8.37 (d, *J* = 8.2 Hz, 1H), 8.21 (dd, *J* = 8.0, 1.7 Hz, 1H), 7.97 (d, *J* = 7.9 Hz, 1H), 7.81 (td, *J* = 8.2, 7.8, 1.7 Hz, 1H), 7.79 – 7.69 (m, 2H), 3.77 (s, 3H), 3.57 (q, *J* = 7.3 Hz, 2H), 1.55 (t, *J* = 7.3 Hz, 3H). ^{13}C NMR (100 MHz, DMSO-d_6) δ 163.9, 152.1, 147.8, 143.9, 135.7, 135.1, 132.7, 132.6, 130.2, 129.7, 129.4, 128.6, 128.3, 127.5, 126.0, 116.4, 63.3, 21.7, 11.0. HRMS: calcd for $C_{19}H_{17}N_5O_2$ 347.1382, found *m/z* = 370.1280 [M + Na]$^+$.

5-(1-ethyl-[1,2,4]triazolo[4,3-a]quinoxalin-4-yl)-2-fluoro-N-(2-

hydroxyethyl)benzamide (29)

29
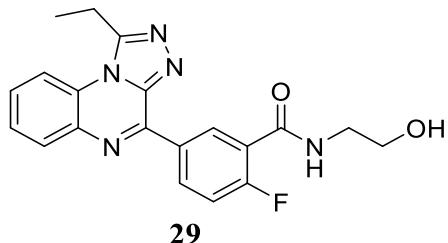
Compound **29** was obtained following the general synthetic procedure (**D**) (25%

yield). ^{1}H NMR (400 MHz, DMSO-d_6) δ 9.06 (dd, J = 7.1, 2.4 Hz, 1H), 9.02 – 8.97

(m, 1H), 8.43 (brs, 1H), 8.38 (d, J = 8.2 Hz, 1H), 8.21 (dd, J = 7.9, 1.6 Hz, 1H), 7.86

– 7.71 (m, 2H), 7.57 (t, J = 9.4 Hz, 1H), 4.78 (t, J = 5.5 Hz, 1H), 3.62 – 3.52 (m, 4H),

3.39 (q, J = 5.9 Hz, 2H), 1.55 (t, J = 7.3 Hz, 3H). ^{13}C NMR (100 MHz, DMSO-d_6) δ

163.4, 160.8 (d, J = 254.3 Hz), 152.1, 146.8, 143.8, 135.6, 133.5 (d, J = 9.2 Hz), 131.5

(d, J = 3.4 Hz), 131.1 (d, J = 3.1 Hz), 130.2, 129.7, 127.5, 125.9, 124.4 (d, J = 15.9

Hz), 116.5, 116.4 (d, J = 23.4 Hz), 59.5, 42.2, 21.7, 11.0. HRMS: calcd for

$C_{20}H_{18}FN_5O_2$ 379.1445, found m/z = 402.1361 [M + Na]$^+$.

N-(3-(1-ethyl-[1,2,4]triazolo[4,3-a]quinoxalin-4-yl)benzyl)methanesulfonamide (30)

30
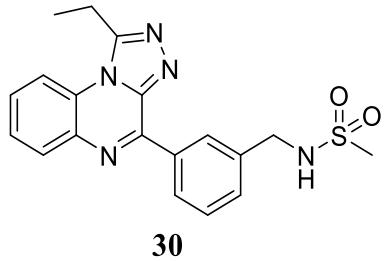
Compound **30** was obtained following the general synthetic procedure (**D**) (67%

yield). ^{1}H NMR (400 MHz, DMSO-d_6) δ 8.72 – 8.67 (m, 2H), 8.31 (d, J = 7.7 Hz, 1H),

8.13 (dd, J = 7.8, 1.7 Hz, 1H), 7.80 – 7.66 (m, 3H), 7.61 (d, J = 5.1 Hz, 2H), 4.32 (d,

J = 6.3 Hz, 2H), 3.53 (q, J = 7.3 Hz, 2H), 2.95 (s, 3H), 1.54 (t, J = 7.3 Hz, 3H). ^{13}C

NMR (100 MHz, DMSO-d_6) δ 152.0, 148.4, 143.9, 138.6, 135.7, 134.9, 130.5, 130.0, 129.4, 128.6, 128.5, 128.4, 127.3, 125.8, 116.3, 46.1, 39.9, 21.7, 11.0. HRMS: calcd for $C_{19}H_{19}N_5O_2S$ 381.1259, found m/z = 404.1153 [M + Na]$^+$.

3-(1-ethyl-[1,2,4]triazolo[4,3-a]quinoxalin-4-yl)phenol (31)

31
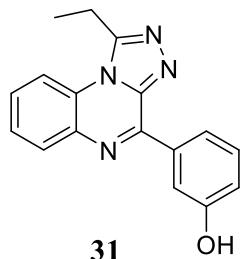
Compound **31** was obtained following the general synthetic procedure (**D**) (45% yield). ^{1}H NMR (600 MHz, DMSO-d_6) δ 9.79 (s, 1H), 8.36 (d, J = 8.0 Hz, 1H), 8.25 – 8.22 (m, 2H), 8.16 (dd, J = 7.9, 1.6 Hz, 1H), 7.79 (td, J = 8.5, 7.9, 1.7 Hz, 1H), 7.77 – 7.71 (m, 1H), 7.42 (t, J = 8.1 Hz, 1H), 7.01 (dd, J = 8.0, 1.4 Hz, 1H), 3.56 (q, J = 7.3 Hz, 2H), 1.54 (t, J = 7.3 Hz, 3H). ^{13}C NMR (150 MHz, DMSO-d_6) δ 157.3, 152.0, 148.5, 144.0, 136.0, 135.8, 130.1, 129.4, 129.4, 127.4, 125.9, 120.5, 118.4, 116.4, 116.2, 21.8, 11.1. HRMS: calcd for $C_{17}H_{14}N_4O$ 290.1168, found m/z = 291.1244 [M + H]$^+$.

*3-(1-ethyl-[1,2,4]triazolo[4,3-a]quinoxalin-4-yl)-5-fluorophenol (32)*

32
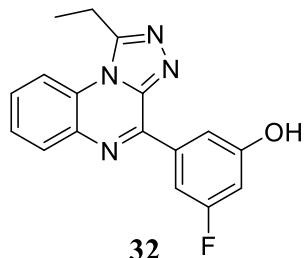
Compound **32** was obtained following the general synthetic procedure (**D**) (35% yield). ^{1}H NMR (400 MHz, DMSO-d_6) δ 10.29 (s, 1H), 8.37 (d, J = 8.3 Hz, 1H), 8.22

– 8.14 (m, 2H), 8.06 (d, J = 10.4 Hz, 1H), 7.81 (t, J = 7.9 Hz, 1H), 7.75 (t, J = 7.7 Hz, 1H), 6.83 (d, J = 10.8 Hz, 1H), 3.56 (q, J = 7.3 Hz, 2H), 1.54 (t, J = 7.3 Hz, 3H). ^{13}C NMR (100 MHz, DMSO-d_6) δ 162.7 (d, J = 241.1 Hz), 158.9 (d, J = 12.1 Hz), 152.1, 147.0 (d, J = 2.8 Hz), 143.8, 137.1 (d, J = 10.9 Hz), 135.5, 130.2, 129.8, 127.5, 126.0, 116.4, 112.8, 106.7 (d, J = 24.2 Hz), 105.3 (d, J = 24.2 Hz), 21.7, 11.0. HRMS: calcd for $C_{17}H_{13}FN_4O$ 308.1073, found m/z = 331.0976 [M + Na]$^+$.

3-(1-ethyl-[1,2,4]triazolo[4,3-a]quinoxalin-4-yl)-5-(trifluoromethyl)phenol (33)
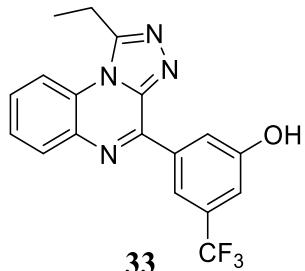
Compound **33** was obtained following the general synthetic procedure (**D**) (54% yield). ^{1}H NMR (400 MHz, DMSO-d_6) δ 8.60 (s, 1H), 8.55 (s, 1H), 8.34 (d, J = 8.3 Hz, 1H), 8.17 (d, J = 8.0 Hz, 1H), 7.80 (t, J = 7.8 Hz, 1H), 7.73 (t, J = 7.6 Hz, 1H), 7.28 (s, 1H), 3.54 (q, J = 7.4 Hz, 2H), 1.54 (t, J = 7.3 Hz, 3H). ^{13}C NMR (100 MHz, DMSO-d_6) δ 158.0, 152.1, 146.7, 143.8, 137.0, 135.5, 130.4 (q, J = 31.3 Hz), 130.3, 129.9, 127.5, 126.0, 124.0 (q, J = 273.7 Hz), 120.0, 116.4, 114.2, 114.2, 21.7, 11.0. HRMS: calcd for $C_{18}H_{13}F_3N_4O$ 358.1041, found m/z = 381.0944 [M + Na]$^+$.

*2-chloro-5-(1-ethyl-[1,2,4]triazolo[4,3-a]quinoxalin-4-yl)phenol (**34**)*
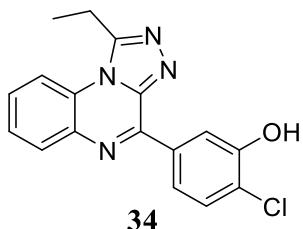
Compound **34** was obtained following the general synthetic procedure (**D**) (41%

yield). ^{1}H NMR (400 MHz, DMSO-d_6) δ 10.62 (s, 1H), 8.54 (d, J = 2.2 Hz, 1H), 8.34

(d, J = 8.1 Hz, 1H), 8.29 (dd, J = 8.4, 2.2 Hz, 1H), 8.12 (dd, J = 7.9, 1.7 Hz, 1H), 7.80

– 7.70 (m, 2H), 7.57 (d, J = 8.4 Hz, 1H), 3.54 (q, J = 7.0 Hz, 2H), 1.53 (t, J = 7.3 Hz,

3H). ^{13}C NMR (100 MHz, DMSO-d_6) δ 153.0, 152.0, 147.3, 143.8, 135.6, 134.5,

130.0, 129.8, 129.5, 127.4, 125.9, 123.0, 121.2, 117.3, 116.4, 21.7, 11.0. HRMS: calcd

for $C_{17}H_{13}ClN_4O$ 324.0778, found m/z = 347.0684 [M + Na]$^+$.


*(3-(1-ethyl-[1,2,4]triazolo[4,3-a]quinoxalin-4-yl)phenyl)methanol (**35**)*
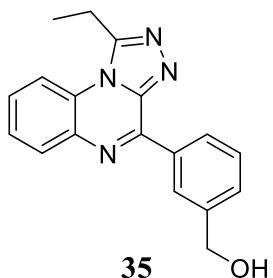
Compound **35** was obtained following the general synthetic procedure (**D**) (74 %

yield). ^{1}H NMR (600 MHz, DMSO-d_6) δ 8.70 – 8.66 (m, 2H), 8.34 (d, J = 7.8 Hz, 1H),

8.16 (dd, J = 7.9, 1.6 Hz, 1H), 7.77 (td, J = 8.5, 7.9, 1.6 Hz, 1H), 7.72 (td, J = 7.6, 1.3

Hz, 1H), 7.61 – 7.55 (m, 2H), 4.66 (s, 2H), 3.54 (q, J = 7.3 Hz, 2H), 1.54 (t, J = 7.3

Hz, 3H). ^{13}C NMR (125 MHz, DMSO-d_6) δ 152.1, 148.7, 144.0, 142.8, 135.8, 134.7,

130.1, 129.4, 129.4, 128.2, 127.4, 127.3, 125.9, 116.4, 62.9, 21.8, 11.0. HRMS: calcd

for $C_{18}H_{16}N_4O$ 304.1324, found m/z = 327.1221 [M + Na]$^+$.

(5-(1-ethyl-[1,2,4]triazolo[4,3-a]quinoxalin-4-yl)-2-fluorophenyl)methanol (36)

36
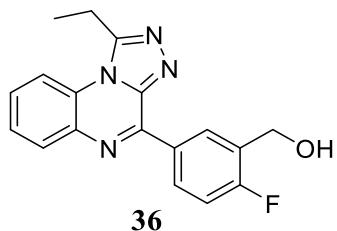
Compound **36** was obtained following the general synthetic procedure (**D**) (64% yield). ^{1}H NMR (400 MHz, DMSO-d_6) δ 8.91 (d, J = 7.5 Hz, 1H), 8.86 – 8.78 (m, 1H), 8.35 (d, J = 8.2 Hz, 1H), 8.17 (dd, J = 7.8, 1.8 Hz, 1H), 7.83 – 7.69 (m, 2H), 7.41 (t, J = 9.3 Hz, 1H), 5.49 (t, J = 5.6 Hz, 1H), 4.69 (d, J = 5.1 Hz, 2H), 3.56 (q, J = 7.3 Hz, 2H), 1.54 (t, J = 7.3 Hz, 3H). ^{13}C NMR (150 MHz, DMSO-d_6) δ 161.5 (d, J = 250.4 Hz), 152.1, 147.6, 143.9, 135.8, 131.0 (d, J = 3.1 Hz), 130.6 (d, J = 8.8 Hz), 130.3 (d, J = 5.5 Hz), 130.1, 129.5, 129.5 (d, J = 15.6 Hz), 127.5, 125.9, 116.5, 115.0 (d, J = 22.1 Hz) 79.2, 56.8, 21.7, 11.0. HRMS: calcd for $C_{18}H_{15}FN_4O$ 322.1230, found m/z = 345.1132 [M + Na]$^+$.

*(4-(1-ethyl-[1,2,4]triazolo[4,3-a]quinoxalin-4-yl)thiophen-2-yl)methanol (37)*

37
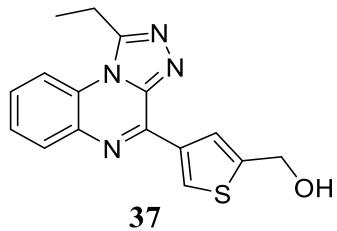
Compound **37** was obtained following the general synthetic procedure (**D**) (98% yield). ^{1}H NMR (600 MHz, DMSO-d_6) δ 9.14 (d, J = 1.4 Hz, 1H), 8.33 (d, J = 8.3 Hz, 1H), 8.11 (dd, J = 7.9, 1.6 Hz, 1H), 8.03 (d, J = 1.2 Hz, 1H), 7.79 – 7.73 (m, 1H), 7.72 (td, J = 7.5, 1.3 Hz, 1H), 5.68 (t, J = 5.7 Hz, 1H), 4.76 (d, J = 4.4 Hz, 2H), 3.55 (q, J = 7.3 Hz, 2H), 1.54 (t, J = 7.4 Hz, 3H). ^{13}C NMR (150 MHz, DMSO-d_6) δ 152.2,

147.1, 144.4, 143.5, 136.4, 135.9, 131.0, 129.8, 129.2, 127.5, 125.7, 123.7, 116.5, 58.4, 21.8, 11.1. HRMS: calcd for $C_{16}H_{14}N_4OS$ 310.0888, found m/z = 333.0793 $[M + Na]^+$.

*N-(3-acetamidophenyl)-3-chloroquinoxaline-2-carboxamide (**1g-I**)*

1g-I
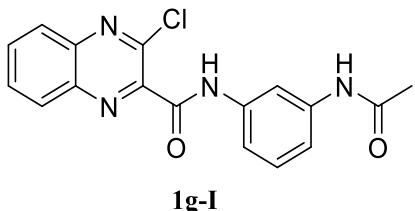
Compound **1g-I** was obtained following the general synthetic procedure (**E**) (45% yield). ^1H NMR (400 MHz, CDCl$_3$) δ 9.62 (s, 1H), 8.22 (dd, J = 7.8, 1.9 Hz, 1H), 8.14 – 8.07 (m, 2H), 7.99 – 7.86 (m, 2H), 7.62 (d, J = 7.5 Hz, 1H), 7.40 – 7.32 (m, 2H), 2.21 (s, 3H). HRMS: calcd for $C_{17}H_{13}ClN_4O_2$ 340.0727, found m/z = 363.0634 $[M + Na]^+$.

*3-chloro-N-(4-(cyanomethyl)phenyl)quinoxaline-2-carboxamide (**1g-II**)*
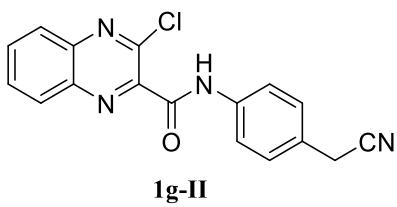
1g-II

Compound **1g-II** was obtained following the general synthetic procedure (**E**) (68% yield). ^1H NMR (600 MHz, MeOD) δ 8.23 (dd, J = 8.3, 1.4 Hz, 1H), 8.10 (dd, J = 8.4, 1.3 Hz, 1H), 8.02 – 7.93 (m, 2H), 7.80 (d, J = 8.5 Hz, 2H), 7.43 (d, J = 8.5 Hz, 2H), 3.93 (s, 2H). HRMS: calcd for $C_{17}H_{11}ClN_4O$ 322.0621, found m/z = 345.0514 $[M + Na]^+$.

Experimental Section

*N-(3-acetamidophenyl)-3-hydrazineylquinoxaline-2-carboxamide (**1h-I**)*

1h-I
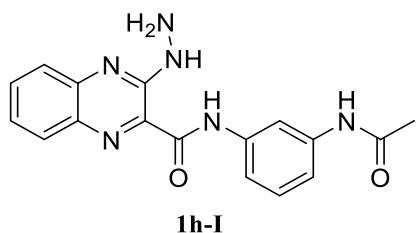
Compound **1h-I** was obtained following the general synthetic procedure (**F**) (50% yield). ^{1}H NMR (400 MHz, DMSO-d_6) δ 10.75 (s, 1H), 10.04 (s, 1H), 9.28 (s, 1H), 8.17 (s, 1H), 8.00 (d, J = 8.3 Hz, 1H), 7.78 – 7.66 (m, 2H), 7.52 – 7.44 (m, 2H), 7.40 (d, J = 8.1 Hz, 1H), 7.31 (t, J = 8.0 Hz, 1H), 2.07 (s, 3H). HRMS: calcd for $C_{17}H_{16}N_6O_2$ 336.1335, found m/z = 337.1470 $[M + H]^+$.

*N-(4-(cyanomethyl)phenyl)-3-hydrazineylquinoxaline-2-carboxamide (**1h-II**)*
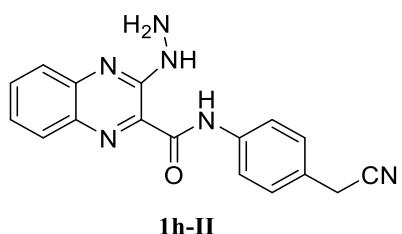
1h-II

Compound **1h-II** was obtained following the general synthetic procedure (**F**) (85% yield). ^{1}H NMR (400 MHz, CDCl$_3$) δ 10.09 (s, 1H), 9.56 (s, 1H), 7.93 (d, J = 8.3 Hz, 1H), 7.82 – 7.74 (m, 3H), 7.70 (t, J = 7.5 Hz, 1H), 7.46 (t, J = 7.5 Hz, 1H), 7.38 (d, J = 8.2 Hz, 2H), 4.22 (s, 2H), 3.77 (s, 2H). HRMS: calcd for $C_{17}H_{14}N_6O$ 318.1229, found m/z = 319.1299 $[M + H]^+$.

N-(3-acetamidophenyl)-1-ethyl-[1,2,4]triazolo[4,3-a]quinoxaline-4-carboxamide

(38)
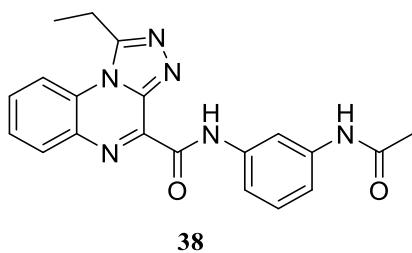
38

Compound **38** was obtained following the general synthetic procedure (**G**) (42% yield). ^{1}H NMR (400 MHz, DMSO-d_6) δ 11.15 (s, 1H), 10.06 (s, 1H), 8.42 (dd, J = 8.5, 1.2 Hz, 1H), 8.25 (dd, J = 8.0, 1.6 Hz, 1H), 8.13 (s, 1H), 7.96 – 7.87 (m, 1H), 7.81 (td, J = 7.7, 1.2 Hz, 1H), 7.50 (d, J = 8.1 Hz, 1H), 7.41 (d, J = 8.5 Hz, 1H), 7.33 (t, J = 8.0 Hz, 1H), 3.58 (q, J = 7.3 Hz, 2H), 2.06 (s, 3H), 1.54 (t, J = 7.3 Hz, 3H). ^{13}C NMR (100 MHz, DMSO-d_6) δ 168.4, 160.3, 152.3, 145.6, 142.9, 139.9, 138.4, 134.9, 131.2, 130.7, 129.2, 127.8, 126.6, 116.8, 115.1, 114.6, 110.5, 24.0, 21.5, 11.0. HRMS: calcd for $C_{20}H_{18}N_6O_2$ 374.1491, found m/z = 397.1391 [M + Na]$^+$.

N-(4-(cyanomethyl)phenyl)-1-ethyl-[1,2,4]triazolo[4,3-a]quinoxaline-4-carboxamide

(39)
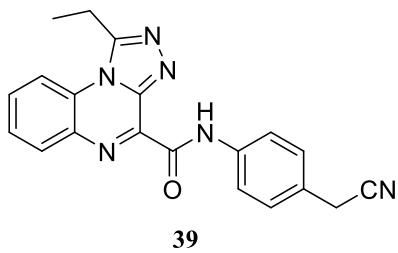
39

Compound **39** was obtained following the general synthetic procedure (**G**) (30% yield). ^{1}H NMR (400 MHz, CDCl$_3$) δ 11.96 (s, 1H), 8.50 (d, J = 7.7 Hz, 1H), 8.25 (d, J = 8.3 Hz, 1H), 7.98 (d, J = 8.3 Hz, 2H), 7.86 (t, J = 7.2 Hz, 1H), 7.79 (t, J = 7.7 Hz, 1H), 7.40 (d, J = 8.2 Hz, 2H), 3.78 (s, 2H), 3.60 (q, J = 7.4 Hz, 2H), 1.74 (t, J = 7.4

Hz, 3H). ^{13}C NMR (100 MHz, CDCl$_3$) δ 158.1, 152.5, 144.1, 142.0, 138.0, 136.2, 133.2, 132.0, 128.9, 128.4, 126.8, 126.5, 121.2, 117.9, 115.5, 23.4, 22.8, 11.3. HRMS: calcd for C$_{20}$H$_{16}$N$_6$O 356.1386, found m/z = 379.1288 [M + Na]$^+$.

5.3 Synthesis of pyrazolopyridine compound 43

Synthesis of the intermediate methyl 1-ethyl-6-(thiophen-2-yl)-1H-pyrazolo[3,4-b]pyridine-4-carboxylate (1m)
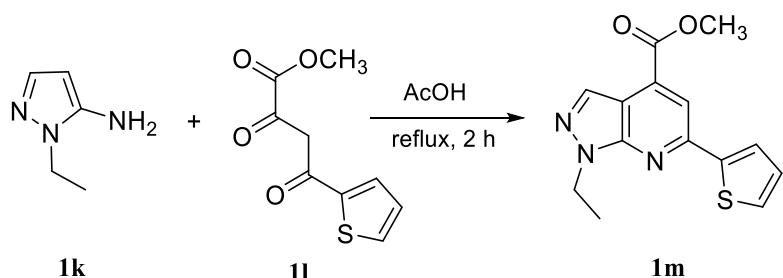
A mixture containing the commercially available 1-ethyl-1H-pyrazol-5-amine **1k** (1 equiv., 0.72 mmol, 80 mg) and 2,4-dioxo-4-thiophen-2-yl-butyric acid methyl ester

1l (1 equiv., 0.72 mmol, 153 mg) in acetic acid (3.6 mL) was refluxed for 2 h. The solvent was then removed under reduced atmosphere and water was added to the obtained solid. The aqueous mixture was then filtered and the obtained precipitate was collected and recrystallized from 2-propanol to give the desired intermediate that was used without further purification (90% yield). ^{1}H NMR (400 MHz, CDCl$_3$) δ 8.31 (s, 1H), 8.07 (s, 1H), 7.76 (d, J = 3.3 Hz, 1H), 7.45 (d, J = 4.9 Hz, 1H), 7.14 (dd, J = 5.0, 3.7 Hz, 1H), 4.61 (q, J = 7.3 Hz, 2H), 4.06 (s, 3H), 1.57 (t, J = 7.3 Hz, 3H). HRMS: calcd for C$_{14}$H$_{13}$N$_3$O$_2$S 287.0728, found m/z = 310.0622 [M + Na]$^+$.

Synthesis of the intermediate 1-ethyl-6-(thiophen-2-yl)-1H-pyrazolo[3,4-b]pyridine-4-carboxylic acid (1n)
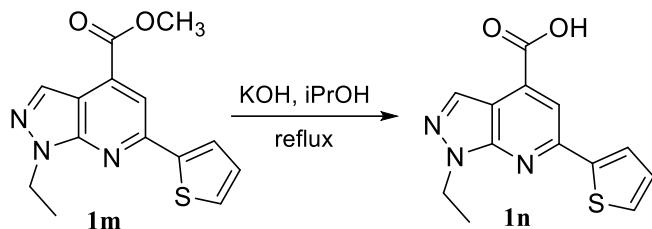
A solution of the obtained ester **1m** (1 equiv., 0.65 mmol, 187 mg) and potassium hydroxide (2 equiv., 1.30 mmol, 73 mg) was refluxed in 2-propanol (9.8 mL) for 2.5 h. After completion, the mixture was cooled to room temperature, diluted with 9.8 mL of water and then neutralized with 2 mL of acetic acid. The obtained precipitate was collected by filtration and dried *in vacuo* overnight. The obtained compound was used for the next step without further purification (100% yield). ^{1}H NMR (400 MHz, MeOD) δ 8.37 (s, 1H), 8.09 (s, 1H), 7.86 (dd, J = 3.7, 1.1 Hz, 1H), 7.56 (dd, J = 5.1, 1.1 Hz, 1H), 7.17 (dd, J = 5.0, 3.7 Hz, 1H), 4.58 (q, J = 7.3 Hz, 2H), 1.53 (t, J = 7.3 Hz, 3H). HRMS: calcd for $C_{13}H_{11}N_3O_2S$ 273.0572, found m/z = 272.0500 [M − H]$^-$.

Synthesis of the final compound 1-ethyl-N-phenyl-6-(thiophen-2-yl)-1H-pyrazolo[3,4-b]pyridine-4-carboxamide (43)
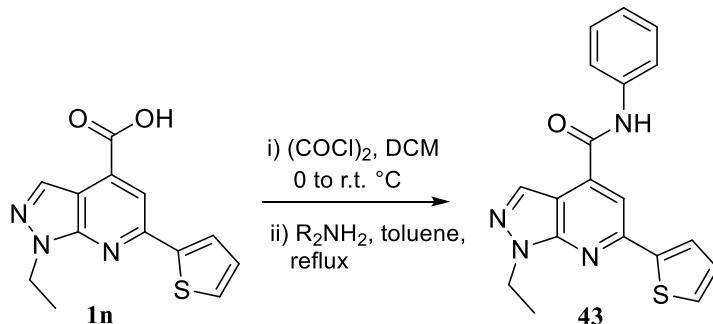
To a solution of the intermediate **1n** (1 equiv., 0.77 mmol, 210 mg) in anhydrous DCM (7.7 mL) was added dropwise oxalyl chloride (13 equiv., 10.00 mmol, 1.5 mL) while

stirring in an ice-bath under nitrogen atmosphere. Then a small amount of anhydrous DMF (0.2 mL) was added and the reaction mixture was stirred at room temperature for 2 h. The solvent was then removed under reduce atmosphere and anhydrous toluene (23.0 mL) was added to the residue. After the addition of aniline (5 equiv., 3.84 mmol, 358 mg), the mixture was refluxed under nitrogen atmosphere for 12 h. After completion of the reaction, the mixture was cooled to room temperature and ethyl acetate was added. The organic phase was then washed with 2 M aqueous solution of HCl and brine, dried over anhydrous sodium sulfate, filtered, and condensed to afford a crude that was purified by silica gel column chromatography in hexane/ethyl acetate (9:1). In order to achieve the desired biology testing purity (>96%), semi-preparative reversed-phase HPLC was carried out by using the gradient conditions from 5% B to 100% B over 50 min, flow rate of 4 mL/min, $\lambda = 240$ nm. The final compound **43** was obtained with 75% overall yield. ^{1}H NMR (500 MHz, DMSO-d_6) δ 10.68 (s, 1H), 8.32 (d, $J = 1.1$ Hz, 1H), 8.26 (s, 1H), 8.08 (d, $J = 3.5$ Hz, 1H), 7.83 (d, $J = 8.0$ Hz, 2H), 7.78 (d, $J = 5.0$ Hz, 1H), 7.42 (t, $J = 8.0$ Hz, 2H), 7.29 – 7.26 (m, 1H), 7.18 (t, $J = 7.4$ Hz, 1H), 4.54 (q, $J = 7.3$ Hz, 2H), 1.49 (t, $J = 7.3$ Hz, 3H). ^{13}C NMR (125 MHz, DMSO-d_6) δ 163.4, 151.3, 150.0, 143.9, 138.5, 137.2, 132.1, 129.9, 128.8, 128.6, 127.8, 124.3, 120.6, 111.4, 111.3, 41.6, 14.7.

5.4 Syntheses of aryl sulfonamide derivatives 3 and 49-74

General synthetic procedure (H) for the syntheses of compounds 3, 49-69 and the

intermediate 1t

3, 49-69 and the
intermediate **1t**
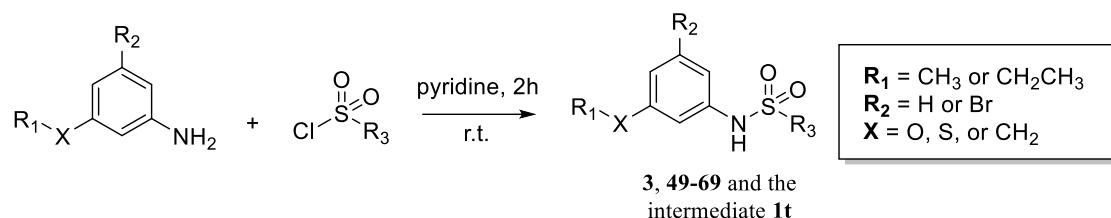
To a solution of the appropriate aniline (1 equiv., 0.49 mmol) in anhydrous pyridine

(2.4 mL) was added the appropriate aryl sulfonyl chloride (1.1 equiv., 0.54 mmol) at

0 °C. The reaction mixture was stirred for 2 hours at room temperature, then pyridine

was removed by rotary evaporator. At the obtained residue was added water that was

extracted with DCM (x3). The organic phase was then dried over sodium sulfate,

filtered, and condensed to afford a crude that was purified either by reversed-phase

HPLC or by silica gel column chromatography, depending on the compound. All final

compounds were characterized by mass spectrometry experiments and NMR analysis

and showed >96% purity.

General synthetic procedure (I) for the syntheses of compounds 70-74

70-74
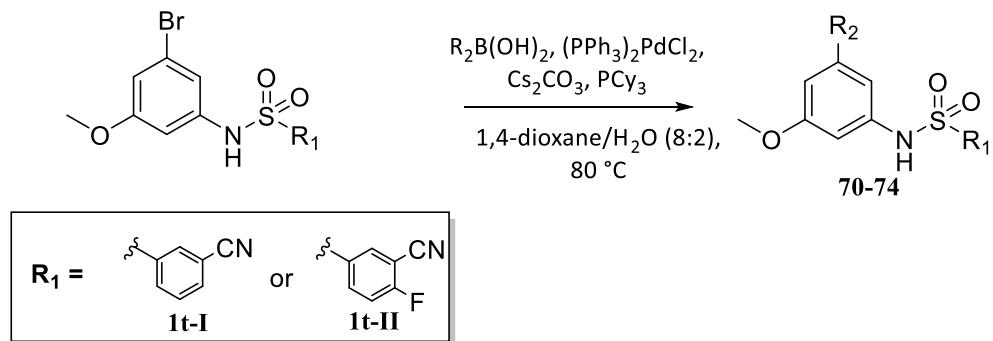
In a two-neck flask were added the previously synthesized intermediate N-(3-bromo-

5-methoxyphenyl)benzenesulfonamide-derivative (1.00 equiv., 0.142 mmol), the

selected phenyl boronic acid (1.50 equiv., 0.212 mmol), PCy_3 (0.05 equiv. 0.007 mmol), $(PPh_3)_2PdCl_2$ (0.05 equiv. 0.007 mmol) and Cs_2CO_3 (3.90 equiv., 0.552 mmol). The flask was evacuated and backfilled with nitrogen three times. Then a degassed solution (1.1 mL) of 1,4-dioxane (80%) and water (20%) was added and the mixture was stirred overnight at 80 °C under nitrogen atmosphere. After completion of the reaction, the mixture was cooled to room temperature, ethyl acetate was added and extracted with distilled water (x2) and brine (x1). The organic phase was dried over anhydrous Na_2SO_4, filtered and concentrated under vacuum. The crude was purified by semi-preparative reversed-phase HPLC by using the gradient conditions from 5% B to 100% B over 50 min, flow rate of 4 mL/min, $\lambda = 240$ nm, to achieve the final compounds **70-74**, whose purity was determined by HPLC (>96%). All final products were characterized by mass spectrometry experiments and NMR analysis.

2,3-dichloro-N-(3-(methylthio)phenyl)benzenesulfonamide (3)
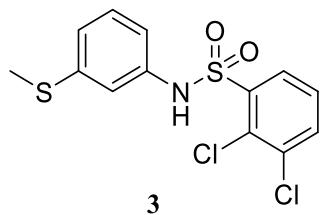
Compound **3** was obtained following the general synthetic procedure (**H**) and purified by semi-preparative reversed-phase HPLC using the gradient conditions from 5% B to 100% B over 50 min, flow rate of 4 mL/min, $\lambda = 240$ nm (87% yield). ^{1}H NMR (400 MHz, DMSO-d_6) δ 10.85 (s, 1H), 8.06 (dd, $J = 8.0$, 1.5 Hz, 1H), 7.92 (dd, $J = 8.0$, 1.5 Hz, 1H), 7.56 (t, $J = 8.0$ Hz, 1H), 7.16 (t, $J = 8.0$ Hz, 1H), 6.94 (t, $J = 1.9$ Hz, 1H), 6.90 (d, $J = 8.0$ Hz, 1H), 6.85 (dd, $J = 8.0$, 2.2 Hz, 1H), 2.36 (s, 3H). ^{13}C NMR (100 MHz, DMSO-d_6) δ 139.4, 138.6, 137.3, 135.1, 134.3, 130.5, 129.8, 128.9, 128.7,

121.3, 115.9, 115.4, 14.4. HRMS: calcd for $C_{13}H_{11}Cl_2NO_2S_2$ 346.9608, found $m/z =$ 369.9504 $[M + Na]^+$.

*2-cyano-N-(3-(methylthio)phenyl)benzenesulfonamide (**49**)*
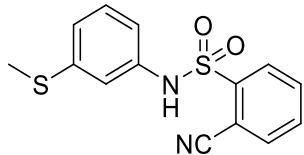
49

Compound **49** was obtained following the general synthetic procedure (**H**) and purified by semi-preparative reversed-phase HPLC using the gradient conditions from 5% B to 100% B over 50 min, flow rate of 4 mL/min, $\lambda = 240$ nm (35% yield). ^{1}H NMR (400 MHz, DMSO-d_6) δ 10.85 (s, 1H), 8.11 – 8.02 (m, 2H), 7.91 (td, $J = 7.8$, 1.4 Hz, 1H), 7.82 (td, $J = 7.8$, 1.4 Hz, 1H), 7.18 (t, $J = 8.3$ Hz, 1H), 6.98 – 6.91 (m, 2H), 6.84 (d, $J = 7.8$ Hz, 1H), 2.38 (s, 3H). ^{13}C NMR (100 MHz, DMSO-d_6) δ 141.0, 139.5, 137.3, 136.0, 134.0, 133.6, 129.7, 129.5, 121.8, 116.9, 116.3, 115.7, 109.3, 14.4. HRMS: calcd for $C_{14}H_{12}N_2O_2S_2$ 304.0340, found $m/z = 327.0234$ $[M + Na]^+$.

*4-bromo-N-(3-(methylthio)phenyl)benzenesulfonamide (**50**)*

50
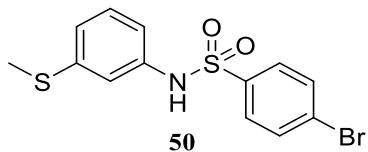
Compound **50** was obtained following the general synthetic procedure (**H**) and purified by semi-preparative reversed-phase HPLC using the gradient conditions from 5% B to 100% B over 50 min, flow rate of 4 mL/min, $\lambda = 240$ nm (95% yield). ^{1}H NMR (400 MHz, DMSO-d_6) δ 10.42 (s, 1H), 7.79 (d, $J = 8.5$ Hz, 2H), 7.68 (d, $J = 8.5$ Hz, 2H), 7.17 (t, $J = 8.1$ Hz, 1H), 6.96 – 6.89 (m, 2H), 6.86 (d, $J = 8.1$ Hz, 1H), 2.38 (s, 3H).

^{13}C NMR (100 MHz, DMSO-d_6) δ 139.8, 139.1, 138.4, 132.9, 130.2, 129.2, 127.4, 122.0, 117.4, 116.8, 14.9. HRMS: calcd for $C_{13}H_{12}BrNO_2S_2$ 356.9493, found m/z = 379.9389 [M + Na]$^+$.

2,6-dichloro-N-(3-(methylthio)phenyl)benzenesulfonamide (51)
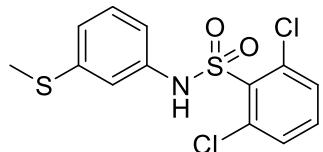
51

Compound **51** was obtained following the general synthetic procedure (**H**) and purified by semi-preparative reversed-phase HPLC using the gradient conditions from 5% B to 100% B over 50 min, flow rate of 4 mL/min, λ = 240 nm (79% yield). ^{1}H NMR (400 MHz, DMSO-d_6) δ 10.88 (s, 1H), 7.66 – 7.61 (m, 2H), 7.57 – 7.52 (m, 1H), 7.17 (t, J = 8.0 Hz, 1H), 6.97 (t, J = 2.0 Hz, 1H), 6.89 (d, J = 7.7 Hz, 1H), 6.85 (dd, J = 8.0, 1.3 Hz, 1H), 2.37 (s, 3H). ^{13}C NMR (100 MHz, DMSO-d_6) δ 139.5, 137.5, 134.5, 134.3, 133.7, 131.9, 129.7, 121.1, 115.0, 114.7, 14.4. HRMS: calcd for $C_{13}H_{11}Cl_2NO_2S_2$ 346.9608, found m/z = 369.9518 [M + Na]$^+$.

2,5-dichloro-N-(3-(methylthio)phenyl)benzenesulfonamide (52)

52

Compound **52** was obtained following the general synthetic procedure (**H**) and purified by semi-preparative reversed-phase HPLC using the gradient conditions from 5% B to 100% B over 50 min, flow rate of 4 mL/min, λ = 240 nm (98% yield). ^{1}H NMR (600

MHz, DMSO-d_6) δ 10.85 (s, 1H), 8.01 (d, J = 2.5 Hz, 1H), 7.74 (dd, J = 8.5, 2.5 Hz,

1H), 7.69 (d, J = 8.5 Hz, 1H), 7.18 (t, J = 8.0 Hz, 1H), 6.94 (t, J = 2.0 Hz, 1H), 6.92

(d, J = 8.0 Hz, 1H), 6.87 (ddd, J = 8.0, 2.0, 0.8 Hz, 1H), 2.38 (s, 3H). ^{13}C NMR (150

MHz, DMSO-d_6) δ 139.4, 137.9, 137.2, 134.6, 133.7, 132.2, 130.8, 129.8, 129.6,

121.5, 116.1, 115.6, 14.4. HRMS: calcd for $C_{13}H_{11}Cl_2NO_2S_2$ 346.9608, found m/z =

369.9518 [M + Na]$^+$.

N-(3-(methylthio)phenyl)-2-nitrobenzenesulfonamide (53)
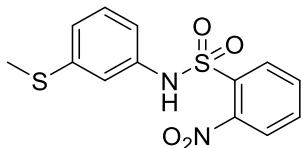
53

Compound **53** was obtained following the general synthetic procedure (**H**) and purified

by semi-preparative reversed-phase HPLC using the gradient conditions from 5% B to

100% B over 50 min, flow rate of 4 mL/min, λ = 240 nm (91% yield). ^{1}H NMR (400

MHz, DMSO-d_6) δ 10.79 (s, 1H), 8.01 – 7.95 (m, 2H), 7.88 – 7.80 (m, 2H), 7.20 (t, J

= 8.0 Hz, 1H), 6.99 – 6.92 (m, 2H), 6.88 (dd, J = 8.0, 2.2 Hz, 1H), 2.38 (s, 3H). ^{13}C

NMR (100 MHz, DMSO-d_6) δ 148.0, 139.5, 137.3, 134.8, 132.6, 131.2, 129.9, 129.8,

129.8, 14.4. HRMS: calcd for $C_{13}H_{12}N_2O_4S_2$ 324.0238, found m/z = 347.0128 [M +

Na]$^+$.

*1-(2,4-dichlorophenyl)-N-(3-(methylthio)phenyl)methanesulfonamide (**54**)*
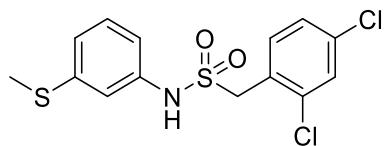
54

Compound **54** was obtained following the general synthetic procedure (**H**) and purified by semi-preparative reversed-phase HPLC using the gradient conditions from 5% B to 100% B over 50 min, flow rate of 4 mL/min, λ = 240 nm (80% yield). ^{1}H NMR (400 MHz, DMSO-d_6) δ 10.09 (s, 1H), 7.62 (d, J = 1.8 Hz, 1H), 7.48 – 7.42 (m, 2H), 7.23 (t, J = 8.0 Hz, 1H), 7.02 (t, J = 2.0 Hz, 1H), 6.97 – 6.92 (m, 2H), 4.64 (s, 2H), 2.43 (s, 3H). ^{13}C NMR (150 MHz, DMSO-d_6) δ 139.3, 138.8, 135.4, 134.6, 134.2, 129.7, 129.0, 127.5, 126.7, 120.6, 115.4, 115.0, 54.0, 14.6. HRMS: calcd for $C_{14}H_{13}Cl_2NO_2S_2$ 360.9765, found m/z = 383.9644 [M + Na]$^{+}$.

*N-(3-(methylthio)phenyl)-1-(3-(trifluoromethyl)phenyl)methanesulfonamide (**55**)*
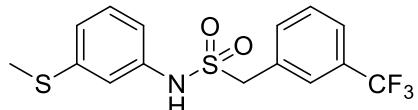
55

Compound **55** was obtained following the general synthetic procedure (**H**) and purified by semi-preparative reversed-phase HPLC using the gradient conditions from 5% B to 100% B over 50 min, flow rate of 4 mL/min, λ = 240 nm (66% yield). ^{1}H NMR (400 MHz, DMSO-d_6) δ 9.92 (s, 1H), 7.71 (d, J = 7.3 Hz, 1H), 7.63 – 7.55 (m, 3H), 7.24 (t, J = 8.0 Hz, 1H), 7.01 (t, J = 2.0 Hz, 1H), 6.96 (dd, J = 8.0, 2.0 Hz, 2H), 4.65 (s, 2H), 2.44 (s, 3H). ^{13}C NMR (100 MHz, DMSO-d_6) δ 139.4, 138.8, 135.1, 131.0, 129.7, 129.4, 129.1 (q, J = 31.3 Hz), 127.5 (q, J = 3.0 Hz), 125.0 (q, J = 3.0 Hz), 124.0 (q, J

= 272.4 Hz), 120.8, 115.8, 115.2, 56.3, 14.5. HRMS: calcd for $C_{15}H_{14}F_3NO_2S_2$ 361.0418, found m/z = 384.0306 [M + Na]$^+$.

1-(3-cyanophenyl)-N-(3-(methylthio)phenyl)methanesulfonamide (56)
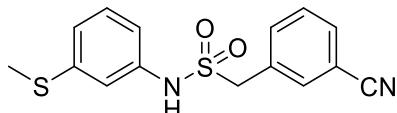
56

Compound **56** was obtained following the general synthetic procedure (**H**) and purified by semi-preparative reversed-phase HPLC using the gradient conditions from 5% B to 100% B over 50 min, flow rate of 4 mL/min, λ = 240 nm (88% yield). ^{1}H NMR (400 MHz, DMSO-d_6) δ 9.93 (s, 1H), 7.82 (dt, J = 7.3, 1.7 Hz, 1H), 7.66 (s, 1H), 7.63 – 7.54 (m, 2H), 7.25 (t, J = 8.0 Hz, 1H), 7.00 (t, J = 2.0 Hz, 1H), 6.98 – 6.94 (m, 2H), 4.61 (s, 2H), 2.45 (s, 3H). ^{13}C NMR (100 MHz, DMSO-d_6) δ 139.4, 138.7, 135.8, 134.4, 131.9, 131.3, 129.7, 129.6, 120.9, 118.4, 115.9, 115.4, 111.3, 56.3, 14.5. HRMS: calcd for $C_{15}H_{14}N_2O_2S_2$ 318.0497, found m/z = 341.0384 [M + Na]$^+$.

N-(3-(methylthio)phenyl)-1-(4-(trifluoromethoxy)phenyl)methanesulfonamide (57)
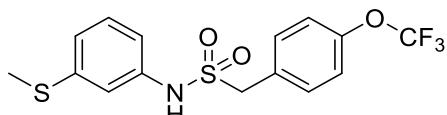

57

Compound **57** was obtained following the general synthetic procedure (**H**) and purified by semi-preparative reversed-phase HPLC using the gradient conditions from 5% B to 100% B over 50 min, flow rate of 4 mL/min, λ = 240 nm (60% yield). ^{1}H NMR (400 MHz, DMSO-d_6) δ 9.91 (s, 1H), 7.42 – 7.33 (m, 4H), 7.24 (t, J = 8.0 Hz, 1H), 7.03 (t, J = 2.9 Hz, 1H), 6.98 – 6.93 (m, 2H), 4.55 (s, 2H), 2.44 (s, 3H). ^{13}C NMR (100 MHz,

DMSO-d_6) δ 148.3, 139.3, 138.8, 132.9, 129.7, 129.0, 120.9, 120.7, 120.0 (q, J = 256.5 Hz), 115.9, 115.3, 56.2, 14.5. HRMS: calcd for $C_{15}H_{14}F_3NO_3S_2$ 377.0367, found *m/z* = 400.0258 [M + Na]$^+$.

*2,3-dichloro-N-(3-methoxyphenyl)benzenesulfonamide (58)*
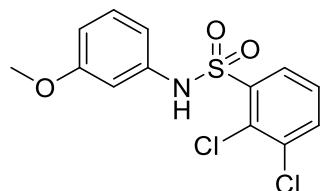
58

Compound **58** was obtained following the general synthetic procedure (**H**) and purified by semi-preparative reversed-phase HPLC using the gradient conditions from 5% B to 100% B over 50 min, flow rate of 4 mL/min, λ = 240 nm (80% yield). ^{1}H NMR (400 MHz, DMSO-d_6) δ 10.79 (s, 1H), 8.06 (dd, J = 8.0, 1.5 Hz, 1H), 7.93 (dd, J = 8.0, 1.5 Hz, 1H), 7.56 (t, J = 8.0 Hz, 1H), 7.14 (t, J = 8.0 Hz, 1H), 6.69 – 6.64 (m, 2H), 6.61 (dd, J = 8.0, 2.1 Hz, 1H), 3.66 (s, 3H). ^{13}C NMR (100 MHz, DMSO-d_6) δ 159.7, 138.7, 137.9, 135.0, 134.2, 130.4, 130.2, 128.9, 128.6, 111.2, 109.1, 105.1, 55.0. HRMS: calcd for $C_{13}H_{11}Cl_2NO_3S$ 330.9837, found *m/z* = 353.9731 [M + Na]$^+$.

*2-cyano-N-(3-methoxyphenyl)benzenesulfonamide (59)*

59

Compound **59** was obtained following the general synthetic procedure (**H**) and purified by semi-preparative reversed-phase HPLC using the gradient conditions from 5% B to 100% B over 50 min, flow rate of 4 mL/min, λ = 240 nm (35% yield). ^{1}H NMR (600

MHz, DMSO-d_6) δ 10.83 (s, 1H), 8.08 (dd, J = 7.8, 1.3 Hz, 1H), 8.06 (dd, J = 8.0, 1.2

Hz, 1H), 7.92 (td, J = 7.8, 1.3 Hz, 1H), 7.83 (td, J = 7.8, 1.3 Hz, 1H), 7.15 (t, J = 8.0

Hz, 1H), 6.69 – 6.63 (m, 3H), 3.67 (s, 3H). ^{13}C NMR (150 MHz, DMSO-d_6) δ 159.8,

141.0, 137.9, 136.1, 134.0, 133.6, 130.2, 129.5, 115.7, 112.1, 109.7, 109.3, 105.9, 55.1.

HRMS: calcd for $C_{14}H_{12}N_2O_3S$ 288.0569, found m/z = 311.0454 $[M + Na]^+$.

4-bromo-N-(3-methoxyphenyl)benzenesulfonamide (60)

60
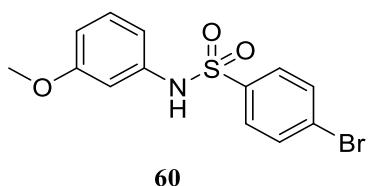
Compound **60** was obtained following the general synthetic procedure (**H**) and purified

by semi-preparative reversed-phase HPLC using the gradient conditions from 5% B to

100% B over 50 min, flow rate of 4 mL/min, λ = 240 nm (94% yield). ^{1}H NMR (400

MHz, DMSO-d_6) δ 10.37 (s, 1H), 7.79 (d, J = 8.6 Hz, 2H), 7.68 (d, J = 8.6 Hz, 2H),

7.14 (t, J = 8.4 Hz, 1H), 6.71 – 6.61 (m, 3H), 3.67 (s, 3H). ^{13}C NMR (100 MHz,

DMSO-d_6) δ 159.7, 138.7, 138.6, 132.4, 130.1, 128.7, 126.8, 112.1, 109.4, 106.0, 55.0.

HRMS: calcd for $C_{13}H_{12}BrNO_3S$ 340.9721, found m/z = 363.9605 $[M + Na]^+$.

*2,5-dichloro-N-(3-methoxyphenyl)benzenesulfonamide (61)*

61
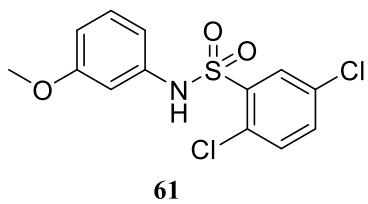
Compound **61** was obtained following the general synthetic procedure (**H**) and purified

by semi-preparative reversed-phase HPLC using the gradient conditions from 5% B to

100% B over 50 min, flow rate of 4 mL/min, λ = 240 nm (70% yield). ^{1}H NMR (400 MHz, CDCl$_3$) δ 8.01 (t, *J* = 1.5 Hz, 1H), 7.42 (d, *J* = 1.5 Hz, 2H), 7.18 (s, 1H), 7.13 (t, *J* = 8.0 Hz, 1H), 6.72 (t, *J* = 2.3 Hz, 1H), 6.71 – 6.62 (m, 2H), 3.74 (s, 3H). ^{13}C NMR (100 MHz, DMSO-*d*$_6$) δ 159.7, 138.0, 137.8, 134.5, 133.7, 132.1, 130.7, 130.2, 129.6, 111.5, 109.4, 105.4, 55.0. HRMS: calcd for C$_{13}$H$_{11}$Cl$_2$NO$_3$S 330.9837, found *m/z* = 353.9744 [M + Na]$^+$.

*N-(3-methoxyphenyl)-2-nitrobenzenesulfonamide (**62**)*

62

Compound **62** was obtained following the general synthetic procedure (**H**) and purified by semi-preparative reversed-phase HPLC using the gradient conditions from 5% B to 100% B over 50 min, flow rate of 4 mL/min, λ = 240 nm (62% yield). ^{1}H NMR (500 MHz, MeOD) δ 7.91 (dd, *J* = 8.0, 1.5 Hz, 1H), 7.83 (dd, *J* = 8.0, 1.5 Hz, 1H), 7.75 (t, *J* = 7.7 Hz, 1H), 7.67 (t, *J* = 7.7 Hz, 1H), 7.13 (t, *J* = 8.0 Hz, 1H), 6.81 – 6.71 (m, 2H), 6.67 (d, *J* = 8.3 Hz, 1H), 3.72 (s, 3H). ^{13}C NMR (125 MHz, MeOD) δ 161.8, 149.9, 139.0, 135.4, 133.2, 133.1, 132.3, 131.1, 125.9, 114.8, 111.9, 108.5, 55.7. HRMS: calcd for C$_{13}$H$_{12}$N$_2$O$_5$S 308.0467, found *m/z* = 331.0368 [M + Na]$^+$.

*1-(2,4-dichlorophenyl)-N-(3-methoxyphenyl)methanesulfonamide (**63**)*

63
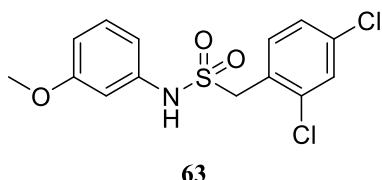
Compound **63** was obtained following the general synthetic procedure (**H**) and purified by semi-preparative reversed-phase HPLC using the gradient conditions from 5% B to 100% B over 50 min, flow rate of 4 mL/min, $\lambda = 240$ nm (76% yield). ^{1}H NMR (400 MHz, DMSO-d_6) δ 10.04 (s, 1H), 7.64 (d, $J = 2.0$ Hz, 1H), 7.50 – 7.41 (m, 2H), 7.22 (t, $J = 8.0$ Hz, 1H), 6.80 – 6.74 (m, 2H), 6.68 – 6.63 (m, 1H), 4.63 (s, 2H), 3.72 (s, 3H). ^{13}C NMR (100 MHz, DMSO-d_6) δ 159.8, 139.4, 135.4, 134.5, 134.1, 130.0, 129.0, 127.4, 126.7, 110.9, 108.6, 104.5, 55.0, 53.7. HRMS: calcd for $C_{14}H_{13}Cl_2NO_3S$ 344.9993, found $m/z = 367.9899$ [M + Na]$^+$.

*1-(3-cyanophenyl)-N-(3-methoxyphenyl)methanesulfonamide (**64**)*

64
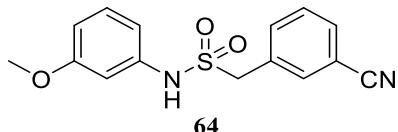
Compound **64** was obtained following the general synthetic procedure (**H**) and purified by semi-preparative reversed-phase HPLC using the gradient conditions from 5% B to 100% B over 50 min, flow rate of 4 mL/min, $\lambda = 240$ nm (93% yield). ^{1}H NMR (600 MHz, MeOD) δ 7.68 (d, $J = 7.7$ Hz, 1H), 7.61 – 7.56 (m, 2H), 7.50 (t, $J = 8.2$ Hz, 1H), 7.21 (t, $J = 8.0$ Hz, 1H), 6.78 – 6.73 (m, 2H), 6.68 (dd, $J = 8.2, 1.5$ Hz, 1H), 4.49 (s, 2H), 3.77 (s, 3H). ^{13}C NMR (150 MHz, MeOD) δ 162.0, 140.6, 136.8, 135.7, 133.2, 132.8, 131.3, 130.7, 119.2, 113.6, 112.5, 110.7, 106.2, 57.3, 55.7. HRMS: calcd for $C_{15}H_{14}N_2O_3S$ 302.0725, found $m/z = 325.0625$ [M + Na]$^+$.

N-(3-methoxyphenyl)-1-(4-(trifluoromethoxy)phenyl)methanesulfonamide (65)


65
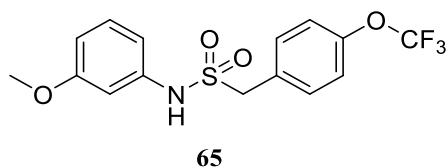
Compound **65** was obtained following the general synthetic procedure (**H**) and purified by semi-preparative reversed-phase HPLC using the gradient conditions from 5% B to 100% B over 50 min, flow rate of 4 mL/min, $\lambda = 240$ nm (78% yield). ^{1}H NMR (400 MHz, DMSO-d_6) δ 9.87 (s, 1H), 7.42 – 7.33 (m, 4H), 7.22 (t, $J = 8.0$ Hz, 1H), 6.80 – 6.74 (m, 2H), 6.67 (d, $J = 8.0$ Hz, 1H), 4.54 (s, 2H), 3.73 (s, 3H). ^{13}C NMR (100 MHz, DMSO-d_6) δ 159.9, 148.3, 139.5, 132.9, 130.1, 129.1, 120.9, 120.0 (q, $J = 256.3$ Hz), 111.1, 108.6, 104.8, 56.0, 55.0. HRMS: calcd for $C_{15}H_{14}F_3NO_4S$ 361.0596, found m/z = 384.0483 $[M + Na]^+$.

2,3-dichloro-N-(3-ethoxyphenyl)benzenesulfonamide (66)

66
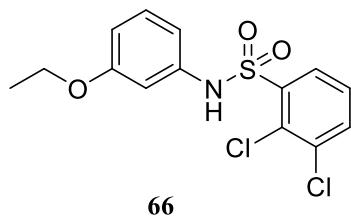
Compound **66** was obtained following the general synthetic procedure (**H**) and purified by semi-preparative reversed-phase HPLC using the gradient conditions from 5% B to 100% B over 50 min, flow rate of 4 mL/min, $\lambda = 240$ nm (96% yield). ^{1}H NMR (400 MHz, DMSO-d_6) δ 10.76 (s, 1H), 8.05 (dd, $J = 8.0$, 1.5 Hz, 1H), 7.91 (dd, $J = 8.1$, 1.5 Hz, 1H), 7.55 (t, $J = 8.0$ Hz, 1H), 7.11 (t, $J = 8.1$ Hz, 1H), 6.68 – 6.62 (m, 2H), 6.57 (dd, $J = 8.2$, 2.0 Hz, 1H), 3.90 (q, $J = 6.9$ Hz, 2H), 1.26 (t, $J = 6.9$ Hz, 3H). ^{13}C NMR

(100 MHz, DMSO-d_6) δ 158.9, 138.7, 137.9, 135.0, 134.2, 130.4, 130.1, 128.8, 128.6, 111.1, 109.7, 105.5, 63.0, 14.5.

2,5-dichloro-N-(3-ethoxyphenyl)benzenesulfonamide (67)
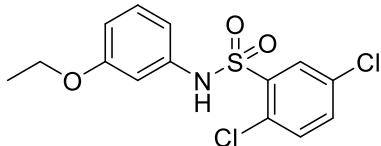
Compound **67** was obtained following the general synthetic procedure (**H**) and purified by semi-preparative reversed-phase HPLC using the gradient conditions from 5% B to 100% B over 50 min, flow rate of 4 mL/min, λ = 240 nm (81% yield). ^{1}H NMR (400 MHz, DMSO-d_6) δ 10.76 (s, 1H), 7.99 (d, J = 2.5 Hz, 1H), 7.74 – 7.66 (m, 2H), 7.13 (t, J = 8.0 Hz, 1H), 6.67 (dd, J = 8.0, 2.2 Hz, 1H), 6.64 (t, J = 2.2 Hz, 1H), 6.59 (dd, J = 8.3, 2.5 Hz, 1H), 3.91 (q, J = 6.9 Hz, 2H), 1.26 (t, J = 6.9 Hz, 3H). ^{13}C NMR (100 MHz, DMSO-d_6) δ 159.0, 138.0, 137.7, 134.4, 133.7, 132.1, 130.7, 130.2, 129.6, 111.4, 110.0, 105.8, 63.0, 14.4.

2,3-dichloro-N-(3-ethylphenyl)benzenesulfonamide (68)
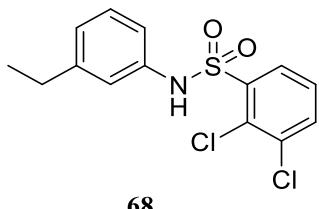

Compound **68** was obtained following the general synthetic procedure (**H**) and purified by semi-preparative reversed-phase HPLC using the gradient conditions from 5% B to 100% B over 50 min, flow rate of 4 mL/min, λ = 240 nm (74% yield). ^{1}H NMR (400 MHz, DMSO-d_6) δ 10.68 (s, 1H), 8.03 (dd, J = 8.0, 1.50 Hz, 1H), 7.91 (dd, J = 8.0,

1.5 Hz, 1H), 7.53 (t, *J* = 8.0 Hz, 1H), 7.12 (t, *J* = 8.0 Hz, 1H), 6.93 (s, 1H), 6.91 – 6.84

(m, 2H), 2.51 – 2.44 (m, 2H), 1.05 (t, *J* = 7.6 Hz, 3H). ^{13}C NMR (100 MHz, DMSO-

d$_6$) δ 145.4, 139.3, 137.2, 135.4, 134.7, 130.9, 129.6, 129.4, 129.0, 124.2, 119.2, 117.3,

28.5, 15.8. HRMS: calcd for $C_{14}H_{13}Cl_2NO_2S$ 329.0044, found *m/z* = 351.9929 [M +

Na]$^+$.

*2,3-dichloro-N-phenylbenzenesulfonamide (69)*

69
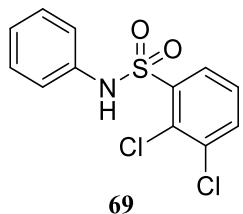
Compound **69** was obtained following the general synthetic procedure (**H**) and purified

by semi-preparative reversed-phase HPLC using the gradient conditions from 5% B to

100% B over 50 min, flow rate of 4 mL/min, λ = 240 nm (77% yield). ^{1}H NMR (600

MHz, DMSO-*d*$_6$) δ 10.79 (s, 1H), 8.03 (dd, *J* = 8.0, 1.5 Hz, 1H), 7.91 (dd, *J* = 8.0, 1.5

Hz, 1H), 7.53 (t, *J* = 8.0 Hz, 1H), 7.25 – 7.21 (m, 2H), 7.10 – 7.07 (m, 2H), 7.02 (t, *J*

= 7.4 Hz, 1H). ^{13}C NMR (150 MHz, DMSO-*d*$_6$) δ 138.7, 136.8, 135.1, 134.2, 130.5,

129.3, 128.9, 128.7, 124.2, 119.4. HRMS: calcd for $C_{12}H_9Cl_2NO_2S$ 300.9731, found

m/z = 323.9611 [M + Na]$^+$.

N-(3-bromo-5-methoxyphenyl)-3-cyanobenzenesulfonamide (1t-I)

1t-I
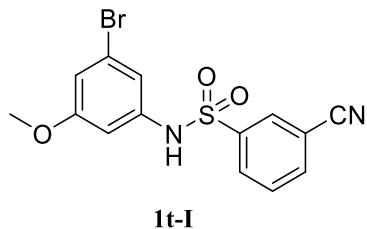
Compound **1t-I** was obtained following the general synthetic procedure (**H**) and

purified on silica gel column chromatography in hexane/ethyl acetate (6:4) (92%

yield). ^{1}H NMR (400 MHz, CDCl$_3$) δ 8.10 (t, *J* = 1.8 Hz, 1H), 8.00 (dt, *J* = 8.0, 1.5 Hz, 1H), 7.85 (dt, *J* = 8.0, 1.5 Hz, 1H), 7.63 (t, *J* = 8.0 Hz, 1H), 6.84 (t, *J* = 1.8 Hz, 1H), 6.82 (s, 1H), 6.78 (t, *J* = 1.8 Hz, 1H), 6.64 (t, *J* = 2.1 Hz, 1H), 3.75 (s, 3H). ^{13}C NMR (100 MHz, CDCl$_3$) δ 161.2, 140.7, 137.7, 136.6, 131.3, 130.9, 130.4, 123.6, 117.1, 116.7, 114.8, 114.1, 106.7, 55.9.

*N-(3-bromo-5-methoxyphenyl)-3-cyano-4-fluorobenzenesulfonamide (***1t-II***)*
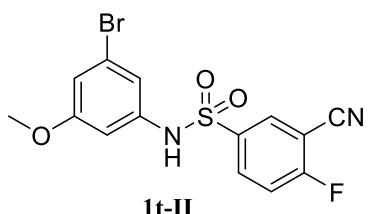
1t-II

Compound **1t-II** was obtained following the general synthetic procedure (**H**) and purified on silica gel column chromatography in hexane/ethyl acetate (6:4) (95% yield). ^{1}H NMR (400 MHz, CDCl$_3$) δ 8.11 (dd, *J* = 5.7, 2.4 Hz, 1H), 8.05 – 7.97 (m, 1H), 7.35 (t, *J* = 8.5 Hz, 1H), 6.86 (t, *J* = 1.8 Hz, 1H), 6.79 (t, *J* = 1.8 Hz, 1H), 6.77 (s, 1H), 6.63 (t, *J* = 2.1 Hz, 1H), 3.77 (s, 3H). ^{13}C NMR (150 MHz, DMSO-d_6) δ 164.7 (d, *J* = 264.3 Hz), 160.6, 139.4, 136.6 (d, *J* = 3.0 Hz), 134.4 (d, *J* = 10.6 Hz), 132.9, 122.5, 118.3 (d, *J* = 21.1 Hz), 114.7, 112.6 (d, *J* = 3.0 Hz), 105.1, 102.0 (d, *J* = 15.1 Hz), 79.2, 55.6.

N-(3'-amino-5-methoxy-[1,1'-biphenyl]-3-yl)-3-cyanobenzenesulfonamide (70)
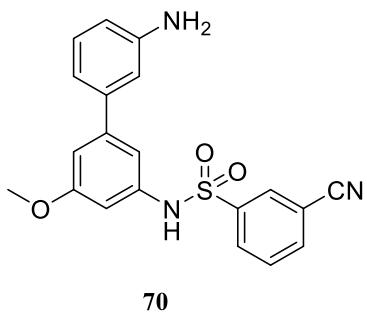
70

Compound **70** was obtained following the general synthetic procedure (**I**) (79% yield).

^{1}H NMR (400 MHz, MeOD) δ 8.13 (t, J = 1.8 Hz, 1H), 8.06 (d, J = 7.1 Hz, 1H), 7.94 (d, J = 7.9 Hz, 1H), 7.70 (t, J = 7.9 Hz, 1H), 7.56 – 7.51 (m, 2H), 7.44 (s, 1H), 7.28 (dt, J = 7.1, 2.1 Hz, 1H), 7.00 (t, J = 1.7 Hz, 1H), 6.91 (t, J = 1.9 Hz, 1H), 6.67 (t, J = 2.1 Hz, 1H), 3.79 (s, 3H). ^{13}C NMR (100 MHz, MeOD) δ 162.4, 143.6, 143.4, 142.5, 140.2, 137.4, 136.1, 132.4, 131.8, 131.6, 131.6, 126.5, 121.8, 121.0, 118.2, 114.6, 113.0, 110.5, 107.3, 56.0. HRMS: calcd for $C_{20}H_{17}N_3O_3S$ 379.0991, found m/z = 380.1058 [M + H]$^+$.

N-(3'-acetyl-5-methoxy-[1,1'-biphenyl]-3-yl)-3-cyanobenzenesulfonamide (71)
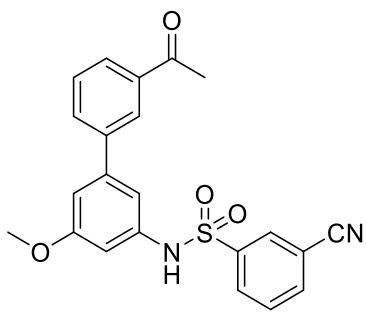
71

Compound **71** was obtained following the general synthetic procedure (**I**) (57% yield).

^{1}H NMR (400 MHz, MeOD) δ 8.14 (t, J = 1.5 Hz, 1H), 8.08 – 8.03 (m, 2H), 7.98 (dt, J = 7.8, 1.4 Hz, 1H), 7.94 (dt, J = 7.8, 1.4 Hz, 1H), 7.76 – 7.68 (m, 2H), 7.56 (t, J = 7.8 Hz, 1H), 6.94 (t, J = 2.0 Hz, 1H), 6.89 (t, J = 1.7 Hz, 1H), 6.75 (t, J = 2.0 Hz, 1H),

3.81 (s, 3H), 2.65 (s, 3H). ^{13}C NMR (100 MHz, MeOD) δ 200.3, 162.4, 143.8, 142.5, 142.1, 140.1, 138.9, 137.4, 132.8, 132.4, 131.8, 131.5, 130.4, 129.0, 127.6, 118.2, 114.6, 113.2, 110.5, 107.4, 56.0, 26.8. HRMS: calcd for $C_{22}H_{18}N_2O_4S$ 406.0987, found $m/z = 429.0873$ [M + Na]$^+$.

*3-cyano-N-(3',5-dimethoxy-[1,1'-biphenyl]-3-yl)benzenesulfonamide (**72**)*
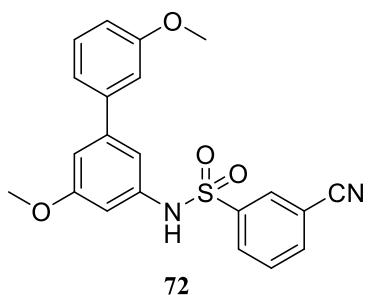
72

Compound **72** was obtained following the general synthetic procedure (**I**) (56% yield). ^{1}H NMR (400 MHz, MeOD) δ 8.13 (s, 1H), 8.04 (d, $J = 8.0$ Hz, 1H), 7.93 (dt, $J = 7.9$, 1.3 Hz, 1H), 7.69 (t, $J = 7.9$ Hz, 1H), 7.31 (t, $J = 7.9$ Hz, 1H), 7.04 (d, $J = 8.5$ Hz, 1H), 6.98 (t, $J = 2.1$ Hz, 1H), 6.92 – 6.83 (m, 3H), 6.70 (t, $J = 2.1$ Hz, 1H), 3.83 (s, 3H), 3.79 (s, 3H). ^{13}C NMR (100 MHz, CDCl$_3$) δ 160.9, 160.1, 144.0, 141.5, 140.9, 137.0, 136.4, 131.3, 131.0, 130.3, 130.1, 119.7, 117.1, 113.9, 113.4, 113.1, 113.1, 110.8, 106.8, 55.7, 55.5. HRMS: calcd for $C_{21}H_{18}N_2O_4S$ 394.0987, found $m/z = 417.0870$ [M + Na]$^+$.

3-cyano-N-(3',5'-difluoro-5-methoxy-[1,1'-biphenyl]-3-yl)-4-

fluorobenzenesulfonamide (73)

73
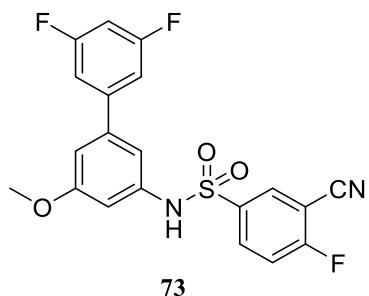
Compound **73** was obtained following the general synthetic procedure (**I**) (76% yield).

^{1}H NMR (600 MHz, CDCl$_3$) δ 8.13 (dd, J = 5.7, 2.3 Hz, 1H), 8.07 – 8.01 (m, 1H), 7.80

(s, 1H), 7.31 (t, J = 8.5 Hz, 1H), 7.01 – 6.96 (m, 2H), 6.86 – 6.82 (m, 2H), 6.80 (tt, J

= 8.8, 2.3 Hz, 1H), 6.75 (t, J = 2.1 Hz, 1H), 3.82 (s, 3H). ^{13}C NMR (150 MHz, CDCl$_3$)

δ 165.3 (d, J = 267.3 Hz), 163.4 (dd, J = 163.4, 12.1 Hz), 161.1, 143.4 (t, J = 9.1 Hz),

141.7 (t, J = 3.0 Hz), 137.7, 137.0 (d, J = 3.0 Hz), 134.2 (d, J = 10.6 Hz), 133.3, 117.8

(d, J = 21.1 Hz), 112.5, 112.3, 110.3, 110.2 (dd, J = 15.1, 6.0 Hz), 107.4, 103.4 (t, J =

25.7 Hz), 103.1 (d, J = 16.6 Hz), 55.8.

3-cyano-4-fluoro-N-(5-methoxy-3'-(trifluoromethyl)-[1,1'-biphenyl]-3-

yl)benzenesulfonamide (74)

74
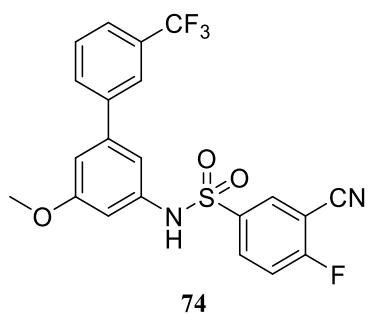
Compound **74** was obtained following the general synthetic procedure (**I**) (42% yield).

^{1}H NMR (400 MHz, MeOD) δ 8.22 (dd, J = 5.9, 2.4 Hz, 1H), 8.14 – 8.06 (m, 1H),

7.78 (d, *J* = 7.2 Hz, 1H), 7.72 (s, 1H), 7.69 – 7.60 (m, 2H), 7.52 (t, *J* = 8.9 Hz, 1H),

6.94 (t, *J* = 1.9 Hz, 1H), 6.90 (t, *J* = 1.7 Hz, 1H), 6.78 (t, *J* = 2.1 Hz, 1H), 3.82 (s, 3H).

^{13}C NMR (125 MHz, MeOD) δ 166.5 (d, *J* = 264.6 Hz), 162.5, 143.3, 142.6, 140.1,

138.6 (d, *J* = 3.8 Hz), 135.7 (d, *J* = 10.1 Hz), 134.3 (d, *J* = 1.3 Hz), 132.3 (q, *J* = 32.8

Hz), 131.8 (q, *J* = 1.3 Hz), 130.9, 125.6 (q, *J* = 272.2 Hz), 125.5 (q, *J* = 3.8 Hz), 124.5

(q, *J* = 3.8 Hz), 118.7 (d, *J* = 21.4 Hz), 113.3, 113.2, 110.6, 107.7, 103.6 (d, *J* = 6.4

Hz), 56.0. HRMS: calcd for $C_{21}H_{14}F_4N_2O_3S$ 450.0661, found *m/z* = 473.0560 [M +

Na]$^+$.

CHAPTER 6

Syntheses of new BRD9 PROTACs and multi-target probe

6.1 Chemistry general information

All commercially available starting materials were used as purchased from Sigma-Aldrich and Fluorochem without further purification. All solvents used for the synthesis were of HPLC grade (Sigma-Aldrich). Chemical reactions were monitored on silica gel 60 F254 plates (Merck) and spots were visualized under UV light (λ = 254 nm). Proton (^{1}H) and carbon (^{13}C) NMR spectra were recorded on Bruker Avance 400 or 600 MHz spectrometer at T = 298 K. All compounds were dissolved in 0.5 mL of CDCl$_3$, CD$_3$OD or DMSO-d_6 (Sigma-Aldrich, 99.8 Atom % D). Chemical shifts (δ) are given in parts per million (ppm) relative to the solvent peak as internal reference: CDCl$_3$ (δH = 7.26 ppm/δC = 77.16 ppm), CD$_3$OD (δH = 3.31 ppm/δC = 49.00 ppm), or DMSO-d_6 (δH = 2.50 ppm/δC = 39.52 ppm). Coupling constants (J) are reported in Hertz (Hz). Signal patterns are reported as: s = singlet, d = doublet, t = triplet, q = quartet, m = multiplet, or a combination of the listed splitting patterns. High resolution mass spectrometry experiments were performed using a LTQ Orbitrap XL mass spectrometer (Thermo Scientific). Semi-preparative reversed-phase HPLC was performed on Agilent Technologies 1200 Series high-performance liquid chromatography using Luna C18 reversed-phase column (250 × 10 mm, 5 μm, 100 Å, flow rate = 4 mL/min, Phenomenex®). The binary solvent system (A/ B) was as follows: 0.1% TFA in water (A) and 0.1% TFA in CH$_3$CN (B). The absorbance was detected at 240 nm. The purity of all biologically tested compounds (>96%) was determined following HPLC and NMR spectra evaluation. Microwave irradiation reactions were carried out in a dedicated CEM-Discover SP focused microwave synthesizer, operating with continuous irradiation power from 0 to 300 W utilizing the standard absorbance level of 300 W maximum power. Reactions were carried out in 10 mL sealed microwave glass vials. The Discover system also included controllable

ramp time, hold time (reaction time), and uniform stirring. After the irradiation period, reaction vessels were cooled rapidly (60–120 s) to ambient temperature by air jet cooling.

6.2 Syntheses of PROTACs compounds 75-80

Synthesis of compound N^1-(1-ethyl-[1,2,4]triazolo[4,3-a]quinoxalin-4-yl)benzene-1,3-diamine (1u)
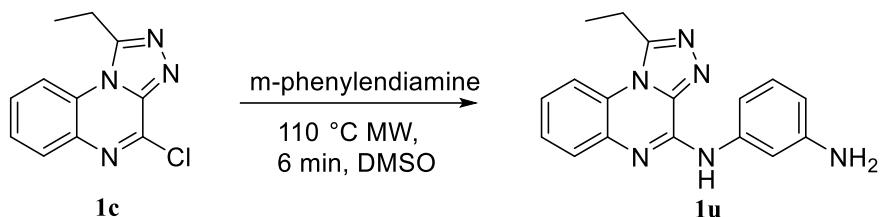
A mixture of 4-chloro-1-ethyl-[1,2,4]triazolo[4,3-*a*]quinoxaline (**1c**) (1.0 equiv., 0.205 mmol, 48 mg), synthesized following general synthetic procedure (**A**), and m-phenylendiamine (3.0 equiv., 0.615 mmol, 67 mg) in DMSO (0.6 mL) was heated under microwave irradiation at 110 °C for 8 min. The vial was then cooled to ambient temperature by air jet cooling and the reaction mixture was diluted with CH_2Cl_2 (1.6 mL) and acidified with 1 N HCl. The resulting crude precipitate was filtered using a Büchner funnel under reduced pressure. The solid was then collected and purified by semi-preparative reversed-phase HPLC using the gradient conditions from 5% B to 100% B over 50 min, flow rate of 4 mL/min, $\lambda = 240$ nm, yielding the desired compound **1u** (86% yield). ^{1}H NMR (400 MHz, MeOD) δ 8.56 (t, $J = 2.1$ Hz, 1H), 8.05 (d, $J = 8.1$ Hz, 1H), 7.87 (dd, $J = 8.3, 2.0$ Hz, 1H), 7.76 (dd, $J = 8.0, 1.6$ Hz, 1H), 7.54 – 7.46 (m, 2H), 7.42 (t, $J = 7.8$ Hz, 1H), 7.12 (dd, $J = 7.9, 2.1$ Hz, 1H), 3.43 (q, $J = 7.4$ Hz, 2H), 1.58 (t, $J = 7.3$ Hz, 3H). HRMS: calcd for $C_{17}H_{16}N_6$ 304.1436, found $m/z = 305.1515$ [M + H]$^+$.

General synthetic procedure (J) for the syntheses of PROTAC compounds 75-80

1u → **75-80**

RCOOH, HATU, TEA
DMF, r.t.
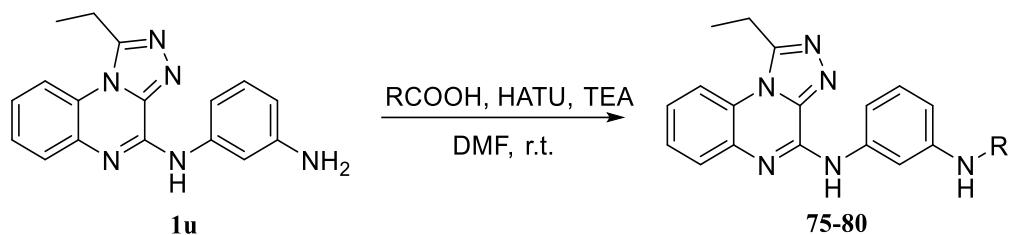
To a solution of compound **1u** (1.0 equiv., 0.033 mmol) in anhydrous DMF (0.2 M) was added TEA (5.0 equiv., 0.165 mmol), HATU (1.05 equiv., 0.035 mmol), and the carboxylic acid building blocks (linker + E3 ligase ligands) (1.0 equiv., 0.033 mmol). After stirring at room temperature for 1 h, volatiles were dried over nitrogen flux and the obtained residue was purified by semi-preparative reversed-phase HPLC using the gradient conditions from 5% B to 100% B over 50 min, flow rate of 4 mL/min, λ = 240 nm, to achieve the final compounds **75-80**, whose purity was determined by HPLC (>96%). All final products were characterized by mass spectrometry experiments and NMR analysis.

(2S,4R)-1-((S)-2-(2-(2-((7-((3-((1-ethyl-[1,2,4]triazolo[4,3-a]quinoxalin-4-yl)amino)phenyl)amino)-7-oxoheptyl)oxy)ethoxy)acetamido)-3,3-dimethylbutanoyl)-4-hydroxy-N-(4-(4-methylthiazol-5-yl)benzyl)pyrrolidine-2-carboxamide (75)


75
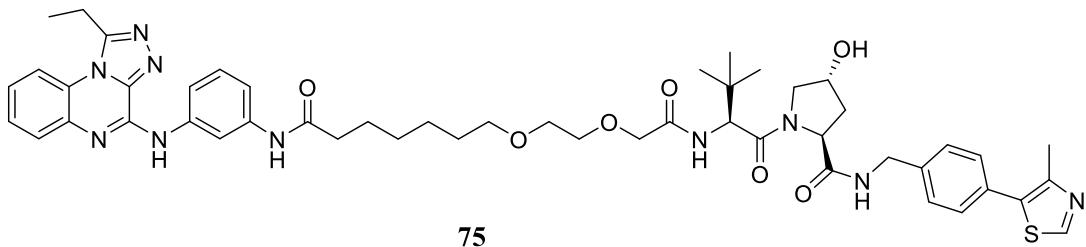
Compound **75** was obtained following the general synthetic procedure (**J**) (93% yield).

^{1}H NMR (400 MHz, MeOD) δ 8.86 (s, 1H), 8.48 (s, 1H), 8.16 (dd, *J* = 8.3, 1.3 Hz, 1H), 7.89 (dd, *J* = 8.1, 1.6 Hz, 1H), 7.72 – 7.69 (m, 1H), 7.63 (d, *J* = 9.4 Hz, 1H), 7.55

(td, *J* = 8.1, 7.7, 1.3 Hz, 1H), 7.47 (td, *J* = 7.8, 7.3, 1.6 Hz, 1H), 7.41 (d, *J* = 7.9 Hz,

2H), 7.38 – 7.31 (m, 3H), 4.68 (d, *J* = 9.4 Hz, 1H), 4.63 – 4.53 (m, 1H), 4.52 – 4.47

(m, 2H), 4.35 (s, 1H), 4.01 (d, *J* = 2.3 Hz, 2H), 3.91 – 3.84 (m, 1H), 3.79 (dd, *J* = 11.0,

3.7 Hz, 1H), 3.70 – 3.66 (m, 2H), 3.64 – 3.58 (m, 2H), 3.56 – 3.48 (m, 4H), 2.43 (s,

3H), 2.42 – 2.36 (m, 1H), 2.25 – 2.17 (m, 1H), 2.12 – 2.01 (m, 1H), 1.78 – 1.67 (m,

2H), 1.66 – 1.58 (m, 4H), 1.47 – 1.38 (m, 4H), 1.33 – 1.26 (m, 2H), 1.03 (s, 9H). ^{13}C

NMR (100 MHz, DMSO-d_6) δ 171.7, 171.2, 169.1, 168.6, 153.0, 151.4, 147.7, 143.4,

139.8, 139.6, 139.5, 139.4, 136.7, 131.1, 129.6, 128.6, 128.4, 127.4, 127.2, 127.1,

124.6, 124.0, 116.0, 115.6, 114.0, 111.8, 70.5, 70.4, 69.6, 69.2, 68.9, 58.7, 56.5, 55.7,

41.7, 37.9, 36.4, 35.7, 29.0, 28.6, 26.1, 25.4, 25.2, 21.6, 15.9, 11.0. HRMS: calcd for

$C_{50}H_{62}N_{10}O_7S$ 946.4524, found *m/z* = 969.4448 [M + Na]$^+$.

(2S,4R)-1-((S)-2-((7-((3-((1-ethyl-[1,2,4]triazolo[4,3-a]quinoxalin-4-

yl)amino)phenyl)amino)-7-oxoheptyl)amino)-3,3-dimethylbutanoyl)-4-hydroxy-N-(4-

*(4-methylthiazol-5-yl)benzyl)pyrrolidine-2-carboxamide (**76**)*

76
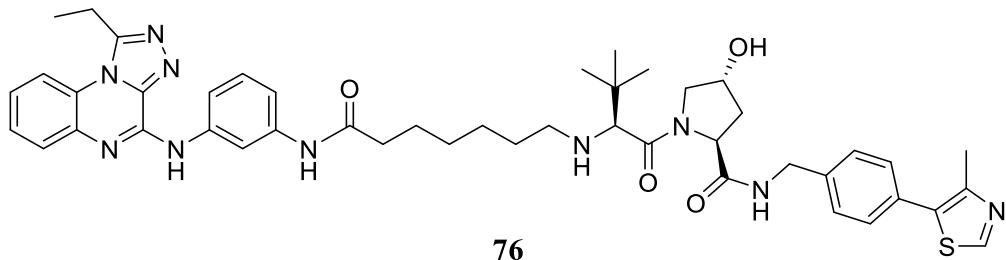
Compound **76** was obtained following the general synthetic procedure (**J**) (30% yield).

^{1}H NMR (400 MHz MeOD) δ 8.48 (s, 1H), 8.16 (d, *J* = 8.2 Hz, 1H), 7.89 (d, *J* = 8.0

Hz, 1H), 7.74 (d, *J* = 7.9 Hz, 1H), 7.55 (t, *J* = 7.5 Hz, 1H), 7.47 (t, *J* = 7.7 Hz, 1H),

7.42 (d, *J* = 7.9 Hz, 2H), 7.39 – 7.27 (m, 5H), 4.74 – 4.65 (m, 1H), 4.58 – 4.49 (m,

2H), 4.33 (s, 1H), 4.09 (s, 1H), 3.88 (d, *J* = 11.4 Hz, 1H), 3.66 (dd, *J* = 11.3, 3.4 Hz,

1H), 3.56 – 3.48 (m, 2H), 3.06 – 2.89 (m, 2H), 2.48 – 2.39 (m, 4H), 2.33 – 2.26 (m,

1H), 2.13 – 2.02 (m, 1H), 1.79 – 1.73 (m, 2H), 1.65 – 1.58 (m, 5H), 1.48 – 1.42 (m, 3H), 1.31 – 1.27 (m, 7H), 1.15 (s, 9H). ^{13}C NMR (100 MHz, MeOD) δ 173.9, 173.9, 167.5, 140.3, 140.2, 139.0, 138.4, 131.5, 130.4, 128.9, 128.8, 126.3, 125.5, 117.2, 117.1, 116.4, 113.4, 71.0, 67.7, 61.1, 58.3, 43.7, 39.0, 37.8, 36.3, 30.7, 29.5, 27.2, 26.8, 26.4, 26.1, 23.7, 23.1, 11.3. HRMS: calcd for $C_{46}H_{56}N_{10}O_4S$ 844.4207, found m/z = 845.4266 [M + H]$^+$.

7-((2-(2,6-dioxopiperidin-3-yl)-1,3-dioxoisoindolin-4-yl)amino)-N-(3-((1-ethyl-[1,2,4]triazolo[4,3-a]quinoxalin-4-yl)amino)phenyl)heptanamide (77)
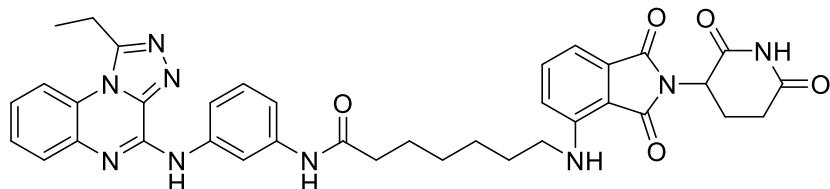
77

Compound **77** was obtained following the general synthetic procedure (**J**) (95% yield). ^{1}H NMR (400 MHz, CDCl$_3$) δ 8.40 (s, 1H), 8.21 (s, 1H), 7.97 (d, J = 7.8 Hz, 1H), 7.91 (dd, J = 8.1, 1.5 Hz, 1H), 7.68 (d, J = 8.1 Hz, 1H), 7.59 – 7.50 (m, 2H), 7.50 – 7.39 (m, 2H), 7.40 – 7.33 (m, 1H), 7.30 (t, J = 8.0 Hz, 1H), 7.05 (d, J = 7.1 Hz, 1H), 6.87 (d, J = 8.5 Hz, 1H), 4.92 (dd, J = 12.2, 5.3 Hz, 1H), 3.49 (q, J = 7.4 Hz, 2H), 3.29 (t, J = 6.7 Hz, 2H), 2.91 – 2.68 (m, 4H), 2.41 (t, J = 7.4 Hz, 2H), 2.18 – 2.07 (m, 1H), 1.83 – 1.75 (m, 2H), 1.75 – 1.67 (m, 2H), 1.65 (t, J = 7.4 Hz, 3H), 1.52 – 1.42 (m, 4H). ^{13}C NMR (100 MHz, CDCl$_3$) δ 171.5, 171.2, 169.8, 169.0, 167.8, 147.2, 143.1, 139.5, 138.8, 137.3, 136.3, 132.6, 129.7, 128.5, 127.7, 125.1, 124.4, 116.9, 115.5, 115.4, 114.9, 111.6, 110.8, 110.0, 77.4, 49.1, 42.6, 41.0, 37.5, 31.6, 28.7, 28.6, 26.4, 25.2, 22.9, 22.5, 11.4. HRMS: calcd for $C_{37}H_{37}N_9O_5$ 687.2918, found m/z = 710.2809 [M + Na]$^+$.

3-(2-((2-(2,6-dioxopiperidin-3-yl)-1,3-dioxoisoindolin-4-yl)amino)ethoxy)-N-(3-((1-

*ethyl-[1,2,4]triazolo[4,3-a]quinoxalin-4-yl)amino)phenyl)propanamide (**78**)*

78
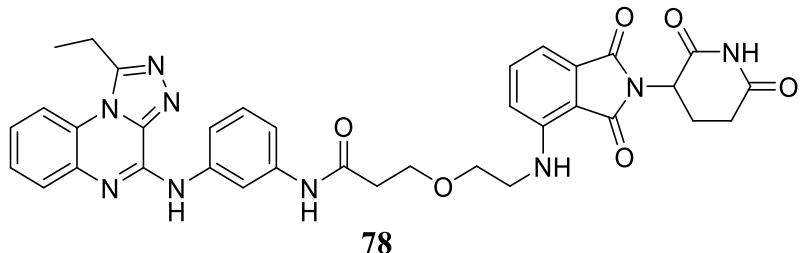
Compound **78** was obtained following the general synthetic procedure (**J**) (94% yield).

^{1}H NMR (400 MHz, MeOD) δ 8.38 (s, 1H), 8.13 (d, J = 8.7 Hz, 1H), 7.85 (dd, J = 8.0,

1.5 Hz, 1H), 7.69 – 7.63 (m, 1H), 7.52 (td, J = 7.7, 1.4 Hz, 1H), 7.45 (td, J = 8.0, 7.5,

1.5 Hz, 1H), 7.38 – 7.33 (m, 1H), 7.30 – 7.26 (m, 2H), 6.99 (d, J = 8.6 Hz, 1H), 6.83

(d, J = 7.1 Hz, 1H), 4.91 – 4.88 (m, 1H), 3.90 (t, J = 5.8 Hz, 2H), 3.75 (t, J = 5.1 Hz,

2H), 3.55 – 3.48 (m, 4H), 2.81 – 2.71 (m, 1H), 2.72 – 2.61 (m, 3H), 2.62 – 2.48 (m,

1H), 2.02 – 1.93 (m, 1H), 1.62 (t, J = 7.4 Hz, 3H). ^{13}C NMR (100 MHz, MeOD) δ

174.6, 172.3, 171.6, 170.5, 169.2, 148.2, 144.4, 140.9, 140.3, 138.4, 137.0, 133.6,

130.0, 129.0, 128.7, 126.2, 125.5, 118.2, 117.1, 116.5, 113.5, 111.9, 111.2, 70.9, 68.2,

50.1, 43.3, 38.8, 32.2, 23.7, 23.1, 11.4. HRMS: calcd for $C_{35}H_{33}N_9O_6$ 675.2554, found

m/z = 698.2378 [M + Na]$^+$.

3-(2-(2-((2-(2,6-dioxopiperidin-3-yl)-1,3-dioxoisoindolin-4-yl)amino)ethoxy)ethoxy)-

*N-(3-((1-ethyl-[1,2,4]triazolo[4,3-a]quinoxalin-4-yl)amino)phenyl)propanamide (**79**)*

79
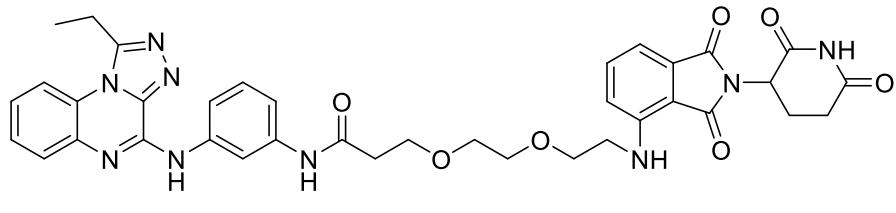
Compound **79** was obtained following the general synthetic procedure (**J**) (95% yield).

^{1}H NMR (400 MHz, CDCl$_3$) δ 8.90 (s, 1H), 8.45 (s, 1H), 8.24 (s, 0H), 7.97 (d, J = 8.1

Hz, 1H), 7.89 (dd, J = 8.1, 1.5 Hz, 1H), 7.60 – 7.50 (m, 2H), 7.47 – 7.40 (m, 1H), 7.34

– 7.25 (m, 3H), 7.20 (t, J = 8.1 Hz, 1H), 6.89 (d, J = 7.0 Hz, 1H), 6.68 (d, J = 8.5 Hz,

1H), 4.85 – 4.79 (m, 1H), 3.89 (t, J = 5.6 Hz, 3H), 3.81 – 3.71 (m, 6H), 3.50 (q, J =

7.4 Hz, 2H), 3.33 (t, J = 5.3 Hz, 2H), 2.85 – 2.77 (m, 1H), 2.74 (t, J = 5.5 Hz, 2H),

2.71 – 2.62 (m, 2H), 2.17 – 2.03 (m, 1H), 1.65 (t, J = 7.4 Hz, 3H). ^{13}C NMR (150

MHz, CDCl$_3$) δ 171.4, 171.0, 169.4, 169.0, 167.6, 153.4, 146.6, 142.7, 139.6, 139.1,

138.7, 137.1, 135.9, 132.3, 129.3, 128.4, 128.1, 125.3, 123.9, 116.6, 116.1, 115.6,

115.4, 111.7, 111.6, 110.3, 70.3, 70.2, 69.3, 67.1, 49.0, 42.3, 37.9, 31.5, 22.8, 22.4,

11.3. HRMS: calcd for C$_{37}$H$_{37}$N$_9$O$_7$ 719.2816, found m/z = 742.2705 [M + Na]$^+$.

Experimental Section

3-(2-(2-(2-((2-(2,6-dioxopiperidin-3-yl)-1,3-dioxoisoindolin-4-

yl)amino)ethoxy)ethoxy)ethoxy)-N-(3-((1-ethyl-[1,2,4]triazolo[4,3-a]quinoxalin-4-

yl)amino)phenyl)propanamide (80)
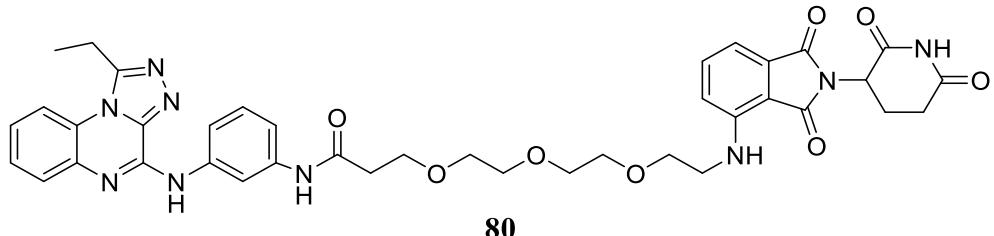
80

Compound **80** was obtained following the general synthetic procedure (**J**) (96% yield).

^{1}H NMR (600 MHz, MeOD) δ 8.48 (t, J = 2.1 Hz, 1H), 8.05 (dd, J = 8.5, 1.3 Hz, 1H),

7.82 (dd, J = 8.1, 1.5 Hz, 1H), 7.63 (d, J = 8.0 Hz, 1H), 7.50 (td, J = 7.9, 1.3 Hz, 1H),

7.41 (td, J = 7.9, 7.3, 1.5 Hz, 1H), 7.35 (d, J = 8.0 Hz, 1H), 7.30 – 7.26 (m, 2H), 6.79

(d, J = 7.0 Hz, 1H), 6.75 (d, J = 8.4 Hz, 1H), 4.95 (dd, J = 12.8, 5.5 Hz, 1H), 3.85 (t,

J = 5.9 Hz, 2H), 3.67 (s, 4H), 3.65 – 3.63 (m, 2H), 3.57 – 3.53 (m, 4H), 3.45 (q, J =

7.4 Hz, 2H), 3.27 (t, J = 5.4 Hz, 2H), 2.86 – 2.79 (m, 1H), 2.76 – 2.71 (m, 1H), 2.72 –

2.63 (m, 3H), 2.14 – 2.07 (m, 1H), 1.60 (t, J = 7.4 Hz, 3H). ^{13}C NMR (150 MHz,

MeOD) δ 174.7, 172.6, 171.6, 170.5, 169.1, 147.8, 144.3, 141.0, 140.4, 138.4, 136.8,

133.5, 130.0, 129.0, 128.7, 126.1, 125.4, 117.8, 117.0, 116.2, 113.2, 111.6, 111.0, 71.7,

71.7, 71.5, 70.4, 68.3, 50.2, 43.1, 38.9, 32.2, 23.8, 23.2, 11.4. HRMS: calcd for

$C_{39}H_{41}N_9O_8$ 763.3078, found m/z = 786.2976 [M + Na]$^+$.

6.3 Synthesis of the SWI/SNF multi-target probe compound 81

Synthesis   of   the   intermediate   tert-butyl   4-(4-bromo-2,6-dimethoxybenzyl)piperazine-1-carboxylate (1w)
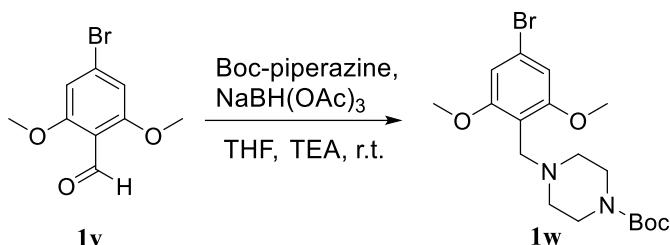
A mixture of the commercially available 4-bromo-2,6-dimethoxybenzaldehyde **1w** (1.0 equiv., 0.408 mmol, 100 mg), Boc-piperazine (1.1 equiv., 0.449 mmol, 84 mg), and TEA (1.1 equiv., 0.449 mmol, 63 μL) in dry THF (9.6 mL) was stirred at room temperature for 15 min. Then, NaBH(OAc)$_3$ (1.5 equiv., 0.612 mmol, 130 mg) was added and the reaction was stirred overnight under nitrogen flux at room temperature. After completion, the reaction was quenched with a saturated solution of NaHCO$_3$ and extracted three times with DCM. The organic phase was then washed with water and brine, dried over sodium sulfate, filtered, and condensed to afford the desired compound **1w** which was used without any further purification (98% yield). ^{1}H NMR (400 MHz, CDCl$_3$) δ 6.67 (s, 2H), 3.77 (s, 6H), 3.60 (s, 2H), 3.36 (t, J = 5.1 Hz, 4H), 2.40 (t, J = 5.1 Hz, 4H), 1.42 (s, 9H). ^{13}C NMR (100 MHz, CDCl$_3$) δ 159.7, 154.6, 121.8, 112.8, 107.9, 79.2, 55.9, 52.3, 48.8, 28.3. HRMS: calcd for C$_{18}$H$_{27}$BrN$_2$O$_4$ 414.1154, found m/z = 415.1216 [M + H]$^+$.

Synthesis of compound 4-iodo-2-methyl-2,7-naphthyridin-1(2H)-one (1y)
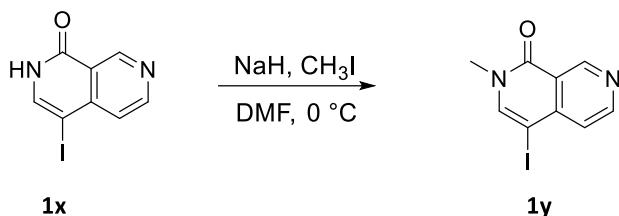
To a solution of the commercially available 4-iodo-2,7-naphthyridin-1-(2*H*)-one **1x** (1.0 equiv., 0.368 mmol, 100 mg), in dry DMF (5.5 mL), NaH (2.0 equiv., 0.735 mmol, 18 mg) was added while stirring in an ice-bath for 30 min. Then CH$_3$I (1.6 equiv., 0.588 mmol, 83 mg) was added and the reaction mixture was stirred for 5 h at 0 °C. After completion, water was poured into the reaction mixture and the precipitate was filtered and collected, yielding the final compound **1y** that was used without further purification (87% yield). ^{1}H NMR (400 MHz, MeOD) δ 9.36 (s, 1H), 8.78 (d, *J* = 5.7 Hz, 1H), 8.15 (s, 1H), 7.63 (d, *J* = 5.7 Hz, 1H), 3.62 (s, 3H). ^{13}C NMR (100 MHz, DMSO-d_6) δ 160.3, 152.0, 150.3, 144.8, 143.0, 122.4, 120.7, 67.9, 36.2. HRMS: calcd for C$_9$H$_7$IN$_2$O 285.9603, found *m/z* = 308.9503 [M + Na]$^+$.

Synthesis of compound 4-(3,5-dimethoxy-4-(piperazin-1-ylmethyl)phenyl)-2-methyl-2,7-naphthyridin-1(2H)-one (1z)
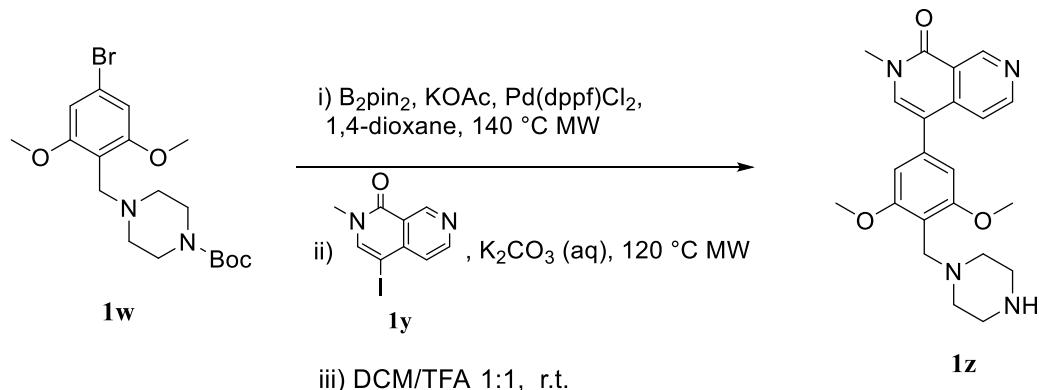
In a glass vial containing a solution of the intermediate **1w** (1.0 equiv., 0.299 mmol, 124 mg) in dioxane (12.4 mL) was evacuated and backfilled with nitrogen three time.

Then, bis(pinacolato)diboron (1.2 equiv., 0.359 mmol, 91 mg), Pd(dppf)Cl$_2$ (0.1 equiv., 0.030 mmol, 22 mg), and KOAc (3.0 equiv., 0.897 mmol, 88 mg) were added and the system was again evacuated and backfilled with nitrogen. The mixture was heated under microwave at 140 °C for 40 min. Then, the intermediate **1y** (1.0 equiv., 0.299 mmol, 86 mg) and 0.3 mL of a 2 M degassed solution of K$_2$CO$_3$ were added. The reaction mixture was heated under microwave conditions at 120 °C for 34 min, then the mixture was filtered through Celite and washed with DCM. The organic layer was then extracted with water and brine, dried over sodium sulfate, filtered, and condensed to afford a crude that was purified on silica gel column chromatography in ethyl acetate/methanol to give the boc-protected intermediate (24% yield, HRMS: calcd for C$_{27}$H$_{34}$N$_4$O$_5$ 494.2529, found m/z = 495.2599 [M + H]$^+$). The boc-protected compound was dissolved in 0.25 mL of DCM and then 0.25 mL of TFA were added. The reaction mixture was then stirred at room temperature for 1 h, after completion the volatiles were removed under vacuum to give the desired compound **1z** (100% yield). ^{1}H NMR (400 MHz, MeOD) δ 9.62 (s, 1H), 8.69 (d, J = 6.6 Hz, 1H), 8.13 (s, 1H), 8.04 (d, J = 6.6 Hz, 1H), 6.87 (s, 2H), 4.54 (s, 2H), 3.94 (s, 6H), 3.75 (s, 3H), 3.70 – 3.65 (m, 4H), 3.63 – 3.60 (m, 4H). HRMS: calcd for C$_{22}$H$_{26}$N$_4$O$_3$ 394.2005, found *m/z* = 395.2063 [M + H]$^+$.

Synthesis of compound 4-(4-((4-(3-amino-6-chloropyridazin-4-yl)piperazin-1-yl)methyl)-3,5-dimethoxyphenyl)-2-methyl-2,7-naphthyridin-1(2H)-one (2a)
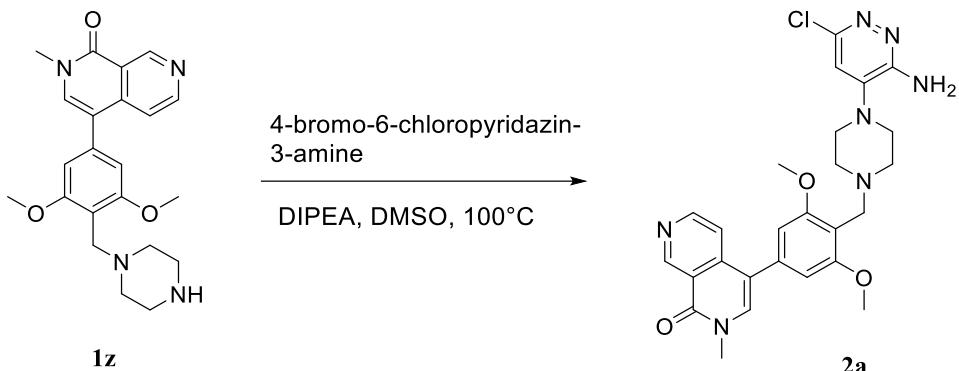
To a solution of the intermediate **1z** (1.1 equiv., 0.080 mmol, 32 mg) and 4-bromo-6-chloropyridazin-3-amine (1.0 equiv., 0.072 mmol, 15 mg) in DMSO (181 μL) was added DIPEA (5.0 equiv., 0.360 mmol, 70 μL) and the reaction was stirred overnight at 100 °C. Then water was added while stirring in an ice-bath and the aqueous phase was extracted three times with ethyl acetate. The organic phase was then washed with water and brine, dried over sodium sulfate, filtered, and condensed to afford a residue that was purified by semi-preparative reversed-phase HPLC using the gradient conditions from 5% B to 100% B over 50 min, flow rate of 4 mL/min, $\lambda = 240$ nm, to achieve the desired compound **2a** (35% yield). ^{1}H NMR (400 MHz, DMSO-d_6) δ 9.45 (s, 1H), 8.72 (d, $J = 5.6$ Hz, 1H), 8.30 (s, 1H), 7.87 (s, 1H), 7.58 (d, $J = 5.6$ Hz, 1H), 6.85 (s, 1H), 6.74 (s, 2H), 3.82 (s, 6H), 3.63 (s, 2H), 3.60 (s, 3H), 2.99 – 2.93 (m, 4H), 2.65 – 2.59 (m, 4H). ^{13}C NMR (150 MHz, DMSO-d_6) δ 160.5, 159.0, 155.5, 151.0, 150.5, 145.9, 141.0, 138.0, 135.3, 131.4, 119.8, 116.0, 114.3, 112.7, 105.5, 56.3, 56.0, 51.9, 48.4, 36.5. HRMS: calcd for $C_{26}H_{28}ClN_7O_3$ 521.1942, found $m/z = 522.2004$ [M + H]$^+$.

Synthesis of compound 4-(4-((4-(3-amino-6-(2-hydroxyphenyl)pyridazin-4-yl)piperazin-1-yl)methyl)-3,5-dimethoxyphenyl)-2-methyl-2,7-naphthyridin-1(2H)-one (81)

2a

(2-hydroxyphenyl)boronic acid, Xphos-Pd-G3, K_2CO_3

dioxane/H_2O, 90 °C

81
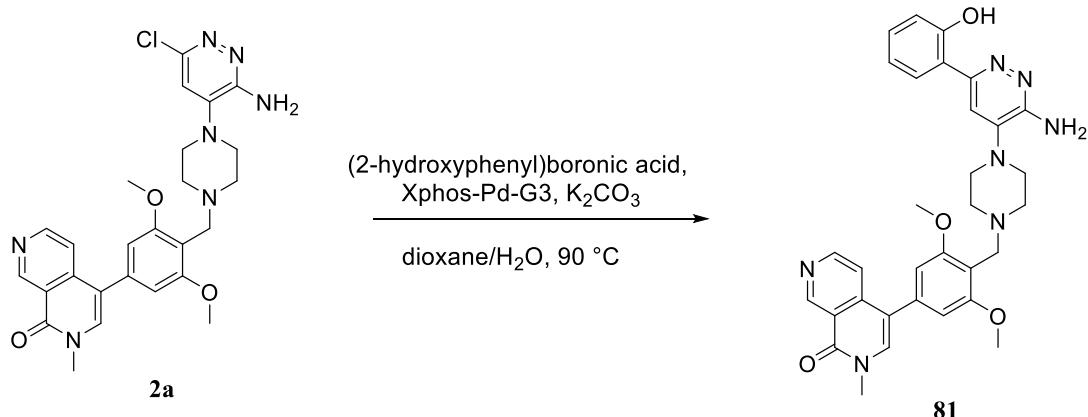
To a solution of the intermediate **2a** (1.0 equiv., 0.014 mmol, 7 mg) in 240 μL of dioxane/H_2O (8:2) was added the commercially available (2-hydroxyphenyl)boronic acid (1.3 equiv., 0.018 mmol, 3 mg) and the system was evacuated and backfilled with nitrogen three time. Then Xphos-Pd-G3 (0.1 equiv., 0.001 mmol, 1 mg) and K_2CO_3 (2.0 equiv., 0.028 mmol, 4 mg) were added, and the system was again evacuated and backfilled with nitrogen. After stirring at 90 °C overnight, the mixture was cooled down and concentrated. The residue was purified by semi-preparative reversed-phase HPLC using the gradient conditions from 5% B to 100% B over 50 min, flow rate of 4 mL/min, $\lambda = 240$ nm, to achieve the desired pure compound **81** (37% yield). ^{1}H NMR (400 MHz, MeOD) δ 7.93 (s, 1H), 7.82 (s, 1H), 7.73 (s, 1H), 7.64 (d, $J = 8.0$ Hz, 1H), 7.43 (t, $J = 7.7$ Hz, 1H), 7.35 (t, $J = 8.0$ Hz, 1H), 7.07 − 7.00 (m, 3H), 6.99 (d, $J = 7.7$ Hz, 1H), 6.88 (s, 1H), 3.97 (s, 6H), 3.73 (s, 3H), 3.60 (s, 2H), 2.70 (s, 6H), 2.66 (s, 2H). HRMS: calcd for $C_{32}H_{33}N_7O_4$ 579.2594, found $m/z = 580.2670$ [M + H]$^+$.

6.4 Synthesis of the PROTAC 82 based on the 9*H*-purine scaffold

Synthesis of the intermediate 3-(2-amino-9H-purin-6-yl)-4-methoxybenzoic acid (2c)
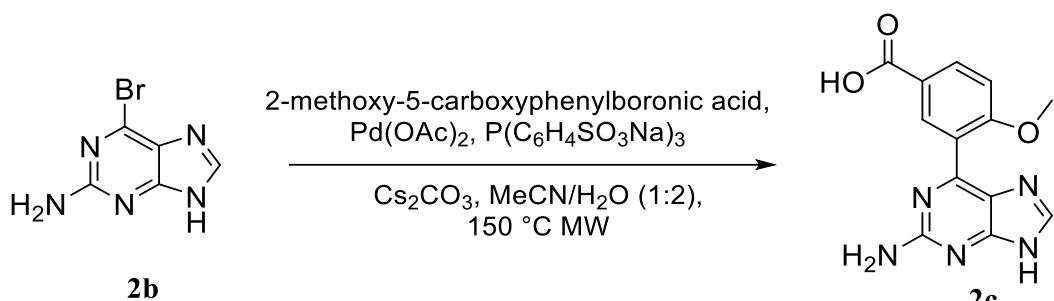
The commercially available 2-amino-6-bromopurine **2b** (0.80 equiv., 0.327 mmol, 70 mg), 2-methoxy-5-carboxyphenylboronic acid (1.30 equiv., 0.531 mmol, 104 mg), Pd(OAc)$_2$ (0.04 equiv., 0.016 mmol, 4 mg), TPPTS (0.20 equiv., 0.082 mmol, 47 mg), and Cs$_2$CO$_3$ (2.40 equiv., 0.981 mmol, 320 mg) were added to a sealed glass vial. The vial was evacuated and backfilled with nitrogen three times, then 0.5 mL of a degassed acetonitrile/water solution (1:2) was added and the mixture was heated under microwave irradiation for 15 min at 150 °C. After completion, 2 mL of cold water and 1 mL of HCl 1.5 M were added to the reaction mixture that was left at 4 °C overnight. The obtained precipitate was filtered and purified by semi-preparative reversed-phase HPLC using the gradient conditions from 5% B to 100% B over 50 min, flow rate of 4 mL/min, λ = 240 nm, to achieve the desired intermediate **2c** (72% yield). ^{1}H NMR (400 MHz, MeOD) *δ* 8.64 (d, *J* = 2.2 Hz, 1H), 8.55 (s, 1H), 8.31 (dd, *J* = 8.8, 2.2 Hz, 1H), 7.39 (d, *J* = 8.8 Hz, 1H), 4.03 (s, 3H). HRMS: calcd for C$_{13}$H$_{11}$N$_5$O$_3$ 285.0862, found *m/z* = 286.0931 [M + H]$^+$.

Synthesis of the final compound (2S,4R)-1-((S)-1-(3-(2-amino-9H-purin-6-yl)-4-methoxyphenyl)-12-(tert-butyl)-1,10-dioxo-5,8-dioxa-2,11-diazatridecan-13-oyl)-4-hydroxy-N-(4-(4-methylthiazol-5-yl)benzyl)pyrrolidine-2-carboxamide (82)
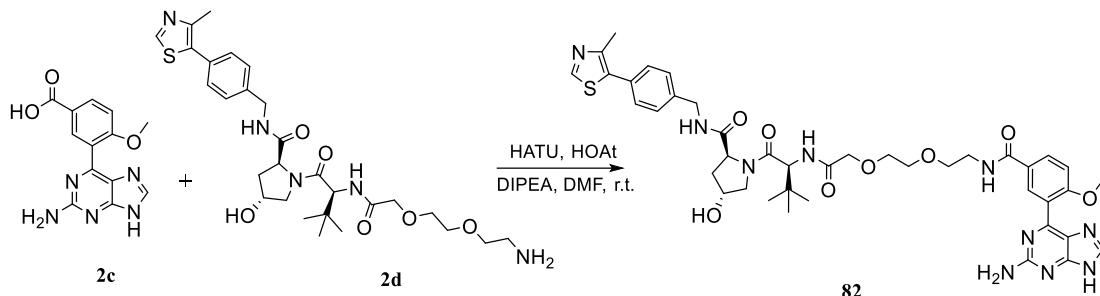
To a solution of compound **2c** (1.0 equiv., 0.042 mmol, 12 mg) in anhydrous DMF (1.9 mL) was added DIPEA (5.0 equiv., 0.210 mmol, 29 μL), HATU (1.0 equiv., 0.042 mmol, 16 mg), HOAt (1.0 equiv., 0.042 mmol, 6 mg) and the commercially available building block **2d** (1.0 equiv., 0.042 mmol, 24 mg). After stirring at room temperature for 2 h, volatiles were dried over nitrogen flux and the resulting residue was purified by semi-preparative reversed-phase HPLC using the gradient conditions from 5% B to 100% B over 50 min, flow rate of 4 mL/min, λ = 240 nm, to achieve the final pure compound **82** (53% yield). ^{1}H NMR (600 MHz, DMSO-d_6) δ 9.25 (s, 1H), 8.69 – 8.63 (m, 2H), 8.47 (dd, J = 8.4, 1.4 Hz, 1H), 8.34 (s, 1H), 7.48 – 7.43 (m, 2H), 7.39 (d, J = 6.8 Hz, 2H), 4.57 (t, J = 9.5 Hz, 1H), 4.47 – 4.41 (m, 1H), 4.40 – 4.32 (m, 1H), 4.32 – 4.21 (m, 1H), 3.99 – 3.94 (m, 1H), 3.64 – 3.52 (m, 8H), 3.49 – 3.34 (m, 1H), 3.33 – 3.24 (m, 1H), 3.11 (q, J = 7.4 Hz, 4H), 2.94 – 2.85 (m, 4H), 2.68 (s, 1H), 2.43 (d, J = 7.1 Hz, 2H), 2.12 – 2.05 (m, 1H), 1.93 – 1.86 (m, 1H), 1.31 – 1.27 (m, 9H). ^{13}C NMR (150 MHz, DMSO-d_6) δ 171.8, 171.7, 169.2, 168.7, 168.6, 161.6, 151.5, 151.5, 150.6, 147.8, 147.7, 139.7, 139.5, 134.6, 131.2, 129.8, 128.7, 128.7, 128.6, 127.5, 127.5,

120.4, 70.4, 70.3, 69.6, 69.4, 68.9, 58.8, 56.7, 55.7, 53.4, 44.1, 41.6, 26.2, 18.0, 16.7,

12.3. HRMS: calcd for $C_{41}H_{50}N_{10}O_8S$ 842.3534, found m/z = 843.3621 $[M + H]^+$.

CHAPTER 7

Syntheses, biophysical and biological evaluation of new VHL

ligands and LRRK2 PROTACs

7.1 Chemistry

7.1.1 General information

All commercially available starting materials were used as purchased from Apollo Scientific, Sigma-Aldrich, Fluorochem, and Enamine without further purification. All solvents used for the syntheses were anhydrous. Chemical reactions were monitored both on silica gel plates (spots were visualized under UV light ($\lambda = 254$ nm)), or by Liquid chromatography-mass spectrometry (LC-MS). (LC-MS) was carried out on a Shimadzu HPLC/MS 2020 equipped with a Hypersil Gold column (1.9 μm, 50 $\times$ 2.1 mm^2), a photodiode array detector, and an electrospray ionization (ESI) detector. The samples were eluted with a 3 min gradient of 5−95% acetonitrile (ACN) in water containing 0.1% formic acid at a flow rate of 0.8 mL/min. Crude reaction mixtures were purified on Flash column chromatography by means of Teledyne ISCO Combiflash Companion installed with disposable normal phase RediSep Rf columns (230-400 mesh, 40-63 mm; SiliCycle). Proton (^{1}H), carbon (^{13}C) and fluorine (^{19}F) NMR spectra were recorded on a Bruker 500 Ultra shield or on a Bruker Ascend 400 spectrometer. Chemical shifts (δ) are given in parts per million (ppm) relative to the solvent peak as internal reference: CDCl$_3$-d_1 (δH $= 7.26$ ppm/δC $= 77.16$ ppm), CD$_3$OD-d_4 (δH $= 3.31$ ppm/δC $= 49.00$ ppm), or DMSO-d_6 (δH $= 2.50$ ppm/δC $= 39.52$ ppm). Coupling constants (J) are reported in Hertz (Hz). Signal patterns are reported as: s = singlet, d = doublet, t = triplet, q = quartet, m = multiplet, brs = broad, or a combination of the listed splitting patterns. High resolution mass spectrometry experiments were performed on a Bruker MicroTOF II focus ESI mass spectrometer connected in parallel to a Dionex Ultimate 3000 RSLC system with a diode array

detector and a Waters X-Bridge C18 column (50 mm × 2.1 mm, 3.5 μm particle size).

All final compounds are >95% pure following LC-MS and NMR spectra evaluation.

7.1.2 Syntheses and characterization of truncated compounds MP-1-21, MP-1-23, MP-1-39, MP-1-85, MP-1-95, MP-1-105, and MP-1-106

Synthesis of the intermediate tert-butyl (4-(4-methylthiazol-5-yl)benzyl)carbamate (2f)
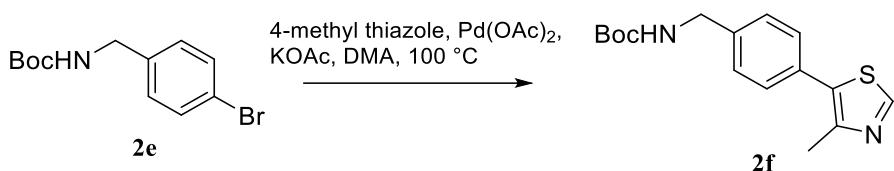
To a round bottom flask, a solution of the commercially available *tert*-butyl 4-bromobenzylcarbamate **2e** (1 equiv., 1.00 g, 3.49 mmol), 4-methylthiazole (3 equiv., 0.95 mL, 10.48 mmol), KOAc (3 equiv., 1.03 g, 10.48 mmol), in *N,N*-dimethylacetamide (30 mL) was added. The flask was then evacuated and backfilled with nitrogen three times, Pd(OAc)$_2$ (0.1 equiv., 0.08 g, 0.35 mmol) was added and the reaction mixture was stirred at 100 °C overnight under nitrogen atmosphere. After completion of the reaction, the mixture was filtered on celite and the filtrate was diluted with DCM and washed several times with water. The organic layer was then dried over sodium sulfate, filtered, and condensed to afford a crude, which was purified with flash column chromatography (0-5% methanol in DCM) on silica gel to give compound **2f** (77% yield). ^{1}H NMR (500 MHz, CDCl$_3$) δ 8.51 (s, 1H), 7.24 (d, J = 7.9 Hz, 2H), 7.18 (d, J = 7.9 Hz, 2H), 4.84 (s, 1H), 4.20 (d, J = 6.0 Hz, 2H), 2.36 (s, 3H), 1.31 (s, 9H). ^{13}C NMR (125 MHz, CDCl$_3$) δ 156.1, 152.8, 150.4, 148.6, 139.0, 131.1, 129.6, 127.8, 79.8, 44.4, 28.5, 16.2. LC-MS, ESI$^+$, m/z = 305.3 [M + H]$^+$.

Synthesis of the intermediate tert-butyl (2R,4R)-4-hydroxy-2-((4-(4-methylthiazol-5-yl)benzyl) carbamoyl) pyrrolidine-1-carboxylate (2g)
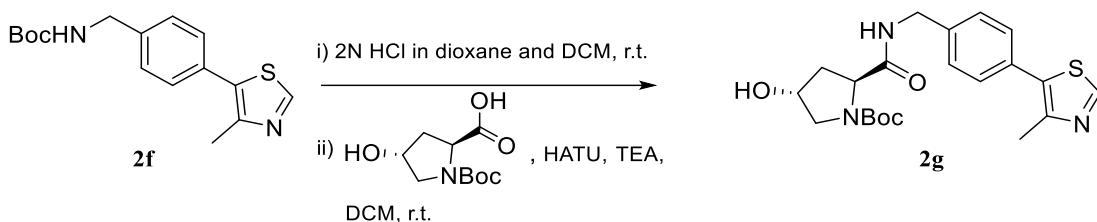
To a solution of the intermediate **2f** (1 equiv., 791 mg, 2.60 mmol) in DCM (5.2 mL) was added 4 N HCl in 1,4-dioxane (5.2 mL) dropwise. After stirring 1 h at room temperature, the mixture was concentrated under reduced pressure, washed with diethyl ether, and dried to give the boc-deprotected product as a HCl salt (93% yield, LC-MS, ESI$^+$, m/z = 205.3 [M + H]$^+$), which was used for the next step. To a suspension of the obtained solid (1 equiv., 669 mg, 2.41 mmol) in DCM (20.0 mL) were added TEA (3 equiv., 1.01 mL, 7.20 mmol), (2S,4R)-1-(tert-butoxycarbonyl)-4-hydroxypyrrolidine-2-carboxylic acid (1 equiv., 558 mg, 2.41 mmol), and HATU (1.05 equiv., 962 mg, 2.53 mmol). After stirring 1.5 h at room temperature, the mixture was washed with water and brine, dried over sodium sulfate, filtered, and condensed to afford a crude residue, which was purified through flash column chromatography on silica gel (0-5% methanol in DCM) to give compound **2g** (91% yield). ^{1}H NMR (500 MHz, CDCl$_3$) δ 8.65 (s, 1H), 7.50 – 7.27 (m, 5H), 4.55 – 4.29 (m, 4H), 3.65 (s, 1H), 3.54 – 3.38 (m, 2H), 2.48 (s, 3H), 2.41 – 2.24 (m, 1H), 2.17 – 2.00 (m, 1H), 1.42 (s, 5H), 1.36 – 1.27 (m, 4H). ^{13}C NMR (125 MHz, CDCl$_3$) δ 172.7, 172.0, 156.2, 155.1, 150.5, 148.5, 138.2, 131.7, 130.9, 129.6, 128.5, 127.8, 80.9, 69.9, 69.3, 60.2, 58.9, 55.2, 54.8, 43.1, 39.8, 37.1, 28.4, 16.1. LC-MS, ESI$^+$, m/z = 418.3 [M + H]$^+$.

Synthesis of the intermediate (9H-fluoren-9-yl)methyl((R)-1-((2S,4R)-4-hydroxy-2-((4-(4-methylthiazol-5-yl)benzyl)carbamoyl)pyrrolidin-1-yl)-3-methyl-1-oxo-3-(tritylthio)butan-2-yl)carbamate (2h)
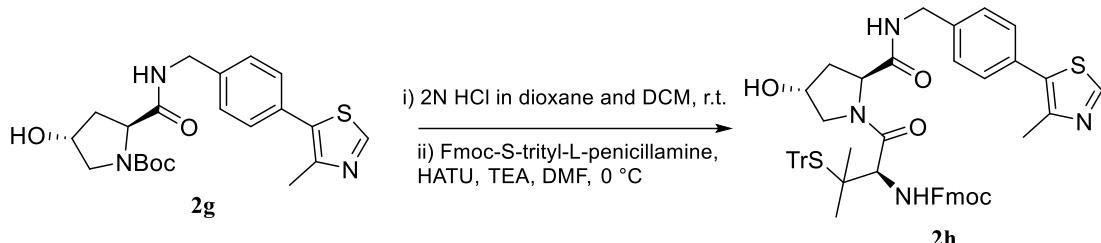
To a solution of compound **2g** (1 equiv., 914 mg, 2.20 mmol) in DCM (4.2 mL) was added 4 N HCl in 1,4-dioxane (4.2 mL) dropwise and the reaction was stirred 1 h at room temperature. After completion of the reaction, the mixture was concentrated under reduced pressure, washed with diethyl ether, and dried to give the boc-deprotected product as a HCl salt (88% yield, LC-MS, ESI$^+$, m/z = 317.9 [M + H]$^+$), which was used in the next step. To a suspension of the obtained solid (1 equiv., 200 mg, 0.57 mmol) in DMF (3.0 mL) was added TEA (2.5 equiv., 197 μL, 1.41 mmol) and stirred at room temperature. In parallel, in a round bottom flask, to a solution of Fmoc-*S*-trityl-L-penicillamine (1 equiv., 347 mg, 0.57 mmol) in DMF (2.0 mL) were added HATU (1 equiv., 215 mg, 0.57 mmol) and TEA (1 equiv., 79 μL, 0.57 mmol) while stirring in an ice-bath. After 10 min, the two solutions were combined and the reaction mixture was stirred for 1 h at 0 °C. After completion of the reaction, water was added and the aqueous phase was extracted several times with ethyl acetate. The organic layer was then collected and dried over sodium sulfate, filtered, and condensed to afford a residue, which was purified with flash column chromatography (0-5% methanol in DCM) on silica gel to give compound **2h** (87% yield). ^{1}H NMR (500 MHz, CDCl$_3$) δ 8.70 (s, 1H), 7.74 (t, J = 7.3 Hz, 2H), 7.57 (d, J = 7.5 Hz, 1H), 7.54 –

7.48 (m, 7H), 7.44 (t, *J* = 6.1 Hz, 1H), 7.40 – 7.33 (m, 2H), 7.29 (d, *J* = 8.2 Hz, 2H),

7.25 – 7.16 (m, 13H), 5.71 (d, *J* = 5.8 Hz, 1H), 4.65 (t, *J* = 8.0 Hz, 1H), 4.38 – 4.28

(m, 2H), 4.30 – 4.21 (m, 2H), 4.20 – 4.09 (m, 2H), 3.60 (d, *J* = 5.8 Hz, 1H), 3.45 (d, *J*

= 11.3 Hz, 1H), 3.38 – 3.28 (m, 2H), 2.50 (s, 3H), 2.27 – 2.19 (m, 1H), 2.13 – 2.07 (m,

1H), 1.19 (s, 3H), 1.00 (s, 3H). ^{13}C NMR (125 MHz, CDCl$_3$) δ 171.0, 170.3, 156.4,

150.4, 148.5, 144.4, 143.9, 143.5, 141.4, 141.3, 138.3, 131.8, 130.7, 129.9, 129.4,

127.9, 127.8, 127.2, 127.2, 127.0, 125.2, 125.1, 120.1, 77.4, 70.1, 7.6, 59.0, 58.2, 56.7,

54.4, 47.0, 42.8, 36.8, 26.0, 25.4, 16.2. LC-MS, ESI$^+$, *m/z* = 913.4 [M + H]$^+$.

Synthesis of the intermediate (2S,4R)-1-((R)-2-amino-3-methyl-3-(tritylthio)butanoyl)-4-hydroxy-N-(4-(4-methylthiazol-5-yl)benzyl)pyrrolidine-2-carboxamide (2i)
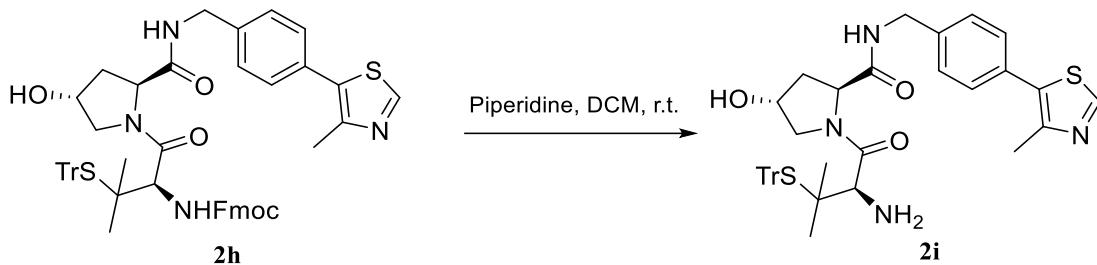
Compound **2h** (1 equiv., 448 mg, 0.49 mmol) was dissolved in 2.0 mL of DCM. Then

piperidine (8 equiv., 0.388 mL, 3.93 mmol) was added and the reaction mixture was

stirred for 1 h at room temperature. After completion of reaction, volatiles were

removed under vacuum and the crude was purified *via* flash column chromatography

(0-10% 0.7 M ammonia-containing methanol in DCM) on silica gel to give compound

2i (96% yield). ^{1}H NMR (500 MHz, CDCl$_3$) δ 8.69 (s, 1H), 7.62 – 7.51 (m, 8H), 7.33

– 7.25 (m, 9H), 7.23 – 7.20 (m, 5H), 4.55 (t, *J* = 8.3 Hz, 1H), 4.32 (s, 1H), 4.28 – 4.16

(m, 2H), 3.15 (d, *J* = 3.2 Hz, 1H), 3.09 (d, *J* = 11.3 Hz, 1H), 2.75 (s, 1H), 2.52 (s, 4H),

2.09 – 2.01 (m, 2H), 1.22 (s, 3H), 1.10 (s, 3H). ^{13}C NMR (125 MHz, CDCl$_3$) δ 172.0, 171.7, 150.3, 148.4, 144.8, 138.4, 131.7, 130.7, 129.9, 129.4, 127.9, 127.7, 126.9, 69.8, 68.2, 59.2, 58.2, 58.1, 57.1, 42.7, 37.6, 25.2, 24.7, 16.2. LC-MS, ESI$^-$, *m/z* = 689.5 [M − H]$^-$.

Synthesis of the intermediate (2S,4R)-1-((R)-2-(1-fluorocyclopropane-1-carboxamido)-3-methyl-3-(tritylthio)butanoyl)-4-hydroxy-N-(4-(4-methylthiazol-5-yl)benzyl)pyrrolidine-2-carboxamide (2j)
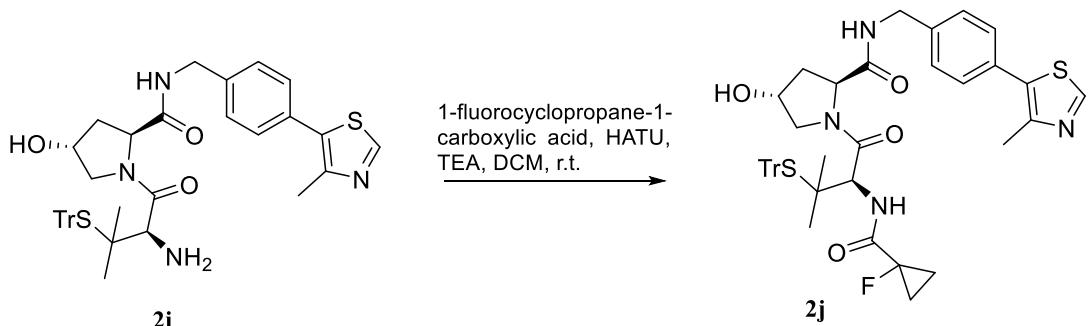
To a solution of the amine compound **2i** (1 equiv., 292 mg, 0.42 mmol) in DCM (2.7 mL) was added TEA (2 equiv., 0.12 mL, 0.85 mmol), HATU (1.05 equiv., 169 mg, 0.44 mmol), and 1-fluorocyclopropane-1-carboxylic acid (1 equiv., 44 mg, 0.42 mmol). After stirring at room temperature for 1 h, water was added and the aqueous phase was extracted three times with DCM. The organic phase was then washed with brine, dried over sodium sulfate, filtered, and condensed to afford a crude product, which was purified through flash column chromatography (0-5% methanol in DCM) on silica gel to give the desired product **2j** (68% yield). ^{1}H NMR (500 MHz, CDCl$_3$) δ 8.70 (s, 1H), 7.53 (d, *J* = 7.2 Hz, 6H), 7.40 (t, *J* = 6.0 Hz, 1H), 7.30 (d, *J* = 8.3 Hz, 2H), 7.24 – 7.17 (m, 12H), 4.63 (t, *J* = 8.1 Hz, 1H), 4.36 (brs, 1H), 4.30 – 4.26 (m, 1H), 4.23 – 4.16 (m, 1H), 3.59 (d, *J* = 5.2 Hz, 1H), 3.46 (d, *J* = 11.5 Hz, 1H), 3.28 (dd, *J* = 11.4, 3.8 Hz, 1H), 2.51 (s, 3H), 2.31 – 2.23 (m, 1H), 2.14 – 2.07 (m, 1H), 1.38 –

1.18 (m, 8H), 1.03 (s, 3H). ^{13}C NMR (125 MHz, CDCl$_3$) δ 171.0, 170.4 (d, J = 20.7 Hz), 170.3, 169.9, 150.5, 148.6, 144.5, 138.4, 131.9, 130.9, 130.0, 129.6, 128.1, 127.1, 78.3 (d, J = 232.2 Hz), 70.3, 68.5, 58.9, 57.1, 56.9, 54.1, 43.0, 36.8, 26.2, 25.7, 16.3, 13.9 (d, J = 11.3 Hz), 13.8 (d, J = 11.3 Hz). ^{19}F NMR (470 MHz, CDCl$_3$) δ -197.30. LC-MS, ESI⁻, m/z = 775.4 [M − H]⁻.

Synthesis of the intermediate (2S,4R)-1-((R)-2-(1-fluorocyclopropane-1-carboxamido)-3-mercapto-3-methylbutanoyl)-4-hydroxy-N-(4-(4-methylthiazol-5-yl)benzyl)pyrrolidine-2-carboxamide (2k)
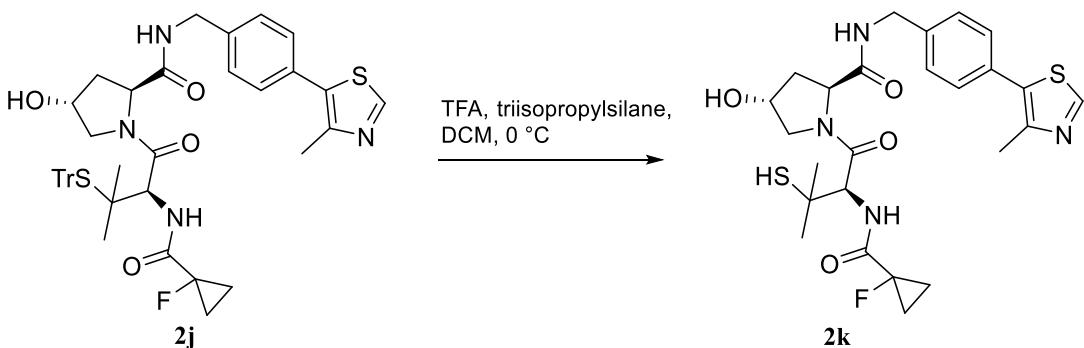
To a solution of compound **2j** (1 equiv., 136 mg, 0.18 mmol) in DCM (8.0 mL) was added triisopropylsilane (0.44 mL) and TFA (0.44 mL) in an ice-bath. The resulting mixture was stirred at 0 °C for 10 min and condensed to afford a residue, which was purified through flash column chromatography (0-5% methanol in DCM) on silica gel to yield compound **2k** (87% yield). ^{1}H NMR (500 MHz, CDCl$_3$) δ 8.68 (s, 1H), 7.43 (dd, J = 8.8, 3.3 Hz, 1H), 7.39 − 7.31 (m, 5H), 4.69 − 4.61 (m, 2H), 4.53 − 4.48 (m, 2H), 4.37 − 4.32 (m, 1H), 4.02 (d, J = 11.1 Hz, 1H), 3.78 (dd, J = 11.1, 3.8 Hz, 1H), 3.71 (brs, 1H), 2.58 (s, 1H), 2.49 (s, 3H), 2.38 − 2.30 (m, 1H), 2.17 − 2.11 (m, 1H), 1.40 (s, 3H), 1.34 (s, 3H), 1.33 − 1.25 (m, 4H). ^{13}C NMR (125 MHz, CDCl$_3$) δ 171.1, 170.6 (d, J = 20.6 Hz), 170.1, 150.7, 148.5, 138.2, 131.9, 131.1, 129.7, 128.2, 78.3 (d, J = 232.2 Hz), 70.2, 59.4, 57.8, 56.9, 46.6, 43.4, 37.1, 30.5, 28.8, 16.2, 14.1 (d, J =

10.1 Hz), 14.1 (d, J = 10.1 Hz). ^{19}F NMR (470 MHz, CDCl$_3$) δ -197.60. LC-MS, ESI$^+$,

m/z = 535.0 [M + H]$^+$.

Synthesis of the intermediate (trans-cyclohexane-1,4-diyl)bis(methylene) bis(4-methylbenzenesulfonate) (2m)
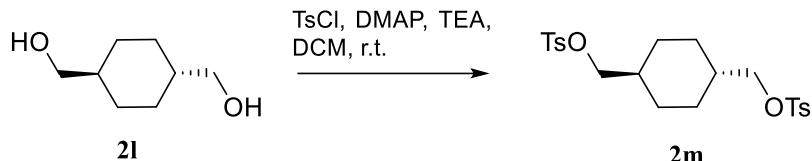
A round bottom flask containing a solution of the commercially available *trans*-cyclohexane-dimethanol **2l** (1.0 equiv., 3.00 g, 20.80 mmol), TEA (2.5 equiv., 7.25 mL, 52.00 mmol), and DMAP (0.005 equiv., 0.01 g, 0.10 mmol) in DCM (144.0 mL) was placed in an ice-bath and TsCl (2.5 equiv., 8.13 g, 42.65 mmol) was added portion wise. The reaction mixture was stirred overnight at room temperature and then quenched with water. The organic phase was then washed with water and brine, dried over sodium sulfate, filtered, and condensed to afford a crude product, which was purified through flash column chromatography (0-10% methanol in DCM) on silica gel to give the desired product **2m** (70% yield). ^{1}H NMR (500 MHz, CDCl$_3$) δ 7.76 (d, J = 8.3 Hz, 4H), 7.33 (d, J = 8.1 Hz, 4H), 3.79 (d, J = 6.4 Hz, 4H), 2.44 (s, 6H), 1.77 – 1.67 (m, 4H), 1.60 – 1.56 (m, 2H), 0.93 – 0.87 (m, 4H). ^{13}C NMR (125 MHz, CDCl$_3$) δ 144.9, 133.1, 130.0, 128.0, 75.0, 37.1, 28.2, 21.8.

Synthesis of the intermediate trans-1,4-bis(bromomethyl)cyclohexane (2n)
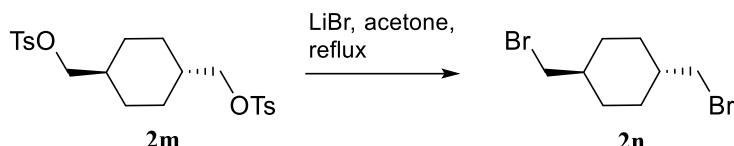
The intermediate compound **2m** (1 equiv., 5.52 g, 12.20 mmol) was dissolved in acetone (41.0 mL) and LiBr was added (4 equiv., 4.24 g, 48.80 mmol). The suspension was stirred overnight at reflux. After completion of the reaction, water was added and extracted several times with ethyl acetate. The organic phase was then washed with brine, dried over sodium sulfate, filtered, and condensed to afford a crude product, which was purified through flash column chromatography (0-10% ethyl acetate in heptane) on silica gel to give the desired product **2n** (63% yield). ^{1}H NMR (500 MHz, CDCl$_3$) δ 3.29 (d, J = 6.2 Hz, 4H), 1.98 – 1.91 (m, 4H), 1.62 (qd, J = 5.5, 2.7 Hz, 2H), 1.11 – 1.00 (m, 4H). ^{13}C NMR (125 MHz, CDCl$_3$) δ 77.4, 77.2, 76.9, 40.1, 39.9, 31.2.

Synthesis of the intermediate 4-(((1R,4R)-4-(bromomethyl)cyclohexyl)methyl)morpholine (2o)
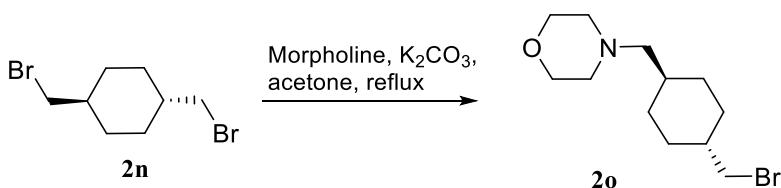
A suspension of compound **2n** (3 equiv., 500 mg, 1.85 mmol), morpholine (1 equiv., 54 μL, 0.62 mmol), and potassium carbonate (3 equiv., 256 mg, 1.85 mmol) in acetone (8.6 mL) was heated to reflux and stirred overnight. The solvent was then evaporated under vacuum to obtain a residue that was dissolved in DCM and extracted with water and brine. The organic phase was then dried over sodium sulfate, filtered, and condensed to afford a crude, which was purified through flash column chromatography (0-55% ethyl acetate in heptane) on silica gel to give the desired product **2o** (48%

yield). ^{1}H NMR (500 MHz, CDCl$_3$) δ 3.63 (t, J = 4.5 Hz, 4H), 3.23 (d, J = 6.3 Hz, 2H), 2.31 (s, 4H), 2.07 (d, J = 7.2 Hz, 2H), 1.87 – 1.76 (m, 4H), 1.59 – 1.49 (m, 1H), 1.43 – 1.33 (m, 1H), 0.99 – 0.92 (m, 2H), 0.90 – 0.80 (m, 2H). ^{13}C NMR (125 MHz, CDCl$_3$) δ 67.0, 65.7, 54.2, 40.6, 40.3, 31.3, 31.0, 29.3. LC-MS, ESI$^+$, *m/z* = 277.8 [M + H]$^+$.

Synthesis of the intermediate 1-((1R,4R)-4-(bromomethyl)cyclohexyl)-N,N-dimethylmethanamine (2u)
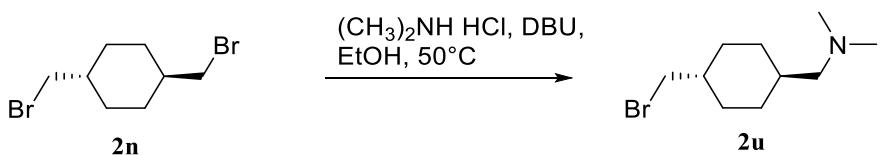
In a sealed glass vial, a solution of compound **2n** (3 equiv., 150 mg, 0.56 mmol), dimethylamine hydrochloride (1 equiv., 15 mg, 0.19 mmol), and DBU (6 equiv., 166 μL, 1.11 mmol) in ethanol (1.1 mL) was heated to 50 °C and stirred overnight. The mixture was then condensed and purified *via* flash column chromatography (0-30% 0.7 M ammonia-containing methanol in DCM) on silica gel to give compound **2u** (37% yield). ^{1}H NMR (500 MHz, CDCl$_3$) δ 3.29 (d, J = 6.1 Hz, 2H), 2.87 (d, J = 7.0 Hz, 2H), 2.82 (s, 6H), 2.16 – 2.08 (m, 2H), 2.02 – 1.95 (m, 2H), 1.80 – 1.74 (m, 1H), 1.66 – 1.57 (m, 1H), 1.19 – 1.13 (m, 2H), 1.13 – 1.07 (m, 2H). ^{13}C NMR (125 MHz, CDCl$_3$) δ 64.4, 44.2, 39.8, 39.5, 34.0, 31.0, 30.8. LC-MS, ESI$^+$, *m/z* = 235.8 [M + H]$^+$.

Synthesis of the intermediate cis-1,4-cyclohexanedimethanol (2q)
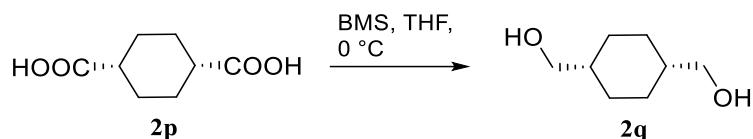
A round bottom flask, containing a solution of the commercially available *cis*-cyclohexane-1,4-dicarboxylic acid **2p** (1 equiv., 1.00 g, 5.81 mmol) in THF (10.0 mL) was evacuated and backfilled with nitrogen three times. Then a solution 2 M of borane dimethyl sulfide in THF (3 equiv., 8.7 mL, 17.42 mmol) was slowly added while stirring in an ice-bath. The reaction mixture was stirred overnight at 0 °C under nitrogen atmosphere and then quenched with methanol. The volatiles were removed under vacuum to afford a residue which was purified with flash column chromatography (0-5% methanol in DCM) on silica gel to give compound **2q** (93% yield). ^{1}H NMR (500 MHz, MeOD) δ 3.46 (d, J = 7.0 Hz, 4H), 1.69 – 1.59 (m, 2H), 1.57 – 1.47 (m, 4H), 1.47 – 1.38 (m, 4H). ^{13}C NMR (125 MHz, MeOD) δ 66.2, 39.3, 26.4.

Synthesis of the intermediate (cis-cyclohexane-1,4-diyl)bis(methylene) bis(4-methylbenzenesulfonate) (2r)
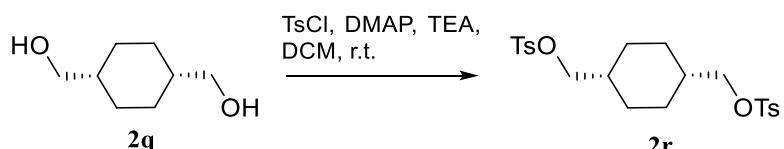
To a solution of *cis*-1,4-cyclohexanedimethanol **2q** (1 equiv., 719 mg, 4.99 mmol) in DCM (41.0 mL) was added TEA (3 equiv., 2.1 mL, 14.96 mmol), DMAP (0.01 equiv., 6.1 mg, 0.05 mmol) and then TsCl (2.5 equiv., 2376 mg, 12.47 mmol) portion wise at 0 °C. The resulting mixture was then warmed to room temperature and stirred overnight. DCM was added, and the mixture was washed with water and brine, dried

over sodium sulfate, filtered, condensed under reduced pressure to afford a residue which was purified through flash column chromatography on silica gel (0-30% ethyl acetate in heptane) to give the title compound (63% yield). ^{1}H NMR (500 MHz, CDCl$_3$) δ 7.71 (d, *J* = 8.4 Hz, 4H), 7.30 (d, *J* = 8.1 Hz, 4H), 3.80 (d, *J* = 7.2 Hz, 4H), 2.39 (s, 6H), 1.82 – 1.73 (m, 2H), 1.43 – 1.34 (m, 4H), 1.23 – 1.15 (m, 4H). ^{13}C NMR (125 MHz, CDCl$_3$) δ 144.8, 132.8, 129.8, 127.7, 72.7, 34.3, 24.4, 21.5.

Synthesis of the intermediate cis-1,4-bis(bromomethyl)cyclohexane (2s)
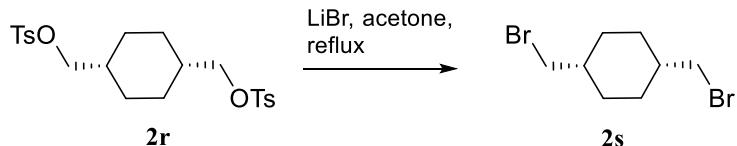
To a solution of **2r** (1 equiv., 1.43 g, 3.15 mmol) in acetone (50.0 mL) was added LiBr (4 equiv., 1.10 g, 12.60 mmol). After stirring at reflux overnight, the mixture was cooled down, ethyl acetate was added and washed with water and brine. The organic phase was then dried over sodium sulfate, filtered, and condensed under reduced pressure to give a residue which was purified with flash column chromatography on silica gel (0-10% ethyl acetate in heptane) to give the title compound (82% yield). ^{1}H NMR (500 MHz, CDCl$_3$) δ 3.34 (d, *J* = 7.0 Hz, 4H), 1.89 – 1.80 (m, 2H), 1.64 – 1.55 (m, 4H), 1.53 – 1.43 (m, 4H). ^{13}C NMR (125 MHz, CDCl$_3$) δ 38.2, 37.5, 27.0.

Synthesis   ***of***   ***the***   ***intermediate***   ***4-(((1S,4S)-4-(bromomethyl)cyclohexyl)methyl)morpholine (2t)***
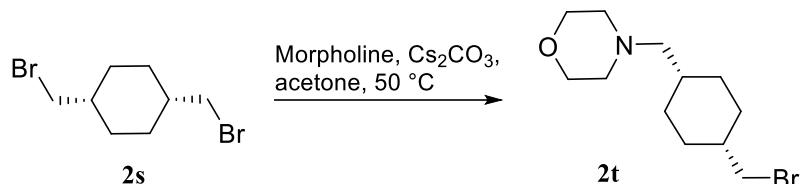
A suspension of compound **2s** (3 equiv., 350 mg, 1.30 mmol), morpholine (1 equiv., 38 μL, 0.43 mmol), and cesium carbonate (5 equiv., 705 mg, 2.17 mmol) in acetone (7.8 mL) was heated to reflux and stirred overnight. The solvent was then evaporated under vacuum to obtain a residue that was dissolved in DCM and extracted with water and brine. The organic phase was then dried over sodium sulfate, filtered, and condensed to afford a crude, which was purified through flash column chromatography (0-55% ethyl acetate in heptane) on silica gel to give the desired product **2t** (12% yield). ^{1}H NMR (500 MHz, CDCl$_3$) δ 3.69 (t, J = 4.6 Hz, 4H), 3.37 (d, J = 7.0 Hz, 2H), 2.38 (s, 4H), 2.20 (d, J = 7.5 Hz, 2H), 1.88 – 1.80 (m, 1H), 1.77 – 1.70 (m, 1H), 1.65 – 1.56 (m, 2H), 1.56 – 1.48 (m, 2H), 1.50 – 1.35 (m, 4H). ^{13}C NMR (125 MHz, CDCl$_3$) δ 67.2, 62.7, 54.3, 39.1, 38.4, 31.6, 27.4, 27.0. LC-MS, ESI$^+$, m/z = 277.8 [M + H]$^+$.

Synthesis of the intermediate 1-((1S,4S)-4-(bromomethyl)cyclohexyl)-N,N-dimethylmethanamine (2v)
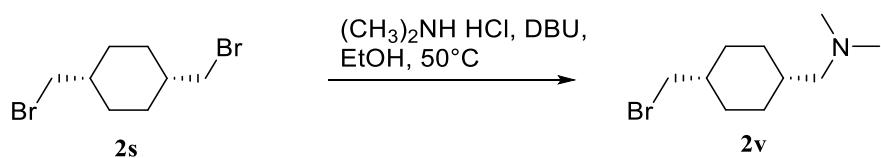
An ethanol (1.1 mL) solution of compound **2s** (3 equiv., 150 mg, 0.56 mmol), dimethylamine hydrochloride (1 equiv., 15 mg, 0.19 mmol), and DBU (8 equiv., 221 μL, 1.48 mmol) was heated to 50 °C in a sealed glass vial and stirred overnight. The mixture was then condensed and purified through flash column chromatography (0-

30% 0.7 M ammonia-containing methanol in DCM) on silica gel to give compound **2v**

(53% yield). ^{1}H NMR (500 MHz, CDCl$_3$) δ 3.36 (d, J = 7.0 Hz, 2H), 2.19 (s, 6H), 2.14

(d, J = 7.5 Hz, 2H), 1.88 – 1.78 (m, 1H), 1.72 – 1.64 (m, 1H), 1.64 – 1.58 (m, 2H),

1.57 – 1.48 (m, 2H), 1.47 – 1.36 (m, 4H). ^{13}C NMR (125 MHz, CDCl$_3$) δ 63.7, 46.1,

39.1, 38.6, 32.7, 27.5, 27.1. LC-MS, ESI$^+$, m/z = 235.8 [M + H]$^+$.

Synthesis of the intermediate (3-methoxyphenyl)(piperazin-1-yl)methanone hydrochloride (2x)
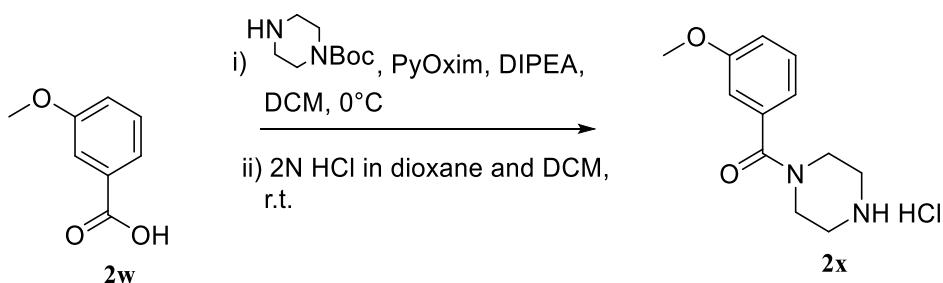
To a solution of the commercially available 3-methoxybenzoic acid **2w** (1 equiv., 0.50

g, 3.29 mmol) in DCM (20.0 mL) was added PyOxim (1 equiv., 1.74 g, 3.29 mmol),

DIPEA (2 equiv., 1.15 mL, 6.58 mmol), and 1-Boc-piperazine (1 equiv., 0.61 g, 3.29

mmol), at 0 °C. After stirring in an ice-bath for 2 h, the mixture was diluted with water

and the organic phase was washed with water and brine. The organic layer was then

concentrated to give a residue that was purified by flash column chromatography on

silica (0-10% methanol in DCM) to give the Boc-protected intermediate (84% yield,

LC-MS, ESI$^+$, m/z = 343.4 [M + Na]$^+$), which was used in the next step. To a solution

of the obtained boc-protected intermediate (1 equiv., 0.59 g, 1.84 mmol) in DCM (3.7

mL) was added a 4N solution of HCl in dioxane (8 equiv., 3.7 mL, 14.74 mmol) at

room temperature. After stirring at room temperature for 2.5 h, volatiles were

evaporated and the residue was diluted with Et$_2$O to give a precipitate which was

filtered, washed with Et$_2$O and air dried overnight to give the title compound (90%

yield) as HCl salt. ^{1}H NMR (500 MHz, DMSO-d_6) δ 9.61 (s, 2H), 7.37 (t, J = 8.0 Hz, 1H), 7.03 (dd, J = 8.2, 2.5, 1H), 7.01 – 6.97 (m, 2H), 3.78 (s, 3H), 3.42 – 3.31 (m, 5H), 3.12 (s, 3H). ^{13}C NMR (125 MHz, DMSO-d_6) δ 168.9, 159.1, 136.3, 129.7, 118.9, 115.5, 112.3, 55.2, 42.3. LC-MS, ESI[+], m/z = 220.9 [M + H][+].

Synthesis of the intermediate (4-(((1R,4R)-4-(bromomethyl)cyclohexyl)methyl)piperazin-1-yl)(3-methoxyphenyl)methanone (2y)
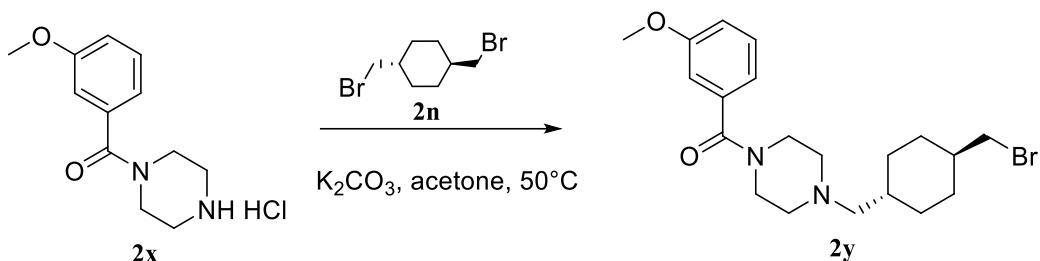
To a suspension of **2x** (1 equiv., 100 mg, 0.39 mmol) in acetone (6.0 mL) was added the previously synthesized intermediate **2n** (3 equiv., 316 mg, 1.17 mmol) and K_2CO_3 (7 equiv., 377 mg, 2.73 mmol). After stirring at 50 °C overnight, the resulting mixture was diluted with DCM, washed with water and brine, dried over sodium sulfate, filtered, and condensed to afford a residue which was purified on flash column chromatography on silica gel (0-5% methanol in DCM) to give the title compound (59% yield). ^{1}H NMR (500 MHz, CDCl$_3$) δ 7.30 – 7.22 (m, 1H), 6.97 – 6.86 (m, 3H), 3.78 (s, 3H), 3.72 (s, 2H), 3.38 (s, 2H), 3.25 (d, J = 6.3 Hz, 2H), 2.47 – 2.26 (m, 4H), 2.12 (d, J = 7.1 Hz, 2H), 1.91 – 1.79 (m, 4H), 1.62 – 1.52 (m, 1H), 1.45 – 1.35 (m, 1H), 0.98 (q, J = 12.6 Hz, 2H), 0.87 (q, J = 13.1 Hz, 2H). ^{13}C NMR (125 MHz, CDCl$_3$) δ 169.9, 159.6, 137.3, 129.5, 119.1, 115.4, 112.4, 65.1, 55.3, 54.0, 53.4, 47.7, 42.2, 40.5, 40.3, 34.9, 31.3, 31.1. LC-MS, ESI[+], m/z = 410.9 [M + H][+].

Synthesis of the intermediate (4-(((1S,4S)-4-(bromomethyl)cyclohexyl)methyl)piperazin-1-yl)(3-methoxyphenyl)methanone (2z)
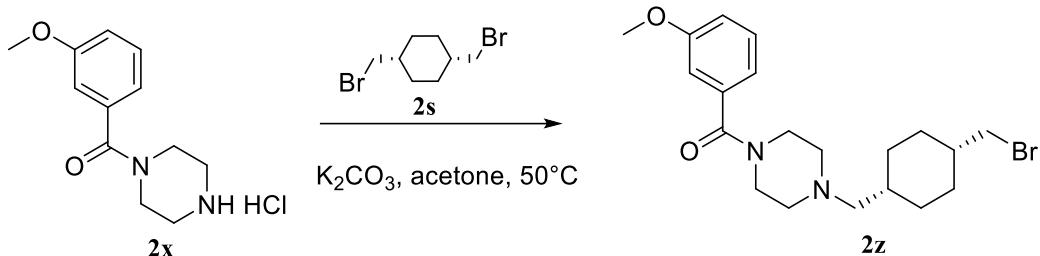
A suspension of compound **2x** (1 equiv., 100 mg, 0.39 mmol), the intermediate **2s** (3 equiv., 316 mg, 1.17 mmol), and potassium carbonate (7 equiv., 377 mg, 2.73 mmol) in acetone (6.0 mL) was heated to 50 °C and stirred overnight. After completion of the reaction, the solvent mixture was diluted with DCM and extracted with water and brine. The organic phase was then dried over sodium sulfate, filtered, and condensed to afford a crude, which was purified through flash column chromatography (0-5% methanol in DCM) on silica gel to give the desired product **2z** (66% yield). ^{1}H NMR (400 MHz, CDCl$_3$) δ 7.28 – 7.22 (m, 1H), 6.93 – 6.85 (m, 3H), 3.77 (s, 3H), 3.70 (s, 2H), 3.37 (s, 2H), 3.32 (d, J = 7.0 Hz, 2H), 2.47 – 2.25 (m, 4H), 2.19 (d, J = 7.5 Hz, 2H), 1.84 – 1.75 (m, 1H), 1.73 – 1.64 (m, 1H), 1.62 – 1.49 (m, 2H), 1.50 – 1.45 (m, 2H), 1.44 – 1.30 (m, 4H). ^{13}C NMR (125 MHz, CDCl$_3$) δ 169.9, 159.6, 137.3, 129.5, 119.1, 115.4, 112.5, 61.8, 55.3, 54.0, 53.3, 47.7, 42.2, 38.8, 38.2, 31.7, 27.3, 26.8. LC-MS, ESI$^+$, m/z = 410.9 [M + H]$^+$.

Synthesis of the final compound (2S,4R)-1-((R)-2-(1-fluorocyclopropane-1-carboxamido)-3-methyl-3-(methylthio)butanoyl)-4-hydroxy-N-(4-(4-methylthiazol-5-yl)benzyl)pyrrolidine-2-carboxamide (MP-1-23)
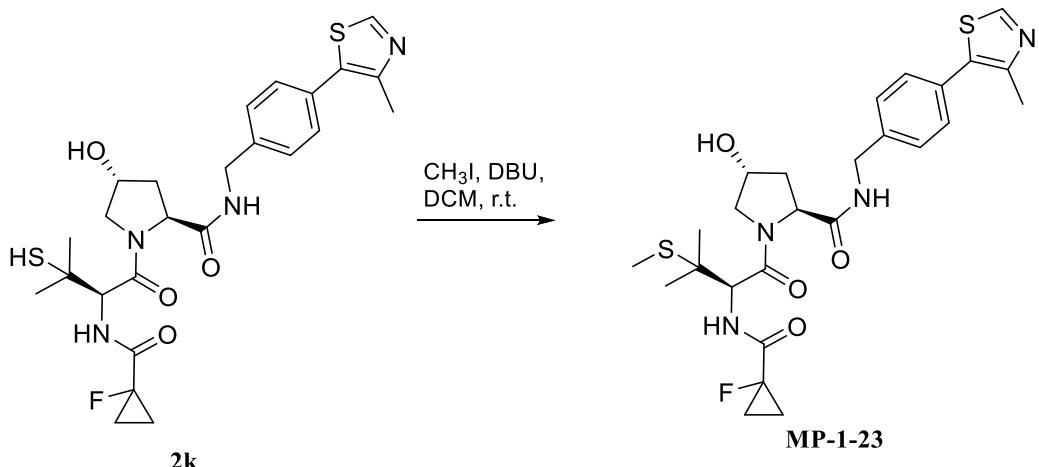
To a solution of the intermediate compound **2k** (1 equiv., 20 mg, 0.037 mmol) in DCM (0.84 mL), CH_3I (1.5 equiv., 4 μL, 0.056 mmol) and DBU (2 equiv., 11 μL, 0.074 mmol) were added. The reaction mixture was stirred overnight at room temperature and, after completion, the mixture was condensed and purified *via* flash column chromatography (0-5% methanol in DCM) on silica gel to give the final pure product **MP-1-23** (23% yield). ^1H NMR (500 MHz, $CDCl_3$) δ 8.68 (s, 1H), 7.38 (d, *J* = 8.3 Hz, 2H), 7.37 – 7.31 (m, 3H), 7.24 (dd, *J* = 8.3, 3.5 Hz, 3H), 4.79 (t, *J* = 8.0 Hz, 1H), 4.75 (d, *J* = 8.0 Hz, 1H), 4.53 (brs, 1H), 4.45 (qd, *J* = 14.9, 5.9 Hz, 2H), 4.04 (d, *J* = 11.3 Hz, 1H), 3.73 (dd, *J* = 11.2, 3.9 Hz, 1H), 2.85 (d, *J* = 4.6 Hz, 1H), 2.52 (s, 3H), 2.50 – 2.41 (m, 1H), 2.26 – 2.21 (m, 1H), 1.97 (s, 3H), 1.35 – 1.30 (m, 6H), 1.31 – 1.25 (m, 4H). ^{13}C NMR (125 MHz, $CDCl_3$) δ 171.0, 170.7 (d, *J* = 20.5 Hz), 170.1, 150.6, 148.7, 138.2, 131.8, 131.2, 129.7, 129.7, 128.4, 78.4 (d, *J* = 232.0 Hz), 70.3, 59.3, 56.9, 55.9, 47.2, 43.4, 37.1, 25.2, 24.9, 16.3, 14.2, 14.1, 11.6. ^{19}F NMR (470 MHz, $CDCl_3$) δ -197.57. HRMS calcd for $C_{26}H_{33}FN_4O_4S_2$: 548.1927, found (ESI$^+$) *m/z* = 549.2900 [M+H]$^+$

General synthetic procedure (K) for the syntheses of the final compounds MP-1-21,

MP-1-39, MP-1-85, MP-1-95, MP-1-105, MP-1-106
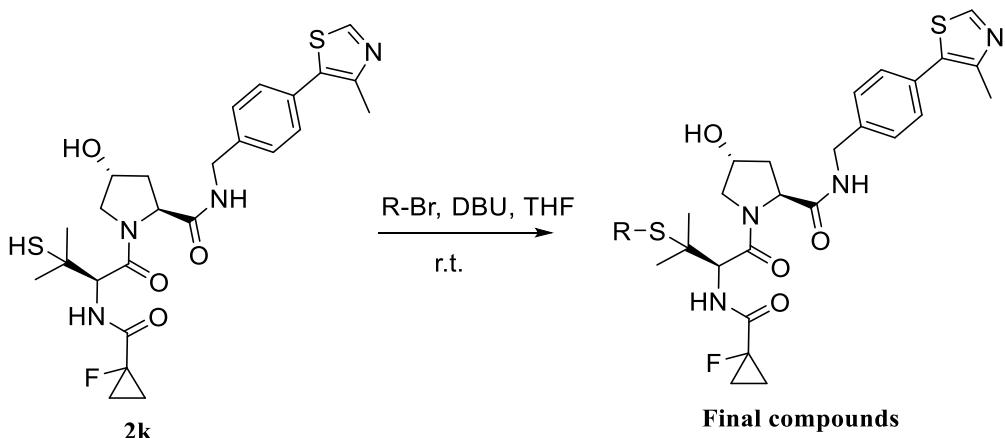
In a round bottom flask, to a solution of compound **2k** (1 equiv., 0.028 mmol) in THF

(1.5 mL) were added the previously synthesized bromine derivatives (1 equiv., 0.028

mmol) and DBU (8 equiv., 0.224 mmol). After stirring at room temperature overnight,

the mixture was condensed and purified *via* flash column chromatography on silica gel

to give the final pure compounds.

*(2S,4R)-1-((R)-2-(1-fluorocyclopropane-1-carboxamido)-3-methyl-3-((((1r,4R)-4-(morpholinomethyl)cyclohexyl)methyl)thio)butanoyl)-4-hydroxy-N-(4-(4-methylthiazol-5-yl)benzyl)pyrrolidine-2-carboxamide (**MP-1-21**)*
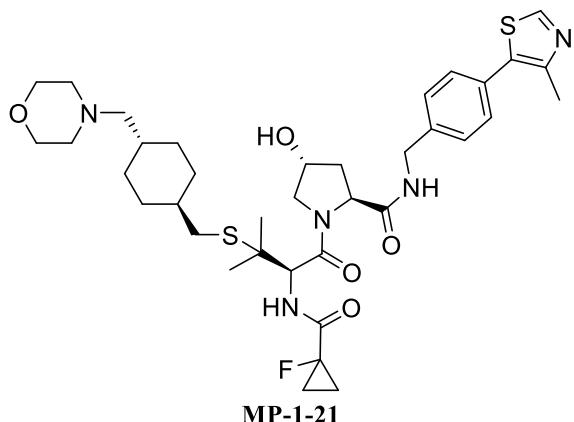
MP-1-21

Compound **MP-1-21** was prepared from **2o** following the general synthetic procedure (**K**). The crude was purified *via* flash column chromatography on silica gel employing 0-5% methanol in DCM to give the final pure compound (78% yield). ^{1}H NMR (500 MHz, CDCl$_3$) δ 8.67 (s, 1H), 7.44 (t, J = 5.9 Hz, 1H), 7.36 (d, J = 8.0 Hz, 2H), 7.32 (d, J = 8.0 Hz, 2H), 4.77 (t, J = 8.0 Hz, 1H), 4.73 (d, J = 7.8 Hz, 1H), 4.51 (brs, 1H), 4.47 – 4.41 (m, 2H), 4.01 (d, J = 11.0 Hz, 1H), 3.73 (dd, J = 11.1, 4.0 Hz, 1H), 3.68 (t, J = 4.5 Hz, 4H), 2.51 (s, 3H), 2.42 – 2.31 (m, 7H), 2.26 – 2.22 (m, 1H), 2.07 (d, J = 7.1 Hz, 2H), 1.83 – 1.74 (m, 4H), 1.40 – 1.25 (m, 13H), 0.95 – 0.78 (m, 4H). ^{13}C NMR (125 MHz, CDCl$_3$) δ 171.1, 170.6 (d, J = 20.5 Hz), 170.1, 150.5, 148.7, 138.3, 131.8, 131.1, 129.7, 128.2, 78.3 (d, J = 232.2 Hz), 70.3, 67.2, 66.0, 59.3, 56.8, 56.3, 54.4, 48.0, 43.2, 38.6, 37.1, 35.5, 34.8, 32.9, 32.8, 31.5, 25.8, 25.5, 16.3, 14.1 (d, J = 10.1 Hz), 14.1 (d, J = 10.1 Hz). ^{19}F NMR (470 MHz, CDCl$_3$) δ -197.64. HRMS calcd for C$_{37}$H$_{52}$FN$_5$O$_5$S$_2$ = 729.3394, found (ESI$^+$) *m/z*: 730.4665

*(2S,4R)-1-((R)-2-(1-fluorocyclopropane-1-carboxamido)-3-methyl-3-((((1s,4S)-4-(morpholinomethyl)cyclohexyl)methyl)thio)butanoyl)-4-hydroxy-N-(4-(4-methylthiazol-5-yl)benzyl)pyrrolidine-2-carboxamide (**MP-1-39**)*
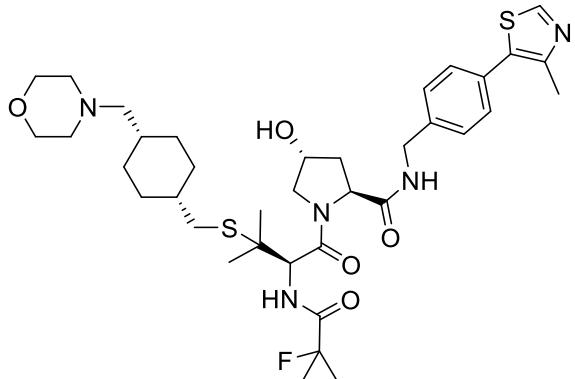
MP-1-39

Compound **MP-1-39** was prepared from **2t** following the general synthetic procedure (**K**). The crude was purified *via* flash column chromatography on silica gel employing 0-5% methanol in DCM to give the final pure product (35% yield). ^{1}H NMR (500 MHz, CDCl$_3$) δ 8.67 (s, 1H), 7.40 (t, J = 6.2 Hz, 1H), 7.37 (d, J = 8.2 Hz, 2H), 7.33 (d, J = 8.0 Hz, 2H), 7.25 (d, J = 3.5 Hz, 1H), 4.78 (t, J = 8.0 Hz, 1H), 4.73 (d, J = 7.8 Hz, 1H), 4.52 (s, 1H), 4.45 (d, J = 5.9 Hz, 2H), 4.03 (d, J = 11.4 Hz, 1H), 3.73 (dd, J = 11.1, 3.8 Hz, 1H), 3.68 (t, J = 4.6 Hz, 4H), 2.51 (s, 3H), 2.48 – 2.34 (m, 7H), 2.27 – 2.21 (m, 1H), 2.17 (d, J = 7.4 Hz, 2H), 1.71 – 1.64 (m, 1H), 1.57 – 1.41 (m, 5H), 1.37 – 1.22 (m, 15H). ^{13}C NMR (125 MHz, CDCl$_3$) δ 171.0, 170.7 (d, J = 20.4 Hz), 170.2, 150.5, 148.7, 138.3, 131.8, 131.2, 129.7, 128.2, 78.4 (d, J = 232.1 Hz), 70.3, 67.2, 63.0, 59.2, 56.8, 56.4, 54.4, 47.9, 43.3, 37.0, 35.9, 33.0, 31.9, 28.8, 28.6, 27.2, 25.9, 25.5, 16.3, 14.2 (d, J = 10.8 Hz), 14.1 (d, J = 10.7 Hz). ^{19}F NMR (470 MHz, CDCl$_3$) δ -197.68. HRMS calcd for C$_{37}$H$_{52}$FN$_5$O$_5$S$_2$: 729.3394, found (ESI$^+$) *m/z* = 730.4651 [M+H]$^+$.

*(2S,4R)-1-((R)-3-((((1r,4R)-4-((dimethylamino)methyl)cyclohexyl)methyl)thio)-2-(1-fluorocyclopropane-1-carboxamido)-3-methylbutanoyl)-4-hydroxy-N-(4-(4-methylthiazol-5-yl)benzyl)pyrrolidine-2-carboxamide (**MP-1-85**)*
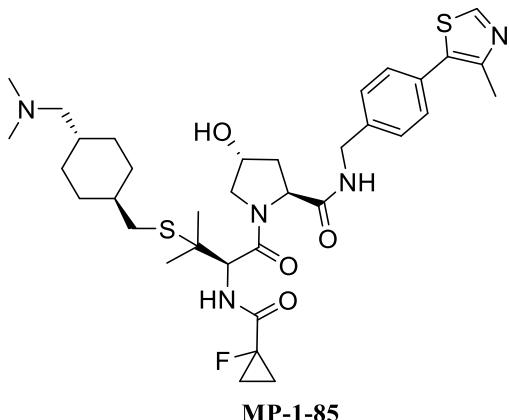
MP-1-85

Compound **MP-1-85** was prepared from **2u** following the general synthetic procedure (**K**). The crude was purified *via* flash column chromatography on silica gel employing 0-25% 0.7 M ammonia-containing methanol in DCM to give the final pure product (87% yield). ^{1}H NMR (500 MHz, CDCl$_3$) δ 8.67 (s, 1H), 7.42 (t, J = 6.0 Hz, 1H), 7.37 (d, J = 8.3 Hz, 2H), 7.33 (d, J = 8.4 Hz, 2H), 7.26 – 7.21 (m, 1H), 4.78 (t, J = 8.0 Hz, 1H), 4.73 (d, J = 8.0 Hz, 1H), 4.51 (s, 1H), 4.50 – 4.41 (m, 2H), 4.03 (d, J = 11.4 Hz, 1H), 3.73 (dd, J = 11.2, 3.9 Hz, 1H), 2.51 (s, 3H), 2.45 – 2.37 (m, 2H), 2.36 – 2.30 (m, 1H), 2.27 – 2.22 (m, 1H), 2.16 (s, 6H), 2.01 (d, J = 7.1 Hz, 2H), 1.82 – 1.75 (m, 4H), 1.38 – 1.23 (m, 13H), 0.96 – 0.87 (m, 2H), 0.86 – 0.77 (m, 2H). ^{13}C NMR (125 MHz, CDCl$_3$) δ 171.0, 170.5 (d, J = 20.5 Hz), 170.0, 150.4, 148.6, 138.2, 131.7, 131.0, 129.6, 128.1, 78.2 (d, J = 232.3 Hz), 74.9, 70.1, 66.9, 59.2, 56.7, 56.2, 47.9, 46.1, 43.1, 38.4, 37.1, 35.7, 35.4, 32.8, 32.7, 31.3, 25.8, 25.3, 16.2, 14.0 (d, J = 10.1 Hz), 14.0 (d, J = 10.1 Hz). ^{19}F NMR (470 MHz, CDCl$_3$) δ -197.68. LC-MS, ESI$^-$, m/z = 686.2 [M − H]$^-$.

*(2S,4R)-1-((R)-3-((((1s,4S)-4-((dimethylamino)methyl)cyclohexyl)methyl)thio)-2-(1-fluorocyclopropane-1-carboxamido)-3-methylbutanoyl)-4-hydroxy-N-(4-(4-methylthiazol-5-yl)benzyl)pyrrolidine-2-carboxamide (**MP-1-95**)*
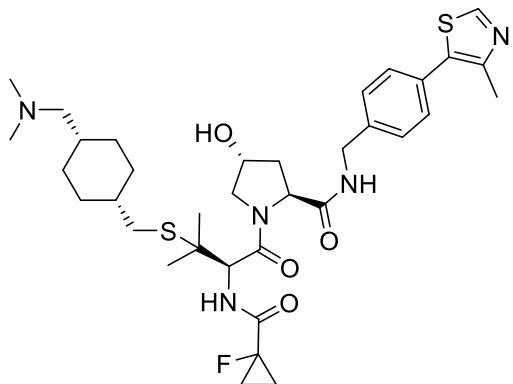
MP-1-95

Compound **MP-1-95** was prepared from **2v** following the general synthetic procedure (**K**). The crude was purified *via* flash column chromatography on silica gel employing 0-25% 0.7 M ammonia-containing methanol in DCM to give the final pure product (40% yield). ^{1}H NMR (500 MHz, CDCl$_3$) δ 8.66 (s, 1H), 7.40 (t, *J* = 6.0 Hz, 1H), 7.37 (d, *J* = 8.3 Hz, 2H), 7.33 (d, *J* = 8.3 Hz, 2H), 7.24 (dd, *J* = 8.0, 3.4 Hz, 1H), 4.80 – 4.74 (m, 2H), 4.71 (s, 1H), 4.54 – 4.48 (m, 1H), 4.49 – 4.41 (m, 2H), 4.01 (d, *J* = 11.3 Hz, 1H), 3.74 (dd, *J* = 11.1, 4.1 Hz, 1H), 2.51 (s, 3H), 2.49 – 2.40 (m, 3H), 2.25 – 2.21 (m, 1H), 2.17 (s, 6H), 2.15 – 2.08 (m, 2H), 1.66 – 1.61 (m, 1H), 1.54 – 1.44 (m, 5H), 1.35 – 1.28 (m, 14H). ^{13}C NMR (125 MHz, CDCl$_3$) δ 170.9, 170.6 (d, *J* = 20.3 Hz), 170.1, 150.4, 148.7, 138.2, 131.8, 131.1, 129.6, 128.2, 78.3 (d, *J* = 232.4 Hz), 75.0, 70.2, 63.9, 59.2, 56.7, 56.3, 47.9, 46.0, 43.2, 36.9, 36.0, 33.1, 32.9, 28.7, 28.6, 27.2, 27.1, 25.8, 25.4, 16.2, 14.0 (d, *J* = 8.8 Hz), 14.0 (d, *J* = 8.8 Hz). ^{19}F NMR (470 MHz, CDCl$_3$) δ -197.70. LC-MS, ESI$^-$, *m/z* = 686.2 [M − H]$^-$.

*(2S,4R)-1-((R)-2-(1-fluorocyclopropane-1-carboxamido)-3-((((1r,4R)-4-((4-(3-methoxybenzoyl)piperazin-1-yl)methyl)cyclohexyl)methyl)thio)-3-methylbutanoyl)-4-hydroxy-N-(4-(4-methylthiazol-5-yl)benzyl)pyrrolidine-2-carboxamide (**MP-1-105**)*
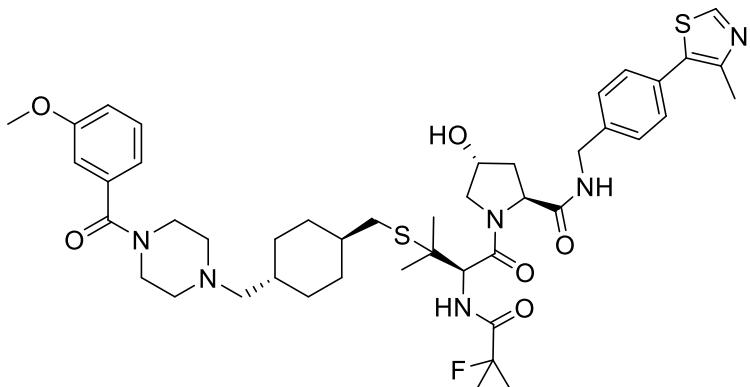
MP-1-105

Compound **MP-1-105** was prepared from **2y** following the general synthetic procedure (**K**). The crude was purified *via* flash column chromatography on silica gel employing 0-5% methanol in DCM to give the final pure product (94% yield). ^{1}H NMR (500 MHz, CDCl$_3$) δ 8.65 (s, 1H), 7.40 (t, J = 5.98 Hz, 1H), 7.36 (d, J = 8.36 Hz, 2H), 7.34 – 7.27 (m, 3H), 7.27 – 7.21 (m, 1H), 6.97 – 6.90 (m, 3H), 4.81 – 4.71 (m, 2H), 4.50 (s, 1H), 4.43 (d, J = 5.93 Hz, 2H), 3.99 (d, J = 11.39 Hz, 1H), 3.81 (s, 3H), 3.76 – 3.69 (m, 2H), 3.39 (brs, 1H), 3.29 (s, 1H), 2.50 (s, 3H), 2.45 – 2.27 (m, 7H), 2.23 – 2.18 (m, 1H), 2.10 (d, J = 7.11 Hz, 2H), 1.98 (s, 1H), 1.79 (t, J = 10.99 Hz, 4H), 1.40 – 1.25 (m, 13H), 0.93 – 0.78 (m, 4H). ^{13}C NMR (125 MHz, CDCl$_3$) δ 171.0, 170.5 (d, J = 20.8 Hz), 170.1, 170.0, 159.8, 150.3, 148.6, 138.2, 137.4, 131.7, 131.1, 129.7, 129.6, 128.1, 119.2, 115.6, 112.6, 78.2 (d, J = 231.9 Hz), 70.2, 65.3, 59.2, 56.7, 56.3, 55.5, 54.2, 53.5, 47.9, 43.2, 42.3, 38.5, 37.0, 35.4, 35.1, 32.8, 32.7, 31.4, 25.7, 25.5, 16.2, 14.0 (d, J = 10.0 Hz), 13.9 (d, J = 8.8 Hz). ^{19}F NMR (470 MHz, CDCl$_3$) δ -197.66. LC-MS, ESI$^-$, m/z = 861.5 [M − H]$^-$.

*(2S,4R)-1-((R)-2-(1-fluorocyclopropane-1-carboxamido)-3-((((1s,4S)-4-((4-(3-methoxybenzoyl)piperazin-1-yl)methyl)cyclohexyl)methyl)thio)-3-methylbutanoyl)-4-hydroxy-N-(4-(4-methylthiazol-5-yl)benzyl)pyrrolidine-2-carboxamide (**MP-1-106**)*
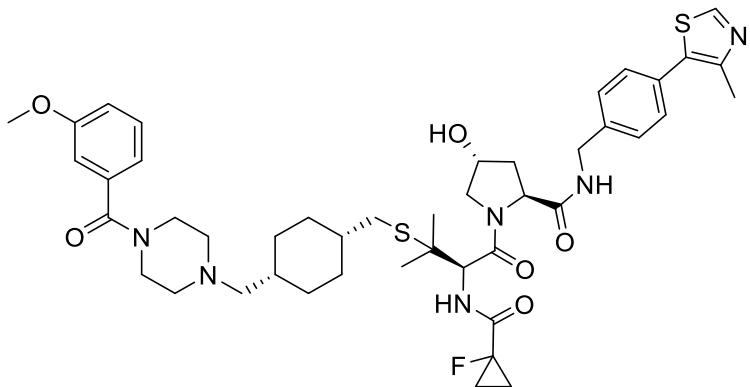
MP-1-106

Compound **MP-1-106** was prepared from **2z** following the general synthetic procedure (**K**). The crude was purified *via* flash column chromatography on silica gel employing 0-5% methanol in DCM to give the final pure product (71% yield). ^{1}H NMR (500 MHz, CDCl₃) δ 8.66 (s, 1H), 7.39 (t, *J* = 5.9 Hz, 1H), 7.36 (d, *J* = 8.3 Hz, 2H), 7.33 – 7.27 (m, 3H), 7.26 – 7.23 (m, 1H), 6.96 – 6.91 (m, 3H), 4.79 – 4.71 (m, 2H), 4.50 (s, 1H), 4.44 (d, *J* = 5.9 Hz, 2H), 4.00 (d, *J* = 11.3 Hz, 1H), 3.81 (s, 3H), 3.73 (dd, *J* = 11.1, 4.0 Hz, 2H), 3.39 (brs, 1H), 3.24 (s, 1H), 2.50 (s, 3H), 2.48 – 2.37 (m, 5H), 2.36 – 2.27 (m, 2H), 2.24 – 2.17 (m, 3H), 1.95 (s, 1H), 1.67 (s, 1H), 1.57 – 1.42 (m, 5H), 1.36 – 1.25 (m, 15H). ^{13}C NMR (125 MHz, CDCl₃) δ 170.9, 170.5 (d, *J* = 20.4 Hz), 170.1, 170.0, 159.8, 150.4, 148.6, 138.2, 137.4, 131.7, 131.1, 129.7, 129.6, 128.1, 119.2, 115.6, 112.6, 78.3 (d, *J* = 232.2 Hz), 70.2, 62.3, 59.2, 56.7, 56.4, 55.5, 54.0, 53.4, 47.9, 43.2, 42.3, 37.0, 35.9, 33.0, 32.1, 28.7, 28.5, 27.1, 25.7, 25.6, 16.2, 14.0 (d, *J* = 7.9 Hz), 13.9 (d, *J* = 8.8 Hz). ^{19}F NMR (470 MHz, CDCl₃) δ -197.66. LC-MS, ESI⁻, *m/z* = 861.2 [M − H]⁻.

7.1.3 Syntheses and characterization of new LRRK2 PROTACs

Synthesis of the intermediate tert-butyl(2S,4R)-2-((4-chlorobenzyl)carbamoyl)-4-hydroxypyrrolidine-1-carboxylate (3c)
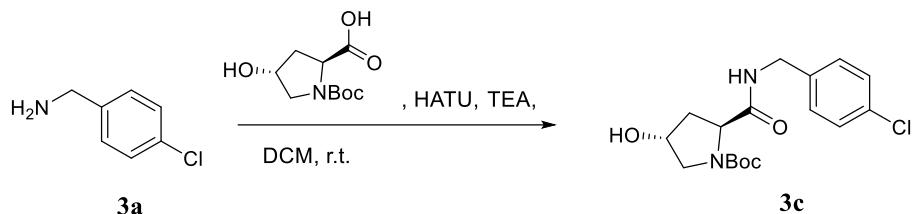
To a solution of the commercially available 4-chlorobenzylamine **3a** (1 equiv., 0.86 mL, 7.06 mmol) in DCM/methanol mixed solvent (38.0/2.0 mL) were added TEA (1.2 equiv., 1.18 mL, 8.47 mmol), (2*S*,4*R*)-1-(tert-butoxycarbonyl)-4-hydroxypyrrolidine-2-carboxylic acid (1 equiv., 1.63 g, 7.06 mmol), and HATU (1.05 equiv., 2.82 g, 7.42 mmol). The reaction mixture was stirred at room temperature for 1.5 h, then water was added and the organic phase was washed two times with water and one with brine, dried over sodium sulfate, filtered, and condensed to afford a crude residue. The obtained solid was purified *via* flash column chromatography on silica gel (0-10% methanol in DCM) to give compound **3c** (71% yield). ^{1}H NMR (500 MHz, CDCl$_3$) δ 7.34 (brs, 1H), 7.27 (d, J = 7.7 Hz, 2H), 7.19 (d, J = 8.0 Hz, 2H), 4.53 – 4.29 (m, 4H), 3.52 – 3.38 (m, 2H), 2.52 – 2.32 (m, 2H), 2.13 – 1.99 (m, 1H), 1.43 (s, 9H). ^{13}C NMR (125 MHz, CDCl$_3$) δ 173.2, 172.7, 155.9, 155.0, 136.8, 133.0, 129.3, 128.7, 80.9, 69.8, 69.2, 59.9, 59.1, 54.9, 42.6, 39.6, 37.6, 28.3. LC-MS, ESI$^+$, *m/z* = 376.9 [M + Na]$^+$.

Experimental Section

Synthesis of the intermediate tert-butyl(2S,4R)-2-((4-cyanobenzyl)carbamoyl)-4-hydroxypyrrolidine-1-carboxylate (3d)

3b   **3d**
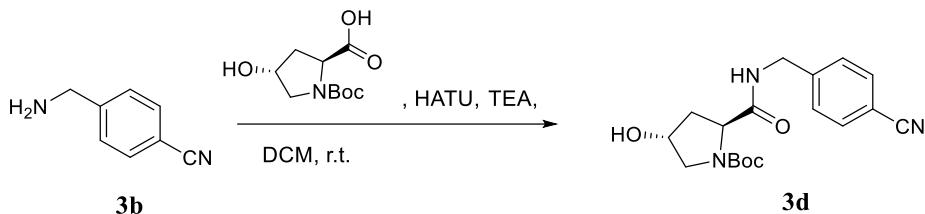
In a round bottom flask, a DCM (40.0 mL) solution containing the commercially available 4-cyanobenzylamine **3b** (1 equiv., 1.00 g, 7.57 mmol), TEA (1.2 equiv., 1.27 mL, 9.08 mmol), (2*S*,4*R*)-1-(tert-butoxycarbonyl)-4-hydroxypyrrolidine-2-carboxylic acid (1 equiv., 1.75 g, 7.57 mmol), and HATU (1.05 equiv., 3.02 g, 7.94 mmol) was stirred at room temperature for 1.5 h. After completion, water was added and the organic phase was washed two times with water and one with brine, dried over sodium sulfate, filtered, and condensed to afford a solid residue. The crude was then purified *via* flash column chromatography on silica gel (0-5% methanol in DCM) to give the title compound (36% yield). ^{1}H NMR (500 MHz, CDCl$_3$) δ 7.55 (d, *J* = 7.8 Hz, 2H), 7.35 (d, *J* = 7.9 Hz, 2H), 4.62 – 4.25 (m, 4H), 3.65 – 3.21 (m, 3H), 2.32 (s, 1H), 2.06 (s, 1H), 1.48 – 1.23 (m, 9H). ^{13}C NMR (125 MHz, CDCl$_3$) δ 173.2, 172.4, 156.0, 154.9, 143.9, 132.4, 128.4, 127.8, 118.8, 111.2, 110.9, 81.0, 69.9, 69.2, 60.0, 58.9, 55.1, 54.8, 42.9, 39.7, 37.2, 28.3.

Synthesis of the intermediate (9H-fluoren-9-yl)methyl((R)-1-((2S,4R)-2-((4-chlorobenzyl)carbamoyl)-4-hydroxypyrrolidin-1-yl)-3-methyl-1-oxo-3-(tritylthio)butan-2-yl)carbamate (3e)
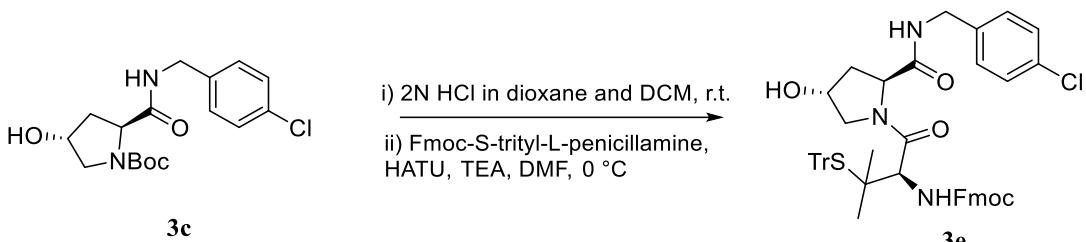
To a solution of the boc-protected intermediate **3c** (1 equiv., 1.79 g, 5.04 mmol) in DCM (10.1 mL) was slowly added 4 N HCl in 1,4-dioxane (10.1 mL). After stirring 1 h at room temperature, the volatiles were removed under reduced pressure. The obtained solid was washed with diethyl ether and air-dried to give the deprotected product as HCl salt (92% yield, LC-MS, ESI^+, $m/z = 254.8$ $[M + H]^+$), which was used for the next step. To a suspension of the obtained derivative (1 equiv., 150 mg, 0.52 mmol) and TEA (2.5 equiv., 179 μL, 1.29 mmol) in DMF (2.7 mL) was added dropwise, in an ice-bath, a mixture of Fmoc-*S*-trityl-L-penicillamine (1 equiv., 316 mg, 0.52 mmol), HATU (1 equiv., 196 mg, 0.52 mmol), and TEA (1 equiv., 72 μL, 0.52 mmol) in DMF (1.8 mL). After stirring at 0 °C for 1 h, water was added and extracted three times with ethyl acetate. Then the organic phase was washed with brine, dried over sodium sulfate, filtered, and condensed to afford a crude, which was purified with flash column chromatography (0-5% methanol in DCM) to afford compound **3e** (81% yield). ^{1}H NMR (500 MHz, MeOD) δ 7.73 (dd, $J = 7.6, 3.5$ Hz, 2H), 7.62 (dd, $J = 7.6, 3.5$ Hz, 2H), 7.51 (d, $J = 7.6$ Hz, 6H), 7.35 – 7.27 (m, 2H), 7.24 – 7.09 (m, 17H), 4.49 (t, $J = 8.1$ Hz, 1H), 4.41 – 4.34 (m, 2H), 4.26 – 4.15 (m, 3H), 4.12 – 4.07 (m, 2H), 3.53 (d, $J = 11.1$ Hz, 1H), 3.43 (dd, $J = 11.0, 4.2$ Hz, 1H), 2.16 – 2.09 (m, 1H), 2.01 – 1.92 (m, 1H), 1.23 (s, 3H), 1.00 (s, 3H). ^{13}C NMR (125 MHz, CDCl$_3$) δ 171.2, 170.1, 156.4, 144.4, 143.8, 143.5, 141.3, 141.3, 136.9, 132.7, 129.9, 128.8, 128.5, 127.9, 127.2, 127.2, 126.9, 125.1, 125.0, 120.1, 77.4, 70.0, 68.5, 67.5,

59.1, 58.3, 56.7, 54.6, 46.9, 42.3, 37.1, 26.0, 25.2. LC-MS, ESI$^+$, *m/z* = 872.4 [M + Na]$^+$.

Synthesis of the intermediate (9H-fluoren-9-yl)methyl((R)-1-((2S,4R)-2-((4-cyanobenzyl)carbamoyl)-4-hydroxypyrrolidin-1-yl)-3-methyl-1-oxo-3-(tritylthio)butan-2-yl)carbamate (3f)
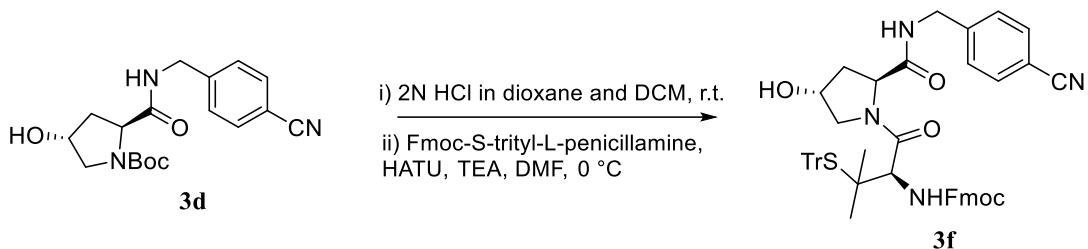
To a solution of compound **3d** (1 equiv., 933 mg, 2.70 mmol) in DCM (5.4 mL) was added 4 N HCl in 1,4-dioxane (5.4 mL) dropwise and the reaction was stirred 1 h at room temperature. The mixture was then concentrated under reduced pressure, washed with diethyl ether, and air-dried to give the boc-deprotected product as a HCl salt (86% yield, LC-MS, ESI$^+$, *m/z* = 246.0 [M + H]$^+$), which was used in the next step without further purification. To a suspension of the obtained salt (1 equiv., 150 mg, 0.53 mmol) in DMF (2.8 mL) was added TEA (2.5 equiv., 185 μL, 1.33 mmol) and stirred at room temperature. In parallel, in a round bottom flask, to a solution of Fmoc-*S*-trityl-L-penicillamine (1 equiv., 327 mg, 0.53 mmol) in DMF (1.9 mL) were added HATU (1 equiv., 202 mg, 0.53 mmol) and TEA (1 equiv., 74 μL, 0.53 mmol) while stirring in an ice-bath. After 10 min, the two solutions were combined and the reaction mixture was stirred for 1 h at 0 °C. After completion, water was added and the aqueous phase was extracted several times with ethyl acetate. The organic layers were then collected and dried over sodium sulfate, filtered, and condensed to afford a residue, which was purified with flash column chromatography (0-5% methanol in DCM) on silica gel to

give compound **3f** (74% yield). ^{1}H NMR (500 MHz, CDCl$_3$) δ 7.76 (t, J = 8.2 Hz, 2H), 7.60 (d, J = 7.5 Hz, 1H), 7.56 – 7.51 (m, 8H), 7.44 – 7.34 (m, 5H), 7.25 – 7.20 (m, 12H), 5.83 (d, J = 5.8 Hz, 1H), 4.59 (t, J = 8.2 Hz, 1H), 4.40 – 4.33 (m, 2H), 4.25 – 4.17 (m, 3H), 4.11 (dd, J = 16.3, 6.3 Hz, 1H), 3.61 (d, J = 5.8 Hz, 2H), 3.47 (d, J = 11.3 Hz, 1H), 3.37 (dd, J = 11.2, 4.0 Hz, 1H), 2.16 – 2.09 (m, 1H), 2.08 – 1.99 (m, 1H), 1.20 (s, 3H), 1.07 (s, 3H). ^{13}C NMR (125 MHz, CDCl$_3$) δ 171.7, 170.2, 156.4, 144.3, 144.0, 143.8, 143.5, 141.4, 141.3, 132.2, 129.9, 128.0, 127.7, 127.3, 127.1, 125.1, 125.0, 120.2, 118.9, 110.7, 77.5, 70.1, 68.6, 67.6, 59.4, 58.4, 57.0, 54.7, 47.0, 42.6, 37.4, 26.1, 25.3.

Synthesis of the intermediate (2S,4R)-1-((R)-2-amino-3-methyl-3-(tritylthio)butanoyl)-N-(4-chlorobenzyl)-4-hydroxypyrrolidine-2-carboxamide (3g)
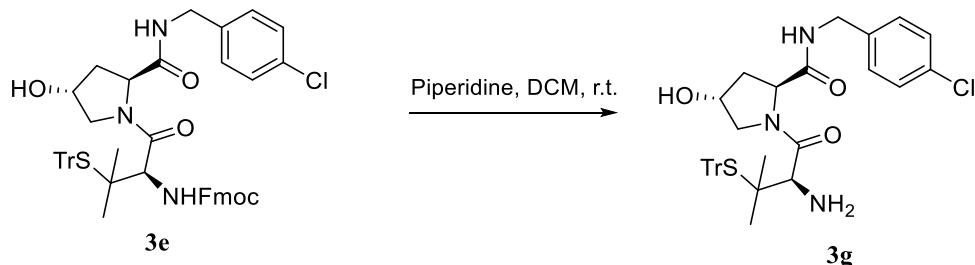
To a solution of the Fmoc-protected compound **3e** (1 equiv., 214 mg, 0.25 mmol) in DCM (0.8 mL) was added piperidine (8 equiv., 0.2 mL, 2.02 mmol) dropwise. The resulting mixture was stirred at room temperature for 1 h, and then condensed under vacuum to give a residue which was purified by flash column chromatography on silica gel (0-15% 0.7 M ammonia-containing methanol in DCM) to give the desired product (90% yield). ^{1}H NMR (500 MHz, CDCl$_3$) δ 7.55 (d, J = 7.5 Hz, 6H), 7.30 – 7.26 (m, 7H), 7.23 – 7.17 (m, 5H), 7.06 (d, J = 8.4 Hz, 2H), 5.09 (brs, 1H), 4.49 (t, J = 8.3 Hz, 1H), 4.28 (s, 1H), 4.11 (dd, J = 6.2, 2.5 Hz, 2H), 3.14 (dd, J = 11.3, 3.8 Hz, 1H), 3.08 (d, J = 11.3 Hz, 1H), 2.77 (s, 1H), 2.05 – 1.96 (m, 2H), 1.19 (s, 3H), 1.03 (s, 3H). ^{13}C

NMR (125 MHz, CDCl$_3$) δ 171.9, 171.6, 144.8, 137.1, 133.0, 130.0, 128.9, 128.7, 128.0, 127.0, 70.0, 68.3, 59.2, 58.2, 58.0, 57.1, 42.5, 37.5, 25.3, 24.7. LC-MS, ESI⁻, *m/z* = 626.5 [M − H]⁻.

Synthesis of the intermediate (2S,4R)-1-((R)-2-amino-3-methyl-3-(tritylthio)butanoyl)-N-(4-cyanobenzyl)-4-hydroxypyrrolidine-2-carboxamide (3h)
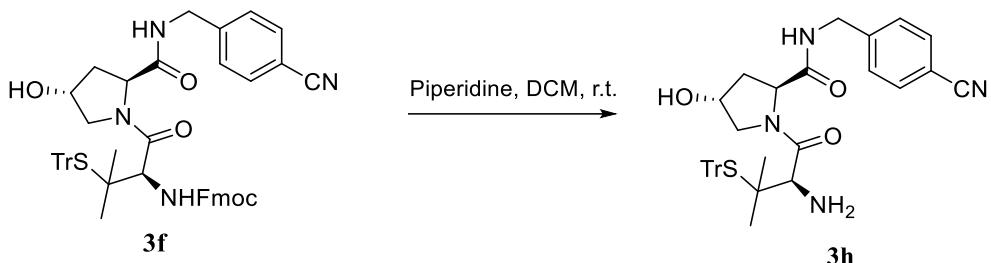
The Fmoc-protected compound **3f** (1 equiv., 329 mg, 0.39 mmol) was dissolved in 1.2 mL of DCM. Then piperidine (8 equiv., 0.3 mL, 3.13 mmol) was added and the reaction mixture was stirred for 1 h at room temperature. After completion of reaction, volatiles were removed under vacuum and the crude was purified *via* flash column chromatography (0-25% 0.7 M ammonia-containing methanol in DCM) on silica gel to give compound **3h** (82% yield). ¹H NMR (500 MHz, CDCl$_3$) δ 7.34 – 7.23 (m, 9H), 7.08 – 6.92 (m, 13H), 4.78 (s, 1H), 4.37 (t, *J* = 8.5 Hz, 1H), 4.10 (s, 1H), 3.97 – 3.88 (m, 2H), 3.00 (dd, *J* = 11.3, 3.7 Hz, 1H), 2.93 (d, *J* = 11.2 Hz, 1H), 2.62 (s, 1H), 1.90 – 1.80 (m, 1H), 1.81 – 1.72 (m, 1H), 0.98 (s, 3H), 0.78 (s, 3H). ¹³C NMR (125 MHz, CDCl$_3$) δ 172.4, 172.2, 144.8, 144.2, 132.4, 130.1, 128.0, 127.8, 127.1, 119.0, 110.9, 70.0, 68.4, 59.4, 58.6, 58.0, 57.4, 42.7, 38.0, 25.0, 24.9. LC-MS, ESI⁻, *m/z* = 617.4 [M − H]⁻.

Synthesis of the intermediate (2S,4R)-N-(4-chlorobenzyl)-1-((R)-2-(1-fluorocyclopropane-1-carboxamido)-3-methyl-3-(tritylthio)butanoyl)-4-hydroxypyrrolidine-2-carboxamide (3i)
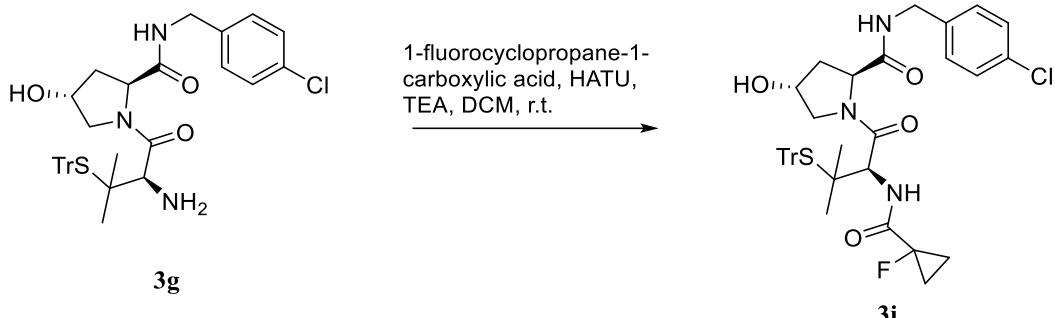
To a solution of the amine compound **3g** (1 equiv., 192 mg, 0.31 mmol) in DMF (1.9 mL) was added TEA (2 equiv., 0.9 mL, 0.61 mmol), HATU (1.05 equiv., 122 mg, 0.32 mmol), and 1-fluorocyclopropane-1-carboxylic acid (1 equiv., 32 mg, 0.31 mmol). After stirring at room temperature for 1 h, water was added and extracted three times with ethyl acetate. The organic phase was then washed with brine, dried over sodium sulfate, filtered, and condensed to afford a crude product, which was purified through flash column chromatography (0-5% methanol in DCM) on silica gel to give the title compound (65% yield). ^{1}H NMR (500 MHz, CDCl$_3$) δ 7.54 (d, J = 7.2 Hz, 6H), 7.38 (t, J = 6.1 Hz, 1H), 7.27 – 7.22 (m, 7H), 7.21 – 7.18 (m, 3H), 7.16 (d, J = 8.4 Hz, 2H), 7.07 (d, J = 8.4 Hz, 2H), 4.54 (t, J = 8.1 Hz, 1H), 4.32 (s, 1H), 4.16 (dd, J = 15.2, 6.0 Hz, 1H), 4.09 (dd, J = 15.2, 6.2 Hz, 1H), 3.74 (d, J = 5.4 Hz, 1H), 3.57 (d, J = 5.2 Hz, 1H), 3.42 (d, J = 11.5 Hz, 1H), 3.28 (dd, J = 11.3, 3.9 Hz, 1H), 2.14 – 2.03 (m, 2H), 1.36 – 1.26 (m, 2H), 1.25 – 1.13 (m, 5H), 1.06 (s, 3H). ^{13}C NMR (125 MHz, CDCl$_3$) δ 171.1, 170.1 (d, J = 20.5 Hz), 169.4, 144.4, 137.0, 132.8, 129.8, 128.9, 128.6, 127.9, 127.0, 78.2 (d, J = 232.2 Hz), 70.1, 68.4, 59.1, 57.0, 56.9, 54.2, 42.5, 37.0, 26.0, 25.5, 13.7, 13.6. ^{19}F NMR (471 MHz, CDCl$_3$) δ -197.21.

Synthesis of the intermediate (2S,4R)-N-(4-cyanobenzyl)-1-((R)-2-(1-fluorocyclopropane-1-carboxamido)-3-methyl-3-(tritylthio)butanoyl)-4-hydroxypyrrolidine-2-carboxamide (3j)
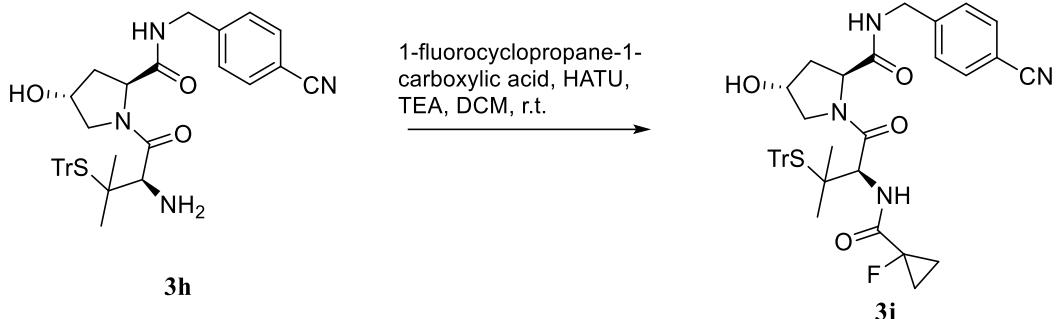
To a DCM solution (2.0 mL) of the synthesized **3h** (1 equiv., 199 mg, 0.32 mmol), it was added TEA (2 equiv., 0.9 mL, 0.64 mmol), HATU (1.05 equiv., 129 mg, 0.34 mmol), and 1-fluorocyclopropane-1-carboxylic acid (1 equiv., 34 mg, 0.32 mmol). The reaction was stirred at room temperature for 1 h, then water was added and the reaction mixture was extracted three times with DCM. The organic phase was then washed with brine, dried over sodium sulfate, filtered, and condensed to afford a crude product, which was purified through flash column chromatography (0-5% methanol in DCM) on silica gel to give compound **3j** (74% yield). ^{1}H NMR (500 MHz, CDCl$_3$) δ 7.57 (d, J = 7.7 Hz, 6H), 7.51 (t, J = 6.2 Hz, 1H), 7.45 (d, J = 8.1 Hz, 2H), 7.33 (t, J = 4.3 Hz, 1H), 7.30 – 7.22 (m, 11H), 4.58 (t, J = 8.2 Hz, 1H), 4.37 (s, 1H), 4.23 (d, J = 6.1 Hz, 2H), 3.73 (d, J = 5.2 Hz, 1H), 3.61 (d, J = 5.1 Hz, 1H), 3.49 (d, J = 11.3 Hz, 1H), 3.36 (dd, J = 11.2, 3.8 Hz, 1H), 2.18 – 2.04 (m, 2H), 1.43 – 1.32 (m, 2H), 1.31 – 1.17 (m, 5H), 1.13 (s, 3H). ^{13}C NMR (125 MHz, CDCl$_3$) δ 171.7, 170.2 (d, J = 20.5 Hz), 169.7, 144.4, 144.1, 132.3, 129.9, 128.0, 127.9, 127.1, 118.9, 110.9, 78.3 (d, J = 232.3 Hz), 70.3, 68.5, 59.4, 57.2, 57.2, 54.3, 42.8, 37.4, 26.2, 25.6, 13.8 (d, J = 11.3 Hz), 13.7 (d, J = 11.3 Hz). ^{19}F NMR (470 MHz, CDCl$_3$) δ -197.16. LC-MS, ESI$^-$, m/z = 703.1 [M − H]$^-$.

Synthesis of the intermediate (2S,4R)-N-(4-chlorobenzyl)-1-((R)-2-(1-fluorocyclopropane-1-carboxamido)-3-mercapto-3-methylbutanoyl)-4-hydroxypyrrolidine-2-carboxamide (3k)
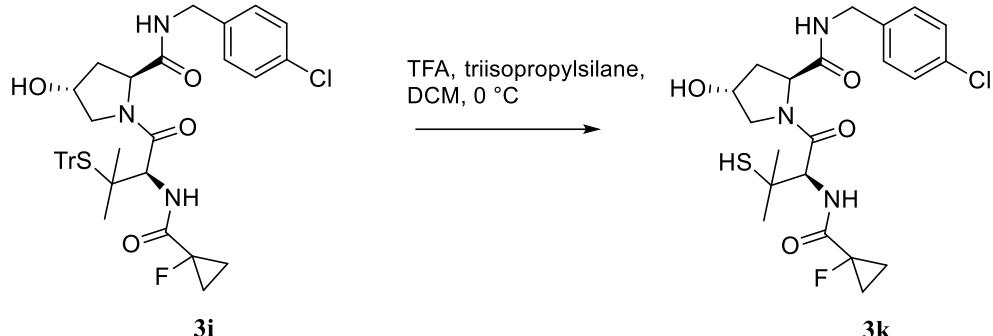
To a solution of the previously synthesized compound **3i** (1 equiv., 142 mg, 0.20 mmol) in DCM (9.0 mL) was added triisopropylsilane (0.5 mL) and TFA (0.5 mL) in an ice-bath. The resulting mixture was stirred at 0 °C for 10 min and condensed to afford a crude, which was purified *via* flash column chromatography (0-5% methanol in DCM) on silica gel to yield compound **3k** (97% yield). ^{1}H NMR (500 MHz, CDCl$_3$) δ 7.42 (dd, J = 8.8, 3.3 Hz, 1H), 7.36 (t, J = 6.1 Hz, 1H), 7.22 (d, J = 8.5 Hz, 2H), 7.18 (d, J = 8.3 Hz, 2H), 4.67 (d, J = 8.7 Hz, 1H), 4.57 (t, J = 8.1 Hz, 1H), 4.44 (s, 1H), 4.39 (dd, J = 15.1, 6.4 Hz, 1H), 4.23 (dd, J = 15.1, 5.5 Hz, 1H), 3.94 (d, J = 11.1 Hz, 1H), 3.76 (dd, J = 11.1, 3.7 Hz, 1H), 3.61 (s, 1H), 2.56 (s, 1H), 2.26 – 2.17 (m, 1H), 2.12 – 2.03 (m, 1H), 1.41 (s, 3H), 1.34 (s, 3H), 1.32 – 1.22 (m, 4H). ^{13}C NMR (125 MHz, CDCl$_3$) δ 171.2, 170.6 (d, J = 20.4 Hz), 170.0, 136.9, 133.3, 129.1, 128.9, 78.3 (d, J = 232.3 Hz), 70.2, 59.5, 57.8, 56.9, 46.7, 43.0, 37.3, 30.3, 28.8, 14.1 (d, J = 10.2 Hz), 14.0 (d, J = 10.2 Hz). ^{19}F NMR (470 MHz, CDCl$_3$) δ -197.54. LC-MS, ESI$^+$, *m/z* = 494.1 [M + Na]$^+$.

Synthesis of the intermediate (2S,4R)-N-(4-cyanobenzyl)-1-((R)-2-(1-fluorocyclopropane-1-carboxamido)-3-mercapto-3-methylbutanoyl)-4-hydroxypyrrolidine-2-carboxamide (3l)
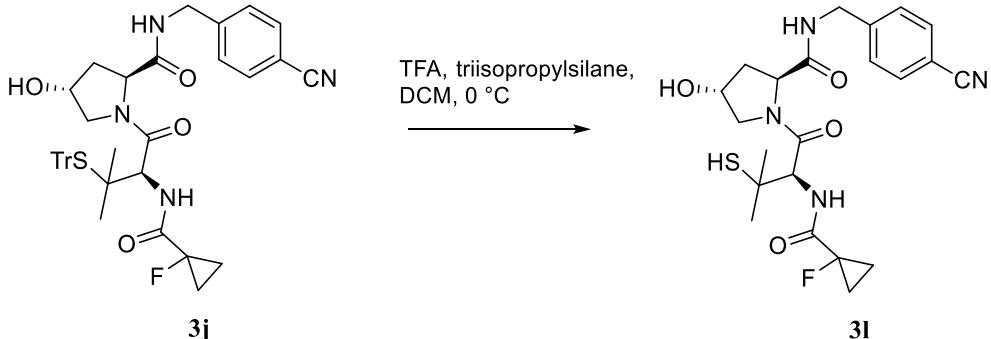
To a solution of compound **3j** (1 equiv., 167 mg, 0.24 mmol) in DCM (10.7 mL) was added triisopropylsilane (0.6 mL) and TFA (0.6 mL) while stirring in an ice-bath. The resulting mixture was stirred at 0 °C for 10 min and condensed to afford a crude, which was purified *via* flash column chromatography (0-5% methanol in DCM) on silica gel to yield compound **3l** (81% yield). ^{1}H NMR (500 MHz, CDCl$_3$) δ 7.54 (d, J = 8.3 Hz, 2H), 7.50 – 7.42 (m, 2H), 7.38 (d, J = 8.1 Hz, 2H), 4.66 (d, J = 8.6 Hz, 1H), 4.62 (t, J = 8.2 Hz, 1H), 4.54 (dd, J = 15.8, 6.7 Hz, 1H), 4.49 (s, 1H), 4.31 (dd, J = 15.8, 5.6 Hz, 1H), 4.03 (d, J = 11.3 Hz, 1H), 3.78 (dd, J = 11.2, 3.7 Hz, 1H), 3.70 (d, J = 3.9 Hz, 1H), 2.55 (s, 1H), 2.39 (s, 1H), 2.28 – 2.19 (m, 1H), 2.17 – 2.09 (m, 1H), 1.42 (s, 3H), 1.37 (s, 3H), 1.36 – 1.23 (m, 4H). ^{13}C NMR (125 MHz, CDCl$_3$) δ 171.5, 170.7 (d, J = 20.6 Hz), 170.2, 143.9, 132.6, 128.2, 118.9, 111.3, 78.3 (d, J = 232.3 Hz), 70.3, 59.5, 57.9, 57.0, 46.7, 43.2, 37.3, 30.5, 29.0, 14.2 (d, J = 10.2 Hz), 14.0 (d, J = 10.2 Hz). ^{19}F NMR (470 MHz, CDCl$_3$) δ -197.59. LC-MS, ESI$^-$, m/z = 461.4 [M − H]$^-$.

Synthesis of the intermediate (4-(((1R,4R)-4-(bromomethyl)cyclohexyl)methyl)piperazin-1-yl)(4-((5-chloro-4-(methylamino)pyrimidin-2-yl)amino)-3-methoxyphenyl)methanone (3n)
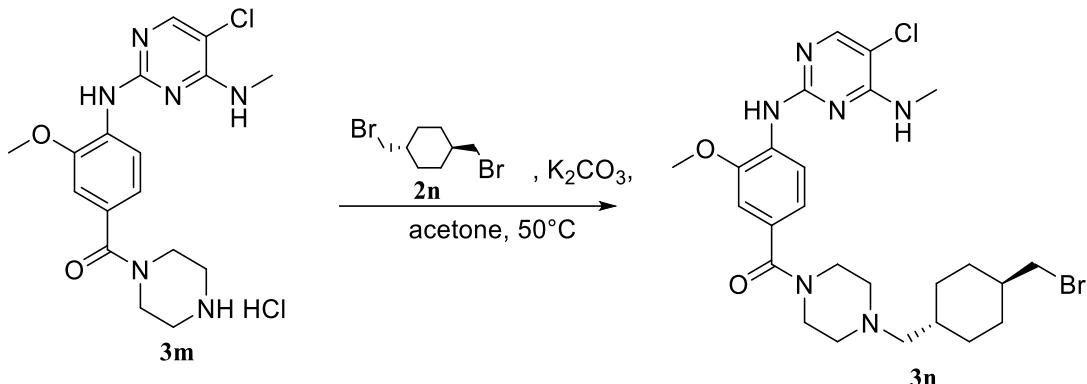
To suspension of the amine hydrochloride compound **3m** (1 equiv., 100 mg, 0.24 mmol), the intermediate **2n** (3 equiv., 196 mg, 0.73 mmol), and potassium carbonate (7 equiv., 234 mg, 1.69 mmol) in acetone (12.0 mL) was heated to 50 °C and stirred overnight. The mixture was then cooled down and diluted with DCM. The organic phase was washed with water and brine, dried over sodium sulfate, filtered, and condensed to afford a crude, which was purified through flash column chromatography (0-5% methanol in DCM) on silica gel to give the desired product **3n** (50% yield). ^{1}H NMR (500 MHz, CDCl$_3$) δ 8.53 (d, J = 8.6 Hz, 1H), 7.91 (s, 1H), 7.62 (s, 1H), 7.02 – 6.96 (m, 2H), 5.34 (q, J = 4.9 Hz, 1H), 3.91 (s, 3H), 3.77 – 3.50 (s, 4H), 3.28 (d, J = 6.3 Hz, 2H), 3.09 (d, J = 4.9 Hz, 3H), 2.39 (s, 3H), 2.15 (d, J = 7.2 Hz, 2H), 1.97 – 1.81 (m, 5H), 1.65 – 1.54 (m, 1H), 1.49 – 1.38 (m, 1H), 1.01 (q, J = 12.7 Hz, 2H), 0.90 (q, J = 12.6 Hz, 2H). ^{13}C NMR (125 MHz, CDCl$_3$) δ 170.6, 158.7, 158.0, 152.8, 147.6, 131.4, 128.1, 120.3, 116.9, 109.7, 105.7, 65.4, 56.0, 54.0, 40.8, 40.5, 35.0, 31.5, 31.3, 28.3. LC-MS, ESI$^+$, m/z = 567.3 [M + H]$^+$.

Experimental Section

Synthesis of the intermediate (4-(((1S,4S)-4-(bromomethyl)cyclohexyl)methyl)piperazin-1-yl)(4-((5-chloro-4-(methylamino)pyrimidin-2-yl)amino)-3-methoxyphenyl)methanone (3o)
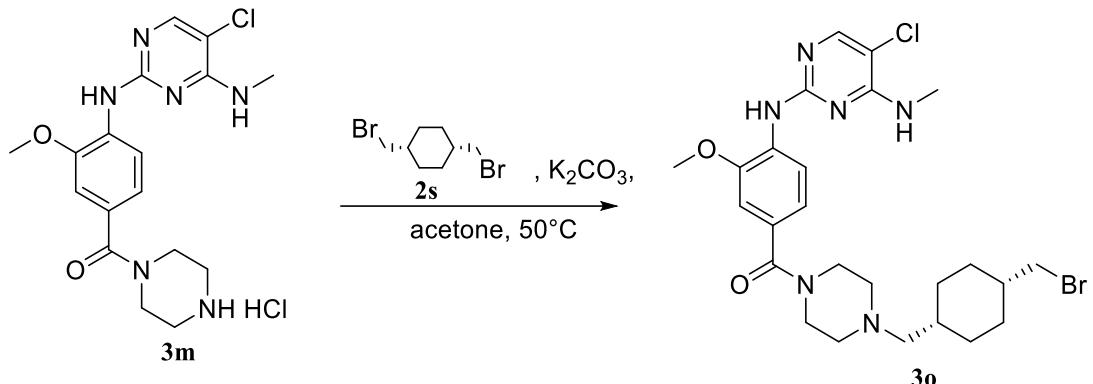
To a suspension of the amine hydrochloride compound **3m** (1 equiv., 100 mg, 0.24 mmol), the intermediate **2s** (3 equiv., 196 mg, 0.73 mmol), and potassium carbonate (7 equiv., 234 mg, 1.69 mmol) in acetone (6.0 mL) was heated to 50 °C and stirred overnight. The mixture was then diluted with DCM and the organic phase was washed with water and brine, dried over sodium sulfate, filtered, and condensed to afford a residue, which was purified *via* flash column chromatography (0-5% methanol in DCM) on silica gel to give the title compound (75% yield). ^{1}H NMR (500 MHz, CDCl$_3$) δ 8.52 (d, J = 8.7 Hz, 1H), 7.89 (s, 1H), 7.62 (s, 1H), 7.00 – 6.95 (m, 2H), 5.36 (q, J = 4.9 Hz, 1H), 3.90 (s, 3H), 3.80 – 3.41 (s, 4H), 3.35 (d, J = 6.9 Hz, 2H), 3.07 (d, J = 4.9 Hz, 3H), 2.48 – 2.28 (s, 4H), 2.22 (d, J = 7.5 Hz, 2H), 1.87 – 1.79 (m, 1H), 1.76 – 1.66 (m, 1H), 1.64 – 1.54 (m, 2H), 1.56 – 1.47 (m, 2H), 1.47 – 1.33 (m, 4H). ^{13}C NMR (125 MHz, CDCl$_3$) δ 170.5, 158.7, 157.9, 152.8, 147.5, 131.4, 128.1, 120.3, 116.8, 109.7, 105.6, 62.0, 56.0, 53.9, 39.1, 38.4, 31.9, 28.3, 27.4, 27.0. LC-MS, ESI$^+$, m/z = 567.5 [M + H]$^+$.

Synthesis of the final compound (2S,4R)-1-((R)-3-((((1r,4R)-4-((4-(4-((5-chloro-4-(methylamino)pyrimidin-2-yl)amino)-3-methoxybenzoyl)piperazin-1-yl)methyl)cyclohexyl)methyl)thio)-2-(1-fluorocyclopropane-1-carboxamido)-3-methylbutanoyl)-N-(4-chlorobenzyl)-4-hydroxypyrrolidine-2-carboxamide (MP01077)
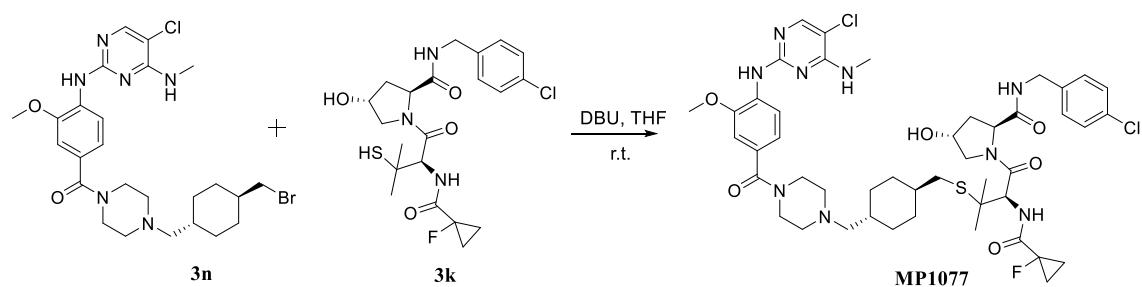
A solution containing **3k** (1 equiv., 13 mg, 0.027 mmol), **3n** (1 equiv., 15 mg, 0.027 mmol), and DBU (8 equiv., 32 μL, 0.216 mmol) in THF (1.5 mL), was stirred at room temperature overnight. After completion of the reaction, the mixture was condensed and the resulting residue was purified through flash column chromatography (0-5% methanol in DCM) on silica gel to give the final pure product **MP01077** (92% yield). ^{1}H NMR (500 MHz, CDCl$_3$) δ 8.53 (d, J = 8.7 Hz, 1H), 7.91 (s, 1H), 7.62 (s, 1H), 7.34 (t, J = 6.0 Hz, 1H), 7.29 – 7.21 (m, 4H), 7.19 (d, J = 8.4 Hz, 2H), 7.02 – 6.98 (m, 2H), 5.32 (q, J = 4.9 Hz, 1H), 4.76 – 4.70 (m, 2H), 4.48 (s, 1H), 4.40 (dd, J = 15.1, 6.2 Hz, 1H), 4.32 (dd, J = 15.1, 5.8 Hz, 1H), 3.99 (d, J = 11.4 Hz, 1H), 3.91 (s, 3H), 3.70 (dd, J = 11.1, 4.0 Hz, 1H), 3.63 (s, 3H), 3.09 (d, J = 4.9 Hz, 3H), 2.41 – 2.32 (m, 6H), 2.24 – 2.15 (m, 1H), 2.13 (d, J = 7.0 Hz, 2H), 1.90 (s, 1H), 1.80 (d, J = 12.3 Hz, 4H), 1.44 – 1.36 (m, 1H), 1.35 – 1.26 (m, 12H), 0.97 – 0.77 (m, 4H). ^{13}C NMR (125 MHz, CDCl$_3$) δ 171.0, 170.6, 170.6 (d, J = 19.8 Hz), 170.1, 158.8, 158.1, 152.9, 147.6, 137.0, 133.3, 131.5, 129.2, 128.9, 128.2, 120.4, 117.0, 109.8, 105.8, 78.3 (d, J = 232.2 Hz), 70.3, 65.5, 59.3, 56.8, 56.4, 56.1, 54.1, 48.0, 43.0, 38.6, 37.1, 35.5, 35.2, 32.9, 32.8,

31.6, 28.3, 25.8, 25.6, 14.1 (d, J = 7.7 Hz), 14.0 (d, J = 7.7 Hz). ^{19}F NMR (470 MHz,

CDCl$_3$) δ -197.68. LC-MS, ESI$^-$, m/z = 954.3 [M − H]$^-$.

Synthesis of the final compound (2S,4R)-1-((R)-3-(((((1s,4S)-4-((4-(4-((5-chloro-4-

(methylamino)pyrimidin-2-yl)amino)-3-methoxybenzoyl)piperazin-1-

yl)methyl)cyclohexyl)methyl)thio)-2-(1-fluorocyclopropane-1-carboxamido)-3-

methylbutanoyl)-N-(4-chlorobenzyl)-4-hydroxypyrrolidine-2-carboxamide

(MP01083)
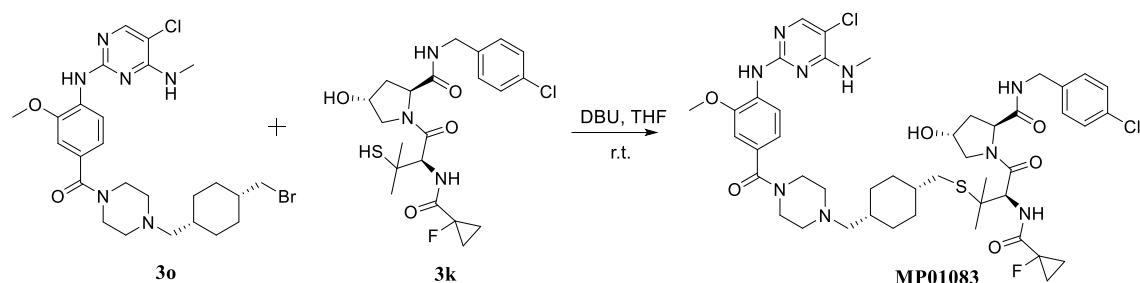
A THF solution (1.5 mL) containing **3k** (1 equiv., 13 mg, 0.027 mmol), **3o** (1 equiv.,

15 mg, 0.027 mmol), and DBU (8 equiv., 32 μL, 0.216 mmol), was stirred at room

temperature overnight. The mixture was condensed under vacuum and the resulting

crude was purified through flash column chromatography (0-5% methanol in DCM)

on silica gel to give the final pure product **MP01083** (85% yield). ^{1}H NMR (500 MHz,

CDCl$_3$) δ 8.54 (d, J = 8.8 Hz, 1H), 7.92 (s, 1H), 7.63 (s, 1H), 7.29 (t, J = 6.0 Hz, 1H),

7.28 – 7.23 (m, 4H), 7.24 – 7.18 (m, 2H), 7.02 – 6.99 (m, 2H), 5.29 (q, J = 4.9 Hz,

1H), 4.78 – 4.70 (m, 2H), 4.50 (s, 1H), 4.41 (dd, J = 15.0, 6.2 Hz, 1H), 4.34 (dd, J =

15.1, 5.8 Hz, 1H), 4.04 (d, J = 11.4 Hz, 1H), 3.92 (s, 3H), 3.70 (dd, J = 11.2, 3.9 Hz,

1H), 3.64 (s, 3H), 3.11 (d, J = 4.9 Hz, 3H), 2.75 (s, 1H), 2.46 – 2.37 (m, 6H), 2.26 –

2.17 (m, 3H), 1.75 – 1.65 (m, 1H), 1.56 – 1.45 (m, 5H), 1.40 – 1.24 (m, 15H). ^{13}C

NMR (125 MHz, CDCl$_3$) δ 170.9, 170.5, 170.5 (d, J = 20.5 Hz), 170.0, 158.7, 158.0,

152.8, 147.5, 136.9, 133.2, 131.4, 129.2, 128.8, 128.1, 120.3, 116.9, 109.7, 105.7, 78.3

(d, *J* = 231.9 Hz), 70.2, 62.3, 59.2, 56.7, 56.4, 56.0, 53.9, 47.9, 42.9, 37.0, 36.0, 33.0,

32.1, 28.6, 28.5, 28.2, 27.1, 25.8, 25.5, 14.0 (d, *J* = 7.8 Hz), 13.9 (d, *J* = 8.8 Hz). [19]F

NMR (470 MHz, CDCl$_3$) *δ* -197.70. LC-MS, ESI⁻, *m/z* = 956.0 [M − H]⁻.

Synthesis of the final compound (2S,4R)-1-((R)-3-((((1r,4R)-4-((4-(4-((5-chloro-4-
(methylamino)pyrimidin-2-yl)amino)-3-methoxybenzoyl)piperazin-1-
yl)methyl)cyclohexyl)methyl)thio)-2-(1-fluorocyclopropane-1-carboxamido)-3-
methylbutanoyl)-N-(4-cyanobenzyl)-4-hydroxypyrrolidine-2-carboxamide
(MP01088)
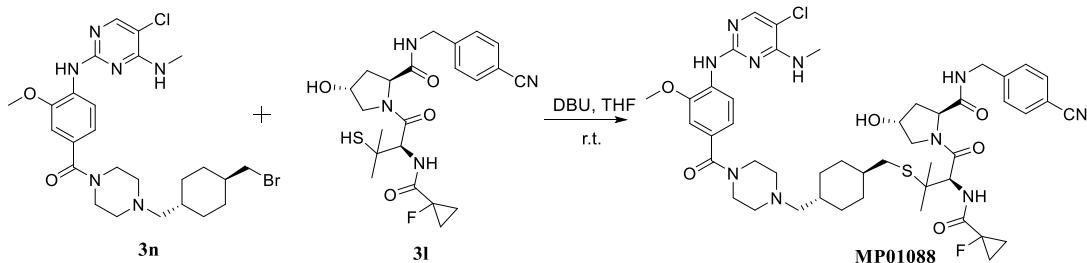
A solution containing **3n** (1 equiv., 15 mg, 0.027 mmol), **3l** (1 equiv., 12 mg, 0.027

mmol), and DBU (8 equiv., 32 *μ*L, 0.216 mmol) in THF (1.5 mL), was stirred at room

temperature overnight. After completion, the mixture was evaporated under vacuum

and the resulting residue was purified *via* flash column chromatography (0-5%

methanol in 1:1 ethyl acetate/DCM) on silica gel to give the final pure product

MP01088 (88% yield). ^{1}H NMR (500 MHz, CDCl$_3$) *δ* 8.53 (d, *J* = 8.7 Hz, 1H), 7.90

(s, 1H), 7.63 (s, 1H), 7.56 (d, *J* = 8.2 Hz, 2H), 7.51 (t, *J* = 6.3 Hz, 1H), 7.37 (d, *J* = 8.0

Hz, 2H), 7.27 (d, *J* = 3.4 Hz, 1H), 7.01 – 6.97 (m, 2H), 5.34 (q, *J* = 4.9 Hz, 1H), 4.76

– 4.69 (m, 2H), 4.50 – 4.46 (m, 1H), 4.47 – 4.38 (m, 2H), 4.01 (d, *J* = 11.1 Hz, 1H),

3.91 (s, 3H), 3.71 (dd, *J* = 11.1, 3.8 Hz, 1H), 3.63 (s, 3H), 3.09 (d, *J* = 4.8 Hz, 3H),

2.42 – 2.29 (m, 6H), 2.32 – 2.25 (m, 1H), 2.26 – 2.20 (m, 1H), 2.12 (d, *J* = 7.1 Hz,

2H), 2.03 (s, 1H), 1.79 (d, J = 11.3 Hz, 4H), 1.40 – 1.24 (m, 12H), 0.95 – 0.78 (m, 4H). ^{13}C NMR (125 MHz, CDCl$_3$) δ 171.4, 170.5, 170.5 (d, J = 20.3 Hz), 170.0, 158.6, 157.9, 152.7, 147.5, 143.9, 132.5, 131.4, 128.1, 128.0, 120.2, 118.9, 116.8, 111.1, 109.6, 105.6, 78.2 (d, J = 232.4 Hz), 70.1, 65.3, 59.3, 56.8, 56.3, 56.0, 54.0, 48.0, 43.0, 38.5, 37.2, 35.3, 35.0, 32.8, 32.7, 31.4, 28.2, 25.8, 25.4, 14.0, 14.0. ^{19}F NMR (470 MHz, CDCl$_3$) δ -197.62. LC-MS, ESI$^-$, m/z = 945.2 [M − H]$^-$.

Synthesis of the final compound (2S,4R)-1-((R)-3-(((((1s,4S)-4-((4-(4-((5-chloro-4-(methylamino)pyrimidin-2-yl)amino)-3-methoxybenzoyl)piperazin-1-yl)methyl)cyclohexyl)methyl)thio)-2-(1-fluorocyclopropane-1-carboxamido)-3-methylbutanoyl)-N-(4-cyanobenzyl)-4-hydroxypyrrolidine-2-carboxamide (MP01089)
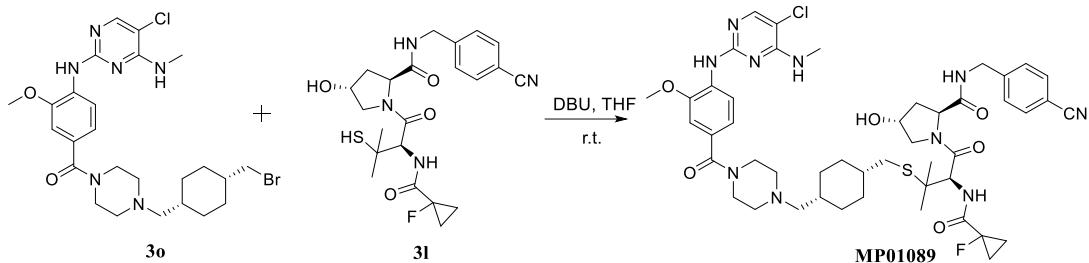
A THF solution (1.5 mL), containing **3l** (1 equiv., 12 mg, 0.027 mmol), **3o** (1 equiv., 15 mg, 0.027 mmol), and DBU (8 equiv., 32 μL, 0.216 mmol), was stirred at room temperature overnight. The volatiles were removed under vacuum and the resulting residue was purified through flash column chromatography (0-15% methanol in DCM) on silica gel to give the final pure product **MP01089** (42% yield). ^{1}H NMR (500 MHz, CDCl$_3$) δ 8.53 (d, J = 8.8 Hz, 1H), 7.92 (s, 1H), 7.62 (s, 1H), 7.57 (d, J = 8.3 Hz, 2H), 7.43 (t, J = 6.1 Hz, 1H), 7.39 (d, J = 8.2 Hz, 2H), 7.24 (dd, J = 7.9, 3.4 Hz, 1H), 7.02 – 6.99 (m, 2H), 5.30 (q, J = 4.9 Hz, 1H), 4.78 – 4.71 (m, 2H), 4.53 – 4.48 (m, 1H), 4.48 – 4.41 (m, 2H), 4.05 (d, J = 11.3 Hz, 1H), 3.92 (s, 3H), 3.71 (dd, J = 11.2, 3.9 Hz,

1H), 3.64 (s, 3H), 3.10 (d, J = 4.9 Hz, 3H), 2.94 (s, 1H), 2.48 – 2.35 (m, 7H), 2.27 – 2.19 (m, 3H), 1.74 (s, 2H), 1.56 – 1.45 (m, 5H), 1.36 – 1.29 (m, 14H). ^{13}C NMR (125 MHz, CDCl$_3$) δ 171.2, 170.7, 170.6, 170.2, 158.7, 158.0, 152.8, 147.6, 143.9, 132.5, 131.5, 128.2, 128.1, 120.3, 118.8, 116.9, 111.3, 109.7, 105.7, 78.3 (d, J = 231.1 Hz), 70.2, 62.3, 59.2, 56.8, 56.5, 56.0, 53.9, 47.8, 43.1, 37.0, 36.0, 33.0, 32.1, 28.7, 28.5, 28.2, 27.1, 25.9, 25.4, 14.1 (d, J = 9.1 Hz), 14.0 (d, J = 9.1 Hz). ^{19}F NMR (470 MHz, CDCl$_3$) δ -197.70. LC-MS, ESI⁻, m/z = 945.2 [M − H]⁻.

7.2 Fluorescence Polarization (FP) assay

FP competitive binding assays measurements were taken on a PHERAstar (BMG LABTECH) plate reader using a filter that sets excitation and emission wavelengths at 485 nm and 520 nm, respectively. 384-well black plates (Coring 3575) were used, and each well was containing 5 nM VCB protein, 5 nM FAM-labeled HIF-1α peptide (FAM-DEALAHypYIPMDDDFQLRSF, "JC9"), and decreasing concentrations of the tested compounds (14 concentrations with a 2-fold serial dilution starting from 250 μM) in FP assay buffer (100 mM bis-tris propane, 100 mM NaCl, 1 mM DTT, pH 7.0) with a final DMSO concentration of 5%. The maximum signal is given by the control wells containing VCB and JC9 with no compound (zero displacement). The minimum signal is given by the control wells containing JC9 in the absence of protein. Control values were used to obtain the percentage (%) of displacement, which was plotted against Log[Compound]. For each titration, the averages of the IC$_{50}$ values were determined using nonlinear regression analysis with GraphPad Prism (v.9.3.1). The K$_i$ values were then back-calculated from the K$_d$ of JC9 (1.5−3.4 nM) and the fitted IC$_{50}$ values obtained, as described in previous works.[174, 183]

7.3 Isothermal Titration Calorimetry (ITC)

ITC experiments were performed in an ITC200 microcalorimeter (GE Healthcare). Titrations were carried out at 25 °C while stirring at 750 rpm. The experiments were performed in reverse mode (*i.e.* protein in the syringe and ligand in the sample cell). Compounds were diluted in ITC buffer (20 mM bis-tris propane, 150 mM NaCl, 1 mM TCEP, pH 7.0) from 10 mM DMSO stock solutions to a final concentration of 20 μM (5% DMSO). Each run consisted of 19 injections of 2 μL of protein solution (ITC buffer with 5% DMSO) at a rate of 0.4 μL/s at 180 s time intervals. An initial injection of 0.2 μL of protein was made and discarded during data analysis, as per manufacturer instruction. VCB (200 μM, in the syringe) was first titrated into compound (20 μM, in the sample cell); at the end of every titration, the excess of solution was removed from the cell and the syringe was washed. The data were fitted to a single binding-site model using the MicroCal PEAQ-ITC analysis software provided by the manufacturer to obtain the stoichiometry (N), the dissociation constant (K_d), and the enthalpy of binding (ΔH).

7.4 Crystallization and structure solution of VCB protein in binary complex with MP-1-39

The binary complex of VCB and compound **MP-1-39** was generated by incubating 121 μM VCB with 242 μM of the compound (from a 10 mM stock in DMSO). Crystals were grown using the vapour diffusion method in 96-well sitting drop plates by mixing equal volumes of the protein and the crystallization solution containing 0.2 NaCl, 0.1M HEPES pH 7.5, 25% PEG3350. Small needle crystals appeared within 24 h but took approximately 1 week to reach a suitable size for harvesting. Once collected, crystals were flash-frozen in liquid nitrogen using 20% ethylene glycol in the crystallization

solution as a cryoprotectant. Diffraction data were collected at Diamond Light Source beamline I24 using a Pilatus3 6M detector at $\lambda = 0.6702$ Å. The structure was solved by molecular replacement using PHASER[184] with VCB structure (PDB entry: 5NVX) as a search model. The initial model underwent iterative rounds of model building and refinement with COOT[185] and Phenix REFINE,[186] respectively. Compound **MP-1-39** geometry restraints for refinement were prepared with Elbow.[187] Model geometry and steric clashes were validated using MOLPROBITY server;[188] Ramachandran plots indicate that 98.2% of backbone torsion angles are in the favored region and there are no outliers. The *R*work and *R*free values of the refined model were 0.196 and 0.218, respectively.

7.5 Western blot

Culturing and passaging of adherent cell lines were carried out using an aseptic technique in CL1 biological safety cabinets. All cells were incubated in a 37 °C incubator with 5% CO_2 and seeded in six-well plates. Cells were then treated with the indicated compounds at 0.1% final concentration of DMSO. Following the treatment with compounds at the indicated concentrations for 4 h, the media was removed and the cells were washed with PBS. The cells were then lysed in a 100 μL ice-cold lysis buffer containing 50 mM tris-HCl pH 7.4, 1 mM EGTA, 10 mM 2-glycerophosphate, 50 mM sodium fluoride, 5 mM sodium pyrophosphate, 270 mM sucrose, supplemented with 1 μg/mL microcystin-LR, 1 mM sodium orthovanadate, complete EDTA-free protease inhibitor cocktail (Roche), and 1% (v/v) Triton X-100. Hence, cells were placed on ice, scraped and collected. Cell lysates were incubated on ice for 10 min and then centrifuged at 15 000 g at 4 °C for 15 min. Pellets were discarded,

while the supernatants were collected for analysis by quantitative immunoblotting. Bradford assay was employed to determine protein concentrations of cell lysates.

Cell lysates containing a quarter of a volume of 4 x NuPAGE LDS sample buffer (NP0007) supplemented with 5% β-mercaptoethanol were heated at 95 °C for 5 min. Samples (15-20 μg) were loaded onto precast 4-12% bis-tris midi 20W or 26W gels (Thermo Fisher Scientific) and resolved at 130 V for 90 min with a NuPAGE MOPS SDS running buffer (Thermo Fisher Scientific). Proteins were electrophoretically transferred onto a 0.45 μm nitrocellulose membrane (GE Healthcare, Amersham Protran Supported 0.45 mm NC) at 90 V for 90 min on ice in a transfer buffer (48 mM tris base and 39 mM glycine supplemented with 20% ethanol). After transferring, the membrane was blocked incubating at room temperature for 1 h with 5% (w/v) skimmed milk powder dissolved in tris-buffered saline with Tween (TBS-T) (50mMtris base, 150 mM sodium chloride (NaCl), 0.1% (v/v) Tween-20). Membranes were washed three times for 15 min with TBS-T 0.1% Tween 20 and were incubated with the primary antibody overnight at 4 °C. Before the secondary antibody incubation, membranes were washed three times for 15 min with TBS-T 0.1% Tween 20. The membranes were then incubated with the secondary antibody for 1 h at room temperature protecting from light. The membranes were then washed with TBS-T 0.1% Tween 20 three times for 15 min, and protein bands were acquired *via* a near-infrared fluorescent detection using the Odyssey CLx imaging system and quantified using Image Studio software. Graphs were generated using Graphpad Prism version 8 software.

The employed antibodies (used at a final concentration of 1 μg/mL) were: monoclonal mouse anti-LRRK2 total, monoclonal rabbit anti-LRRK2 pSer935, monoclonal mouse

anti-Rab10 total, monoclonal rabbit anti-Rab10 pThr73, monoclonal mouse anti-α-tubulin.

List of Abbreviations

3D	Three-dimensional
ACN	Acetonitrile
AML	Acute myeloid leukemia
AR	Androgen receptor
ATP	Adenosine Triphosphate
BAZ2B	Bromodomain adjacent to zinc finger domain 2B
BBB	Blood-brain barrier
BET	Bromodomain and extra-terminal domain
BMS	Borane dimethylsulfide
BRD2	Bromodomain-containing protein 2
BRD2-BD1	Bromodomain-containing protein 2-domain 1
BRD2-BD2	Bromodomain-containing protein 2-domain 2
BRD3	Bromodomain-containing protein 3
BRD3-BD1	Bromodomain-containing protein 3-domain 1
BRD3-BD2	Bromodomain-containing protein 3-domain 2
BRD4	Bromodomain-containing protein 4
BRD4-BD1	Bromodomain-containing protein 4-domain 1
BRD4-BD2	Bromodomain-containing protein 4-domain 2
BRD7	Bromodomain-containing protein 7
BRD9	Bromodomain-containing protein 9
BRDs	Bromodomains
BRDT-BD1	Bromodomain testis-domain 1
BRPF1	Bromodomain and PHD finger containing 1
BRPF1b	Bromodomain and PHD finger containing 1 isoform b
CCK8	Cell Counting Kit 8
CeTPD	Centre for Targeted Protein Degradation
CRBN	Cereblon
CSF	Cerebrospinal fluid
DBU	1,8-Diazabicyclo[5.4.0]undec-7-ene
DCM	Dichloromethane
DEX	Dexamethasone
DIPEA	N,N-Diisopropylethylamine
DMAP	4-Dimethylaminopyridine
DMF	Dimethylformamide
DMSO	Dimethyl sulfoxide
DSF	Differential Scanning Fluorimetry
EDC·HCl	1-ethyl-3-(3-dimethylaminopropyl)carbodiimide hydrochloride
EGFR	Epidermal growth factor receptor
ELISA	Enzyme-linked immunosorbent assay
Erβ	Estrogen receptor β
FP	Fluorescence Polarization
GR	Glucocorticoid receptor
HATs	Histone acetyltransferases
HCC	Hepatocellular carcinoma
HDACs	Histone deacetylases

HOBt	Hydroxybenzotriazole
HPLC	High Performance Liquid Chromatography
HRMS	High-resolution mass spectrometry
HTS	High Throughput Screening
HTVS	High-Throughput Virtual Screening
IC_{50}	Half Maximal Inhibitory Concentration
IL	Interleukin
IL-6	Interleukin 6
ITC	Isothermal Titration Calorimetry
IVS	Inverse Virtual Screening
KAc	Acetyl-lysine
K_D	Dissociation Constant
LC-MS	Liquid Chromatography - Mass Spectrometry
LPS	Lipopolysaccharide
LRKK2	Leucine-rich repeat kinase 2
MEFs	Mouse Embryonic Fibroblasts
MIF	Macrophage migration inhibitory factor
mPGES-1	Microsomal prostaglandin E2 synthase-1
MRT	Malignant rhabdoid tumor
mSWI/SNF	Mammalian SWItch/Sucrose Non-Fermentable
MTD	Multi-target drug
MW	Microwave
ncBAF	Non-canonical BAF
NMR	Nuclear Magnetic Resonance
PD	Parkinson's disease
PDB	Protein Data Bank
PDE6D	Phosphodiesterase 6δ
PEG	Polyethylene glycol
PK	Pharmacokinetic
PROTAC	Proteolysis Targeting Chimera
Ro5	Rule of 5
RXR	Retinoid X receptor
SAR	Structure–activity relationship
sEH	Soluble epoxide hydrolases
SP	Standard precision
SWI/SNF	SWItch/Sucrose Non-Fermentable
TANK2	Tankyrase 2
TEA	Triethylamine
TFA	Trifluoroacetic acid
THF	Tetrahydrofuran
TLC	Thin layer chromatography
TNF-α	Tumor necrosis factor α
TP	Thymidine phosphorylase
TR-FRET	Time-resolved fluorescence energy transfer
TsCl	4-Toluenesulfonyl chloride
UPS	Ubiquitin-proteasome system
VCB	VHL complexed with elongin B and elongin C
VHL	Von Hippel-Lindau
VSW	Virtual screening workflow

WT   Wild Type
XP   Extra precision

References

1.   Ntranos, A.; Casaccia, P., Bromodomains: Translating the words of lysine acetylation into myelin injury and repair. *Neurosci. Lett.* **2016**, 625, 4-10.

2.   Karim, R. M.; Schönbrunn, E., An Advanced Tool To Interrogate BRD9. *J. Med. Chem.* **2016**, 59, 4459-4461.

3.   Lauro, G.; Romano, A.; Riccio, R.; Bifulco, G., Inverse Virtual Screening of Antitumor Targets: Pilot Study on a Small Database of Natural Bioactive Compounds. *J. Nat. Prod.* **2011**, 74, 1401-1407.

4.   Kadoch, C.; Hargreaves, D. C.; Hodges, C.; Elias, L.; Ho, L.; Ranish, J.; Crabtree, G. R., Proteomic and bioinformatic analysis of mammalian SWI/SNF complexes identifies extensive roles in human malignancy. *Nat. Genet.* **2013**, 45, 592-601.

5.   Wang, L.; Oh, T. G.; Magida, J.; Estepa, G.; Obayomi, S. M. B.; Chong, L.-W.; Gatchalian, J.; Yu, R. T.; Atkins, A. R.; Hargreaves, D.; Downes, M.; Wei, Z.; Evans, R. M., Bromodomain containing 9 (BRD9) regulates macrophage inflammatory responses by potentiating glucocorticoid receptor activity. *Proc. Natl. Acad. Sci. U. S. A.* **2021**, 118, e2109517118.

6.   Sharma, S.; Kelly, T. K.; Jones, P. A., Epigenetics in cancer. *Carcinogenesis* **2009**, 31, 27-36.

7.   Waddington, C. H., The Epigenotype. *Int. J. Epidemiol.* **2011**, 41, 10-13.

8.   Jones, P. A.; Baylin, S. B., The fundamental role of epigenetic events in cancer. *Nat. Rev. Genet.* **2002**, 3, 415-428.

9.   Baylin, S. B.; Jones, P. A., A decade of exploring the cancer epigenome — biological and translational implications. *Nat. Rev. Cancer* **2011**, 11, 726-734.

10.   Kouzarides, T., Chromatin Modifications and Their Function. *Cell* **2007**, 128, 693-705.

11.   Dawson, Mark A.; Kouzarides, T., Cancer Epigenetics: From Mechanism to Therapy. *Cell* **2012**, 150, 12-27.

12.   Minucci, S.; Pelicci, P. G., Histone deacetylase inhibitors and the promise of epigenetic (and more) treatments for cancer. *Nat. Rev. Cancer* **2006**, 6, 38-51.

References

13. Bannister, A. J.; Kouzarides, T., Regulation of chromatin by histone modifications. *Cell Res.* **2011**, 21, 381-395.

14. Margueron, R.; Trojer, P.; Reinberg, D., The key to development: interpreting the histone code? *Curr. Opin. Genet. Dev.* **2005**, 15, 163-176.

15. Norton, V. G.; Imai, B. S.; Yau, P.; Bradbury, E. M., Histone acetylation reduces nucleosome core particle linking number change. *Cell* **1989**, 57, 449-457.

16. Jones, P. A.; Issa, J.-P. J.; Baylin, S., Targeting the cancer epigenome for therapy. *Nat. Rev. Genet.* **2016**, 17, 630-641.

17. Marmorstein, R.; Zhou, M.-M., Writers and readers of histone acetylation: structure, mechanism, and inhibition. *Cold Spring Harb. Perspect. Biol.* **2014**, 6, a018762.

18. Seto, E.; Yoshida, M., Erasers of histone acetylation: the histone deacetylase enzymes. *Cold Spring Harb. Perspect. Biol.* **2014**, 6, a018713.

19. Qi, J., Bromodomain and extraterminal domain inhibitors (BETi) for cancer therapy: chemical modulation of chromatin structure. *Cold Spring Harb. Perspect. Biol.* **2014**, 6, a018663.

20. Zaware, N.; Zhou, M.-M., Chemical modulators for epigenome reader domains as emerging epigenetic therapies for cancer and inflammation. *Curr. Opin. Chem. Biol.* **2017**, 39, 116-125.

21. Nicodeme, E.; Jeffrey, K. L.; Schaefer, U.; Beinke, S.; Dewell, S.; Chung, C.-w.; Chandwani, R.; Marazzi, I.; Wilson, P.; Coste, H.; White, J.; Kirilovsky, J.; Rice, C. M.; Lora, J. M.; Prinjha, R. K.; Lee, K.; Tarakhovsky, A., Suppression of inflammation by a synthetic histone mimic. *Nature* **2010**, 468, 1119-1123.

22. Tamkun, J. W.; Deuring, R.; Scott, M. P.; Kissinger, M.; Pattatucci, A. M.; Kaufman, T. C.; Kennison, J. A., brahma: A regulator of Drosophila homeotic genes structurally related to the yeast transcriptional activator SNF2SWI2. *Cell* **1992**, 68, 561-572.

23. Filippakopoulos, P.; Picaud, S.; Mangos, M.; Keates, T.; Lambert, J.-P.; Barsyte-Lovejoy, D.; Felletar, I.; Volkmer, R.; Müller, S.; Pawson, T.; Gingras, A.-C.; Arrowsmith, Cheryl H.; Knapp, S., Histone Recognition and Large-Scale Structural Analysis of the Human Bromodomain Family. *Cell* **2012**, 149, 214-231.

24.   Fujisawa, T.; Filippakopoulos, P., Functions of bromodomain-containing proteins and their roles in homeostasis and cancer. *Nat. Rev. Mol. Cell Biol.* **2017**, 18, 246-262.

25.   Filippakopoulos, P.; Knapp, S., Targeting bromodomains: epigenetic readers of lysine acetylation. *Nat. Rev. Drug Discov.* **2014**, 13, 337-356.

26.   Taniguchi, Y., The Bromodomain and Extra-Terminal Domain (BET) Family: Functional Anatomy of BET Paralogous Proteins. *Int. J. Mol. Sci.* **2016**, 17, 1849.

27.   Dreier, M. R.; de la Serna, I. L., SWI/SNF Chromatin Remodeling Enzymes in Melanoma. *Epigenomes* **2022**, 6, 10.

28.   Zhu, X.; Liao, Y.; Tang, L., Targeting BRD9 for Cancer Treatment: A New Strategy. *Onco Targets Ther.* **2020**, 13, 13191-13200.

29.   Yu, X.; Li, Z.; Shen, J., BRD7: a novel tumor suppressor gene in different cancers. *Am. J. Transl. Res.* **2016**, 8, 742-8.

30.   Euskirchen, G. M.; Auerbach, R. K.; Davidov, E.; Gianoulis, T. A.; Zhong, G.; Rozowsky, J.; Bhardwaj, N.; Gerstein, M. B.; Snyder, M., Diverse Roles and Interactions of the SWI/SNF Chromatin Remodeling Complex Revealed Using Global Approaches. *PLoS Genet.* **2011**, 7, e1002008.

31.   Scotto, L.; Narayan, G.; Nandula, S. V.; Subramaniyam, S.; Kaufmann, A. M.; Wright, J. D.; Pothuri, B.; Mansukhani, M.; Schneider, A.; Arias-Pulido, H.; Murty, V. V., Integrative genomics analysis of chromosome 5p gain in cervical cancer reveals target over-expressed genes, including Drosha. *Mol. Cancer* **2008**, 7, 58.

32.   Kang, J. U.; Koo, S. H.; Kwon, K. C.; Park, J. W.; Kim, J. M., Gain at chromosomal region 5p15.33, containing TERT, is the most frequent genetic event in early stages of non-small cell lung cancer. *Cancer Genet. Cytogenet.* **2008**, 182, 1-11.

33.   Levine, D. A., Integrated genomic characterization of endometrial carcinoma. *Nature* **2013**, 497, 67-73.

34.   Cancer Genome Atlas Research, N., Comprehensive genomic characterization of squamous cell lung cancers. *Nature* **2012**, 489, 519.

35.   Barbieri, C. E.; Baca, S. C.; Lawrence, M. S.; Demichelis, F.; Blattner, M.; Theurillat, J.-P.; White, T. A.; Stojanov, P.; Van Allen, E.; Stransky, N.; Nickerson, E.; Chae, S.-S.; Boysen, G.; Auclair, D.; Onofrio, R. C.; Park, K.; Kitabayashi, N.; MacDonald, T. Y.; Sheikh, K.; Vuong, T.; Guiducci, C.; Cibulskis, K.; Sivachenko, A.; Carter, S. L.; Saksena, G.; Voet, D.; Hussain, W. M.; Ramos, A. H.; Winckler, W.;

Redman, M. C.; Ardlie, K.; Tewari, A. K.; Mosquera, J. M.; Rupp, N.; Wild, P. J.; Moch, H.; Morrissey, C.; Nelson, P. S.; Kantoff, P. W.; Gabriel, S. B.; Golub, T. R.; Meyerson, M.; Lander, E. S.; Getz, G.; Rubin, M. A.; Garraway, L. A., Exome sequencing identifies recurrent SPOP, FOXA1 and MED12 mutations in prostate cancer. *Nat. Genet.* **2012**, 44, 685-689.

36.   Cleary, S. P.; Jeck, W. R.; Zhao, X.; Chen, K.; Selitsky, S. R.; Savich, G. L.; Tan, T.-X.; Wu, M. C.; Getz, G.; Lawrence, M. S.; Parker, J. S.; Li, J.; Powers, S.; Kim, H.; Fischer, S.; Guindi, M.; Ghanekar, A.; Chiang, D. Y., Identification of driver genes in hepatocellular carcinoma by exome sequencing. *Hepatology* **2013**, 58, 1693-1702.

37.   Hohmann, A. F.; Martin, L. J.; Minder, J. L.; Roe, J.-S.; Shi, J.; Steurer, S.; Bader, G.; McConnell, D.; Pearson, M.; Gerstberger, T.; Gottschamel, T.; Thompson, D.; Suzuki, Y.; Koegl, M.; Vakoc, C. R., Sensitivity and engineered resistance of myeloid leukemia cells to BRD9 inhibition. *Nat. Chem. Biol.* **2016**, 12, 672-679.

38.   Krämer, K. F.; Moreno, N.; Frühwald, M. C.; Kerl, K., BRD9 Inhibition, Alone or in Combination with Cytostatic Compounds as a Therapeutic Approach in Rhabdoid Tumors. *Int. J. Mol. Sci.* **2017**, 18, 1537.

39.   Galdeano, C.; Ciulli, A., Selectivity on-target of bromodomain chemical probes by structure-guided medicinal chemistry and chemical biology. *Future Med. Chem.* **2016**, 8, 1655-1680.

40.   Theodoulou, N. H.; Bamborough, P.; Bannister, A. J.; Becher, I.; Bit, R. A.; Che, K. H.; Chung, C.-w.; Dittmann, A.; Drewes, G.; Drewry, D. H.; Gordon, L.; Grandi, P.; Leveridge, M.; Lindon, M.; Michon, A.-M.; Molnar, J.; Robson, S. C.; Tomkinson, N. C. O.; Kouzarides, T.; Prinjha, R. K.; Humphreys, P. G., Discovery of I-BRD9, a selective cell active chemical probe for bromodomain containing protein 9 inhibition. *J. Med. Chem.* **2016**, 59, 1425-1439.

41.   Clark, P. G.; Vieira, L. C.; Tallant, C.; Fedorov, O.; Singleton, D. C.; Rogers, C. M.; Monteiro, O. P.; Bennett, J. M.; Baronio, R.; Müller, S.; Daniels, D. L.; Méndez, J.; Knapp, S.; Brennan, P. E.; Dixon, D. J., LP99: discovery and synthesis of the first selective BRD7/9 bromodomain inhibitor. *Angew. Chem.* **2015**, 127, 6315-6319.

42.   Martin, L. J.; Koegl, M.; Bader, G.; Cockcroft, X.-L.; Fedorov, O.; Fiegen, D.; Gerstberger, T.; Hofmann, M. H.; Hohmann, A. F.; Kessler, D.; Knapp, S.; Knesl, P.; Kornigg, S.; Müller, S.; Nar, H.; Rogers, C.; Rumpel, K.; Schaaf, O.; Steurer, S.;

Tallant, C.; Vakoc, C. R.; Zeeb, M.; Zoephel, A.; Pearson, M.; Boehmelt, G.; McConnell, D., Structure-Based Design of an in Vivo Active Selective BRD9 Inhibitor. *J. Med. Chem.* **2016**, 59, 4462-4475.

43.   Picaud, S.; Strocchia, M.; Terracciano, S.; Lauro, G.; Mendez, J.; Daniels, D. L.; Riccio, R.; Bifulco, G.; Bruno, I.; Filippakopoulos, P., 9 H-purine scaffold reveals induced-fit pocket plasticity of the BRD9 bromodomain. *J. Med. Chem.* **2015**, 58, 2718-2736.

44.   Singh, N.; Baby, D.; Rajguru, J. P.; Patil, P. B.; Thakkannavar, S. S.; Pujari, V. B., Inflammation and cancer. *Ann. Afr. Med.* **2019**, 18, 121-126.

45.   Crawford, T. D.; Vartanian, S.; Côté, A.; Bellon, S.; Duplessis, M.; Flynn, E. M.; Hewitt, M.; Huang, H.-R.; Kiefer, J. R.; Murray, J.; Nasveschuk, C. G.; Pardo, E.; Romero, F. A.; Sandy, P.; Tang, Y.; Taylor, A. M.; Tsui, V.; Wang, J.; Wang, S.; Zawadzke, L.; Albrecht, B. K.; Magnuson, S. R.; Cochran, A. G.; Stokoe, D., Inhibition of bromodomain-containing protein 9 for the prevention of epigenetically-defined drug resistance. *Bioorg. Med. Chem. Lett.* **2017**, 27, 3534-3541.

46.   Del Gaudio, N.; Di Costanzo, A.; Liu, N. Q.; Conte, L.; Migliaccio, A.; Vermeulen, M.; Martens, J. H.; Stunnenberg, H. G.; Nebbioso, A.; Altucci, L., BRD9 binds cell type-specific chromatin regions regulating leukemic cell survival via STAT5 inhibition. *Cell Death Dis.* **2019**, 10, 1-14.

47.   Hügle, M.; Regenass, P.; Warstat, R.; Hau, M.; Schmidtkunz, K.; Lucas, X.; Wohlwend, D.; Einsle, O.; Jung, M.; Breit, B.; Günther, S., 4-Acyl Pyrroles as Dual BET-BRD7/9 Bromodomain Inhibitors Address BETi Insensitive Human Cancer Cell Lines. *J. Med. Chem.* **2020**, 63, 15603-15620.

48.   Hay, D. A.; Rogers, C. M.; Fedorov, O.; Tallant, C.; Martin, S.; Monteiro, O. P.; Müller, S.; Knapp, S.; Schofield, C. J.; Brennan, P. E., Design and synthesis of potent and selective inhibitors of BRD7 and BRD9 bromodomains. *MedChemComm* **2015**, 6, 1381-1386.

49.   Pierri, M.; Gazzillo, E.; Chini, M. G.; Ferraro, M. G.; Piccolo, M.; Maione, F.; Irace, C.; Bifulco, G.; Bruno, I.; Terracciano, S.; Lauro, G., Introducing structure-based three-dimensional pharmacophore models for accelerating the discovery of selective BRD9 binders. *Bioorg. Chem.* **2022**, 118, 105480.

50.   *Phase*, Schrödinger, LLC, New York, NY: 2021.

51.   Dixon, S. L.; Smondyrev, A. M.; Knoll, E. H.; Rao, S. N.; Shaw, D. E.; Friesner, R. A., PHASE: a new engine for pharmacophore perception, 3D QSAR model development, and 3D database screening: 1. Methodology and preliminary results. *J. Comput.-Aided Mol. Des.* **2006**, 20, 647-671.

52.   Dixon, S. L.; Smondyrev, A. M.; Rao, S. N., PHASE: A Novel Approach to Pharmacophore Modeling and 3D Database Searching. *Chem. Biol. Drug Des.* **2006**, 67, 370-372.

53.   *LigPrep*, Schrödinger, LLC, New York, NY: 2021.

54.   *Glide*, Schrödinger, LLC, New York, NY: 2021.

55.   Friesner, R. A.; Banks, J. L.; Murphy, R. B.; Halgren, T. A.; Klicic, J. J.; Mainz, D. T.; Repasky, M. P.; Knoll, E. H.; Shelley, M.; Perry, J. K.; Shaw, D. E.; Francis, P.; Shenkin, P. S., Glide: A New Approach for Rapid, Accurate Docking and Scoring. 1. Method and Assessment of Docking Accuracy. *J. Med. Chem.* **2004**, 47, 1739-1749.

56.   Halgren, T. A.; Murphy, R. B.; Friesner, R. A.; Beard, H. S.; Frye, L. L.; Pollard, W. T.; Banks, J. L., Glide: A New Approach for Rapid, Accurate Docking and Scoring. 2. Enrichment Factors in Database Screening. *J. Med. Chem.* **2004**, 47, 1750-1759.

57.   Daina, A.; Michielin, O.; Zoete, V., SwissADME: a free web tool to evaluate pharmacokinetics, drug-likeness and medicinal chemistry friendliness of small molecules. *Sci. Rep.* **2017**, 7, 42717.

58.   Clark, P. G. K.; Dixon, D. J.; Brennan, P. E., Development of chemical probes for the bromodomains of BRD7 and BRD9. *Drug Discov. Today Technol.* **2016**, 19, 73-80.

59.   Hytti, M.; Tokarz, P.; Määttä, E.; Piippo, N.; Korhonen, E.; Suuronen, T.; Honkakoski, P.; Kaarniranta, K.; Lahtela-Kakkonen, M.; Kauppinen, A., Inhibition of BET bromodomains alleviates inflammation in human RPE cells. *Biochem. Pharmacol.* **2016**, 110-111, 71-79.

60.   Ali, I.; Lee, J.; Go, A.; Choi, G.; Lee, K., Discovery of novel [1,2,4]triazolo[4,3-a]quinoxaline aminophenyl derivatives as BET inhibitors for cancer treatment. *Bioorg. Med. Chem. Lett.* **2017**, 27, 4606-4613.

61.   Philpott, M.; Yang, J.; Tumber, T.; Fedorov, O.; Uttarkar, S.; Filippakopoulos, P.; Picaud, S.; Keates, T.; Felletar, I.; Ciulli, A.; Knapp, S.; Heightman, T. D.,

Bromodomain-peptide displacement assays for interactome mapping and inhibitor discovery. *Mol. Biosyst.* **2011**, 7, 2899-2908.

62.   Eglen, R. M.; Reisine, T.; Roby, P.; Rouleau, N.; Illy, C.; Bossé, R.; Bielefeld, M., The use of AlphaScreen technology in HTS: current status. *Curr. Chem. Genomics* **2008**, 1, 2-10.

63.   *CombiGlide*, Schrödinger, LLC, New York, NY: 2021.

64.   *QikProp*, Schrödinger, LLC, New York, NY: 201.

65.   Laoui, A.; Polyakov, V. R., Web services as applications' integration tool: QikProp case study. *J. Comput. Chem.* **2011**, 32, 1944-1951.

66.   Lipinski, C. A.; Lombardo, F.; Dominy, B. W.; Feeney, P. J., Experimental and computational approaches to estimate solubility and permeability in drug discovery and development settings. *Adv. Drug Del. Rev.* **2012**, 64, 4-17.

67.   Lee, S.; Cil, O.; Diez-Cecilia, E.; Anderson, M. O.; Verkman, A. S., Nanomolar-Potency 1,2,4-Triazoloquinoxaline Inhibitors of the Kidney Urea Transporter UT-A1. *J. Med. Chem.* **2018**, 61, 3209-3217.

68.   Hayes, B. L., Recent advances in microwave-assisted synthesis. *Aldrichimica Acta* **2004**, 37, 66-77.

69.   Thul, P. J.; Lindskog, C., The human protein atlas: A spatial map of the human proteome. *Protein Sci.* **2018**, 27, 233-244.

70.   Bevill, S. M.; Olivares-Quintero, J. F.; Sciaky, N.; Golitz, B. T.; Singh, D.; Beltran, A. S.; Rashid, N. U.; Stuhlmiller, T. J.; Hale, A.; Moorman, N. J.; Santos, C. M.; Angus, S. P.; Zawistowski, J. S.; Johnson, G. L., GSK2801, a BAZ2/BRD9 Bromodomain Inhibitor, Synergizes with BET Inhibitors to Induce Apoptosis in Triple-Negative Breast Cancer. *Mol. Cancer Res.* **2019**, 17, 1503-1518.

71.   Zhou, Q.; Huang, J.; Zhang, C.; Zhao, F.; Kim, W.; Tu, X.; Zhang, Y.; Nowsheen, S.; Zhu, Q.; Deng, M.; Chen, Y.; Qin, B.; Luo, K.; Liu, B.; Lou, Z.; Mutter, R. W.; Yuan, J., The bromodomain containing protein BRD-9 orchestrates RAD51–RAD54 complex formation and regulates homologous recombination-mediated repair. *Nat. Commun.* **2020**, 11, 2639.

72.   Riching, K. M.; Vasta, J. D.; Hughes, S. J.; Zoppi, V.; Maniaci, C.; Testa, A.; Urh, M.; Ciulli, A.; Daniels, D. L., Translating PROTAC chemical series optimization into functional outcomes underlying BRD7 and BRD9 protein degradation. *Current Research in Chemical Biology* **2021**, 1, 100009.

73.   Vangamudi, B.; Paul, T. A.; Shah, P. K.; Kost-Alimova, M.; Nottebaum, L.; Shi, X.; Zhan, Y.; Leo, E.; Mahadeshwar, H. S.; Protopopov, A.; Futreal, A.; Tieu, T. N.; Peoples, M.; Heffernan, T. P.; Marszalek, J. R.; Toniatti, C.; Petrocchi, A.; Verhelle, D.; Owen, D. R.; Draetta, G.; Jones, P.; Palmer, W. S.; Sharma, S.; Andersen, J. N., The SMARCA2/4 ATPase domain surpasses the bromodomain as a drug target in SWI/SNF-mutant cancers: insights from cDNA rescue and PFI-3 inhibitor studies. *Cancer Res.* **2015**, 75, 3865-3878.

74.   Crawford, T. D.; Tsui, V.; Flynn, E. M.; Wang, S.; Taylor, A. M.; Côté, A.; Audia, J. E.; Beresini, M. H.; Burdick, D. J.; Cummings, R., Diving into the water: inducible binding conformations for BRD4, TAF1 (2), BRD9, and CECR2 bromodomains. *J. Med. Chem.* **2016**, 59, 5391-5402.

75.   Suzuki, A., Carbon–carbon bonding made easy. *Chem. Commun.* **2005**, 4759-4763.

76.   Layek, M.; Gajare, V.; Kalita, D.; Islam, A.; Mukkanti, K.; Pal, M., A highly effective synthesis of 2-alkynyl-7-azaindoles: Pd/C-mediated alkynylation of heteroaryl halides in water. *Tetrahedron* **2009**, 65, 4814-4819.

77.   Hegedus, L. S.; Greenberg, M. M.; Wendling, J. J.; Bullock, J. P., Synthesis of 5,12-Dioxocyclam Nickel (II) Complexes Having Quinoxaline Substituents at the 6 and 13 Positions as Potential DNA Bis-Intercalating and Cleaving Agents. *J. Org. Chem.* **2003**, 68, 4179-4188.

78.   Gul, S., Epigenetic assays for chemical biology and drug discovery. *Clin. Epigenetics* **2017**, 9, 41.

79.   Igoe, N.; Bayle, E. D.; Fedorov, O.; Tallant, C.; Savitsky, P.; Rogers, C.; Owen, D. R.; Deb, G.; Somervaille, T. C.; Andrews, D. M.; Jones, N.; Cheasty, A.; Ryder, H.; Brennan, P. E.; Müller, S.; Knapp, S.; Fish, P. V., Design of a biased potent small molecule inhibitor of the bromodomain and PHD finger-containing (BRPF) proteins suitable for cellular and in vivo studies. *J. Med. Chem.* **2017**, 60, 668-680.

80.   Cheng, C. L.-H.; Tsang, F. H.-C.; Wei, L.; Chen, M.; Chin, D. W.-C.; Shen, J.; Law, C.-T.; Lee, D.; Wong, C. C.-L.; Ng, I. O.-L. N., Chun-Ming Wong, Bromodomain-containing protein BRPF1 is a therapeutic target for liver cancer. *Commun. Biol.* **2021**, 4, 1-14.

81.   Xing, Y.; Zuo, J.; Krogstad, P.; Jung, M. E., Synthesis and Structure–Activity Relationship (SAR) Studies of Novel Pyrazolopyridine Derivatives as Inhibitors of Enterovirus Replication. *J. Med. Chem.* **2018**, 61, 1688-1703.

82.   Youn, S. W.; Ko, T. Y.; Jang, Y. H., Palladium-Catalyzed Regioselective Synthesis of 3-Arylindoles from N-Ts-Anilines and Styrenes. *Angew. Chem. Int. Ed.* **2017**, 56, 6636-6640.

83.   De Vita, S.; Chini, M. G.; Lauro, G.; Bifulco, G., Accelerating the repurposing of FDA-approved drugs against coronavirus disease-19 (COVID-19). *RSC advances* **2020**, 10, 40867-40875.

84.   Di Micco, S.; Pulvirenti, L.; Bruno, I.; Terracciano, S.; Russo, A.; Vaccaro, M. C.; Ruggiero, D.; Muccilli, V.; Cardullo, N.; Tringali, C.; Riccio, R.; Bifulco, G., Identification by Inverse Virtual Screening of magnolol-based scaffold as new tankyrase-2 inhibitors. *Biorg. Med. Chem.* **2018**, 26, 3953-3957.

85.   Lauro, G.; Strocchia, M.; Terracciano, S.; Bruno, I.; Fischer, K.; Pergola, C.; Werz, O.; Riccio, R.; Bifulco, G., Exploration of the dihydropyrimidine scaffold for the development of new potential anti-inflammatory agents blocking prostaglandin E2 synthase-1 enzyme (mPGES-1). *Eur. J. Med. Chem.* **2014**, 80, 407-415.

86.   Chini, M. G.; Giordano, A.; Potenza, M.; Terracciano, S.; Fischer, K.; Vaccaro, M. C.; Colarusso, E.; Bruno, I.; Riccio, R.; Koeberle, A.; Werz, O.; Bifulco, G., Targeting mPGES-1 by a Combinatorial Approach: Identification of the Aminobenzothiazole Scaffold to Suppress PGE2 Levels. *ACS Med. Chem. Lett.* **2020**, 11, 783-789.

87.   Brien, G. L.; Remillard, D.; Shi, J.; Hemming, M. L.; Chabon, J.; Wynne, K.; Dillon, E. T.; Cagney, G.; Van Mierlo, G.; Baltissen, M. P.; Vermeulen, M.; Qi, J.; Fröhling, S.; Gray, N. S.; Bradner, J. E.; Vakoc, C. R.; Armstrong, S. A., Targeted degradation of BRD9 reverses oncogenic gene expression in synovial sarcoma. *eLife* **2018**, 7, e41305.

88.   Santos, R.; Ursu, O.; Gaulton, A.; Bento, A. P.; Donadi, R. S.; Bologa, C. G.; Karlsson, A.; Al-Lazikani, B.; Hersey, A.; Oprea, T. I.; Overington, J. P., A comprehensive map of molecular drug targets. *Nat. Rev. Drug Discov.* **2017**, 16, 19-34.

89.   Ciulli, A.; Trainor, N., A beginner's guide to PROTACs and targeted protein degradation. *The Biochemist* **2021**, 43, 74-79.

References

90.   Crooke, S. T.; Baker, B. F.; Crooke, R. M.; Liang, X.-h., Antisense technology: an overview and prospectus. *Nat. Rev. Drug Discov.* **2021**, 20, 427-453.

91.   Nelson, A. L.; Dhimolea, E.; Reichert, J. M., Development trends for human monoclonal antibody therapeutics. *Nat. Rev. Drug Discov.* **2010**, 9, 767-774.

92.   Burnett, John C.; Rossi, John J., RNA-Based Therapeutics: Current Progress and Future Prospects. *Chem. Biol.* **2012**, 19, 60-71.

93.   Kinch, M. S.; Kraft, Z.; Schwartz, T., 2021 in review: FDA approvals of new medicines. *Drug Discov. Today* **2022**, 27, 2057-2064.

94.   Zhou, X.; Dong, R.; Zhang, J.-Y.; Zheng, X.; Sun, L.-P., PROTAC: A promising technology for cancer treatment. *Eur. J. Med. Chem.* **2020**, 203, 112539.

95.   Lai, A. C.; Crews, C. M., Induced protein degradation: an emerging drug discovery paradigm. *Nat. Rev. Drug Discov.* **2017**, 16, 101-114.

96.   Collins, I.; Wang, H.; Caldwell, J. J.; Chopra, R., Chemical approaches to targeted protein degradation through modulation of the ubiquitin–proteasome pathway. *Biochem. J.* **2017**, 474, 1127-1147.

97.   Sakamoto, K. M.; Kim, K. B.; Kumagai, A.; Mercurio, F.; Crews, C. M.; Deshaies, R. J., Protacs: Chimeric molecules that target proteins to the Skp1–Cullin–F box complex for ubiquitination and degradation. **2001**, 98, 8554-8559.

98.   Garber, K., The PROTAC gold rush. *Nat. Biotechnol.* **2022**, 40, 12-16.

99.   Salerno, A.; Seghetti, F.; Caciolla, J.; Uliassi, E.; Testi, E.; Guardigni, M.; Roberti, M.; Milelli, A.; Bolognesi, M. L., Enriching Proteolysis Targeting Chimeras with a Second Modality: When Two Are Better Than One. *J. Med. Chem.* **2022**, 65, 9507-9530.

100.   Cipriano, A.; Sbardella, G.; Ciulli, A., Targeting epigenetic reader domains by chemical biology. *Curr. Opin. Chem. Biol.* **2020**, 57, 82-94.

101.   Roy, M. J.; Winkler, S.; Hughes, S. J.; Whitworth, C.; Galant, M.; Farnaby, W.; Rumpel, K.; Ciulli, A., SPR-Measured Dissociation Kinetics of PROTAC Ternary Complexes Influence Target Degradation Rate. *ACS Chem. Biol.* **2019**, 14, 361-368.

102.   Němec, V.; Schwalm, M. P.; Müller, S.; Knapp, S., PROTAC degraders as chemical probes for studying target biology and target validation. *Chem. Soc. Rev.* **2022**, 51, 7971-7993.

103.   FHD-609 in Subjects With Advanced Synovial Sarcoma or Advanced SMARCB1-Loss Tumors. https://clinicaltrials.gov/ct2/show/NCT04965753

104. Bondeson, D. P.; Mares, A.; Smith, I. E. D.; Ko, E.; Campos, S.; Miah, A. H.; Mulholland, K. E.; Routly, N.; Buckley, D. L.; Gustafson, J. L.; Zinn, N.; Grandi, P.; Shimamura, S.; Bergamini, G.; Faelth-Savitski, M.; Bantscheff, M.; Cox, C.; Gordon, D. A.; Willard, R. R.; Flanagan, J. J.; Casillas, L. N.; Votta, B. J.; den Besten, W.; Famm, K.; Kruidenier, L.; Carter, P. S.; Harling, J. D.; Churcher, I.; Crews, C. M., Catalytic in vivo protein knockdown by small-molecule PROTACs. *Nat. Chem. Biol.* **2015**, 11, 611-617.

105. Bondeson, D. P.; Smith, B. E.; Burslem, G. M.; Buhimschi, A. D.; Hines, J.; Jaime-Figueroa, S.; Wang, J.; Hamman, B. D.; Ishchenko, A.; Crews, C. M., Lessons in PROTAC Design from Selective Degradation with a Promiscuous Warhead. *Cell Chem. Biol.* **2018**, 25, 78-87.e5.

106. Gadd, M. S.; Testa, A.; Lucas, X.; Chan, K.-H.; Chen, W.; Lamont, D. J.; Zengerle, M.; Ciulli, A., Structural basis of PROTAC cooperative recognition for selective protein degradation. *Nat. Chem. Biol.* **2017**, 13, 514-521.

107. Churcher, I., Protac-Induced Protein Degradation in Drug Discovery: Breaking the Rules or Just Making New Ones? *J. Med. Chem.* **2018**, 61, 444-452.

108. Mullard, A., First targeted protein degrader hits the clinic. *Nat. Rev. Drug Discov.* **2019**.

109. Yang, C.-Y.; Qin, C.; Bai, L.; Wang, S., Small-molecule PROTAC degraders of the Bromodomain and Extra Terminal (BET) proteins — A review. *Drug Discov. Today Technol.* **2019**, 31, 43-51.

110. Zoppi, V.; Hughes, S. J.; Maniaci, C.; Testa, A.; Gmaschitz, T.; Wieshofer, C.; Koegl, M.; Riching, K. M.; Daniels, D. L.; Spallarossa, A.; Ciulli, A., Iterative Design and Optimization of Initially Inactive Proteolysis Targeting Chimeras (PROTACs) Identify VZ185 as a Potent, Fast, and Selective von Hippel–Lindau (VHL) Based Dual Degrader Probe of BRD9 and BRD7. *J. Med. Chem.* **2019**, 62, 699-726.

111. Farnaby, W.; Koegl, M.; Roy, M. J.; Whitworth, C.; Diers, E.; Trainor, N.; Zollman, D.; Steurer, S.; Karolyi-Oezguer, J.; Riedmueller, C.; Gmaschitz, T.; Wachter, J.; Dank, C.; Galant, M.; Sharps, B.; Rumpel, K.; Traxler, E.; Gerstberger, T.; Schnitzer, R.; Petermann, O.; Greb, P.; Weinstabl, H.; Bader, G.; Zoephel, A.; Weiss-Puxbaum, A.; Ehrenhöfer-Wölfer, K.; Wöhrle, S.; Boehmelt, G.; Rinnenthal, J.; Arnhof, H.; Wiechens, N.; Wu, M.-Y.; Owen-Hughes, T.; Ettmayer, P.; Pearson,

References

M.; McConnell, D. B.; Ciulli, A., BAF complex vulnerabilities in cancer demonstrated via structure-based PROTAC design. *Nat. Chem. Biol.* **2019**, 15, 672-680.

112. Weisberg, E.; Chowdhury, B.; Meng, C.; Case, A. E.; Ni, W.; Garg, S.; Sattler, M.; Azab, A. K.; Sun, J.; Muz, B.; Sanchez, D.; Toure, A.; Stone, R. M.; Galinsky, I.; Winer, E.; Gleim, S.; Gkountela, S.; Kedves, A.; Harrington, E.; Abrams, T.; Zoller, T.; Vaupel, A.; Manley, P.; Faller, M.; Chung, B.; Chen, X.; Busenhart, P.; Stephan, C.; Calkins, K.; Bonenfant, D.; Thoma, C. R.; Forrester, W.; Griffin, J. D., BRD9 degraders as chemosensitizers in acute leukemia and multiple myeloma. *Blood Cancer J.* **2022**, 12, 110.

113. Kofink, C.; Trainor, N.; Mair, B.; Wöhrle, S.; Wurm, M.; Mischerikow, N.; Roy, M. J.; Bader, G.; Greb, P.; Garavel, G.; Diers, E.; McLennan, R.; Whitworth, C.; Vetma, V.; Rumpel, K.; Scharnweber, M.; Fuchs, J. E.; Gerstberger, T.; Cui, Y.; Gremel, G.; Chetta, P.; Hopf, S.; Budano, N.; Rinnenthal, J.; Gmaschitz, G.; Mayer, M.; Koegl, M.; Ciulli, A.; Weinstabl, H.; Farnaby, W., A selective and orally bioavailable VHL-recruiting PROTAC achieves SMARCA2 degradation in vivo. *Nat. Commun.* **2022**, 13, 5969.

114. Webb, T.; Craigon, C.; Ciulli, A., Targeting epigenetic modulators using PROTAC degraders: Current status and future perspective. *Bioorg. Med. Chem. Lett.* **2022**, 63, 128653.

115. A Study to Assess the Safety and Tolerability of CFT8634 in Locally Advanced or Metastatic SMARCB1-Perturbed Cancers, Including Synovial Sarcoma and SMARCB1-Null Tumors. https://clinicaltrials.gov/ct2/show/NCT05355753

116. Bemis, T. A.; La Clair, J. J.; Burkart, M. D., Unraveling the Role of Linker Design in Proteolysis Targeting Chimeras. *J. Med. Chem.* **2021**, 64, 8042-8052.

117. Clague, M. J.; Heride, C.; Urbé, S., The demographics of the ubiquitin system. *Trends Cell Biol.* **2015**, 25, 417-426.

118. Bolognesi, M. L., Harnessing Polypharmacology with Medicinal Chemistry. *ACS Med. Chem. Lett.* **2019**, 10, 273-275.

119. Hopkins, A. L.; Mason, J. S.; Overington, J. P., Can we rationally design promiscuous drugs? *Curr. Opin. Struct. Biol.* **2006**, 16, 127-136.

120. Anighoro, A.; Bajorath, J.; Rastelli, G., Polypharmacology: Challenges and Opportunities in Drug Discovery. *J. Med. Chem.* **2014**, 57, 7874-7887.

121.   Meunier, B., Hybrid Molecules with a Dual Mode of Action: Dream or Reality? *Acc. Chem. Res.* **2008**, 41, 69-77.

122.   Morphy, R.; Rankovic, Z., Designed Multiple Ligands. An Emerging Drug Discovery Paradigm. *J. Med. Chem.* **2005**, 48, 6523-6543.

123.   Bolognesi, M. L.; Cavalli, A., Multitarget Drug Discovery and Polypharmacology. **2016**, 11, 1190-1192.

124.   de Lera, A. R.; Ganesan, A., Epigenetic polypharmacology: from combination therapy to multitargeted drugs. *Clin. Epigenetics* **2016**, 8, 105.

125.   Cai, X.; Zhai, H.-X.; Wang, J.; Forrester, J.; Qu, H.; Yin, L.; Lai, C.-J.; Bao, R.; Qian, C., Discovery of 7-(4-(3-Ethynylphenylamino)-7-methoxyquinazolin-6-yloxy)-N-hydroxyheptanamide (CUDC-101) as a Potent Multi-Acting HDAC, EGFR, and HER2 Inhibitor for the Treatment of Cancer. *J. Med. Chem.* **2010**, 53, 2000-2009.

126.   Qian, C.; Lai, C.-J.; Bao, R.; Wang, D.-G.; Wang, J.; Xu, G.-X.; Atoyan, R.; Qu, H.; Yin, L.; Samson, M.; Zifcak, B.; Ma, A. W. S.; DellaRocca, S.; Borek, M.; Zhai, H.-X.; Cai, X.; Voi, M., Cancer Network Disruption by a Single Molecule Inhibitor Targeting Both Histone Deacetylase Activity and Phosphatidylinositol 3-Kinase Signaling. *Clin. Cancer. Res.* **2012**, 18, 4104-4113.

127.   Atkinson, S. J.; Soden, P. E.; Angell, D. C.; Bantscheff, M.; Chung, C.-w.; Giblin, K. A.; Smithers, N.; Furze, R. C.; Gordon, L.; Drewes, G.; Rioja, I.; Witherington, J.; Parr, N. J.; Prinjha, R. K., The structure based design of dual HDAC/BET inhibitors as novel epigenetic probes. *MedChemComm* **2014**, 5, 342-351.

128.   Albrecht, B. K.; Cote, A.; Crawford, T.; Duplessis, M.; Good, A. C.; Leblanc, Y.; Magnuson, S. R.; Nasveschuk, C. G.; Romero, F. A.; Tang, Y. Therapeutic pyridazine compounds and uses thereof. 2016.

129.   Hodges, C.; Kirkland, J. G.; Crabtree, G. R., The many roles of BAF (mSWI/SNF) and PBAF complexes in cancer. *Cold Spring Harb. Perspect. Med.* **2016**, 6, a026930.

130.   Balkwill, F.; Mantovani, A., Inflammation and cancer: back to Virchow? *The Lancet* **2001**, 357, 539-545.

131.   Dvorak, H. F., Tumors: Wounds That Do Not Heal. *New Engl. J. Med.* **1986**, 315, 1650-1659.

132.   Pardoll, D. M., Spinning molecular immunology into successful immunotherapy. *Nat. Rev. Immunol.* **2002**, 2, 227-238.

133.   Maiuri, M. C.; Tajana, G.; Iuvone, T.; De Stefano, D.; Mele, G.; Ribecco, M. T.; Cinelli, M. P.; Romano, M. F.; Turco, M. C.; Carnuccio, R., Nuclear Factor-κB Regulates Inflammatory Cell Apoptosis and Phagocytosis in Rat Carrageenin-Sponge Implant Model. *Am. J. Pathol.* **2004**, 165, 115-126.

134.   Savill, J.; Fadok, V., Corpse clearance defines the meaning of cell death. *Nature* **2000**, 407, 784-788.

135.   Pollard, J. W., Tumour-educated macrophages promote tumour progression and metastasis. *Nat. Rev. Cancer* **2004**, 4, 71-78.

136.   Kidane, D.; Chae, W. J.; Czochor, J.; Eckert, K. A.; Glazer, P. M.; Bothwell, A. L. M.; Sweasy, J. B., Interplay between DNA repair and inflammation, and the link to cancer. *Crit. Rev. Biochem. Mol. Biol.* **2014**, 49, 116-139.

137.   Alpsoy, A.; Utturkar, S. M.; Carter, B. C.; Dhiman, A.; Torregrosa-Allen, S. E.; Currie, M. P.; Elzey, B. D.; Dykhuizen, E. C., BRD9 Is a Critical Regulator of Androgen Receptor Signaling and Prostate Cancer Progression. *Cancer Res.* **2021**, 81, 820-833.

138.   Wang, X.; Wang, S.; Troisi, E. C.; Howard, T. P.; Haswell, J. R.; Wolf, B. K.; Hawk, W. H.; Ramos, P.; Oberlick, E. M.; Tzvetkov, E. P.; Ross, A.; Vazquez, F.; Hahn, W. C.; Park, P. J.; Roberts, C. W. M., BRD9 defines a SWI/SNF sub-complex and constitutes a specific vulnerability in malignant rhabdoid tumors. *Nat. Commun.* **2019**, 10, 1881.

139.   Gatchalian, J.; Malik, S.; Ho, J.; Lee, D.-S.; Kelso, T. W. R.; Shokhirev, M. N.; Dixon, J. R.; Hargreaves, D. C., A non-canonical BRD9-containing BAF chromatin remodeling complex regulates naive pluripotency in mouse embryonic stem cells. *Nat. Commun.* **2018**, 9, 5139.

140.   Wei, Z.; Yoshihara, E.; He, N.; Hah, N.; Fan, W.; Pinto, A. F. M.; Huddy, T.; Wang, Y.; Ross, B.; Estepa, G.; Dai, Y.; Ding, N.; Sherman, M. H.; Fang, S.; Zhao, X.; Liddle, C.; Atkins, A. R.; Yu, R. T.; Downes, M.; Evans, R. M., Vitamin D Switches BAF Complexes to Protect β Cells. *Cell* **2018**, 173, 1135-1149.e15.

141.   Aggarwal, B. B., Signalling pathways of the TNF superfamily: a double-edged sword. *Nat. Rev. Immunol.* **2003**, 3, 745-756.

142.   Knüpfer, H.; Preiß, R., Significance of interleukin-6 (IL-6) in breast cancer (review). *Breast Cancer Res. Treat.* **2007**, 102, 129-135.

143. Liu, X.; Kalogeropulou, A.; Domingos, S.; Makukhin, N.; Nirujogi, R.; Singh, F.; Shpiro, N.; Saalfrank, A.; Sammler, E.; Ganley, I. G.; Moreira, R.; Alessi, D. R.; Ciulli, A., Discovery of XL01126: A Potent, Fast, Cooperative, Selective, Orally Bioavailable, and Blood-Brain Barrier Penetrant PROTAC Degrader of Leucine-Rich Repeat Kinase 2. *J. Am. Chem. Soc.* **2022**, 144, 16930-16952.

144. Ishihara, L. S.; Cheesbrough, A.; Brayne, C.; Schrag, A., Estimated life expectancy of Parkinson's patients compared with the UK population. *J. Neurol. Neurosurg. Psychiatry* **2007**, 78, 1304-1309.

145. Feigin, V. L.; Abajobir, A. A.; Abate, K. H.; Abd-Allah, F.; Abdulle, A. M.; Abera, S. F.; Abyu, G. Y.; Ahmed, M. B.; Aichour, A. N.; Aichour, I., Global, regional, and national burden of neurological disorders during 1990–2015: a systematic analysis for the Global Burden of Disease Study 2015. *The Lancet Neurology* **2017**, 16, 877-897.

146. Dorsey, E. R.; Sherer, T.; Okun, M. S.; Bloem, B. R., The Emerging Evidence of the Parkinson Pandemic. *J. Parkinsons Dis.* **2018**, 8, S3-s8.

147. Lesage, S.; Dürr, A.; Tazir, M.; Lohmann, E.; Leutenegger, A.-L.; Janin, S.; Pollak, P.; Brice, A., LRRK2 G2019S as a Cause of Parkinson's Disease in North African Arabs. *New Engl. J. Med.* **2006**, 354, 422-423.

148. Lesage, S.; Condroyer, C.; Lannuzel, A.; Lohmann, E.; Troiano, A.; Tison, F.; Damier, P.; Thobois, S.; Ouvrard-Hernandez, A.-M.; Rivaud-Péchoux, S.; Brefel-Courbon, C.; Destée, A.; Tranchant, C.; Romana, M.; Leclere, L.; Dürr, A.; Brice, A., Molecular analyses of the LRRK2 gene in European and North African autosomal dominant Parkinson's disease. *J. Med. Genet.* **2009**, 46, 458-464.

149. Myasnikov, A.; Zhu, H.; Hixson, P.; Xie, B.; Yu, K.; Pitre, A.; Peng, J.; Sun, J., Structural analysis of the full-length human LRRK2. *Cell* **2021**, 184, 3519-3527.

150. Greggio, E.; Cookson, M. R., Leucine-Rich Repeat Kinase 2 Mutations and Parkinson's Disease: Three Questions. *ASN Neuro* **2009**, 1, 13-24.

151. Di Maio, R.; Hoffman, E. K.; Rocha, E. M.; Keeney, M. T.; Sanders, L. H.; De Miranda, B. R.; Zharikov, A.; Van Laar, A.; Stepan, A. F.; Lanz, T. A.; Kofler, J. K.; Burton, E. A.; Alessi, D. R.; Hastings, T. G.; Greenamyre, J. T., LRRK2 activation in idiopathic Parkinson's disease. *Sci. Transl. Med.* **2018**, 10, eaar5429.

152. Deng, X.; Dzamko, N.; Prescott, A.; Davies, P.; Liu, Q.; Yang, Q.; Lee, J.-D.; Patricelli, M. P.; Nomanbhoy, T. K.; Alessi, D. R.; Gray, N. S., Characterization of a

selective inhibitor of the Parkinson's disease kinase LRRK2. *Nat. Chem. Biol.* **2011**, 7, 203-205.

153.   Choi, H. G.; Zhang, J.; Deng, X.; Hatcher, J. M.; Patricelli, M. P.; Zhao, Z.; Alessi, D. R.; Gray, N. S., Brain Penetrant LRRK2 Inhibitor. *ACS Med. Chem. Lett.* **2012**, 3, 658-662.

154.   Jennings, D.; Huntwork-Rodriguez, S.; Henry, A. G.; Sasaki, J. C.; Meisner, R.; Diaz, D.; Solanoy, H.; Wang, X.; Negrou, E.; Bondar, V. V.; Ghosh, R.; Maloney, M. T.; Propson, N. E.; Zhu, Y.; Maciuca, R. D.; Harris, L.; Kay, A.; LeWitt, P.; King, T. A.; Kern, D.; Ellenbogen, A.; Goodman, I.; Siderowf, A.; Aldred, J.; Omidvar, O.; Masoud, S. T.; Davis, S. S.; Arguello, A.; Estrada, A. A.; de Vicente, J.; Sweeney, Z. K.; Astarita, G.; Borin, M. T.; Wong, B. K.; Wong, H.; Nguyen, H.; Scearce-Levie, K.; Ho, C.; Troyer, M. D., Preclinical and clinical evaluation of the LRRK2 inhibitor DNL201 for Parkinson's disease. *Sci. Transl. Med.* **2022**, 14, eabj2658.

155.   Deniston, C. K.; Salogiannis, J.; Mathea, S.; Snead, D. M.; Lahiri, I.; Matyszewski, M.; Donosa, O.; Watanabe, R.; Böhning, J.; Shiau, A. K.; Knapp, S.; Villa, E.; Reck-Peterson, S. L.; Leschziner, A. E., Structure of LRRK2 in Parkinson's disease and model for microtubule interaction. *Nature* **2020**, 588, 344-349.

156.   Watanabe, R.; Buschauer, R.; Böhning, J.; Audagnotto, M.; Lasker, K.; Lu, T.-W.; Boassa, D.; Taylor, S.; Villa, E., The In Situ Structure of Parkinson's Disease-Linked LRRK2. *Cell* **2020**, 182, 1508-1518.

157.   Andersen, M. A.; Wegener, K. M.; Larsen, S.; Badolo, L.; Smith, G. P.; Jeggo, R.; Jensen, P. H.; Sotty, F.; Christensen, K. V.; Thougaard, A., PFE-360-induced LRRK2 inhibition induces reversible, non-adverse renal changes in rats. *Toxicology* **2018**, 395, 15-22.

158.   Baptista, M. A. S.; Merchant, K.; Barrett, T.; Bhargava, S.; Bryce, D. K.; Ellis, J. M.; Estrada, A. A.; Fell, M. J.; Fiske, B. K.; Fuji, R. N.; Galatsis, P.; Henry, A. G.; Hill, S.; Hirst, W.; Houle, C.; Kennedy, M. E.; Liu, X.; Maddess, M. L.; Markgraf, C.; Mei, H.; Meier, W. A.; Needle, E.; Ploch, S.; Royer, C.; Rudolph, K.; Sharma, A. K.; Stepan, A.; Steyn, S.; Trost, C.; Yin, Z.; Yu, H.; Wang, X.; Sherer, T. B., LRRK2 inhibitors induce reversible changes in nonhuman primate lungs without measurable pulmonary deficits. *Sci. Transl. Med.* **2020**, 12, eaav0820.

159.   A Study to Evaluate the Safety, Tolerability, and Pharmacokinetics of BIIB094 in   Adults   With   Parkinson's   Disease. https://www.clinicaltrials.gov/ct2/show/NCT03976349

160.   Garofalo, A. W.; Bright, J.; De Lombaert, S.; Toda, A. M. A.; Zobel, K.; Andreotti, D.; Beato, C.; Bernardi, S.; Budassi, F.; Caberlotto, L.; Gao, P.; Griffante, C.; Liu, X.; Mengatto, L.; Migliore, M.; Sabbatini, F. M.; Sava, A.; Serra, E.; Vincetti, P.; Zhang, M.; Carlisle, H. J., Selective Inhibitors of G2019S-LRRK2 Kinase Activity. *J. Med. Chem.* **2020**, 63, 14821-14839.

161.   Leśniak, R. K.; Nichols, R. J.; Schonemann, M.; Zhao, J.; Gajera, C. R.; Fitch, W. L.; Lam, G.; Nguyen, K. C.; Smith, M.; Montine, T. J., Discovery of G2019S-Selective Leucine Rich Repeat Protein Kinase 2 inhibitors with in vivo efficacy. *Eur. J. Med. Chem.* **2022**, 229, 114080.

162.   Tasegian, A.; Singh, F.; Ganley, I. G.; Reith, A. D.; Alessi, D. R., Impact of Type II LRRK2 inhibitors on signaling and mitophagy. *Biochem. J.* **2021**, 478, 3555-3573.

163.   Li, T.; Yang, D.; Zhong, S.; Thomas, J. M.; Xue, F.; Liu, J.; Kong, L.; Voulalas, P.; Hassan, H. E.; Park, J.-S.; MacKerell, A. D., Jr; Smith, W. W., Novel LRRK2 GTP-binding inhibitors reduced degeneration in Parkinson's disease cell and mouse models. *Hum. Mol. Genet.* **2014**, 23, 6212-6222.

164.   Li, T.; He, X.; Thomas, J. M.; Yang, D.; Zhong, S.; Xue, F.; Smith, W. W., A Novel GTP-Binding Inhibitor, FX2149, Attenuates LRRK2 Toxicity in Parkinson's Disease Models. *PLoS One* **2015**, 10, e0122461.

165.   Helton, L. G.; Soliman, A.; von Zweydorf, F.; Kentros, M.; Manschwetus, J. T.; Hall, S.; Gilsbach, B.; Ho, F. Y.; Athanasopoulos, P. S.; Singh, R. K.; LeClair, T. J.; Versées, W.; Raimondi, F.; Herberg, F. W.; Gloeckner, C. J.; Rideout, H.; Kortholt, A.; Kennedy, E. J., Allosteric Inhibition of Parkinson's-Linked LRRK2 by Constrained Peptides. *ACS Chem. Biol.* **2021**, 16, 2326-2338.

166.   Konstantinidou, M.; Oun, A.; Pathak, P.; Zhang, B.; Wang, Z.; ter Brake, F.; Dolga, A. M.; Kortholt, A.; Dömling, A., The tale of proteolysis targeting chimeras (PROTACs) for Leucine-Rich Repeat Kinase 2 (LRRK2). *ChemMedChem* **2021**, 16, 959-965.

167.   Gray, N. S.; Hatcher, J. Degraders of Wild-Type and Mutant Forms of Lrrk2. WO2020081682A1, 2020.

168.   Araujo, E.; Berlin, M.; Sparks, S. M.; Wang, J.; Zhang, W. WO2021194879A1, 2021.

169.   Liu, X.; Zhang, X.; Lv, D.; Yuan, Y.; Zheng, G.; Zhou, D., Assays and technologies for developing proteolysis targeting chimera degraders. *Future Med. Chem.* **2020**, 12, 1155-1179.

170.   Bond, A. G.; Craigon, C.; Chan, K.-H.; Testa, A.; Karapetsas, A.; Fasimoye, R.; Macartney, T.; Blow, J. J.; Alessi, D. R.; Ciulli, A., Development of BromoTag: A "Bump-and-Hole"–PROTAC System to Induce Potent, Rapid, and Selective Degradation of Tagged Target Proteins. *J. Med. Chem.* **2021**, 64, 15477-15502.

171.   Casement, R.; Bond, A.; Craigon, C.; Ciulli, A. Mechanistic and Structural Features of PROTAC Ternary Complexes. In *Targeted Protein Degradation: Methods and Protocols*, Cacace, A. M.; Hickey, C. M.; Békés, M., Eds.; Springer US: New York, NY, 2021, pp 79-113.

172.   Danley, D. E., Crystallization to obtain protein–ligand complexes for structure-aided drug design. *Acta Crystallogr. Sect. D. Biol. Crystallogr.* **2006**, 62, 569-575.

173.   Stum, E. A.; Gleichmann, T. Soaking Techniques. In *Crystallization of Nucleic Acids and Proteins: A Practical Approach*, Ducruix, A.; Giegé, R., Eds.; Oxford University Press: 1999, pp 365-390.

174.   Soares, P.; Gadd, M. S.; Frost, J.; Galdeano, C.; Ellis, L.; Epemolu, O.; Rocha, S.; Read, K. D.; Ciulli, A., Group-Based Optimization of Potent and Cell-Active Inhibitors of the von Hippel–Lindau (VHL) E3 Ubiquitin Ligase: Structure–Activity Relationships Leading to the Chemical Probe (2S,4R)-1-((S)-2-(1-Cyanocyclopropanecarboxamido)-3,3-dimethylbutanoyl)-4-hydroxy-N-(4-(4-methylthiazol-5-yl)benzyl)pyrrolidine-2-carboxamide (VH298). *J. Med. Chem.* **2018**, 61, 599-618.

175.   Atilaw, Y.; Poongavanam, V.; Svensson Nilsson, C.; Nguyen, D.; Giese, A.; Meibom, D.; Erdelyi, M.; Kihlberg, J., Solution Conformations Shed Light on PROTAC Cell Permeability. *ACS Med. Chem. Lett.* **2021**, 12, 107-114.

176.   Buckley, D. L.; Van Molle, I.; Gareiss, P. C.; Tae, H. S.; Michel, J.; Noblin, D. J.; Jorgensen, W. L.; Ciulli, A.; Crews, C. M., Targeting the von Hippel–Lindau E3 Ubiquitin Ligase Using Small Molecules To Disrupt the VHL/HIF-1α Interaction. *J. Am. Chem. Soc.* **2012**, 134, 4465-4468.

177.   Buckley, D. L.; Gustafson, J. L.; Van Molle, I.; Roth, A. G.; Tae, H. S.; Gareiss, P. C.; Jorgensen, W. L.; Ciulli, A.; Crews, C. M., Small-Molecule Inhibitors of the Interaction between the E3 Ligase VHL and HIF1α. *Angew. Chem. Int. Ed.* **2012**, 51, 11463-11467.

178.   Hu, J.; Hu, B.; Wang, M.; Xu, F.; Miao, B.; Yang, C.-Y.; Wang, M.; Liu, Z.; Hayes, D. F.; Chinnaswamy, K.; Delproposto, J.; Stuckey, J.; Wang, S., Discovery of ERD-308 as a Highly Potent Proteolysis Targeting Chimera (PROTAC) Degrader of Estrogen Receptor (ER). *J. Med. Chem.* **2019**, 62, 1420-1442.

179.   Steger, M.; Diez, F.; Dhekne, H. S.; Lis, P.; Nirujogi, R. S.; Karayel, O.; Tonelli, F.; Martinez, T. N.; Lorentzen, E.; Pfeffer, S. R.; Alessi, D. R.; Mann, M., Systematic proteomic analysis of LRRK2-mediated Rab GTPase phosphorylation establishes a connection to ciliogenesis. *eLife* **2017**, 6, e31012.

180.   Steger, M.; Tonelli, F.; Ito, G.; Davies, P.; Trost, M.; Vetter, M.; Wachter, S.; Lorentzen, E.; Duddy, G.; Wilson, S.; Baptista, M. A. S.; Fiske, B. K.; Fell, M. J.; Morrow, J. A.; Reith, A. D.; Alessi, D. R.; Mann, M., Phosphoproteomics reveals that Parkinson's disease kinase LRRK2 regulates a subset of Rab GTPases. *eLife* **2016**, 5, e12813.

181.   Dzamko, N.; Deak, M.; Hentati, F.; Reith, Alastair D.; Prescott, Alan R.; Alessi, Dario R.; Nichols, R. J., Inhibition of LRRK2 kinase activity leads to dephosphorylation of Ser910/Ser935, disruption of 14-3-3 binding and altered cytoplasmic localization. *Biochem. J.* **2010**, 430, 405-413.

182.   Reith, A. D.; Bamborough, P.; Jandu, K.; Andreotti, D.; Mensah, L.; Dossang, P.; Choi, H. G.; Deng, X.; Zhang, J.; Alessi, D. R.; Gray, N. S., GSK2578215A; A potent and highly selective 2-arylmethyloxy-5-substitutent-N-arylbenzamide LRRK2 kinase inhibitor. *Bioorg. Med. Chem. Lett.* **2012**, 22, 5625-5629.

183.   Van Molle, I.; Thomann, A.; Buckley, Dennis L.; So, Ernest C.; Lang, S.; Crews, Craig M.; Ciulli, A., Dissecting Fragment-Based Lead Discovery at the von Hippel-Lindau Protein:Hypoxia Inducible Factor 1α Protein-Protein Interface. *Chem. Biol.* **2012**, 19, 1300-1312.

184.   McCoy, A. J.; Grosse-Kunstleve, R. W.; Adams, P. D.; Winn, M. D.; Storoni, L. C.; Read, R. J., Phaser crystallographic software. *J. Appl. Crystallogr.* **2007**, 40, 658-674.

185.   Emsley, P.; Cowtan, K., Coot: model-building tools for molecular graphics. *Acta Crystallogr. Sect. D. Biol. Crystallogr.* **2004**, 60, 2126-2132.

186.   Afonine, P. V.; Grosse-Kunstleve, R. W.; Echols, N.; Headd, J. J.; Moriarty, N. W.; Mustyakimov, M.; Terwilliger, T. C.; Urzhumtsev, A.; Zwart, P. H.; Adams, P. D., Towards automated crystallographic structure refinement with phenix. refine. *Acta Crystallogr. Sect. D. Biol. Crystallogr.* **2012**, 68, 352-367.

187.   Moriarty, N. W.; Grosse-Kunstleve, R. W.; Adams, P. D., electronic Ligand Builder and Optimization Workbench (eLBOW): a tool for ligand coordinate and restraint generation. *Acta Crystallogr. Sect. D. Biol. Crystallogr.* **2009**, 65, 1074-1080.

188.   Chen, V. B.; Arendall, W. B.; Headd, J. J.; Keedy, D. A.; Immormino, R. M.; Kapral, G. J.; Murray, L. W.; Richardson, J. S.; Richardson, D. C., MolProbity: all-atom structure validation for macromolecular crystallography. *Acta Crystallogr. Sect. D. Biol. Crystallogr.* **2010**, 66, 12-21.